PhD-FSTM-2021-038
The Faculty of Sciences, Technology and Medicine

DISSERTATION

Defence held on 18/06/2021 in Esch-sur-Alzette, Luxembourg

to obtain the degree of

DOCTEUR DE L'UNIVERSITÉ DU LUXEMBOURG

EN BIOLOGIE

by

Sunday Ojochegbe OKUTACHI

Born on 23rd December 1990 in Abocho, Nigeria

CHARACTERIZATION OF NOVEL COVALENT AND NON-COVALENT DRUGS AGAINST K-RAS SURROGATE TARGETS

Dissertation defence committee

Prof. Dr. Daniel Abankwa, dissertation supervisor
University of Luxembourg, Luxembourg
Prof. Dr. Iris Behrmann, chairperson
University of Luxembourg, Luxembourg
Prof. Dr. Khrishnaraj Rajalingam
University Medical Center, Mainz, Germany
Prof. Dr. Ian Prior
University of Liverpool, United Kingdom
Dr. Chris Marshall
Princess Margaret cancer center, University of Toronto, Canada

CHARACTERIZATION OF NOVEL COVALENT AND NON-COVALENT DRUGS AGAINST K-RAS SURROGATE TARGETS

OKUTACHI Ojochegbe Sunday

A thesis submitted in partial fulfilment of the

Requirements for the degree of

Doctor of Philosophy in Biology

At the

University of Luxembourg

June 2021

This Doctoral Thesis was performed at the Department of Life Sciences and Medicine at the University of Luxembourg, under the supervision of Prof. Dr. Daniel Abankwa, principal investigator of the Cancer Cell Biology and Drug Discovery Laboratory. The PhD is funded by the University of Luxembourg under the starting grant of Prof. Abankwa's position.

Thesis supervisory committee:

Prof. Dr. Daniel Abankwa

University of Luxembourg, Luxembourg

Prof. Dr. Iris Behrmann

University of Luxembourg, Luxembourg

Prof. Dr. Khrishnaraj Rajalingam

University Medical Center, Mainz, Germany

DLSM | DEPARTMENT OF LIFE SCIENCES AND MEDICINE

UNIVERSITÉ DU LUXEMBOURG

Affidavit

Declaration of Authorship

I hereby confirm that the PhD thesis entitled “characterization of novel covalent and non-covalent drugs against K-Ras surrogate targets” is written independently and without any other external sources other than those cited.

Esch-sur-Alzette, May 03, 2021

OKUTACHI Ojochegbe Sunday

Acknowledgement

In all your ways acknowledge Him and He shall direct your paths

Proverbs 3:6

The past 3 years have been filled with so many lessons, opportunities and memories that would not have been possible without the help of several individuals from my professional and person life.

Firstly, I wish to express my deepest gratitude to **Prof. Dr. Daniel ABANKWA,** my thesis supervisor and academic mentor for allowing me work on this complex and stimulating topic of Ras biology. I will be forever grateful to you for taking a chance on me and welcoming me into your lab. Your academic mentorship and support has ensured that I grew rapidly as a scientist and helped me use my time optimally as demonstrated by this record time to graduation. I appreciate your patience and willingness to go the extra mile to impact knowledge. I appreciate your commitment to excellence and quality work, your frank comments and desire to bring out the best from your graduate students. My experience with you will remain a watershed moment in my life's story.

Also, I will like to specially thank the external jury members of my thesis defense committee **Prof. Ian PRIOR** of the University of Liverpool and **Prof. Chris MARSHALL** of University of Toronto for accepting to examine my thesis. Having read many of your seminal publications in Ras biology, I am honored to have such leading figures evaluate my work. My sincere gratitude goes to my thesis advisory committee members **Prof. Dr. Iris BEHRMANN** and **Prof. Dr. Khrishnaraj RAJALINGAM** for taking out time from your busy schedules to support the progress of my PhD training.

Furthermore, I will like to thank all the members of the Cancer Cell Biology and Drug Discovery Group especially **Dr. Ganesh babu MANOHARAN, Dr. Elisabeth RECKINGER-SCHAFFNER, Marie CATILLON** and **Christina LAURINI** for all the help and support on the bench and off the bench. I am grateful to **Ganesh** who not only served as an unofficial supervisor but also a good friend and support in my darkest hours of need. You so generously offered scientific and personal

advice and helped ensure that I stayed grounded during this PhD. Your kindness is appreciated. Thank you **Lis** for the often resourceful ideas on experiments and assay optimization as well as your hospitality when we first arrived in Luxembourg and subsequently. Interacting with you is always a pleasure, your commitment to common decency and family values has no doubt rubbed off on me. You will be remembered fondly. Thank you **Marie**, our multi-talented research technologist who so gracefully taught me many useful techniques for my project. Your abilities on the bench are rare and so is you willingness to share knowledge. Thank you **Christina** for helping out with microscopy and making sure we did not run-out of critical items during the course of my PhD.

In addition, I wish to thank the more recent senior members of the Abankwa lab **Dr. Rohan CHIPPALKATTI** and **Dr. Karolina PAVIC** for helping out with troubleshooting experiments, data analysis and literature expertise. I will also like to thank my fellow PhD students **Pelin KAYA** and **Candy STEFFEN** for being such kind colleagues and a delight to converse with.

I would like to thank all the current and previous members of the department of life sciences and medicine (DLSM) with whom I had the opportunity to meet and interact with during my visits to BT2. Special thanks to **Prof. Iris BEHRMANN, Sergio ALVAREZ** and **Alexandre SALSMANN** who have been so helpful with my nonprofits efforts to improve biomedical research in my home country of Nigeria. Special thanks go to **Dr. Raquel MACHADO**, Lis's former postdoc for her friendship, support and all round positivity. Also, I will like to thank **Dr. Sotirios GALTSIDIS** who was always helpful troubleshooting experiments. I enjoyed chatting with you both on stimulating and wide ranging topics on science and society. As we were often isolated from the rest of the department at BT2, the friendships I formed with fellow PhD students from the Signal Transduction Group particularly **Nadege Wendkouni MINNOUNGOU** and **Tijana RANDIC** was really helpful in going through this exciting but challenging period. I also wish to thank all the administrative staff at the DLSM and the office of doctoral education particularly **Caroline HERFROY**, **Stephanie CUGNACH** and **Magali GUILLAUME** respectively for facilitating the day to day activities and for organizing and taking care of trips to conferences and managing orders.

This acknowledgement will be incomplete without the mention of the people in my private life who have helped keep me healthy, safe and made me feel loved. First on this list is my beloved wife and life partner **Grace Ebi-ojo EKELE**. You have been and continue to be my rock through thick and thin, you helped console me far from home and all our loved ones when daddy passed and

continue to support me in every possible way. You have given me the greatest gift of all, a family and a future. Thank you for enduring my late nights working nonstop, thank you for taking care of our son **Onu Alexander OKUTACHI** after your long workdays as I stay glued to my PC. Thank you for all the happy memories and moments. Indeed, I am lucky to have you both in my life.

To my late dad **James OKUTACHI,** I am thankful for all the love and support throughout my formative years. You taught me to be decent, to dream beyond my immediate circumstances, work hard and be ambitious. The successes of my life so far are chiefly credited to you. You are the model dad and I know you would be proud of me today. Thank you mum **Elisabeth OKUTACHI,** you have always been there for me through the good and tough times, thank you for the unconditional love, the long nights tending to my needs and enduring a very energetic child. Finally, I wish to specially thank all my siblings **McDonald, Christiana, Moses, Victor and Mary** for your endless love and support all these years. Thank you for all the childhood memories and adventures in our small world in Lokoja. I couldn't have hoped for a better family.

Attah mi, Oma mi, iye mi, kpai oya mi, mè má defi olaiye mi'n, u má neke chi ewundun.

Thank you all.

Dedication

This PhD is dedicated to my wife Grace, my son Onu, my dad James who passed 5 months into my PhD and my mum Elisabeth.

"*Education, then, beyond all other divides of human origin, is a great equalizer of conditions of men—the balance wheel of the social machinery.*"

Horace Mann, 1848

Table of Content

List of Figures

List of Tables

List of Abbreviations

A2ML1	Alpha-2-macroglobulin-like 1
AKT	Protein Kinase B
APC	Adenomatous polyposis coli
Arf	ADP ribosylation factors
Arl2	Arf-like protein 2
ATF2	Activating transcription factor 2
AUC	Area under the curve
BAD	Bcl-2 associated death promoter
BAX	Bcl-2 associated x protein
Bcl-2	B-cell lymphoma 2
BCR-ABL	Breakpoint cluster region protein - Tyrosine protein Kinase ABL1 fusion gene
B-Raf	Rat-1 fibroblast kinase B homolog
BRET	Bioluminescence resonance energy transfer
CaM	Calmodulin
CaMeRas	Calmodulin-K-Ras4b fusion biosensor
cAMP	Cyclic adenosine monophosphate
CBL	E3 ubiquitin-protein ligase CBL
CDC25	Cell division cycle 25, a dual specific phosphatase first isolated from yeast
Cdc42	Cell division control protein 42 homolog
CDK4	Cyclin dependent Kinase 4
CDKs	Cyclin dependent Kinases
cGMP	Cyclic guanosine monophosphate
CIP2A	Cancerous inhibitor of PP2A
C-jun	Jun proto-oncogene
CRC	Colorectal cancer
CSCs	Cancer stem cells
CTLA4	cytotoxic T-lymphocyte-associated protein 4
DSS	Drug sensitivity score
DUSP	Dual specificity phosphatase
EC_{50}	Half maximal effective concentration

EGFR	Epidermal growth factor receptor
ERK	Extracellular signal regulated kinase
FGFR	Fibroblast growth factor receptor
FLIM	Fluorescence life-time imaging microscopy
FRET	Fluorescence resonance energy transfer
FTase	Farnesyl transferase
FTIs	Farnesyl transferase inhibitors
GAPs	GTPase activating proteins
GDP	Guanosine 5' diphosphate
GEFs	Guanine nucleotide exchange factor
GGTase1	Geranylgeranyltransferase
GGTIs	Geranylgeranyltransferase inhibitors
GRB2	Growth factor receptor-bound protein 2
GTP	Guanosine 5' triphosphate
GTPases	Guanosine triphosphatases
HCC	Hepatocellular carcinoma
HEAT	Hungtingtin Elongation factor 3/ PP2A A/TOR1
HIF-1	Hypoxia inducible factor 1
H-Ras	Harvey rat sarcoma viral oncogene homolog
HVR	Hypervariable region of Ras proteins
IC_{50}	Half maximal inhibitory concentration
ICMT	Protein-S-isoprenylcysteine O-methyl transferase
IEX-1	Immediate early response gene X-1
IKK	IkappaB Kinase
iPSCs	Induced pluripotent stem cells
IRS1	Insulin receptor substrate 1
JNK	Jun amino-(N)-terminal kinase
K-Ras	Kirsten rat sarcoma viral oncogene homolog
LCMT-1	Leucine Carboxyl Methyl Transferase 1
LUAD	Lung adenocarcinoma
LZTR1	Leucine-zipper-like transcriptional regulator 1
MAP2K1	Dual specificity mitogen-activated protein kinase kinase 1
MAP4K3	Mitogen-activated protein kinase kinase kinase kinase 3

MAPK	Mitogen-activated protein kinase
MEK	MAPK/ERK Kinase
mTOR	Mammalian target of Rapamycin
mTORC1	mTOR complex 1
NF- kB	Nuclear factor Kappa B
NF1	Neurofibromin 1
N-Ras	Neuroblastoma Ras viral oncogene homolog
NSCLC	Non-small cell lung cancer
OCT4	octamer-binding transcription factor 4
p110α	Phosphatidylinositol-4,5-bisphosphate 3-kinase, catalytic subunit alpha
$p21^{CIP1}$	cyclin-dependent kinase inhibitor 1
PATs	Palmitoyl acyl transferases
PD1	Programmed death protein 1
PDACs	Pancreatic ductal adenocarcinomas
PDE6D	Phospodiesterase 6 delta subunit
PDEs	Phosphodiesterases
PDGR	Platelets derived growth factor receptor
PDK1	Protein Kinase D 1
PDL1	Programmed death ligand 1
PI3K	Phosphoinositide-3-kinase
PIP2	phosphatidylinositol 4,5-bisphosphate
PIP3	phosphatidylinositol 3,4,5-trisphosphate
PKC	Protein Kinase C
PM	Plasma membrane
PME1	PP2A methylesterase-1
PP2A	Protein phosphatase 2 α
PROTACs	Proteolysis targeting chimeras
PTEN	Phospatase and tensin homolog
PTM	Post translational modification
PTPA	Phosphotyrosyl phosphatase activator
PTPN11	Tyrosine-protein phosphatase non-receptor type 11
Rab	Ras-like protein in brain
Rac1	Ras-related C3 botulinum toxin substrate 1
Ral	Ras-like

RalA	Ras-like A
RalB	Ras-like B
RalBP1	Ral binding protein 1
RalGDS	Ral guanine nucleotide dissociation stimulus
Ran	Ras-related nuclear protein
Ras	Rat sarcoma (protein)
RASA1	RAS P21 Protein Activator 1
RCE1	Ras converting enzyme 1
Rheb	Ras homolog enriched in brain
Rho	Ras homologus
RIT1	GTP-binding protein Rit1
RTKs	Receptor tyrosine kinases
S6K	Ribosomal protein S6 Kinase beta-1
Sec5	Exocyst complex component SEC5
SET	Suvar/ Enhancer of zeste/ Trithorax
SHC	Src homology 2 domain containing transforming protein
SH-domain	Src homology domain
SHOC-2	Leucine-rich repeat protein
SHP2	Src homology 2 (SH2) domain–containing phosphatase 2
SMAP	Small molecule activator of PP2A
SOS	Son of sevenless
SPRED1	Sprouty-related, EVH1 domain-containing protein 1
SPRY	Sprouty RTK signaling antagonist
Src	Non-receptor protein tyrosine kinase
SREBP	Sterol regulatory element-binding protein
STAT3	signal transducer and activator of transcription 3
TANK	TRAF Family Member Associated NFKB Activator
TBK1	TANK-binding Kinase 1
TILs	Tumor infiltrating lymphocytes
TSC2	Tuberous sclerosis complex 2
UPS	Ubiquitin proteasome system
VEGF	Vascular endothelial growth factor
Wnt	Wingless type

Abstract

Mutations in the KRAS gene are associated with approximately 15% of all human cancers. This makes it one of the most frequently mutated oncogenes known. Whilst recent breakthroughs in Ras drug discovery have led to the FDA approval of the first direct and covalent inhibitor of the KRAS-G12C mutant, the majority of KRAS driven cancers are not G12C mutated. Furthermore, recent studies have identified resistance mechanisms against the new inhibitors. Consequently, research into other direct and indirect Ras inhibition strategies, as well as synergistic drug combination efforts are being vigorously pursued.

In the first part of this thesis, I describe my contributions to the development and characterization of novel PDE6D inhibitors with activity against KRAS driven cancers. PDE6D is a trafficking chaperone of K-Ras that facilitates its dynamic localization to the plasma membrane. Although some progress had been made in identifying lead drug candidates against this protein, an Arl2 dependent PDE6D cargo ejection mechanism continues to hamper progress. We describe the development of **Deltaflexin 1 and Deltaflexin 2**, into which we engineered a 'molecular spring' to improve resilience to Arl2 ejection of PDE6D cargo. We show that these compounds selectively inhibit K-Ras membrane organization and exhibited K-Ras selective anti-proliferative effects against cancer cell lines from colon and breast tissues whilst blocking the 3D spheroid growth of lung and breast cancer cell lines.

In the second part, I describe my main project, the identification of a novel covalent inhibitor of calmodulin (CaM) with anti-cancer activity in K-Ras mutated cancers named **Calmirasone1.** A relevance of the K-Ras/ CaM interaction for the promotion of cancer cell stemness has been previously suggested. We previously showed that the natural product Ophiobolin A (OphA) blocked K-Ras membrane organization in a CaM dependent manner and cancer cell spheroid formation. However, because of the broad toxicity of OphA, its suitability as a tool compound to further study this K-Ras/CaM associated stemness properties is limited. We have therefore characterized a set of benzazulenones with distant chemical similarity to OphA in a battery of assays. We identified Calmirasone1 which exhibits improved CaM affinity and a significantly lower unspecific toxicity relative to OphA. Furthermore, Calmirasone1 selectively blocked K-Ras membrane organization and inhibited the 3D spheroid growth of K-Ras dependent cancer cell lines.

In the third part of this thesis, I assessed the synergistic potential of targeting CaM and protein phosphatase 2A (PP2A) in Ras-MAPK dependent cancer cell lines. PP2A is a tumor suppressor that catalyze the dephosphorylation of multiple targets in the cell. Using specific

CaM inhibitors and PP2A agonists as well as the already clinically approved phenothiazines (PTZs), our results from this study suggests that synergistic targeting of CaM and PP2A improves anti-cancer effects and that PTZs combine CaM inhibitory and PP2A re-activating properties in their cancer killing activity.

INTRODUCTION

1. INTRODUCTION

Cancer is the second leading cause of death globally, in 2020, 19.3 million new cases and almost 10 million deaths were estimated for the disease (Sung et al., 2021). The global burden of cancer is projected to continue to increase due to factors such as lifestyle changes, increased life expectancy and an increasingly aging population (Sung et al., 2021). With over 70% of cancer mortalities occurring in developing countries whose healthcare systems are often overstretched, the need for innovative approaches to cancer treatment is without question.

Half a century of research in molecular oncology has led researchers to identify many of the genetic alterations that are implicated in cancer development, chief among these being the transformation of proto-onocogenes into onocogenes and the blockade of tumor suppressor gene activity. Several hallmark features of cancer have been extensively characterized (Hanahan and Weinberg, 2011). This deeper understanding of the disease has led to a surge in the development of targeted therapeutics aimed at the onco-proteins such as the BCR-Abl oncofusion Kinase (Gleevec), B-Raf (Sorafenib, Zelboraf), EGFR (Erlotinib) etc. Unfortunately, some oncogenic proteins such as Ras have remained elusive to direct therapeutic intervention.

Ras proteins were among the earliest identified oncogenes. These proteins have been implicated in approximately 19% of all human solid tumors thus making them the most frequently mutated oncogenes in cancer (Prior et al., 2020). After almost 40 years of intense research, recent breakthroughs have led to the clinical development of the first direct and covalent inhibitors of the K-RasG12C mutant of which Amgen's molecule, sotorasib recently received FDA approval (Moore et al., 2020, Amgen, 2021). Importantly, whilst this represents a major breakthrough in Ras drug development, the majority of K-Ras driven cancers are not G12C mutated. Furthermore, recent studies have identified resistance mechanisms against these new inhibitors (Tanaka et al., 2021). Hence, research into other direct and indirect Ras inhibition strategies as well as synergistic drug combinations are being vigorously pursued.

In the first part of this thesis, we developed and characterized novel PDE6D inhibitors with activity against K-Ras driven cancers. PDE6D is a trafficking chaperone of K-Ras that facilitates its dynamic localization to the plasma membrane (Chandra et al., 2011). Although some progress had been made in identifying early leads against this protein, an Arl2 dependent PDE6D cargo ejection mechanism continues to hamper progress in efforts to develop viable drug candidates (Martin-Gago et al., 2017). To this end, we developed and evaluated novel PDE6D inhibitors with a different design principle across a number of cellular and biochemical assays for their K-Ras mediated anti-cancer activities.

In the second part of this thesis, we characterized novel covalent inhibitors of CaM that are able to disrupt the K-Ras/CaM interaction in cells. Recent evidence suggests that K-Ras interacts with CaM to promote cancer cell stemness by suppressing non canonical frizzled-8 mediated Wnt signaling (Wang et al., 2015b). Indeed, CaM has been recently identified as a *bona fide* chaperone protein able to facilitate the dynamic distribution of K-Ras alongside PDE6D (Grant et al., 2020b, Agamasu et al., 2019, Chandra et al., 2011). Ser181 of K-Ras plays an important role in this interaction since phosphorylation of this residue by treatment with prostratin compromises K-Ras binding to CaM and suppressed K-Ras mediated tumorigenicity (Wang et al., 2015b). Also, Ophiobolin A (OphA), a covalent inhibitor of CaM was shown to block K-Ras nanoclustering and sphere formation in K-Ras mutated cancer cell lines (Najumudeen et al., 2016). However, OphA exhibits unspecific toxicity against numerous targets. Hence, our goal here was to develop OphA-like compounds with improves CaM specific activity and cellular activity against K-Ras driven cancers.

In the third part of this thesis, we assessed the synergistic potential of targeting Ras mediated pathways through the combination of CaM inhibitors and Protein phosphatase 2α (PP2A) reactivation. PP2A is a tumor suppressor that catalyze the dephosphorylation of multiple targets in cells, the activity of PP2A is down-regulated in many cancers (Sangodkar et al., 2016). Previous reports have indicated that PP2A reactivation blocks the growth of Ras driven cancers (Kauko et al., 2018). To this end, we explore the synergistic potential of blocking both CaM and re-activing PP2A. We assessed phenothiazines, a class of antipsychotic drugs as well as single agent CaM inhibitors and PP2A agonists in a panel of cells lines within this study.

Conclusively, the findings of our PDE6D study have formed the basis for the development of third generation PDE6D inhibitors. From the CaM study, a new tool compound Calmirasone1 has been identified which can be applied in unravelling K-Ras/CaM associated cancer stemness characteristics in subsequent studies. Furthermore, our results from the synergism study suggest that phenothiazines can integrate the synergistic activities of CaM inhibition and PP2A activation. Importantly, during the course of this thesis, we developed a new highly sensitive live-cell BRET based compound screening assay for the identification and characterization of Ras isoform specific protein-protein interaction (PPI) disrupting small molecules.

1.1 Ras Small GTPases

Small guanosine triphosphatases (GTPases) are a group of proteins defined by their ability to bind GTP and hydrolyze it into GDP, the so-called GTP/GDP cycle (Bourne et al., 1991). Whilst small GTPases are biochemically and functionally similar to the α-subunit of heterotrimeric G proteins, they differ from G-proteins due to their ability to function as monomeric units (Claing, 2013). A total of 167 members of the small GTPase family have been identified in humans till date **(Figure 1)**, these proteins are subdivided on the basis of sequence and functional similarities into five families consisting of 39 Ras proteins, 30 Arf proteins, 22 Rho proteins, 65 Rab proteins, 1 Ran protein and 7 unclassified proteins **(Figure 1)** (Rojas et al., 2012, Liu et al., 2017).

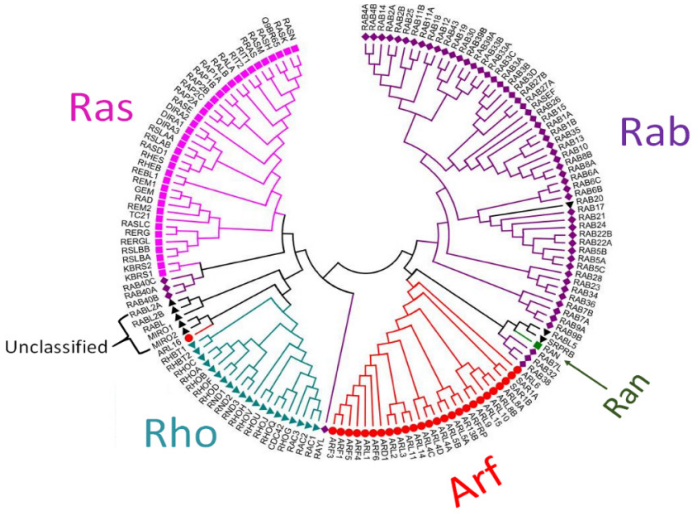

***Figure 1. Phylogeny of the Ras Small GTPase Super-family**. Adapted from (Qu et al., 2019)*

The Ras family members were the first to be identified in this superfamily. They function primarily as signaling nodes that mediate cellular responses to many extracellular stimuli and are known to regulate cellular differentiation, proliferation, morphology and apoptosis through interactions with a variety of downstream effectors, some of the best known proteins in the Ras family are K-Ras, H-Ras and N-Ras (Karnoub and Weinberg, 2008). Rho family members are known for their central role in actin cytoskeletal remodeling and cell polarity. Some well-known and extensively studied members of the Rho family include RhoA, Rac1 and Cdc42 (Etienne-Manneville and Hall, 2002, Hall, 1998). The Rab family is the largest in the Ras superfamily in humans, they are best

known for their role in vesicle formation, movement and fusion as well as vesicular cargo trafficking (Pereira-Leal and Seabra, 2001, Segev, 2001). The 30 member-strong Arf family in addition to facilitating the bi-directional vesicular trafficking of cargo also modulate lipid membrane composition, ciliogenesis, energy metabolism and transcriptional regulation (Donaldson and Jackson, 2011, Sztul et al., 2019). The Ran protein is the only member of its family, this protein is present in all eukaryotes and plays a key role in nuclear transport (Weis, 2003). Importantly, Ran acts as a positional marker of the genome to regulate multiple aspects of the eukaryotic cell cycle (Weis, 2003).

1.1.1 Ras protein structure

Four (4) ubiquitously expressed Ras isoforms derive from three (3) distinct Ras genes in humans. The HRAS gene encodes H-Ras protein, NRAS encodes N-Ras protein and the KRAS gene encodes two alternative splice variant proteins K-Ras4a and K-Ras4b (Ahearn et al., 2018). These proteins show a high degree of sequence identity (between 82-90% amino acid sequence homology). However, only the first 82 amino acids of all 4 Ras isoforms exhibit 100% sequence homology (Ahearn et al., 2018). This structural region contains the G – domain which is involved in GTP binding/hydrolysis as well as the switch I (residues 32-38) and switch II (residues 60-75) regions that serve as allosteric determinants of Ras effector binding (Vetter and Wittinghofer, 2001). Whilst the majority of the sequence divergence of Ras proteins reside in the hypervariable region (HVR), a second level of sequence variation exists from amino acids 86-166 (Zhou et al., 2016). This region which has a 78% sequence identity has been shown to contain the allosteric functionality that plays an important role in S II conformation, membrane orientation and the formation of nanoclusters which in turn regulates effector utilization (Parker and Mattos, 2015, Abankwa et al., 2010). Indeed, a third previously unknown switch region (Switch III) which comprises of the β2-β3-loop and helix α5 was identified by Abankwa et al., (Abankwa et al., 2008b).` This novel region was also found to play a role in defining the membrane orientation of Ras proteins (Abankwa and Gorfe, 2020). Upon GTP-binding, Switch III undergoes structural rearrangements that leads to an alternative engagement of the helix α4, two basic residues on helix α4 then contact membrane lipids leading to the reorientation of the G-domain (Abankwa et al., 2008b). Finally, the HVR consist of roughly 20 amino acids that vary significantly across all Ras isoforms **(Figure 2)**. The HVR is essential for the membrane targeting and prenylation of the various Ras proteins (Hobbs et al., 2016). Indeed the sequence variation on the HVR of Ras proteins defines differential post-translational modification and lipidation (Ahearn et al., 2018). Both K-Ras splice variants have polybasic sequences which in addition to farnesylation (K-Ras4b) and a further palmitoylation (K-Ras4a) facilitates membrane

anchorage (Gelabert-Baldrich et al., 2014). In the case of H-Ras and N-Ras, two and one palmitoyl groups are respectively acquired in addition to the farnesylation at the HVR (Ahearn et al., 2018).

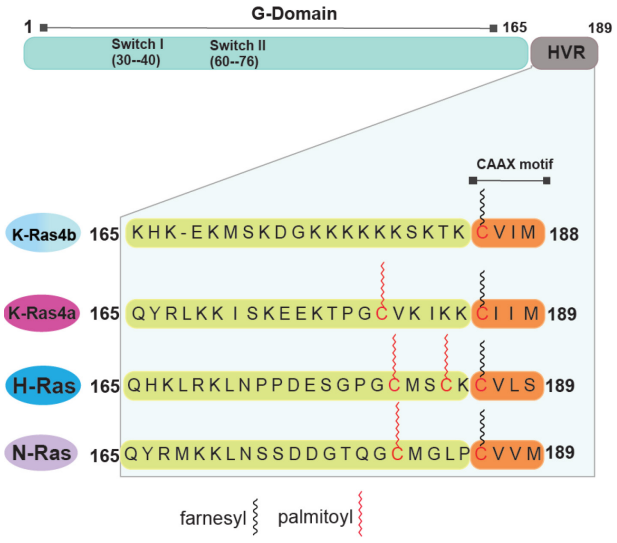

Figure 2. Ras protein structural diversity

Ras proteins have an 82-90% sequence homology in the sequence of the first 165 amino acids. This so called G-domain is responsible for their nucleotide binding and effector engagement functionalities. Ras isoforms differ mostly in the amino acid sequence of their hypervariable region (HVR). This stretch of 24-25 amino acids directs Ras membrane targeting and post translational lipidation.

1.1.2 Ras post-translational modification

Upon cytosolic biosynthesis, Ras proteins and indeed all GTPases containing the CAAX motif are processed by three enzymes; first farnesyl transferase (FTase) catalyses the irreversible farnesylation of the cysteine of the CAAX motif. In the case of K-Ras and N-Ras, an alternative prenylation by genarylgenaryl transferase-1 (GGTase 1) is possible (Whyte et al., 1997). Once prenylated, Ras proteins are targeted to the surface of the endoplasmic reticulum where the Ras-converting enzyme 1 (RCE1) and isoprenylcysteine carboxylmethyltransferase (ICMT) catalyzes respectively the cleavage of AAX and carboxymethylation of the cysteine residue (Ahearn et al., 2018, Boyartchuk et al., 1997, Gutierrez et al., 1989). At this point, the CAAX processing and the polybasic lysine residues on the HVR of K-Ras4b is sufficient for membrane targeting by active transport with the support of trafficking chaperone (Hancock et al., 1990).

N-Ras, H-Ras and K-Ras4a undergoes additional processing by the palmitoylation of additional cysteine residues upstream of the CAAX cysteine; Cys181 for N-Ras, Cys181 and 184 for H-Ras and Cys180 of K-Ras4a (Apolloni et al., 2000, Laude and Prior, 2008). This reversible process is catalyzed by the DHHC family of palmitoyl acyl transferases (PATs), palmitoylation of Cys181 of N-Ras and H-Ras directs sorting from the Golgi apparatus to the recycling endosomes, a necessity for subsequent trafficking to exocytic vesicles destined for the plasma membrane **(Figure 3)** (Apolloni et al., 2000, Laude and Prior, 2008).

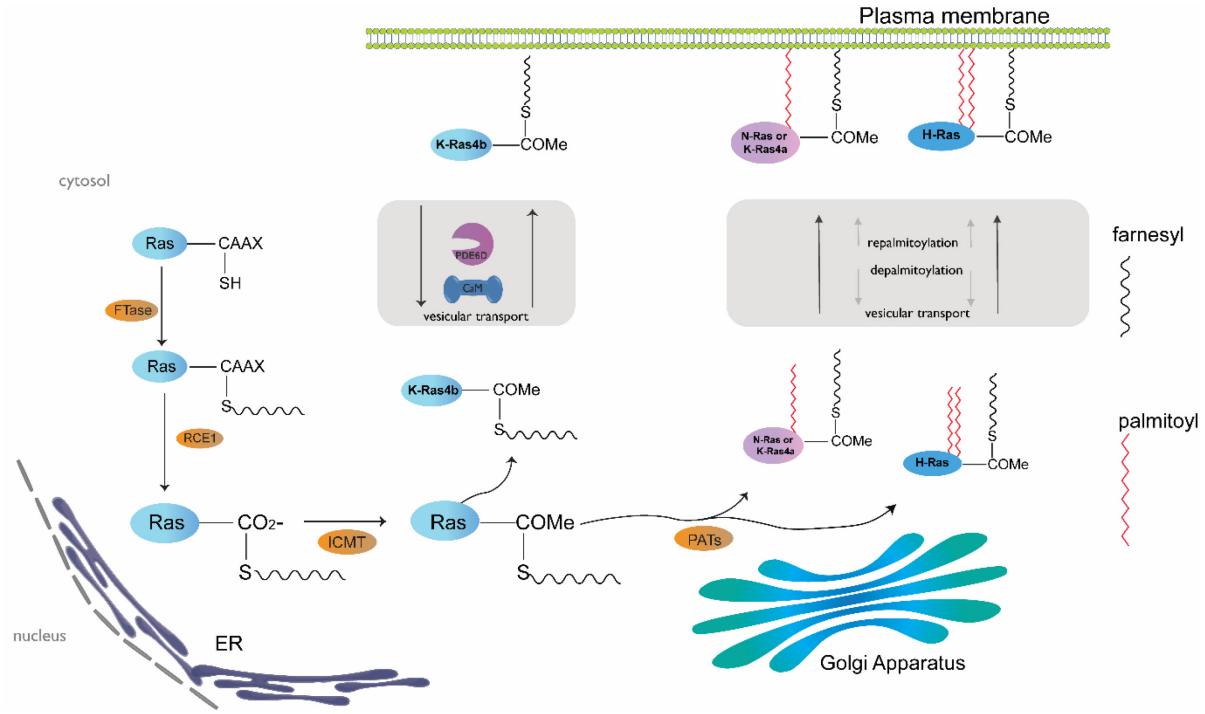

Figure 3. Differential Ras post-translational modification dictates membrane targeting *Newly synthesized Ras proteins undergo a series of enzymatic processing at various subcellular locations including the cytosol, endoplasmic reticulum, and Golgi before membrane localization. Farnesyl transferase, Ras converting enzyme and isoprenylcysteine carboxylmethyltransferase respectively catalyse the farnesylation, AAX cleavage and carboxy methylation of Ras proteins. Carboxymethylated and farnesylated K-Ras4b is actively transported to the plasma membrane via the recycling endosomes, the trafficking chaperones PDE6D and CaM are known to play a role in modulating K-Ras membrane localization and dynamic distribution. Further processing of the other Ras isoforms N-ras, K-Ras4A and H-Ras on the Golgi enhance their respective membrane targeting via the vesicular transport system.*

In addition to the differential palmitoylation of Ras proteins due to their HVR structural variation, Ras proteins undergo a series of additional post-translational modifications on the G-domain (Glucosylation, Sumolyation, ADP-Ribosylation, Acetylation, Ubiquitination and Nitrosylation) (Baker et al., 2013, Yang et al., 2012, Williams et al., 2003, Herrmann et al., 1998).

Phosphorylation of the G-domain has also been reported (e.g Y32 Y64 and Y137) (Bunda et al., 2014). Whilst the HVR can undergo phosphorylation and cis-trans isomerization (Ahearn et al., 2018). Ubiquitination have also been found to be another level of differential Ras protein post-translational modification (Hobbs et al., 2016). The mono and/or di-ubiquitination of H-Ras was shown to facilitate its internalization into endo-membranes thus limiting H-Ras mediated Raf effector engagement (Jura et al., 2006). Importantly, H-Ras ubiquitination on K117 accelerates nucleotide exchange and activation (Baker et al., 2013). N-Ras as well as K-Ras4b are also mono/di-ubiquitinated whilst the mono-ubiquitination of K-Ras4b at K147 was shown to increase effector engagement without enhancing K-Ras4b subcellular localization, the ubiquitination deficient K-RasG12V exhibited reduced oncogenic activity (Sasaki et al., 2011). Following the present evidence, it is plausible to posit that the differential ubiquitination of Ras proteins distinctly affect the Ras isoforms which may result in unique functional consequences. Finally, acetylation is another PTM that occurs at K104 of K-Ras4b, this modification is proposed to disrupt SII conformation, GEF-mediated activation and the reduction of effector activation and oncogenic potential (Yang et al., 2012). So far, acetylation has only been documented for K-Ras (Yang et al., 2012). It therefore remains to be seen if a similar process occurs with the other Ras isoforms.

1.1.3 Ras membrane interaction and cellular localization

The presence of polybasic groups and palmitoyl lipid groups on Ras proteins enables reversible interactions with the plasma membrane and facilitates dynamic associations with a number of subcellular compartments (Prior and Hancock, 2012). K-Ras exhibits a short residency on the PM (a few minutes) and the net negative charge of the PM is responsible for the accumulation of K-Ras on its surface (Prior and Hancock, 2012). A consequence of this short residency is the apparent absence of an intrinsic capacity for K-Ras to be trafficked by classic membrane carriers (Misaki et al., 2010). Palmtoylated Ras proteins on the other hand associate more stably with the PM and are thus trafficked post-Golgi association via membrane carriers like the recycling endosomes to the PM (Misaki et al., 2010).

In addition to plasma membrane and ER/Golgi complex localization, a number of other subcellular compartments accessible to Ras proteins have been identified (Prior and Hancock, 2012, Bivona et al., 2006). The recycling endosomes which plays a critical role in endocytosis and growth factor signaling as well as mitochondrial localization of K-Ras which triggers apoptosis upon PKC mediated S181 phosphorylation are well established alternative point of K-Ras localization (Prior and Hancock, 2012, Bivona et al., 2006). Importantly, recent studies have established the central role of Ras chaperone proteins particularly the delta subunit of phosphodiesterase 6 (PDE6D) and the master calcium signal regulatory protein CaM in promoting K-Ras reversible translocation

between the subcellular space and plasma membrane (Chandra et al., 2011, Sperlich et al., 2016, Agamasu et al., 2019, Grant et al., 2020b).

1.1.4 Ras nanoclustering

Ras anchorage to the plasma membrane is pre-requisite for effector engagement and downstream signaling. The HVR is responsible for directing this membrane localization (Abankwa et al., 2008a). Ras proteins form distinct non-random proteo-lipid clusters on the PM called nanoclusters **(Figure 4)** (Prior et al., 2003). The membrane raft hypothesis evidenced by the work of the Hancock group established some critical hallmark features of Ras nanoclusters namely that; (1) Ras isoforms segregate laterally into distinct dynamic nanoclusters potentiated by their intrinsic HVR differences. (2) The nanoclusters have a 9nm radius containing up to 7 Ras proteins per cluster. (3) Ras nanoclusters have an average lifetime that vary between 0.1 s and 1 s in its inactive and active states respectively and that (4) approximately 40% of Ras proteins are immobilized nanoclusters whilst the remaining proteins freely diffuse as monomeric units (Abankwa and Gorfe, 2020).

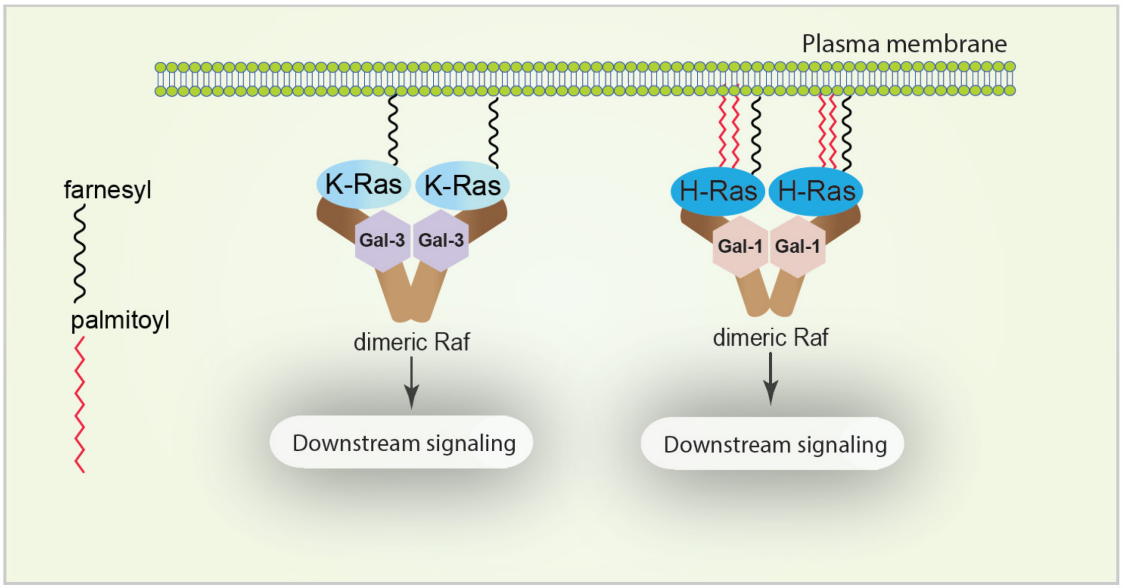

Figure 4. Ras proteins form distinct nanoclusters.

Ras isoforms form distinct proteo-lipid nanoclusters which facilitates isoform specific downstream signaling. Various proteins such as galectin-3 and galectin-1 have been reported to facilitate the K-Raf/Raf and H-Ras/Raf interface respectively.

Ras nanoclusters are required for the recruitment and activation of Ras effectors such as Raf proteins. In fact, previous studies showed that Ras monomeric units fail to activate Raf and various Ras dependent signaling networks (Plowman et al., 2008). Thus, proteins such as galectin-3 and galectin-1 which are known to be important for the respective nanoclustering of K-

RasG12V and H-RasG12V have emerged as attractive drug targeting strategies in Ras driven cancers (Shalom-Feuerstein et al., 2008, Blazevits et al., 2016, Abankwa and Gorfe, 2020).

1.1.5 Cellular Ras activation, signaling and effector engagement

Ras proteins signal downstream of the receptor tyrosine kinases (RTKs) to facilitate key signaling pathways such as the Ras-MAPK-ERK pathway, the PI3K-AKT-mTORC1 pathway as well as the less characterized RalGDS signaling pathway **(Figure 6)**. In normal cells, these pathways are important in controlling critical functions such as growth, proliferation and survival (Downward, 2003, Neel et al., 2011).

The first step in "normal" Ras signaling involves the binding of extracellular growth ligands to a group of transmembrane RTKs e.g the epidermal growth factor receptor (EGFR), fibroblast growth factor receptors (FGFR) or platelet derived growth factor receptors (PDGR). Binding of RTKs to these ligands induces receptor dimerization and phosphorylation (Downward, 2003). The autophosphorylated intracellular domain of the RTKs then binds to the SH2 domain of an adaptor protein called growth-factor-receptor-bound protein 2 (GRB2). GRB2 through its SH3 domain recruits the guanine nucleotide exchange factor (GEF) son of sevenless (SOS) (Downward, 2003). Because Ras small GTPases can only elicit downstream signaling in their GTP bound form, the replacement of GDP with GTP serves as a binary switching mechanism for the regulation of cellular growth signals (Hennig et al., 2015). Upon binding to GTP, Ras proteins undergo significant conformational changes that facilitates effector recruitment for subsequent downstream signaling (Wennerberg et al., 2005). Importantly, after effector recruitment, GTP is hydrolysed by Ras proteins via their intrinsic GTPase activity and the action of GTPase activating proteins (GAPs) that enhances the intrinsic GTPase activity of Ras proteins (e.g neurofibromin 1 aka NF1). By this means, Ras proteins are able to cycle between an "on" and "off" state dictated by its nucleotide binding status **(Figure 5)** (Hennig et al., 2015).

1.1.5.1 RAS/MAPK signaling pathway

Canonical MAPK signaling (also called the Ras-Raf-MEK-ERK signaling pathway) is central to cellular processes such as proliferation, differentiation, apoptosis, angiogenesis etc. (Guo et al., 2020). In this cascade of events involving several mitogen activated protein kinases (MAPKs), GTP-bound Ras promotes Raf dimerization and phosphorylation, this induces Raf kinase activity which is crucial for the phosphorylation of Raf substrates MEK1 and MEK2 (Nussinov et al., 2020). Raf kinase domain dimerization is pre-requisite for full activation of Raf (Zhang et al., 2021, Rajakulendran et al., 2009). Like most other kinases, wild-type Raf proteins remain mostly in a guarded auto-inhibitory state via a mechanism that protects against unregulated activation,

signaling and even degradation of Raf proteins by shielding the Raf kinase dimerization surface (Nussinov et al., 2020). 14-3-3 proteins are universally expressed regulatory scaffold proteins known to be critical for the autoinhibition of Raf proteins (Liau et al., 2020, Zhang et al., 2021). Raf proteins contains two 14-3-3 recognition motifs (Kohler and Brummer, 2016). Phosphorylation of Ser729 (B-Raf), Ser621 (C-Raf) and Ser582 (A-Raf) on the C-terminal tail is known to promote Raf activation (Chong and Guan, 2003, Zhang et al., 2021). Conversely, phosphorylation of Ser365 of the B-Raf CR2 loop, Ser259 (C-Raf) and Ser214 (A-Raf) inhibits Raf activation (Chong and Guan, 2003, Zhang et al., 2021). Recent evidence from a cryoelectron microscopy study confirm that the interaction of 14-3-3 dimers with the two phosphorylation sites keep Raf proteins in the auto-inhibited state (Park et al., 2019).

Following Raf activation, the cascade proceeds with MEK-mediated activation of ERK1 and ERK2 (Park et al., 2019). ERK serine/threonine kinase activity both phosphorylates a range of nuclear transcriptional factors to modulate cellular growth and participate in the negative feedback regulation of the entire cascade by phosphorylating upstream components such as SOS or C-Raf and by altering transcription of dual specific phosphatase (DUSP) family as well as the sprouty (SPRY) family of proteins (Owens and Keyse, 2007, Lake et al., 2016).

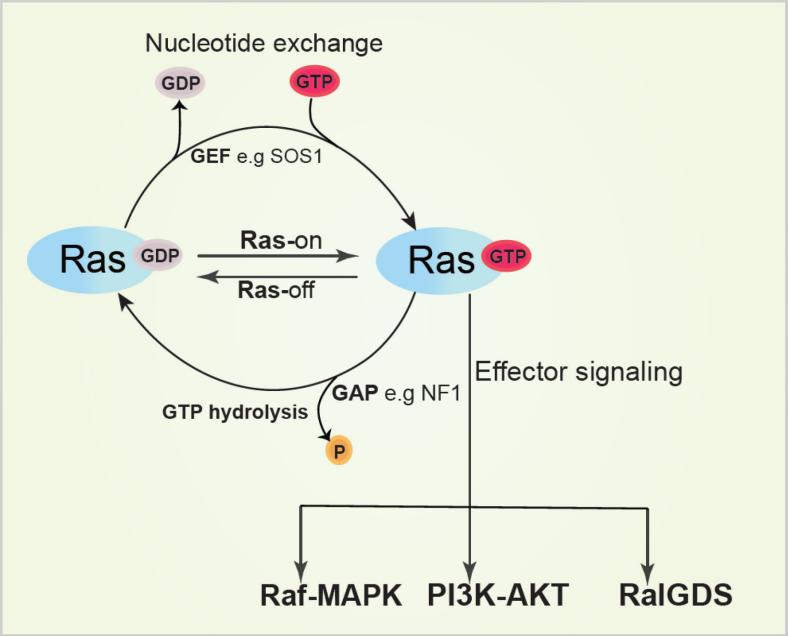

Figure 5. Ras binary switching through GEFs and GAPs activity.

1.1.5.2 The PI3K/AKT signaling pathway

Another pathway downstream of Ras relevant in the regulation of cell proliferation, differentiation, metabolism, migration, mobility and apoptosis is the PI3K/AKT/mTOR signaling pathway.

Dysfunctional PI3K/AKT signaling is generally considered a hallmark cancer feature (Thorpe et al., 2015). Through the activity of phosphatidylinositol-4-5-bisphophate-3-kinases (PI3Ks), protein kinase B (AKT) and eventually the mechanistic target of rapamycin (mTOR) is activated via a series of phosphorylation events. Upon activation, PI3K phosphorylates membrane bound PIP2, converting it to PIP3 to activate the signaling cascade. PIP3 acts as a secondary lipid messenger that recruits both AKT and its serine/threonine kinase activator PDK1 to the plasma membrane through direct binding to their PH domains resulting in the consequent downstream signaling pathway (Zhang et al., 2019, Castellano and Downward, 2011). The phosphatase tumor suppressor and tensin homolog (PTEN) dephosphorylates PIP3 to PIP2 thus terminating the signal and completing the cycle (Castellano and Downward, 2011). PI3K-AKT signaling promotes growth and survival via many mechanisms including the inhibition of pro-apoptotic Bcl-2 family members BAD and BAX as well as the negative regulation of the transcriptional factor NF-kB which results in transcription of pro-survival and anti-apoptotic genes (Engelman et al., 2006, Duronio, 2008). AKT also phosphorylates TSC2 thus inhibiting the TSC1/TSC2-mediated inhibition of Rheb GTPases which are essential for the activation of the mammalian target of rapamycin (mTOR). The mTORC1/mTORC2 protein complexes are important in regulation various anabolic processes such as ribosome biogenesis, protein biosynthesis, nutrient uptake and autophagy. Importantly, mTOR signaling plays a significant role in the development of age-related diseases such as neuropathies and cancer (Cornu et al., 2013).

1.1.5.3 The RalGDS pathway

The least understood Ras effector signaling pathway is the Ras-like (Ral) guanine dissociation stimulus (RalGDS) pathway **(Figure 6)**. Similar to Ras proteins (46-51% sequence homology), the two Ral proteins (RalA and RalB) can interact with multiple downstream effectors when GTP-bound (Neel et al., 2011). Ral proteins through the 2 components of the octameric exocyst complex Sec5 and Exo84 regulate cellular exocytosis (Wu et al., 2008). This exocyst function facilitates movement and tethering of post-Golgi secretory vesicles to the plasma membrane before exocytic fusion. Indeed, this exocytic function has been implicated in a number of cancer associated cellular processes such as cell migration and tumor cell invasion (Spiczka and Yeaman, 2008).

Additionally, RalGDS and/or Ral activation is involved in Ras-mediated activation of various transcriptional factors including the phosphorylation and activation of c-Jun through JNK MAPK activation, ATF2 and STAT3 through Src tyrosine kinase activation (de Ruiter et al., 2000, Okan et al., 2001, Goi et al., 2000).

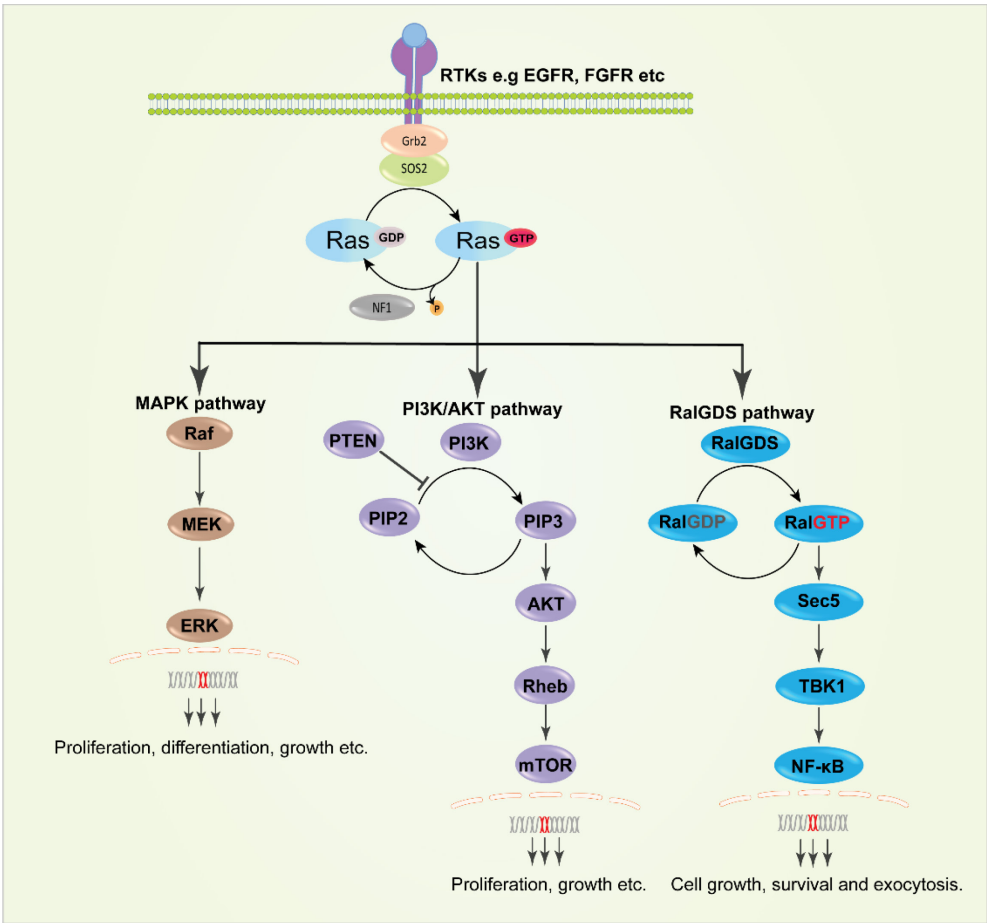

Figure 6. Ras signaling and effector engagement.

Schematic diagram showing 3 major signaling pathways downstream of Ras activation. Membrane bound Ras-GTP facilitates the recruitment of downstream effectors Raf, PI3K and RalGDS for the respective activation of the MAPK, PI3K/AKT and RalGDS signaling cascades that collectively regulate cellular functions like proliferation, differentiation, growth, survival and exocytosis.

Although the Ral-mediated effector signals that regulates these transcriptional factor activation remains sparsely known, Ral-mediated activation of NF-kB has been sufficiently investigated and was shown to be regulated by Sec5 and not Ral binding protein 1 (RalBP1) (Henry et al., 2000). Activated RalB facilitates the interaction of Sec5 with the TANK-binding Kinase 1 (TBK1), an atypical IkappaB Kinase (IKK) (Chien et al., 2006). The recruitment of TBK1 then results in an increase in TBK1 catalytic activity including the direct phosphorylation and promotion of the nuclear localization and activation of NF-kB (Harris et al., 2006).

1.2 K-Ras in Human Disease

1.2.1 The role of Ras proteins in dysfunctional development

Due to the extensive amount of research data collected in over 4 decades, the relevance of normal Ras functioning for healthy embryonic development and the avoidance of a range of malignancies in adult life is now clearly established. Whilst somatic Ras mutations and/or other Ras pathway protein mutations lead to a wide range of cancers **(Figure 7)**. Germline mutations in critical

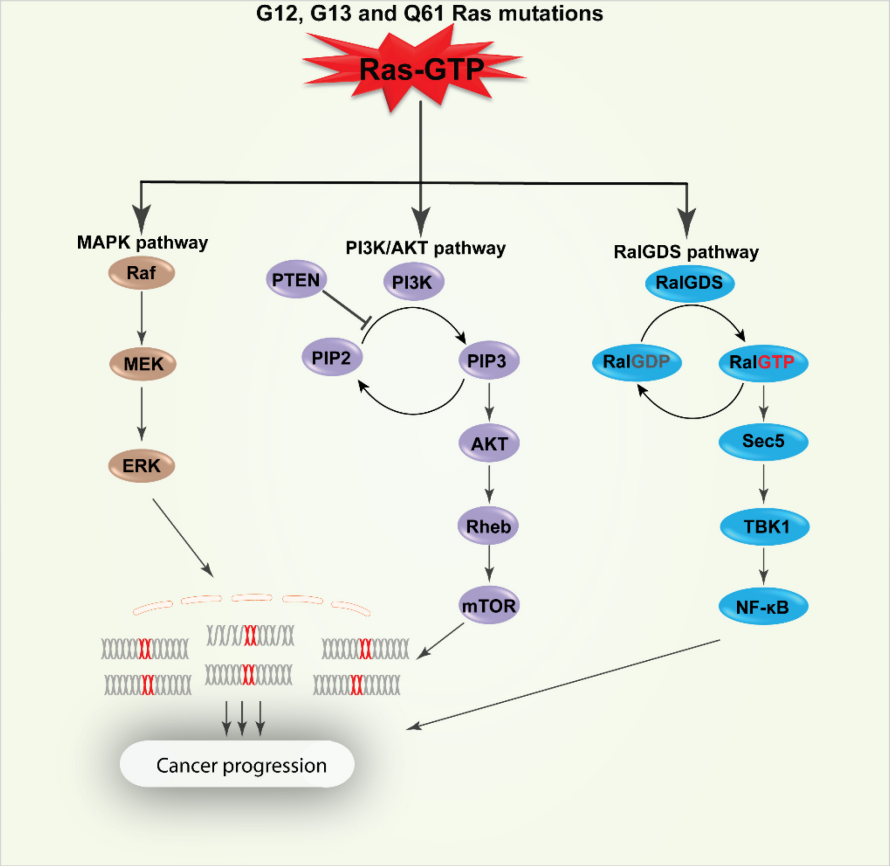

Figure 7. Dysfunctional Ras signaling in Cancer.

components of the Ras-MAPK pathway often result in a number of inherited developmental disease called RASopathies (Rauen, 2013). Although each RASopathy consist of unique phenotypic elements, these syndromes bear many overlapping physiological characteristics including; craniofacial dysmorphia, cardiovascular abnormalities, cutaneous lesions, cognitive and neurological impairments, cardiovascular abnormalities, musculoskeletal abnormalities and a greatly elevated risk of developing malignancies (Rauen, 2013). These diseases **(Figure 8)** include; (1) neurofibromatosis type-1 (NF1) syndrome caused by the haplo-insufficiency of

neurofibromin, a Ras GAP protein central to inactivation of Ras signaling (Cimino and Gutmann, 2018); (2) Noonan syndrome (NS) which can be caused by germline mutations in PTPN11, SOS1,RAF1, KRAS, BRAF, NRAS, MAP2K1, RIT1, SOS2, LZTR1 and A2ML1(El Bouchikhi et al., 2016); (3) Costello syndrome caused by HRAS activating mutations (Aoki et al., 2016); (4) Craniofaciocutaneous (CFC) syndromes which is caused by BRAF, MAP2K1/2 and KRAS mutations (Aoki et al., 2016); (5) NF1-like syndrome aka Legius syndrome caused by haploinsufficiency of SPRED1 (Brems et al., 2007); (6) Noonan-like syndrome caused by Leucine-rich repeat protein (SHOC-2), a protein that enhances MAP kinase activity by binding and forming a complex with Raf-Ras (Li et al., 2000). Noonan-like syndrome can also be caused by CBL mutations (Cordeddu et al., 2009, Martinelli et al., 2010); (7) Capillary malformation-arteriovenous malformation (CM-AVM) caused by haploinsufficiency of p120 Ras-GAP (RASA1) (Eerola et al., 2003) and (8) Noonan syndrome with multiple lentigines (NSML) caused by PTPN11 and RAF1 mutations (Aoki et al., 2016).

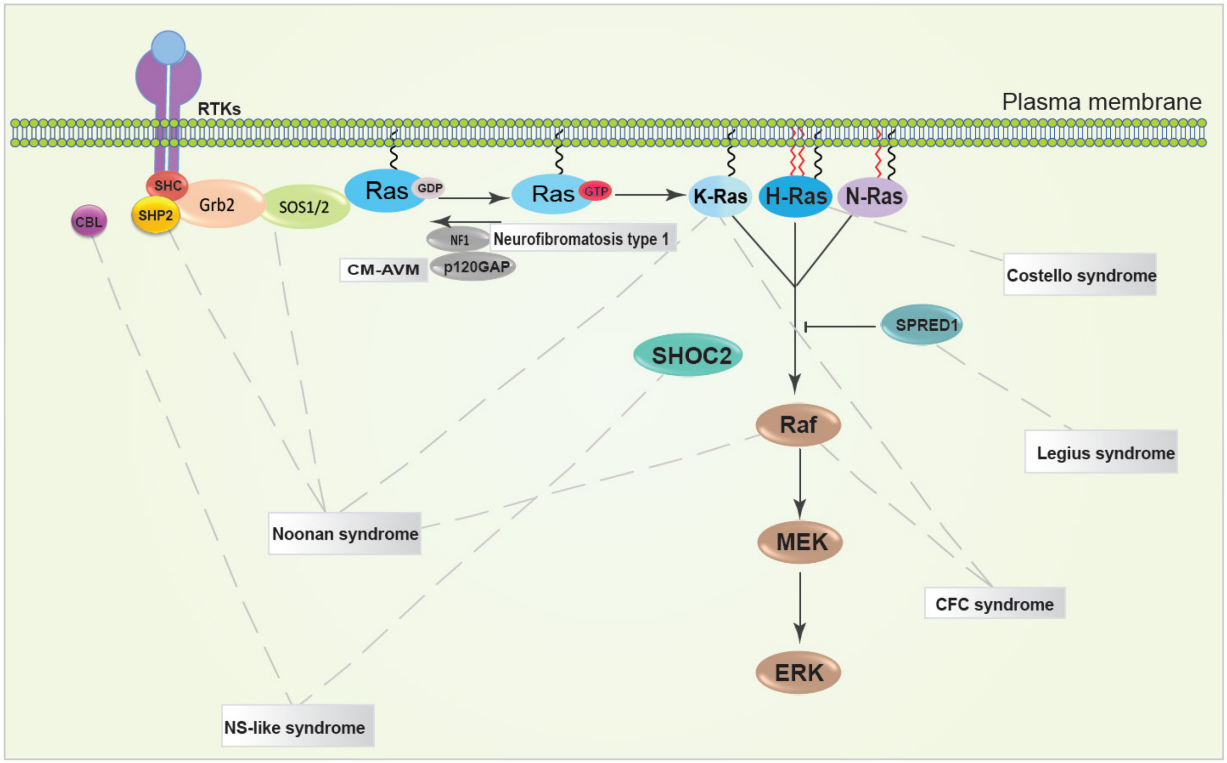

Figure 8. Rasopathies.

Schematic illustration depicting the Ras/MAPK signaling pathway and various effector germline mutations associated with the development of Rasopathies.

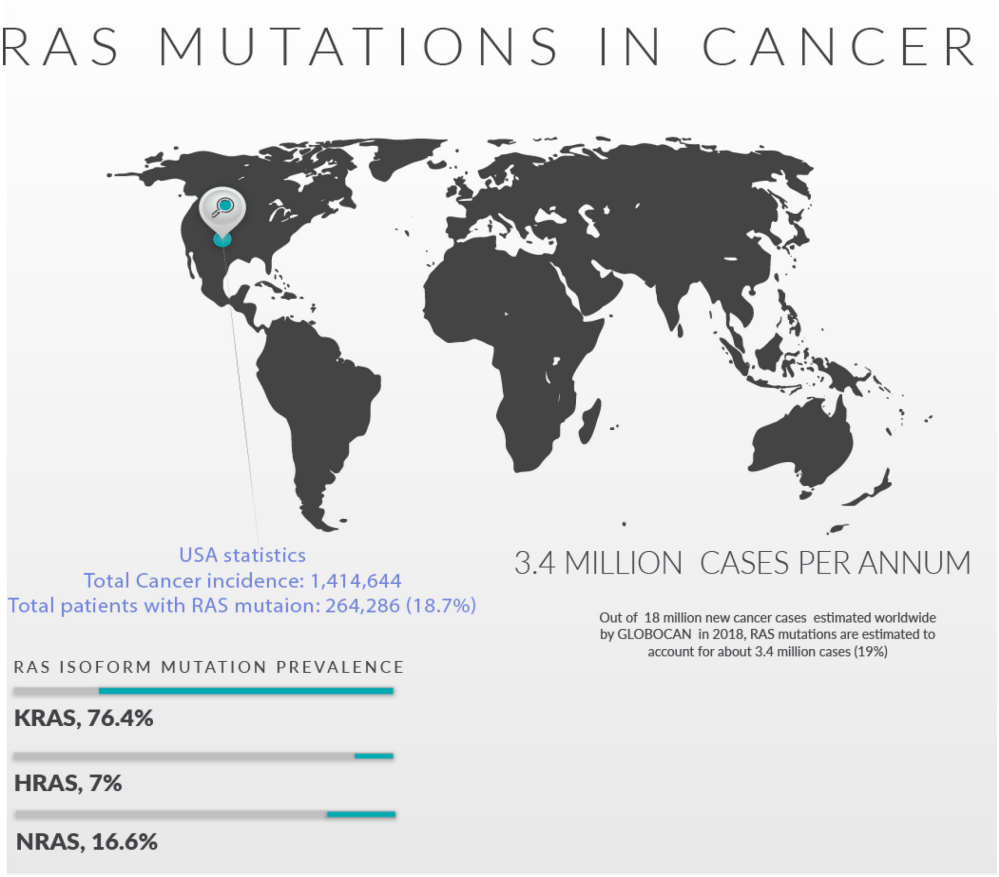

Figure 9. Epidemiology of Ras mutations in cancer.

According to GLOBOCAN, over 18 million cancer cases are reported annually, Ras mutations make up about 19% of these cancers with K-Ras, H-Ras and N-Ras mutations having a 76.6%, 7% and 16.6% of the total Ras mutated cancer burden of 3.4 million (Prior et al., 2020).

The majority of Ras mutated cancers occur in the pancreas (pancreatic ductal adenocarcinomas (PDAC)), colon (colorectal cancer (CRC)), lung (lung adenocarcinomas (LUAD)) and skin (melanomas) (Moore et al., 2020). Interestingly, various Ras isoforms exhibit tumor tissue-type preferences. For instance, PDAC (86%), LUAD (32%) and CRC (41%) are predominantly KRAS driven with the G12 mutation also showing a clear prevalence **(Figure 10)** (Moore et al., 2020). NRAS mutations on the other hand accounts for 29% of melanomas with the Q61 codon point mutation being the preferred activation mutation in these cancer types (Cancer Genome Atlas, 2015b). Conversely, H-Ras mutations are more common in head and neck cancers (5%) and bladder cancer (4%) albeit at a significantly lower frequency in comparison to K-Ras and N-Ras mutation dominated tissue types (Cancer Genome Atlas, 2015a, Robertson et al., 2017).

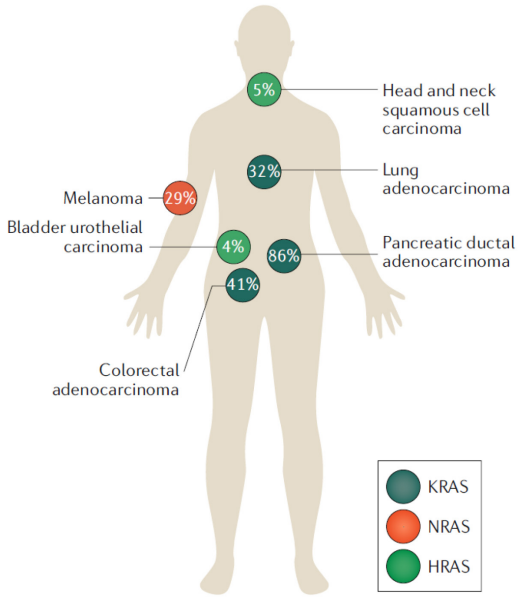

Figure 10. Ras Isoform mutation prevalence and tissue specificity. *Adopted from (Moore et al., 2020)*

The frequency of Ras isoform mutation and the tissue specificity of the Ras isoform mutation prevalence differ across human cancers. The above figure illustrates the tissue distribution and mutational frequency of the Ras isoforms in human cancers.

For long, evidence of differential and unequal patterns in Ras isoform oncogenicity, patient survival data as well as tissue preference has led the Ras research community to posit that Ras isoforms exhibit critical differences in their cancer causing abilities (Prior and Hancock, 2012, Bournet et al., 2016, Blons et al., 2014, Li et al., 2018). In fact, Prior et al recently proposed that the interplay between three main factors determine if conditions are optimal for Ras driven oncogenesis and perhaps even explain isoform and tissue specificity namely; (1) Ras gene dosage which is defined by relative expression levels and activation states; (2) isoform specific signaling and corresponding mutational status and (3) the cellular and tissue context that contributes and/or dictates the genetic, epigenetic and proteomic landscape upon which Ras networks elicit their signaling effects (Prior et al., 2020). Consistently, unravelling this complex interplay will be central in explaining this not fully understood pattern of inequality displayed by Ras proteins.

Evidence for a varied amount of activated Ras protein population (between 30% to 90%) and a difference in activation stability depending on the nature of the Ras mutation (i.e whether the mutations cause Ras proteins to cycle faster or become GAP-insensitive) coupled with differential Ras isoform expression levels (sometimes reaching over 100-fold difference between isoforms

and across tissue types), all point to the importance of Ras gene dosage in defining signaling capacity difference (Li et al., 2018, Prior et al., 2020, Newlaczyl et al., 2017). These differences create a window of permissiveness that is optimal for oncogenic development which may change as tumors progress and acquire resistance to therapeutic interventions (Prior et al., 2020).

Furthermore, the differential localization of Ras proteins within the subcellular space as well as their tendencies to form distinct nanoclusters influences their effector engagement patterns (Zhou and Hancock, 2015, Abankwa and Gorfe, 2020). For instance, in vitro studies have revealed some distinct binding preferences within the Ras-Raf interaction with B-Raf being selective for K-Ras engagement whilst C-Raf showed a clear preference for H-Ras binding (Terrell et al., 2019). Importantly, Galectin 1 and 3 has been shown to respectively act as accessory proteins within the K-Ras/B-Raf and H-Ras/C-Raf interaction interface and therefore plays an important and potentially druggable role in the reported isoform specific signaling **(Figure 4)** (Abankwa and Gorfe, 2020).

1.2.2 K-Ras as a driver of cancer cell stemness

First proposed over 40 years ago, the cancer stem cell (CSC) theory states that a small subset of the tumor population is responsible for fueling the tumor's growth and that this CSC population often evades classic therapeutic intervention (O'Brien et al., 2007). In practice, the CSC theory nicely supports clinical observations, particularly the frequently observed resurgence of tumors after initial seemingly successful treatments **(Figure 11)** (Batlle and Clevers, 2017, Chen et al., 2012). CSCs possess characteristics of normal stemcells including the capacity for self-renewal and differentiation in addition to their ability to initiate tumors. A number of cellular markers such as CD24, CD44, CD133 etc. are used to identify and enrich for the CSC sub-population (Yu et al., 2012). Similarly, a signaling network involving Wnt/β-catenin, Notch, Hedgehog and microRNAs is known to control the CSC phenotype (Yu et al., 2012). CSCs have been identified in many cancer types including brain, colorectal, breast and hematological malignancies. Consequently, CSC targeting has emerged as a major strategy in cancer drug development (Yang et al., 2020).

A significant body of evidence supports K-Ras as an important player in the promotion of cancer stemness signaling pathways such as the sonic hedgehog signaling pathway in PDAC and canonical Wnt/β catenin signaling pathway (Gu et al., 2016, Hwang et al., 2020). Similarly, Oncogenic K-Ras in colon cancer was shown to enhance embryonic stem (ES) cell-like program during colon cancer progression from an adenoma to a carcinoma and also activates CSC properties in APC-mutated cells through the MAPK signaling pathway (Le Rolle et al., 2016, Moon et al., 2014). In fact, the critical role of Ras-MAPK signaling in stemcells is supported by the fact

that embryonic stem cell transformation from their naïve to primed pluripotent state is dependent on Ras-MAPK signaling as well as their subsequent proliferation and differentiation during embryogenesis (Blair et al., 2011).

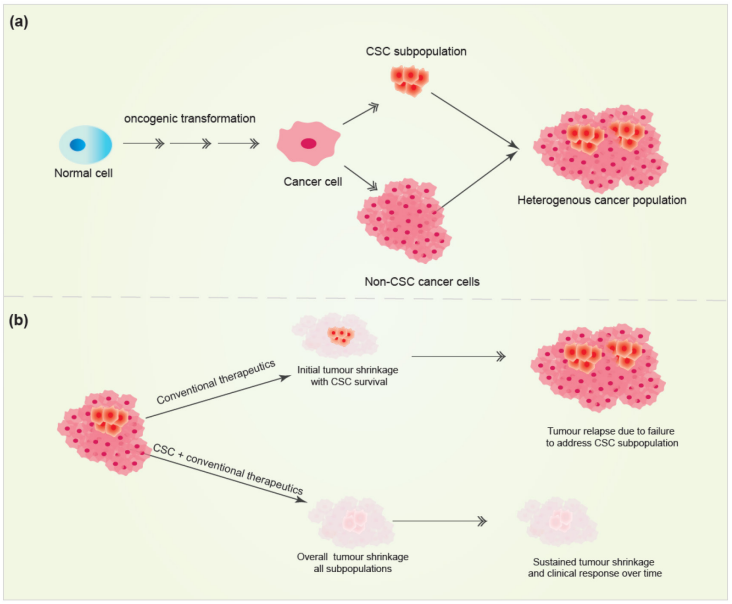

Figure 11. Schematic illustration of the CSC model.

(a) *CSCs arise from normal/progenitor cells which undergo and acquire special mutational changes that bestows stem-like characteristics such as self-renewal, differentiation and de-differentiation to a small subset of a tumor population.* ***(b)*** *Failure to target the CSCs subpopulation with tradition therapeutic interventions have been proposed to ultimately lead to tumor relapse. Hence, the need to develop CSCs targeting drugs in addition to conventional therapy is likely to improve clinical outcomes.*

In addition, induced pluripotent stem cells (iPSCs) derived from patients with K-RasG13C mutations possessed a significantly higher level of stemness marker OCT4 in the heterozygous G13C/wt cells as compared to the homozygous wt/wt populations (Kubara et al., 2018). Interestingly, another study showed that K-Ras (G12D) mutations exclusively caused the increase of the neural stemcell pool in in mouse brain models as similar H-Ras and N-Ras mutations failed to do so thus suggesting a differential isoform specific potential in driving the CSC phenotype (Bender et al., 2015). Importantly, in support of this differential isoform activity, the McCormick group in 2015 showed that K-Ras interacts with CaM to promote cancer cell stemness by suppressing non canonical frizzled-8 mediated Wnt signaling (Wang et al., 2015b). Whilst the underlying mechanisms of K-Ras driven CSC phenotype promotion is still unclear, a growing body of evidence have shown that selective targeting of K-Ras/CaM interaction can be a viable therapeutic strategy against CSCs (Wang et al., 2015b, Najumudeen et al., 2016).

1.3 The K-Ras trafficking chaperone PDE6D

1.3.1 Biochemistry of PDE6D

Phosphodiesterases (PDEs) are a broad family of enzymes consisting of 11 isoenzyme groups and over 50 subunits that catalyse the hydrolysis of cyclic nucleotides and thus play an important role in regulating cellular levels of signaling messengers such as cAMP and cGMP (Boswell-Smith et al., 2006). Phosphodiesterase-6 (PDE6) is primarily expressed in photoreceptors where it plays a critical role in phototransduction, it consists of the catalytic α and β subunits, an inhibitory γ subunit and a non-catalytic δ subunit (Zhang et al., 2015). Phosphodiesterase-6 delta subunit (PDE6δ; also known as PDEδ, PrBP/δ and PDE6D) is a 17kDa prenyl binding and solubilizing factor for Ras and Rab GTPases (Chandra et al., 2011). Originally first identified as a non-catalytic subunit of the photoreceptor PDE6, PDE6D has since been found to be expressed in several other tissue types where it is implicated in the regulation of the dynamic distribution of prenylated proteins (Dharmaiah et al., 2016). PDE6D consists of a hydrophobic prenyl binding pocket located between two β sheets **(Figure 12)**. Consistently, prenylated proteins containing either farnesyl (15 carbon) or geranylgeranyl (20 carbon) units bind to the hydrophobic pocket of PDE6D with the prenylated groups being able to occupy multiple positions inside the hydrophobic pocket of PDE6D (Dharmaiah et al., 2016). PDE6D interacts with farnesylated and carboxymethylated K-Ras with a binding affinity of 2.3 ± 0.3 μM. Absence of the methyl group significantly decreases this affinity (Kd of 82 ± 9 μM) emphasizing the importance of both farnesylation and carboxymethylation for the K-Ras/PDE6D interaction (Dharmaiah et al., 2016). Indeed, an absence of the methyl group resulted in charge repulsion thus diminishing the hydrophobic interactions (Dharmaiah et al., 2016). Conversely, Chandra et al showed that diminishing the positive charge on the polybasic region of K-Ras by S181 phosphorylating agent bryostatin-1 enhanced the hydrophobic interaction and the ability of PDE6D to effectively solubilize K-Ras (Chandra et al., 2011).

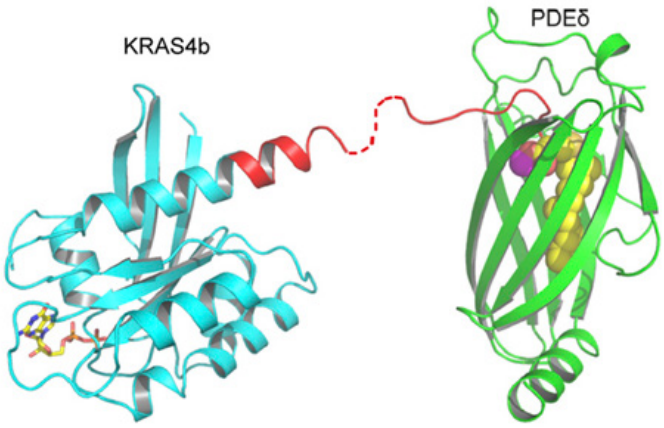

Figure 12. Structure of PDE6D in complex with K-Ras4b. *adopted from (Dharmaiah et al., 2016)*

Structure illustrates GDP-bound K-Ras4b-Fme in complex with PDE6D. The PDE6D, GTPase domain and HVR of K-Ras4b are shown in green, cyan and red respectively. The farnesyl chain is shown as spheres and colored yellow. The carbon and oxygen atoms of the carboxymethyl group are colored magenta and red respectively whilst GDP is shown as a stick and colored yellow (carbon) and red (oxygen).

1.3.2 The PDE6D/K-Ras interaction and the modulation of K-Ras localization

Lipid modified small GTPases will diffuse and equilibrate randomly across cellular membranes driven by entropy, unless specific transport and delivery systems are available to guide their unloading (Chandra et al., 2011). Indeed, cytoplasmic prenyl binding factors have been proposed to facilitate the cellular trafficking of K/H/ and N-Ras (Chandra et al., 2011). For K-Ras, PDE6D has been identified as a major solubilizing factor able to chaperone K-Ras dynamic distribution to the plasma membrane.

Crystal structure studies on the fully processed K-Ras-PDE6D complex show that the protein-protein interaction may assume two binding modes (Dharmaiah et al., 2016). In the first form, the HVR residues as well as the farnesyl and carboxy-methyl group of K-Ras go deep into the hydrophobic pocket of PDE6D whereas in the second crystal form, most of the residues present in the HVR were not involved in complexation with PDE6D. It has been suggested that the crystal form I is more akin to binding of farnesylated K-Ras to PDE6D whilst the second form is assumed when PDE6D binds with the 20-carbon geranyl-geranylated K-Ras (Dharmaiah et al., 2016).

Although the carboxymethyl and farnesyl groups of K-Ras are critical to the PDE6D-K-Ras interaction, no specific interactions between PDE6D and the G-domain of K-Ras have been observed thus indicating that the nucleotide binding state of K-Ras is irrelevant to this interaction (Dharmaiah et al., 2016). Because the hydrophobic pocket on PDE6D is too small to accommodate additional lipid chains, PDE6D selectively chaperones K-Ras and other mono-prenylated GTPases trafficking over H-Ras and other GTPase with additional lipid chains (Dharmaiah et al., 2016, Schmick et al., 2014, Chandra et al., 2011). This property may explain why PDE6D inhibitors selectively disrupt K-Ras nanoclustering and kill K-Ras driven cancers (Siddiqui et al., 2020).

Mechanistically, mislocalized K-Ras and presumably newly synthesized K-Ras proteins are sequestered from the endomembranes by PDE6D (Schmick et al., 2014). The solubilized K-Ras proteins are then pushed out of the hydrophobic pocket of PDE6D upon GTP- Arl2 mediated allosteric changes on PDE6D at the perinuclear area (Ozdemir et al., 2018). Arl-2, actively facilitates the release of K-Ras on the perinuclear membranes (Ismail et al., 2011). Upon release from PDE6D, the recycling endosomes traps K-Ras into the vesicular transport system mediated trafficking to the plasma membranes **(Figure 13)**. Importantly, the Arl2-dependent ejection mechanism of PDE6D cargo is also responsible for the rapid ejection of most small molecule inhibitors developed against PDE6D including deltarasin and deltazinone (Martin-Gago et al., 2017). This explains why despite having compounds with remarkable nanomolar in vitro binding affinity to PDE6D, the cellular anti-cancer effects of the early generation of PDE6D inhibitors are almost a thousand folds lesser (Zimmermann et al., 2013, Papke et al., 2016). Though a new generation of PDE6D inhibitors including deltasonamides and Deltaflexins have been developed that appear to show improved resistance to the Arl2-mediated ejection, efforts towards developing potential clinical candidates for PDE6D inhibition is still in the early stages (Martin-Gago et al., 2017, Siddiqui et al., 2020).

1.3.3 Drug targeting of PDE6D

Recent studies have shown that PDE6D is significantly upregulated in hepatocellular carcinoma and that this overexpression correlated with an enhanced tumor state (Dietrich et al., 2019). It was also found that depletion of PDE6D resulted in a significant reduction in HCC proliferation migration and clonogenicity (Dietrich et al., 2019). In a similar vein another study assessing the expression patterns of PDE6 subunits in breast cancer cell lines found PDE6D to be highly expressed across four breast cancer cell lines irrespective of their estrogen receptor expression status (Dong et al., 2013). As K-Ras is a client of PDE6D chaperone activity, it is plausible to

suggest that PDE6D may facilitate K-Ras mediated oncogenesis. Indeed, a number of drug discovery efforts assessing novel PDE6D inhibitors have consistently shown that inhibition of the protein in cancers harboring K-Ras mutations such as colorectal, pancreatic and lung is a valid strategy (Klein et al., 2019, Martin-Gago et al., 2017, Papke et al., 2016, Siddiqui et al., 2020, Zimmermann et al., 2013). Taken together, current evidence supports PDE6D as a relevant protein in cancer progression either independently or in conjunction with its K-Ras modulating cellular functions.

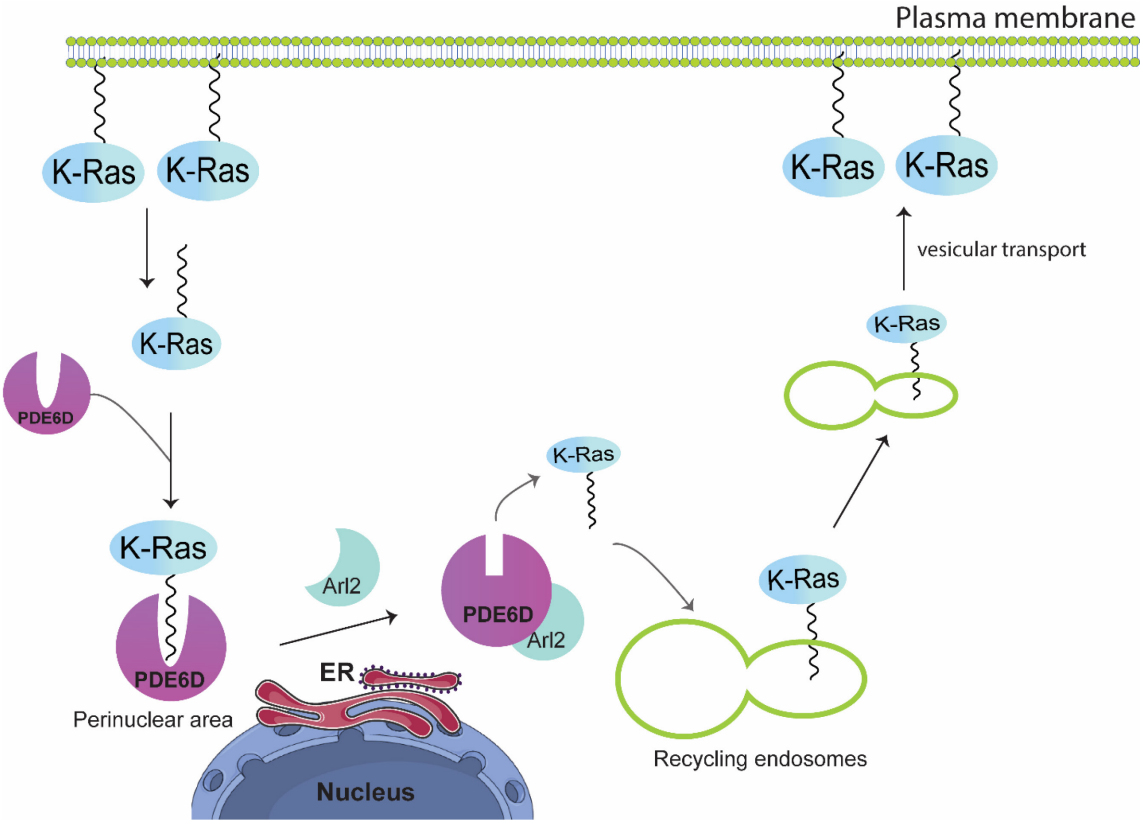

Figure 13. Mechanistic model of PDE6D trafficking of K-Ras.

Mislocalized and potentially newly synthesized K-Ras proteins are sequestered from the endomembranes by PDE6D. The K-Ras cargo on PDE6D is ejected through the action of Arl2-GTP in the perinuclear area. Once released, the recycling endosomes trap K-Ras and facilitates its membrane localization via the vesicular transport system.

The first PDE6D inhibitor is named Deltarasin (Zimmermann et al., 2013). Deltarasin is a benzimidazole small molecule inhibitor that binds at low nanomolar concentrations (K_D = 38 nM) to the prenyl binding hydrophobic pocket of PDE6D (Zimmermann et al., 2013). This compound was found to cause the mislocalization of K-Ras and blocked the growth of K-Ras driven pancreatic cancer in cells as well as in pancreatic cancer xenograft models (Zimmermann et al.,

2013). However, this compound in addition to exhibiting unspecific toxicity also suffers from the Arl2-mediated ejection mechanism previously discussed. A second generation compound deltazinone was developed (Papke et al., 2016). This compound showed improved in vitro affinity for PDE6D (K_D = 8 nM) and better selectivity for inhibiting K-Ras driven cancer cell proliferation. However, this compound in addition to being ejected by Arl2 was found to be unsuitable for animal studies as it is rapidly metabolized in mice (Papke et al., 2016). To counter the challenges of bioavailability and Arl2 ejection, third generation PDE6D inhibitors deltasonamide 1 and 2 with picomolar in vitro affinity to PDE6D (K_D deltasonamide 1 = 203 ± 31 pM; K_D deltasonamide 2 = 385 ± 52 pM) where developed (Martin-Gago et al., 2017). The improved affinity of the deltasonamides was rationalized by their ability to form up to 7 hydrogen bonds with the hydrophobic pocket for PDE6D (Martin-Gago et al., 2017). Importantly, these compounds showed improved cellular activity in addition to selectively inhibiting the growth of K-ras dependent cell lines. Deltasonamides also showed an improved resistance to Arl2 unloading primarily due to the improved binding affinity to the hydrophobic pocket potentiated by its ability to form up to 7 hydrogen bonds with critical amino acid residues within the pocket (Martin-Gago et al., 2017).

A different strategy involving the innovative proteolysis targeting chimera system (PROTACs) has been recently adopted in PDE6D drug development. PROTACs are hetero bifunctional molecules that links a protein of interest (POI) ligand to an E3 ubiquitin ligase thus facilitating the proteosomal degradation of the POI via the ubiquitin proteasome system (UPS) (Sun et al., 2019). The Waldmann group recently developed a PDE6D PROTAC using the deltasonamides as the PDE6D ligand due to their picomolar affinity to PDE6D. Indeed, the PROTACs selectively depleted PDE6D protein levels but surprising revealed a previously unknown role of PDE6D in the regulation of lipid metabolism (Winzker et al., 2020). They specifically showed that the PDE6D inhibitor PROTAC increased the sterol regulatory binding protein (SREBP)-mediated gene expression of lipid metabolism enzymes which was accompanied by an increase in the level of cholesterol biosynthesis precursors (Winzker et al., 2020). Another study that recently assessed potentially unidentified targets of the clinical multikinase inhibitor sorafenib using the PROTAC approach showed that PDE6D is indeed a target of sorafenib as evidenced by the proteosomal degradation of PDE6D in several cell lines treated with the sorafenib based PROTAC (Yang Li, 2020).

1.4 The K-Ras trafficking chaperone calmodulin

1.4.1 Molecular structure and biology of CaM

CaM is a 16.7 KDa, acidic, ubiquitously expressed, master calcium regulator protein that has been implicated in many cellular processes including cell cycle regulation, Muscular contraction, apoptosis as well as cell proliferation (Tidow and Nissen, 2013). Structurally, CaM possess two fairly symmetrical globular lobes separated by a flexible linker (the N and C lobes). Each lobe contains a pair of EF hands each capable of coordinating a calcium ion (4 Ca^{2+} in total) **(Figure 14)** (Tidow and Nissen, 2013). Each lobe of CaM can independently bind protein targets either in the calcium bound holo-enzyme and/or calcium free apo-enzyme states (Marshall et al., 2015). The C lobe of CaM exhibits a 3-fold higher binding affinity for calcium and this binding of calcium to CaM induces conformational changes that results in the exposure of a methionine rich hydrophobic pocket on each lobe (Yang et al., 2003, Crivici and Ikura, 1995, Cox, 1988). Whilst CaM traditionally binds to helical, basic peptides harboring two hydrophobic side chains spaced by 2 to 18 residues, a number of non-canonical binding partners possessing a mono-lipidated polybasic N- or C terminus have been identified (Tidow and Nissen, 2013, Grant et al., 2020c). CaM's exceptional protein target binding spectrum is exemplified by its ability to bind well over 400 proteins in humans and mice including proteins such as cell surface receptors, kinases, phosphatases, ion channels, small GTPases etc. (Tebar et al., 2020). This property is enabled by the protein's flexibility conferred by its linker region and the fact that CaM's N and C lobe are able to assume open and closed conformational cycles depending on their calcium-bound states (Chou et al., 2001).

The protein sequence of CaM is identical across all vertebrate species making it one of the most highly conserved proteins known (Toutenhoofd and Strehler, 2000). Importantly, this ubiquitously expressed protein is also encoded for by 3 identical non-allelic genes which creates a highly debated conundrum of genetic redundancy (Toutenhoofd and Strehler, 2000). It has been suggested that this seemingly redundant evolutionary event is meant to ensure the availability of "back-up" copies of CaM. However, Toutenhoofd and Strehler hypothesize that the three gene copies may not be redundant copies but rather suggest that vertebrate cells exploit this multigene nature of CaM to regulate the local, spatial and temporary availability of CaM (Toutenhoofd and Strehler, 2000). CaM is able to undergo a number of post-translation modifications including carboxymethylation, phosphorylation at Thr26, Thr29, Thr79, Ser81, Tyr138, Tyr99, Ser101 and Thr117 as well as tri-methylation at Lys115 (Murtaugh et al., 1980, Benaim and Villalobo, 2002,

Magnani et al., 2010). Indeed, these differential PTMs may facilitate its selective interaction with various proteins spatio-temporarily.

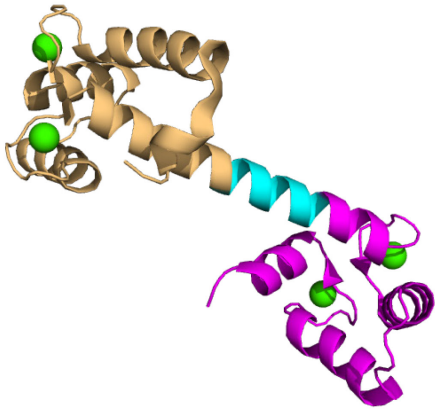

Figure 14. Protein Structure of CaM.

3D structure of fully loaded calmodulin in complex with four (4) calcium ions (green balls). CaM is a 148 amino acid long protein consisting of two fairly symmetrical N and C lobes joined by a flexible linker region. The 3D structure was rendered with Pymol (PDB 4DJC).

1.4.2 The Role of CaM in the cell cycle and MAPK signaling

Cell proliferation is amongst the many processes regulated by Ca^{2+}/CaM (Kahl and Means, 2003). Actively dividing eukaryotic cells undergo proliferation through a series of stages termed the “cell cycle”. The cell cycle consist primarily of; an initial gap phase (G1), a synthesis phase (S) where DNA is replicated, a second gap phase (G2) and a mitosis phase (M) in which cytoplasmic and chromosomal components are divided into two daughter cells (Otto and Sicinski, 2017). The transition through the phases of the cell cycle is tightly regulated by a number of proteins including the cyclin-dependent serine/threonine kinases (CDKs) (Otto and Sicinski, 2017). CaM is required for normal cell cycle progression notably during; re-entry from quiescence (G0), upon mitogenic stimulation, during the G1/S boundary, during G2/M transition, M phase progression as well as during mitotic exit (Kahl and Means, 2003). Studies have shown that CaM binds to the carboxyl terminal of cyclin-dependent kinase inhibitor 1 ($p21^{CIP1}$) (Rodriguez-Vilarrupla et al., 2005). $p21^{CIP1}$ in addition to its CDK inhibitory role, acts as a bridge molecule in the CDK4/ cyclin D1 complex (LaBaer et al., 1997). Similarly, CaM has been shown to bind directly to cyclin E (Choi et al., 2006). Consistently, it was this significant body of evidence implicating CaM in the cell cycle that inspired initial interests in targeting CaM in cancer several decades ago.

The epidermal growth factor receptor, a major upstream regulator of the Ras/MAPK signaling pathway is a CaM binding protein (Li and Villalobo, 2002, Tebar et al., 2002). Murine EGFR was isolated by Ca^{2+} dependent CaM-affinity chromatography (Li and Villalobo, 2002, Tebar et al., 2002). Similarly, a Ca^{2+} dependent direct binding of CaM to the juxtamembrane region of the receptor (amino acids 645-660) was shown (Martin-Nieto and Villalobo, 1998). Taken together, these studies established a relevance of CaM interaction with a critical upstream components of Ras signaling. CaM was first shown to bind exclusively to K-Ras among the major Ras isoforms in affinity chromatography studies by the Neus Agell Group (Villalonga et al., 2001). Their study suggested that the interaction between K-Ras and CaM was direct and that this interaction modulates the Ras-MAPK signaling pathway (Villalonga et al., 2001). Likewise, they showed that binding of CaM to K-Ras prevents the phosphorylation of Ser181 by PKC in vivo (Alvarez-Moya et al., 2010). Their data suggested that the inability of K-Ras to be phosphorylated causes a markedly decreased ability of K-Ras to stimulate proliferation in saturated serum conditions (Alvarez-Moya et al., 2010). Furthermore, they demonstrated that the phosphorylation of K-Ras also regulates oncogenic K-Ras function such as focus formation capacity, apoptosis resistance upon Adriamycin treatment as well as tumor cell mobility (Alvarez-Moya et al., 2010). However, recent studies on the role of Ser181 phosphorylation in modulating the K-Ras/CaM interaction appears to sharply contrast this view (Wang et al., 2015b). It was suggested that PKC mediated phosphorylation of Ser181 of K-Ras compromises its binding to CaM and suppresses tumorigenicity (Wang et al., 2015b).

1.4.3 The K-Ras4b/CaM interaction and the modulation of K-Ras localization

Of the 4 Ras isoforms, CaM interacts exclusively with K-Ras4b (Villalonga et al., 2001). Although some contradictions exist regarding the specific details of the K-Ras/CaM interaction, a significant and robust body of evidence indicates that the interaction is calcium dependent, nucleotide independent , farnesylation dependent , and G-domain independent (Grant et al., 2020b, Sperlich et al., 2016, Agamasu et al., 2019, Jang et al., 2019, Villalonga et al., 2001).

Structurally, the hydrophobic pockets of the N and C lobes of Ca^{2+} CaM can potentially bind to farnesylated K-Ras in a 1:2 stoichiometry involving 1 CaM and 2 K-Ras molecules (Agamasu et al., 2019). The C-lobe was shown to exhibit a 10 fold higher affinity for K-Ras (C lobe K_D = 0.4 μM; N lobe K_D = 4.0 μM) (Agamasu et al., 2019) . Similarly, another group showed using chemical

shift perturbations NMR that farnesylation was absolutely required for specific interactions of K-Ras with CaM (Grant et al., 2020b). Crystal structure of CaM in complex with farnesylated and carboxymethylated K-Ras reveals that the methionine rich hydrophobic pocket on CaM sequesters the farnesyl moiety (Grant et al., 2020b). Importantly, electrostatic interactions between the acidic flexible linker of CaM and the polybasic HVR of K-Ras (KSKTKC) have also been suggested as a significant contributor to this interaction (Wu et al., 2011, Grant et al., 2020b, Agamasu et al., 2019). In addition to C185 farnesylation, Ser181 of K-Ras has also been identified as a critical residue for the interaction with calmodulin (Alvarez-Moya et al., 2010, Wang et al., 2015b). Binding of CaM to K-Ras prevents the phosphorylation of Ser181 and the phosphorylation of this residue by PKC has been shown to compromise the K-Ras/CaM interaction (Alvarez-Moya et al., 2010, Wang et al., 2015b).

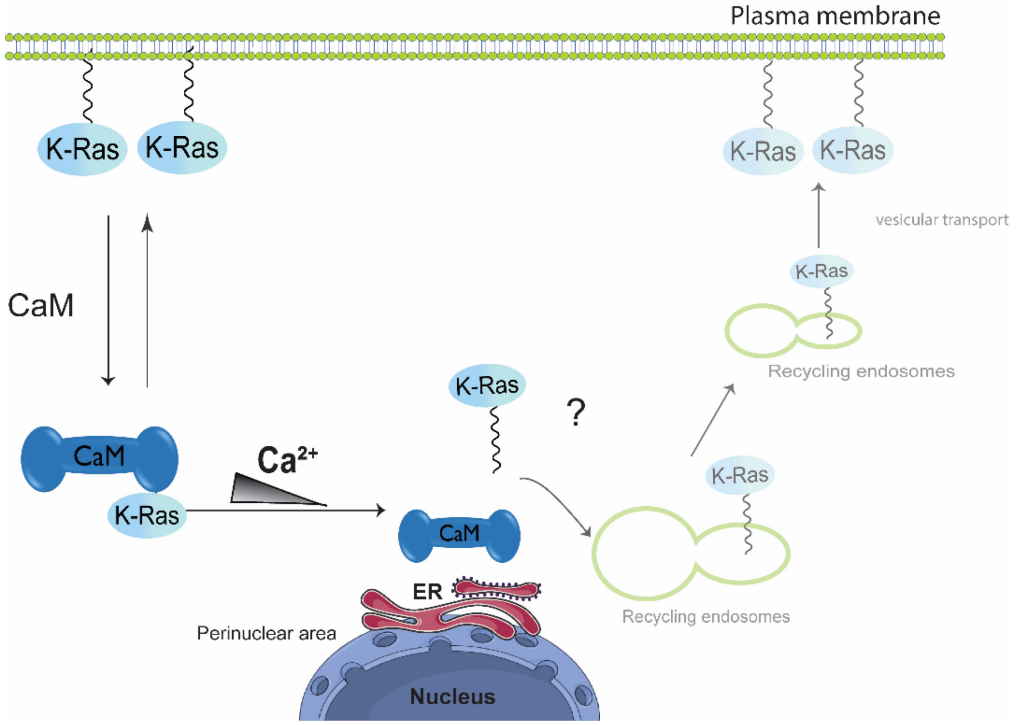

Figure 15. Proposed mechanism of K-Ras trafficking by CaM.

Ca^{2+}/CaM facilitates the reversible translocation of K-Ras from the plasma membrane into the cytoplasmic space. A calcium dependent release mechanism of K-Ras is initiated at subcellular regions with lower Ca^{2+} gradients. Released K-Ras may then be trapped by the recycling endosomes in areas near the recycling endosome. In such a system, the RE subsequently aids plasma membrane enrichment of K-Ras via vesicular transportation.

An earlier study into the effects of CaM interaction on K-Ras localization showed that Ca^{2+}/CaM facilitates the reversible translocation of K-Ras from the plasma membrane in hippocampal neuronal cells (Fivaz and Meyer, 2005). Recent evidence have suggested that CaM is able to

extract K-Ras from the PM (Agamasu et al., 2019, Sperlich et al., 2016). Indeed, in vitro studies using nanodiscs, membrane mimetics and anionic monolayers indicate that CaM sufficiently outcompetes these artificial membranes for the K-Ras farnesyl moiety (Agamasu et al., 2019, Sperlich et al., 2016). Similarly, cellular experiments have shown that CaM is able to sequester K-Ras from the plasma membrane (Grant et al., 2020b, Sidhu et al., 2003). Since both CaM and the PM bind to the same structural elements on K-Ras, the interaction to either partner is mutually exclusive. Using a chimeric CaM-K-Ras fusion protein construct (CaMeRas) in a live cell FRET experimental setup, Grant et al demonstrated a Ca^{2+} and farnesylation dependent reversible K-Ras membrane detachment process in which the CaMeRas-WT construct was internalized upon Ca^{2+} stimulation whereas, the Ca^{2+} deficient CaMeRas mutant failed to be internalized (Grant et al., 2020b).

Furthermore, since Ca^{2+} ion concentrations at different subcellular compartments undergo a dynamic flux through activation and inactivation of Ca^{2+} channels, stores and pumps, K-Ras may be released by CaM at low Ca^{2+} gradient regions within the subcellular space **(Figure 15)**, thus potentially allowing for other K-Ras trafficking chaperones like PDE6D to ferry K-Ras unto the relevant structures for subsequent localization to the membrane (Sperlich et al., 2016, Capiod, 2013, Berchtold and Villalobo, 2014). In such a scenario, CaM and PDE6D act as cooperating units in modulating K-Ras membrane association and signaling. Such cooperativity may become interesting in the context of synergistic targeting of Ras driven cancers.

Co-localization of interacting proteins in various subcellular structures may be indicative of functional activity within such structures. In addition to its plasma membrane localization, K-Ras has been found on the ER, Golgi and Mitochondria (Bivona et al., 2006, Prior and Hancock, 2012). Interestingly, Ca^{2+}/CaM is also reported to localize on and even regulate protein transport to the Mitochondria, ER, Golgi as well as the Nucleus (Berchtold and Villalobo, 2014, Aich and Shaha, 2013). Therefore, it is reasonable to speculate that K-Ras and CaM may interact to modulate other non-canonical cellular functions outside of the PM.

1.4.4 Role of CaM in cancer development

Elevated levels of Ca^{2+}/CaM has been reported in multiple human and animal tumors (Liu et al., 1996, Berchtold and Villalobo, 2014). CaM has been reported to promote cell proliferation, migration, autophagy and apoptosis in cancer (Berchtold and Villalobo, 2014). Consistently, early studies using the CaM antagonists trifluoperazine and W-7 in combination with tamoxifen, an estrogen receptor inhibitor induced apoptosis in breast cancer cell lines indicating the relevance of CaM for cancer growth and survival (Frankfurt et al., 1995). Similarly, CaM has been implicated in the promotion of tumor-associated angiogenesis, a process whereby tumor cells grow new

blood vessels to enhance their oxygen supply (Berchtold and Villalobo, 2014). Hypoxic stress occurs in poorly vasculated tumor microenvironments thereby causing an increase in cytosolic Ca^{2+} and the formation of Ca^{2+}/CaM complexes, this promotes the transcriptional activity of the hypoxia inducible factor (HIF-1) thus increasing the expression of the vascular endothelial growth factor (VEGF) which promotes angiogenesis (Shen et al., 2007). Furthermore, the interaction between K-Ras and CaM has been found to influence both MAPK and PI3K/AKT signaling output (Nussinov et al., 2015). Indeed, recent evidence have implicated this K-Ras/CaM interaction as a promoter of cancer cell stemness by suppressing non-canonical frizzled 8-mediated Wnt signaling (Wang et al., 2015b).

Taken together, the evidence above points to an important role of CaM in the development of the malignant phenotype. Indeed, it is clear that the relevance of CaM for the maintenance of normal cell division and proliferation coupled with its ability to interact with many proteins, some of which are oncogenes (e.g K-Ras) implicates CaM in the development of cancer.

1.4.5 CaM inhibitors

A conditional tetracyclin-dependent CaM knockout system in chicken lymphoma DT40 cells developed by the Berchtold group in which two CaM genes are deleted and the third gene is replaced with an artificially regulated transgene showed that CaM is critical for survival of vertebrate cells (Panina et al., 2012). They also showed that overexpression of ectopic wild-type CaM or CaM with one fully active Ca2+ binding domain restored cell viability (Panina et al., 2012). However, because of the evidence implicating Ca2+/CaM in various malignancies, small molecules against this protein have been sort for several years now. Indeed, many inhibitors with distinct chemical properties have been assessed for their anti-CaM activity in various tumors.

CaM inhibitors including CaM antagonist calmidazolium (CMZ), naphtalenesulfonamides such as the highly soluble and cell penetrating W-7, W-5 and W-13 as well as the clinically approved phenothiazine antipsychotic trifluoperazine have all been shown to reversibly inhibit CaM (Sunagawa et al., 1999, Hidaka et al., 1981, Sengupta et al., 2007, Weiss et al., 1980, Huang et al., 2019). Similarly, natural product E6 berbamine, the wasp venom peptide polistes mastoparan, the small molecule CGS-9343B as well as artemisinin and tehranolide have all been shown to inhibit CaM in several cancer cell lines (Hu et al., 1992, Mou et al., 2019, Barnette et al., 1983, Hilchie et al., 2016, Neuhaus and Reber, 1992, Noori and Hassan, 2014, Black et al., 1989). A group of anti-fungal azole derived compounds including miconazole and econazole have also been shown to inhibit CaM activity (Hegemann et al., 1993). Interestingly, a recent study on miconazole showed that the compound induced an increase in CaM gene expression suggesting

that CaM inhibition by the compound leads to a compensatory protein overexpression in aquatic species (Breitholtz et al., 2020).

1.4.6 CaM covalent inhibitors

Despite a generally cautious attitude towards covalent inhibitor development by the pharmaceutical industry, several covalent compounds have been approved for the treatment of a number of clinical conditions including clopidogrel (a covalent modifier of P2Y purinergic receptor 12), lansoprazole (a H+/K+ ATPase inhibitor) and esomeprazole (also a H+/K+ ATPase inhibitor prescribed for heartburns), these inhibitors featured in the top 10 selling drugs in the US in 2009 (Singh et al., 2011). In oncology, key covalent inhibitors include inhibitors of Aromatase, thymidylate synthase and ribonucleotide reductase (Singh et al., 2011). Many covalent inhibitors act via cysteine residue modification due to the high intrinsic reactivity of this amino acid and structure-guided targeting of non-catalytic cysteine is a widely adopted strategy in drug discovery (Cuesta and Taunton, 2019). Lysine residue targeting covalent inhibitors have been mostly unexplored even though a large set of potentially targetable lysines have been identified (Cuesta and Taunton, 2019).

Ophiobolin A (OphA) is a lysine reactive covalent inhibitor of CaM (Hait et al., 1987, Leung et al., 1984). This potent anti-fungal sesterpenoid natural product was shown to covalently modify lysine residue 75, 77 and 148 on CaM and block K-Ras mutated cancer spheroid growth (Leung et al., 1984, Najumudeen et al., 2016). OphA can react with CaM at a 2:1 ratio, similar to covalent phenothiazine derivative trifluoromethyl phenothiazine (POS-TP) which also react with Lys148 (Faust et al., 1987, Leung et al., 1984). In addition to its potency against CaM, OphA appears to show activity against several other targets including phosphatidylethanolamine (Chidley et al., 2016). The phenothiazine antipsychotic fluphenazine-N-2-chloroethane (fluphenazine mustard) is also known to irreversibly modify CaM **(SI Table 1)** (Hwang et al., 2009).

Due to the critical role CaM plays in many cellular processes, development of inhibitors against this target has been met with extreme caution (Villalobo and Berchtold, 2020). However, the availability of clinically approved compounds that bind to CaM such as the phenothiazine antipsychotics indicates that perhaps, CaM inhibition may be tolerated. Recent studies indicate a stemness context specific collaboration of CaM and K-Ras (Wang et al., 2015b). Disruption of this interaction through PKC mediated S181 phosphorylation as well as the direct inhibition of CaM by OphA demonstrated anti-cancer activity (Wang et al., 2015b, Najumudeen et al., 2016). Taken together, the growing body of evidence suggests that targeting CaM in K-Ras driven cancers may offer a new window of opportunity for drug development (Najumudeen et al., 2016, Wang et al., 2015b, Saito et al., 2017).

1.5 Targeting oncogenic Ras signaling

With the exception of the recently approved K-RasG12C covalent inhibitor sotorasib (Lumakras), K-Ras remains a largely undrugged oncogenic target (Amgen, 2021). The paucity of drug binding pockets on the surface of these proteins has made the prospect of direct inhibition a huge challenge that has only been partly resolved a few years ago (Ostrem et al., 2013). Consequently, indirect targeting of Ras through both upstream and downstream effector inhibition have been the most widely explored and extensively discussed below **(Figure 16)** (Moore et al., 2020).

1.5.1 Inhibition of signaling upstream of Ras

For Ras to be activated, several upstream processes are required including; (1) an intact signal relay system from growth factors through GEFs and GAPs as well as (2) processes that facilitate Ras localization on the plasma membrane. Because these processes consist of several druggable protein players, they have been extensively exploited in efforts to block Ras oncogenic signaling. The development of clinical EGFR inhibitors (Erlotinib, Afatinib, Osimertinib and Gefitinib) and monoclonal antibodies (Cetuximab, nimotuzumab, necitumumab and Panitumumab) are excellent examples of how blocking upstream Ras signaling can be exploited (Huang et al., 2020, Cai et al., 2020). Also, significant effort has been put into developing inhibitors against the GEF SOS1. Indeed, small molecules that interfered with the SOS-Ras interaction were previously developed but whilst these molecules showed low nanomolar affinity to SOS, assessment in cellular assays yielded poor activity (Sun et al., 2012, Leshchiner et al., 2015, Patgiri et al., 2011). Subsequent efforts led to the development of a small molecule Bay-293 which binds to the CDC25 domain of SOS1 and a region adjacent to switch II on the Ras-SOS1-Ras complex at nanomolar concentrations, Bay-293 was more effective against wild-type K-Ras cancer cells relative to the previous compounds (Hillig et al., 2019). Currently, a clinical trial to assess an SOS1 inhibitor BI 701963 as a single agent and in combinations with the MEK inhibitor trametinib is underway for patients with different types of advanced cancers harboring K-Ras mutations (NCT04111458). SHP2, a non-receptor protein tyrosine phosphatase which acts as a scaffold protein that facilitates Ras nucleotide exchange by binding to GRB2 and SOS1 is also another major target currently being assessed in the context of blocking Ras driven cancers (Moore et al., 2020). In fact, 3 potent allosteric SHP2 inhibitors; RMC 4630, JAB-3068 and TN0155 are undergoing clinical trials (Moore et al., 2020).

1.5.2 Targeting downstream of Ras GTPase signaling

1.5.2.1 Ras/Raf/MEK/ERK pathway inhibition

Activated Ras promotes the recruitment and dimerization of Raf proteins which facilitates the activation of other downstream nodes of the MAPK pathway as previously detailed. To effectively address Ras driven cancers, this pathway needs to be suppressed and many therapeutics have been developed to this effect. Clinical BrafV600-mutant kinase inhibitors vemurafenib and dabrafenib which induce an outward shift of the αC helix in the kinase domain of Raf effectively inhibit Raf monomers (Karoulia et al., 2016). Since BrafV600 mutants signal as monomers, these compounds are effective against the mutated target (Karoulia et al., 2016, Moore et al., 2020). Unfortunately, Ras mutant cancers that signal via dimerized Raf proteins are insensitive to these inhibitors. In fact, these inhibitors even paradoxically activate the MAPK pathway by binding wild-type Raf (Poulikakos et al., 2010). Whilst some details remain unclear, paradoxical ERK activation in the presence of inactive B-Raf depends on enhanced dimerization and transactivation of C-Raf (Poulikakos et al., 2010, Holderfield et al., 2014, Rajakulendran et al., 2009). Consequently, Raf inhibitors which are able to bind both monomeric and dimeric Raf such as belvarafenib, AZ-628, LY3009120 and LXH-254 have been reported to show efficacy against both Ras-mutant and Raf-mutant tumors although some show minimal paradoxical activation (Peng et al., 2015, Vakana et al., 2017, Moore et al., 2020).

Various inhibitors have been developed for MEK, another major downstream effector of the MAPK signaling pathway. The inhibitors cobometinib, trametinib and binimetinib are clinically approved MEK drugs that are available for treating B-RafV600 mutant melanoma (Hellmann et al., 2019, Hatzivassiliou et al., 2013). Whilst these compounds show benefits against their intended target, they too fail to be efficacious against Ras-mutated cancer (Blumenschein et al., 2015, Moore et al., 2020).

Efforts to develop ERK inhibitors have not yet yielded any clinically approved compounds. However, some promising agents such as GDC-0994 and ulixertinib have been assessed as monotherapeutic agents in various phase I clinical trials (Varga et al., 2020, Sullivan et al., 2018). Similarly, KO-947 and LY-3214996 are currently undergoing clinical assessment for their efficacy in various cancers (Moore et al., 2020).

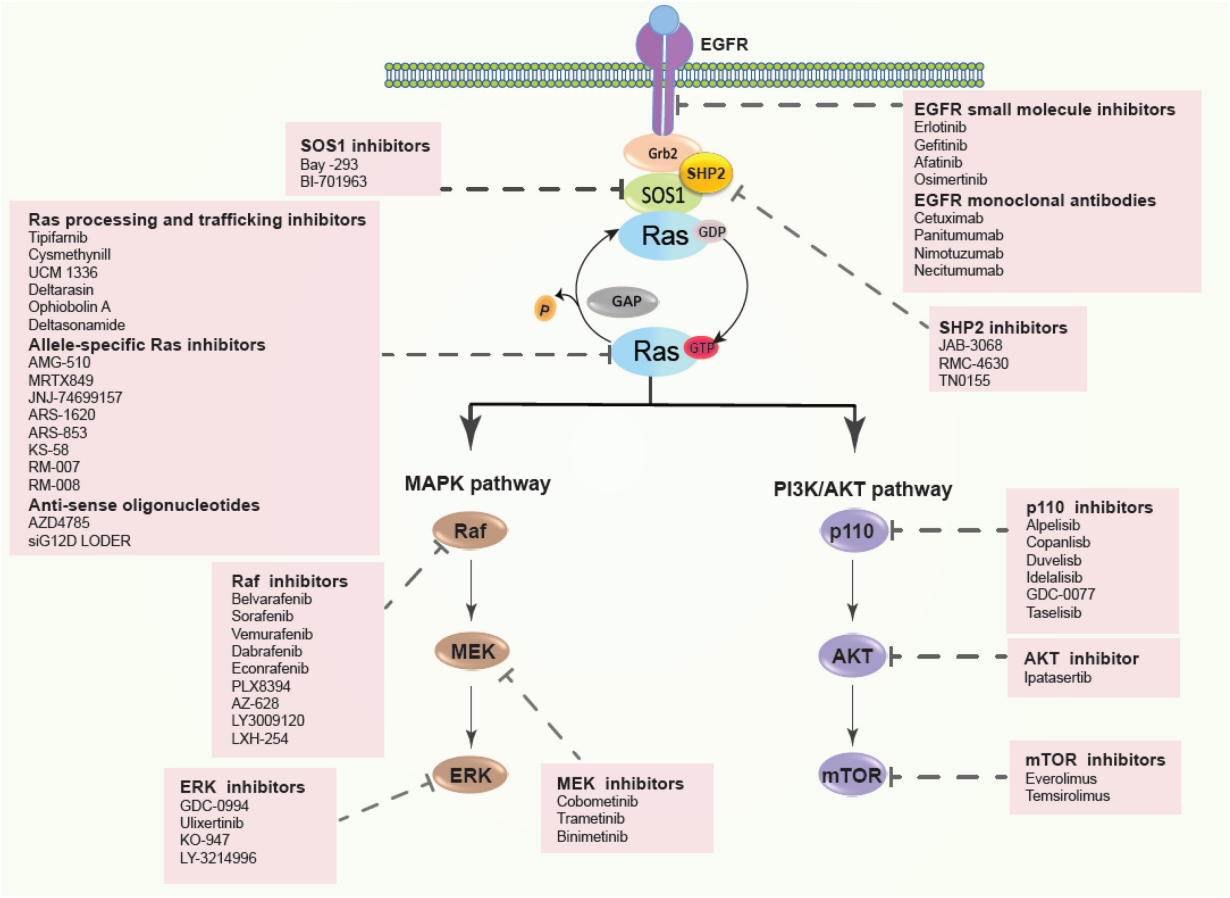

Figure 16. Schematic representation of various Ras targeting approaches. *Figure modified from (Moore et al., 2020).*

Several therapeutic strategies have been/being developed to reduce the activation of Ras for instance, EGFR small molecule inhibitors and monoclonal antibodies have been developed. Inhibition of SOS and SHP2 is another strategy to decrease GDP-GTP nucleotide exchange. The inhibition of Ras processing and trafficking chaperones is also widely exploited in efforts to mitigate Ras oncogenic signaling. Recent efforts in direct Ras targeting has led to the development of the K-RasG12C specific covalent inhibitors as well as a number of other small molecules in development. Several clinical and experimental drugs have been developed to inhibit Ras downstream effectors of the MAPK and PI3K/AKT signaling pathways including Raf, MEK, ERK, p110, AKT and mTOR.

1.5.2.2 Ras-PI3K/Akt pathway inhibition

Another major alternative downstream pathway modulated by Ras proteins which can be blocked is the PI3K/AKT signaling pathway. Class one PI3K protein p110α, a ubiquitously expressed isoform and an exclusive client of Ras proteins has been a major subject of research (Fruman et al., 2017). Interestingly though, the clinically approved inhibitor alpelisib, a p110α inhibitor is not approved for Ras mutated tumors. A combination of multiple redundancies between the MAPK and PI3K pathway continues to facilitate the development of resistance mechanisms (Moore et

al., 2020). Whilst the use of combinatorial and synergistic drug targeting approaches have been employed in many clinical trials, unbearable toxicity issues seem to be widespread with most of these strategies (Wang et al., 2018, Algazi et al., 2019, Moore et al., 2020).

1.5.3 Inhibition of Ras Post-translational processing and trafficking

Another strategy of Ras upstream inhibition involves the blockade of either Ras post-translational processing or the inhibition of key chaperone proteins that facilitate proper localization to the plasma. The development of inhibitors against the post-translational prenylation of Ras proteins include the farnesyl transferase inhibitors (FTIs) and geranylgeranyl transferase inhibitors (GGTIs), inhibitors against the AAX cleavage step i.e Ras-converting enzyme (RCE1) as well as inhibitors of the methylation step of Ras processing; the isoprenylcysteine carboxyl methyltransferase (ICMT) inhibitors is well documented (Moore et al., 2020). The FTI inhibitor tipifarnib shows promise for only patients with H-Ras mutated HNSCC, NSCLC and metastatic urothelial carcinoma due to the fact that K-Ras and N-Ras possessed alternative prenylation mechanism mediated by the GGTases (Gilardi et al., 2020, Zheng et al., 2010, Lee et al., 2020, Whyte et al., 1997). To circumvent the apparent redundancy exhibited by K-Ras and N-Ras mutant cell lines, the RCE1 and ICMT steps which are essential in these cells may be exploited as mutant selective therapeutic approaches. The compounds cysmethynil and UCM 1336 have been developed to block ICMT (Wang et al., 2017).

The dynamic distribution of processed K-Ras to the plasma membrane is facilitated by chaperone proteins notably PDE6D and CaM (Chandra et al., 2011, Dharmaiah et al., 2016, Grant et al., 2020a, Agamasu et al., 2019). Both chaperones and the various strategies to inhibit them have been extensively reviewed in previous sections of this thesis and constitute the majority of the original contribution of this thesis to Ras biology.

1.5.4 Direct K-Ras inhibitors: K-RasG12C inhibitors and beyond

Kevan Shokat and colleagues pioneered the growing field of Ras covalent inhibitors with their seminal work which developed the first series of irreversible covalent compounds capable of binding to the cysteine mutant K-Ras protein (K-RasG12C) in the GDP-bound form. These compounds trapped the G12C mutant in the GDP form, blocked SOS mediated nucleotide exchange and prevented Raf effector engagement of the mutant **(Figure 17)** (Ostrem et al., 2013). Their crystal structural studies revealed a previously unknown pocket beneath the effector binding switch-II region of K-Ras. Indeed this pocket is available in the other K-Ras G12 mutants but because these other mutants have a lower rate of intrinsic GTPase activity, development of

covalent inhibitors against their GDP-bounds forms might not be nearly as successful relative to G12C-mutated K-Ras (Hunter et al., 2015).

From the Shokat group's first generation of G12C inhibitors, the lead compound was optimized by modifying its linker and hydrophobic binding pocket to generate a more potent and cellular active compound ARS-853 (Patricelli et al., 2016). ARS-853 was further improved by introducing a quinazoline-based series with a fluorophenol hydrophobic binding moiety. This significantly improved pharmacological properties leading to the development of ARS-1620 (Janes et al., 2018).

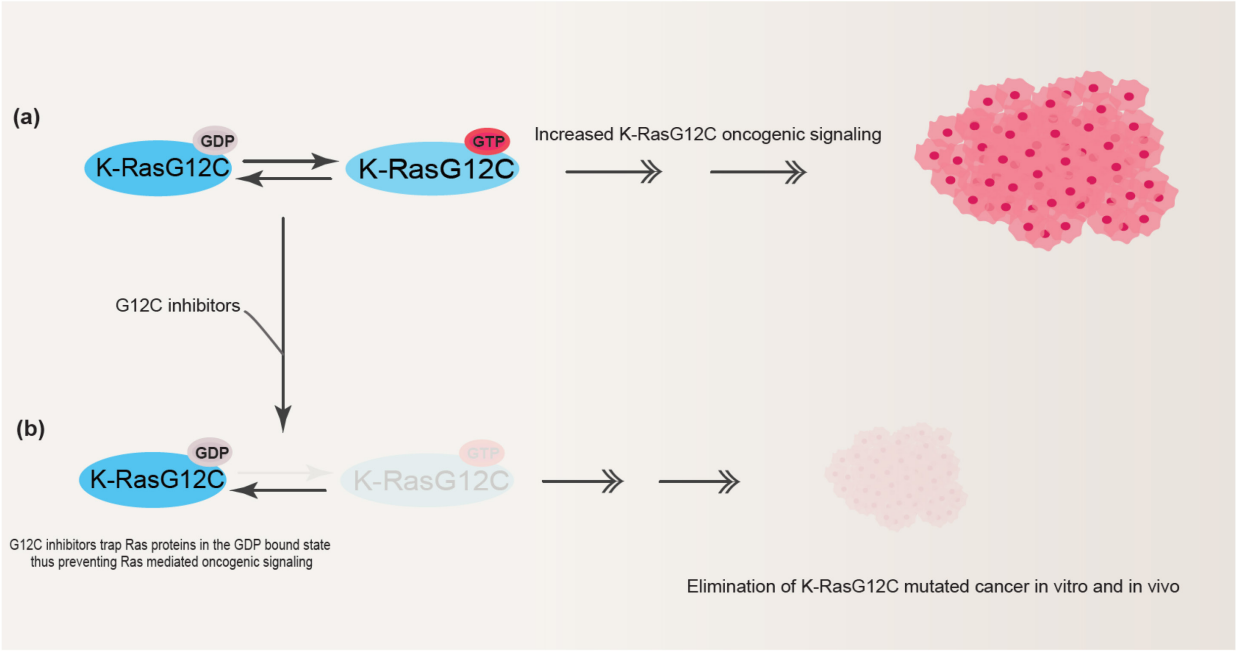

Figure 17. Schematic representation of K-RasG12C inhibition.

Many biopharma companies are developing G12C inhibitors notably Amgen's Sotorasib (AMG-510) which has an addition aromatic ring that improves protein-ligand interactions by exploiting an alternative orientation of His95 in the switch-II pocket (Canon et al., 2019). Sotorasib has been recently granted priority review by the FDA for the treatment of K-RasG12C-mutated locally advanced or metastatic NSCL (Healio, 2021). Approval efforts for sotarasib have made similar progress in Europe and China thus making it potentially the first K-Ras specific inhibitor on track for approval (Biospace, 2021). Mirati's MRTX849 (Adagrasib) is currently also recruiting for a randomized phase 3 clinical trial versus docetaxel in patients with previously treated NSCLC harboring the K-RasG12C mutation (NCT04685135). A third compound ARS-3248 (JNJ-74699157) developed by an exclusive R&D agreement between Wellspring Biosciences, Inc.,

and Janssen Biotech, completed its phase 1 clinical trials in 2020 in patients with the K-RasG12C mutated NSCLC and CRC, the results have not been announced (NCT04006301).

Since the current K-RasG12C inhibitors require the protein to be bound in the GDP form, mutations that facilitate nucleotide exchange and/or prevent GTPase activity will pose a mechanism of resistance to these compounds (Moore et al., 2020). Indeed a recent study has shown that K-RasG12C mutant cancer cells exhibit heterogeneous response to these inhibitors by producing new K-rasG12C proteins in response to reduced MAPK signaling. Importantly, the new proteins are maintained in the GTP bound state whilst the contribution of drug resistance through EGFR, SHP2 and Aurora Kinase A was implicated (Dunnett-Kane et al., 2021, Xue et al., 2020). Similarly, another recent study showed that clinically acquired resistance to K-RasG12C inhibitors is mediated by a novel switch II pocket mutation (K-RasY96D) (Tanaka et al., 2021). It was identified that this mutation results in the interference of key drug-protein interactions and conferred resistance to G12C inhibitors in engineered and patient derived K-RasG12C cancer models (Tanaka et al., 2021). Coupled with the fact that G12C mutations account for only a small proportion of K-Ras mutated cancers, the need to develop inhibitors that can both target other K-Ras alleles whilst functioning independently of the nucleotide binding state is pertinent. To this end, some molecules have been recently discovered that circumvent the nucleotide dependency, these molecules (RM-007 and RM-008) are able to bind a newly discovered groove adjacent the switch II pocket (Gentile et al., 2017, Moore et al., 2020). Whilst developing inhibitors against other alleles such as the G12V and G12D mutants is currently still in early stages, the recent identification of the peptide KS-58 as a selective inhibitor of K-RasG12D mutated cancer highlight an early promise in this area (Sakamoto et al., 2020). Other approaches including the targeting of all K-Ras alleles with the Pan-K-Ras inhibitor RMC-6236 is also under development.

1.6 Protein phosphatase 2A (PP2A)

1.6.1 Biochemistry and structure of PP2A

Homeostasis of cellular phosphorylation level is achieved by tightly controlled activities of two classes of enzymes- protein kinases, which catalyze transfer of a phosphate group to a specific protein residue, and protein phosphatases, which catalyze the reversed reaction. PP2A belongs to a large family of serine/ threonine protein phosphatases and is classified as phosphoprotein phosphatase (PPP), based on specific sequence motifs in the catalytic site (Nasa and Kettenbach, 2018). These sites coordinate two bivalent metal ions (Mn2+, Fe2+, Zn2+), which activate water molecule, thereby aiding substrate dephosphorylation (Zhang et al., 2013). PP2A is one of best established tumor suppressor phosphatases (Kauko and Westermarck, 2018). Structure of PP2A is very complex (Xing et al., 2006). In cells, it functions as a heterotrimer (Sangodkar et al., 2016). Each heterotrimer is built of one unit of the scaffolding (A) (also referred to as PR65), and catalytic (C) subunits, which together comprise the “core enzyme”. Both, A and C subunits, have two different isoforms, α and β, with Aα and Cα accounting for the majority of each subunit expression in most cells (Eichhorn et al., 2009). The A subunit contains 15 tandem HEAT (Hungtingtin/ Elongation factor 3/ PP2A A /TOR1) repeats, with each repeat consisting of a tandem helix connected by a loop (Wlodarchak and Xing, 2016). The core enzyme further complexes with only one member of the regulatory (B) subunits. B subunits are split into four structurally distinct families and are also referred to as B (B55/ PR55), B´(B56/ PR61), B´´ (PR48/ PR72/ PR130) and B´´´(PR93/ PR110)/ Striatin **(Figure 18)** (Sangodkar et al., 2016). Whilst these B subunit families exhibit minimal sequence homology across families, members of the same family are structurally similar (Shi, 2009). Each of the regulatory B subunits has 2-5 different isoforms and splicing variants, adding to combinatorial complexity of PP2A´s structural organization. PP2A in fact comprises over 80 distinct holoenzymes (Sangodkar et al., 2016). The identity of the B subunit determines subcellular localization and substrate specificity of the holoenzyme (Janssens and Goris, 2001). Activity of PP2A is subject to regulation by post-translational modifications, in particular methylation and phosphorylation of the catalytic subunit. Catalytic subunit can be phosphorylated at Thr304 and Tyr307, with the latter one preventing formation of B55 complexes by inhibiting methylation of Leu309 by Leucine Carboxyl Methyl Transferase 1 (LCMT-1) (Perrotti and Neviani, 2013).

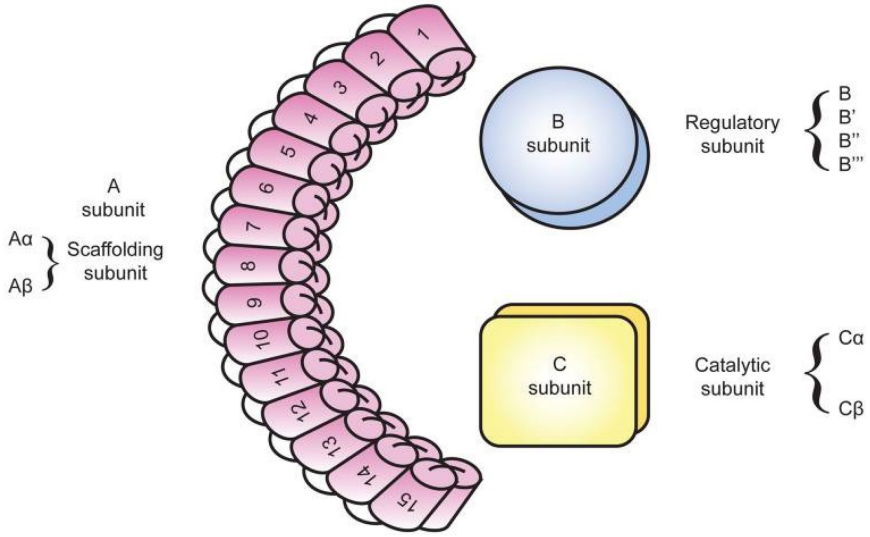

Figure 18. Structural components of the PP2A heterotrimeric complex. *Adopted from (Sangodkar et al., 2016)*

1.6.2 Role of PP2A in the regulation of Ras signaling pathways

Due to its critical function as a master regulator of cellular phosphorylation events capable of regulating up to 70% of pSer/ pThr sites, PP2A is inadvertently implicated in the control of downstream oncogenic signaling events such as Ras-MAPK pathways and the PI3K/AKT/mTOR pathways (Wlodarchak and Xing, 2016). PP2A has been shown to facilitate the negative regulation of the Ras-MAPK pathway through its binding to the phospho-tyrosine domain of SHC, an important member of the growth factor binding complex of GRB2, SOS and SHC that mediates Ras activations (Ugi et al., 2002). Also, PP2A-B56 have been reported to Downregulate phosphorylation of ERK (Letourneux et al., 2006). Importantly, this PP2A-mediated dephosphorylation is reversed in the presence of the immediate early response gene X-1 (IEX-1) (Letourneux et al., 2006). Similarly, PP2A promotes the dephosphorylation and consequent activation of Sprouty2, a negative regulator of MAPK signaling (Lao et al., 2007). Sprouty2, when phosphorylated, cannot bind to GRB2. However, the dephosphorylation of Sprouty2 by PP2A exposes the GRB2 binding motif on the C-terminus, thus resulting in the inhibition of Ras-MAPK signaling **(Figure 19)** (Lao et al., 2007, Wlodarchak and Xing, 2016).

PP2A is also implicated in the regulation of the PI3K/AKT/mTOR pathway (Kuo et al., 2008). PP2A B56 holoenzyme inhibits AKT by dephosphorylating both T308 and S473 residues (Kuo et al., 2008). Similarly, PP2A has been reported to dephosphorylate S6K, a downstream effector of the mTOR signaling pathway, which promotes cell growth and proliferation **(Figure 19)** (Peterson

et al., 1999). Furthermore, PP2A has been shown to inhibit the mTOR pathway by dephosphorylating the insulin receptor substrate 1 (IRS1) in the insulin signaling pathway or MAP4K3 in the amino acid pathway (Yan et al., 2010, Hartley and Cooper, 2002).

1.6.3 Role of PP2A in cancer development

Downregulation of PP2A´s activity is not just implicated in oncogenic development, but also in neurodegenerative and intellectual disorders as well as cardiovascular disease (Mazhar et al., 2019). Cancer remains the primary research focus of PP2A and a number of studies have highlighted the important role of PP2A as a tumor suppressor and indicate that the disruption of the PP2A holoenzyme activity contributes to carcinogenesis (Perrotti and Neviani, 2013). PP2A inactivation can occur through several mechanisms, including low-frequency somatic mutations of its subunits and methylation and/or phosphorylation of the C-terminal tail of the catalytic subunit (Perrotti and Neviani, 2013). The major mechanism of PP2A´s inactivation across different pathological states is over-expression of its endogenous inhibitory proteins, such as SET (Suvar/ Enhancer of zeste/ Trithorax), CIP2A (Cancerous inhibitor of PP2A) or PME-1 (PP2A methylesterase-1), which opposes activity of LCMT-1 (Reynhout and Janssens, 2019).

Inhibitory proteins are structurally and functionally diverse (Kauko and Westermarck, 2018). For example, SET binds directly to the catalytic subunit, CIP2A associates with B56 family members and PME-1 demethylates L309 of the catalytic subunit, since L309 is the C-terminal residue important for carboxymethylation and enzyme activation, this PME-1 mediated demethylation leads to expulsion of the metal ions and loss of enzyme activity (Li et al., 1996, Clark and Ohlmeyer, 2019). Overexpression of PP2A inhibitory proteins such as CIP2A and SET is a prognostic indicator for poor patient survival in cancer (Cristobal et al., 2012, Cristobal et al., 2015). CIP2A over-expression also drives cancer resistance to kinase or epigenetic inhibitors (Kauko et al., 2018). Therefore, PP2A reactivation strategies could be applicable in addressing various malignancies.

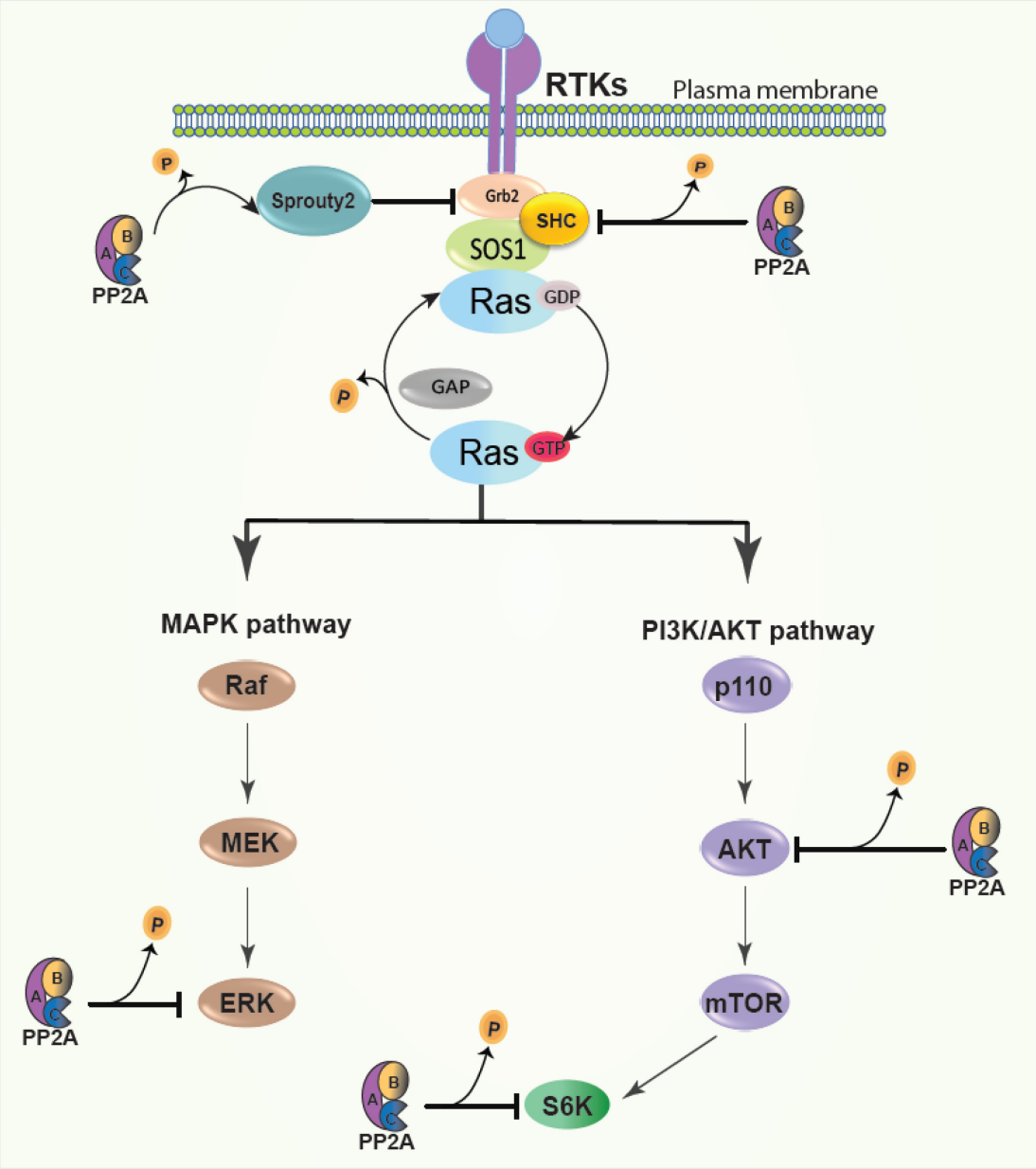

Figure 19. Mechanism of PP2A mediated regulation of Ras downstream signaling

1.6.4 Therapeutic strategies to re-activate PP2A in cancer

Therapeutic efforts aimed at re-activating PP2A in various malignancies are primarily focused on inhibition of the endogenous inhibitors of PP2A and development of small molecules modulators of PP2A activity (Mazhar et al., 2019). For the first strategy, FTY720, the sphingosine analog, has been shown to inhibit SET (Rahman et al., 2016, Neviani et al., 2007). Similarly, SET targeting peptide OP449 is known to reactivate PP2A and was shown to enhance the efficacy of tyrosine kinase inhibitors in myeloid leukemia (Agarwal et al., 2014). Several natural compounds downregulating CIP2A have been reported, for instance ellagic acid contained in red wine was

reported to suppress CIP2A levels in lung cancer although convincing profiling of direct engagement of the target by the compounds is still lacking (Duan et al., 2019). The natural product celastrol induced degradation of CIP2A via CHIP E3 ubiquitin ligase, while its biotinylated derivative was shown to bind to CIP2A in cell lysate (Liu et al., 2014).

PP2A reactivating approach by so-called small molecule activators of PP2A (SMAPs) was pioneered by the Narla group, by re-purposing tricyclic neuroleptics such as phenothiazines, for which potent on and off target effect was known (Kastrinsky et al., 2015). Phenothiazines are antagonists of dopamine D2 receptor with anti-cancer activity (Westermarck and Neel, 2020). Therefore, chemical optimization efforts aimed at improving anti-cancer properties whilst engineering out neuroleptic effects was pursued (Kastrinsky et al., 2015). SMAPs were shown to trigger cell death of K-Ras mutant lung cancer cell lines and to also inhibit tumor growth in a xenograft model (Sangodkar et al., 2017). SMAPs were shown to elicit their anti-cancer effects via PP2A, as presence of a small T antigen from simian virus (SV) 40, a well-established PP2A-binding viral protein, rendered cells resistant to SMAP effect (Sangodkar et al., 2017, Sablina and Hahn, 2008). Recently, crystal structure of the SMAP DT-061 in complex with PP2A-B56α holoenzyme was resolved (Leonard et al., 2020). DT-061 was shown to act as a “molecular glue” able to stabilize B56α-containing PP2A heterotrimers. The binding site for the compound was shown to be at the interface of all three PP2A subunits (Leonard et al., 2020). This demonstrated that in spite of high similarity between different subunits of the same B regulatory family, isoform-specific compounds can be designed (Leonard et al., 2020). Furthermore, high-throughput drug screen using 230 kinase inhibitors across two K-Ras mutated lung cancer cell lines showed that PP2A activation status determines response to MEK inhibitors (Kauko et al., 2018). Inhibition of PP2A by siRNA against the A subunit led to an increase in the activation of PI3K/AKT pathway and rendered resistance to MEK and ERK inhibitors (Kauko et al., 2018). Subsequently, activation of PP2A by siRNA against its inhibitory protein CIP2A sensitized cells to these inhibitors, with synergistic effects observed in the co-treatment with SMAPs (Kauko et al., 2018).

AIMS AND OBJECTIVES

2. AIMS AND OBJECTIVES

The development of therapeutics that directly target K-Ras has been largely unsuccessful until recently with the advent of the G12C inhibitors (Ostrem et al., 2013, Moore et al., 2020, Janes et al., 2018). Still, the majority of K-Ras mutations are not G12C mutated thus not amenable to covalent modification (Moore et al., 2020). Furthermore, the development of resistance mechanisms against these covalent inhibitors have already been report (Dunnett-Kane et al., 2021, Xue et al., 2020, Tanaka et al., 2021). Hence, the need to explore alternative approaches including targeting of Ras membrane trafficking chaperones as well as the adoption of multiple synergistic therapeutic strategies that may effectively block Ras mediated signaling output remain relevant.

In this thesis work, I contribute to the development and characterization of novel inhibitors of K-Ras trafficking chaperones PDE6D and CaM respectively Deltaflexins and Calmirasone1. I also show that the synergistic inhibition of CaM and re-activation of the tumor suppressor PP2A with small molecules improved anti-cancer effects on Ras-MAPK dependent cancer cell lines and show that the phenothiazine fluphenazine mustard may act via this mechanism.

Therefore, the 3 main aims of this thesis work are:

1. The development and characterization of novel PDE6D inhibitors with improved resilience to Arl2 ejection and cell penetration.
2. The development and characterization of novel covalent CaM inhibitors with reduced unspecific cytotoxicity and improved K-Ras mediated anti-cancer effects.
3. The evaluation of the potential of phenothiazines to synergistically block CaM and reactivate PP2A in cancer cells.

MATERIALS AND METHODS

3.0 MATERIALS AND METHODS

3.1 MATERIALS

3.1.1 Cell lines

Table 1. List of cell lines used in thesis

Cell line	Tissue	Tumor type	Ras/MAPK Mutation	Project
MDA-MB-231	Breast	Metastatic adenocarcinoma	K-RasG13D	1, 2, 3
Hs 578T	Breast	Primary Carcinoma	H-RasG12D	1, 2
NCI-H358	Lung	Primary Carcinoma	K-RasG12C	1, 2, 3
MIA PaCa-2	Pancreas	Primary Carcinoma	K-RasG12C	2, 3
A375	Skin	Primary Melanoma	B-RafV600E	1, 2, 3
T24	Bladder	Primary Carcinoma	H-RasG12V	2, 3
HEK-293 EBNA	Human embryonic kidney	N/A	N/A	1, 2, 3
HeLa	Cervix	Primary Adenocarcinoma	N/A	2, 3
MDCK	Kidney (dog)	N/A	N/A	2

3.1.2 Plasmids, siRNAs & Primers

Table 2. Plasmids, siRNAs & Primers

Plasmid / siRNAs / Primers	Project
pDest305-CMV-Rluc8-K-RasG12V	2, 3
pDest305-CMV-Rluc8-H-RasG12V	2, 3
pDest305-CMV-GFP2-K-RasG12V	2, 3
pDest305-CMV-Rluc8-K-RasG12C	2
pDest305-CMV-Rluc8-K-RasG13D	2
pDest305-CMV-Rluc8-K-RasQ61H	2
pDest305-CMV-Rluc8-K-Ras	2
pDest305-CMV-Rluc8	2
pDest305-CMV-GFP2-H-RasG12V	2, 3
pDest312-CMV-CaMwt-GFP2	2, 3
pDest527-His-wtCaM	2
pDest527-His-mtCaM	2
pmGFP-K-RasG12V and pmCherry-K-RasG12V	1
pmGFP-H-RasG12V and pmCherry-H-RasG12V	1

mCit-Rheb and mCherryPDE6D	1
siRNA-CALM1	2
siRNA-KRAS	2
siRNA-HRAS	2
KRAS, forward 5'- tacagtgcaatgagggacca-3', reverse 5'- tcctgagcctgttttgtgtct-3'	2
HRAS, forward 5'- ctgaccatccagctgatcca-3', reverse 5'- tggcaaacacacacaggaag-3'	2
CALM1, forward 5'- gctcgcaccatggctgat-3' , reverse 5'- tgttgggttctgacccagtg-3'	2
ACTB , forward 5'-ggggtgttgaaggtctcaaa-3'; reverse 5'- ggcatcctcaccctgaagta-3'	2

3.1.3 Reagents

Table 3. Reagents

Reagent	**Application**	**Project**
RPMI	Cell Culture	1, 2, 3
DMEM	Cell Culture	1, 2, 3
FBS	Cell Culture	1, 2, 3
L-Glutamate	Cell Culture	1, 2, 3
DMSO	Cell Culture, Compound Profiling	1, 2, 3
B27	Cell Culture	1, 2, 3
EGF	Cell Culture, Western Blotting	1, 2, 3
PFA	FLIM-FRET, Confocal Microscopy	1, 2, 3
JetPRIME	FLIM-FRET, BRET	1, 2, 3
MethoCult H4100	2D Monolayers, 3D Spheroids	1, 2, 3
RIPA buffer	Western Blotting	1, 2, 3
AlamarBlue	2D Monolayers, 3D Spheroids	1, 2, 3
BSA	Western Blotting	1, 2, 3
LR clonase	Gateway Cloning	2, 3
Mini-prep and Midi-prep kits	Gateway Cloning	2, 3
Nitrocellulose membrane	Western Blotting	1, 2, 3
Stained protein ladder	Western Blotting	1, 2, 3
RNAiMax	Gene Knockdown	2
Lipofectamine	Gene Knockdown	2

3.1.4 Antibodies

Table 4. Antibodies

Antigen	Manufacturer	Project
PDE6D	Santa Cruz Biotechnology	1
Actin	Sigma-Aldrich	1
CALM1	Cell Signaling	2
GAPDH	Sigma	2, 3
ERK1/2	Cell Signaling	2, 3
pERK1/2	Santa Cruz Biotechnology	2, 3
Anti-mouse	LI-COR	2, 3
Anti-rabbit	LI-COR	2, 3

3.1.5 Inhibitors

Table 5. Inhibitors

Compound	Source	Catalogue Number	Project
ophiobolin A	Santa Cruz	sc-202266	2, 3
mevastatin	Alfa Aesar	J61357	2
FTI-277	BioVision	2874	2, 3
prostratin	Sigma-Aldrich	P0077	2
calmidazolium	Santa Cruz	sc-201494	2, 3
AMG-510	MedChem Express	HY-114277	2, 3
vemurafenib	Selleckchem	S1267	1, 2
benzethonium chloride	Sigma-Aldrich	53751	1, 2, 3
Deltarasin	Selleckchem	S7224	1
ARS-1620	Medchem express	HY-U00418	1, 3
Fluphenazine	sigma	F0280000	3
Fluphenazine Mustard	Enzo	BML-CA325-0050	3
Trifluoperazine	cayman vwr	15068	3
DT-061	Selleckchem	S8774	3
Trametinib	Bio-connect	SC-364639	2, 3

3.2 METHODS

Most methods employed in this thesis are described in the corresponding manuscripts (Siddiqui et al., 2020), (Okutachi et al., under revision) **(Table 6)**. The methods described here are either critical methods employed in this thesis or part of the methods used in the additional unpublished data.

3.2.1 List of Published methods

Table 6. List of published methods

Name of Method	Manuscript
FLIM-FRET assays for PPI analysis	(Siddiqui et al., 2020)
Confocal Microscopy	(Siddiqui et al., 2020), Okutachi et al., under review
SPR for PPI analysis	(Siddiqui et al., 2020)
2D monolayers	(Siddiqui et al., 2020), Okutachi et al., under review
3D spheroids	(Siddiqui et al., 2020) Okutachi et al., under review
RT-qPCR	(Siddiqui et al., 2020) Okutachi et al., under review
FP assay	(Siddiqui et al., 2020) Okutachi et al., under review
ATARiS Gene sensitivity score	(Siddiqui et al., 2020) Okutachi et al., under review
Composite drug activity score	Okutachi et al., under review
Drug sensitivity score (DSS) analysis	Okutachi et al., under review
Western Blotting	Okutachi et al., under review
Protein purification	Okutachi et al., under review
BRET assay	Okutachi et al., under review

3.2.2 Overview of the BRET method

Protein-protein interactions are critical for almost all biological processes and a number of techniques have been developed to evaluate these dynamic processes. Bioluminescence resonance energy transfer (BRET) is a form of resonance energy transfer (RET) which relies on the non-radiant energy transfer from the light emitted through the luciferase mediated conversion of a light emitting substrate coelenterazine (James et al., 2006). The first version of the BRET technology developed by Xu et al., used *Renilla luciferase* (Rluc) as the bioluminescent energy donor with its substrate being coelenterazine h and an enhanced yellow fluorescent protein (EYFP) as the acceptor (Xu et al., 1999). However, the technology has since expanded to include a sizable collection of donor-acceptor systems in both live cell and in vivo applications (Dale et al., 2019). Upon co-expression of the protein pairs, the transfer of energy in BRET depend upon the critical factors such as the proximal distance between the BRET pairs, the relative orientation of the BRET pairs as well as the spectral properties of the BRET pairs **(Figure 19)** (El Khamlichi et al., 2019, Bacart et al., 2008).

The distance between the BRET pairs is inversely proportional to the resonance energy transfer. Hence, BRET decreases as the distance between the acceptor and donor pairs increase from 10 to 100 Å (1 to 10 nm) (El Khamlichi et al., 2019, Bacart et al., 2008). Secondly, BRET pairs must have a spectral overlap between the emission spectrum of the donor and the excitation spectrum of the acceptor (El Khamlichi et al., 2019). A third condition for BRET is the maintenance of an aligned spatial orientation of the BRET pairs due to the dipole-dipole nature of the resonance energy transfer process **(Figure 19)** (El Khamlichi et al., 2019, Bacart et al., 2008).

BRET differs from foster resonance energy transfer (FRET) in a number of ways. For instance, unlike FRET which must be excited by monochromatic light for signal generation, BRET does not require external illumination. Hence, the quantification of energy transfer is easier in BRET than in FRET (Boute et al., 2002). in BRET, the relative expression of the biosensors can be independently quantified by measuring the luminescence of the donor and fluorescence of the acceptor (Boute et al., 2002). Another challenge of FRET is the photo-bleaching of the donor fluorophore due to repeated exposure to light, this results in the overall loss of signal over time (Boute et al., 2002).

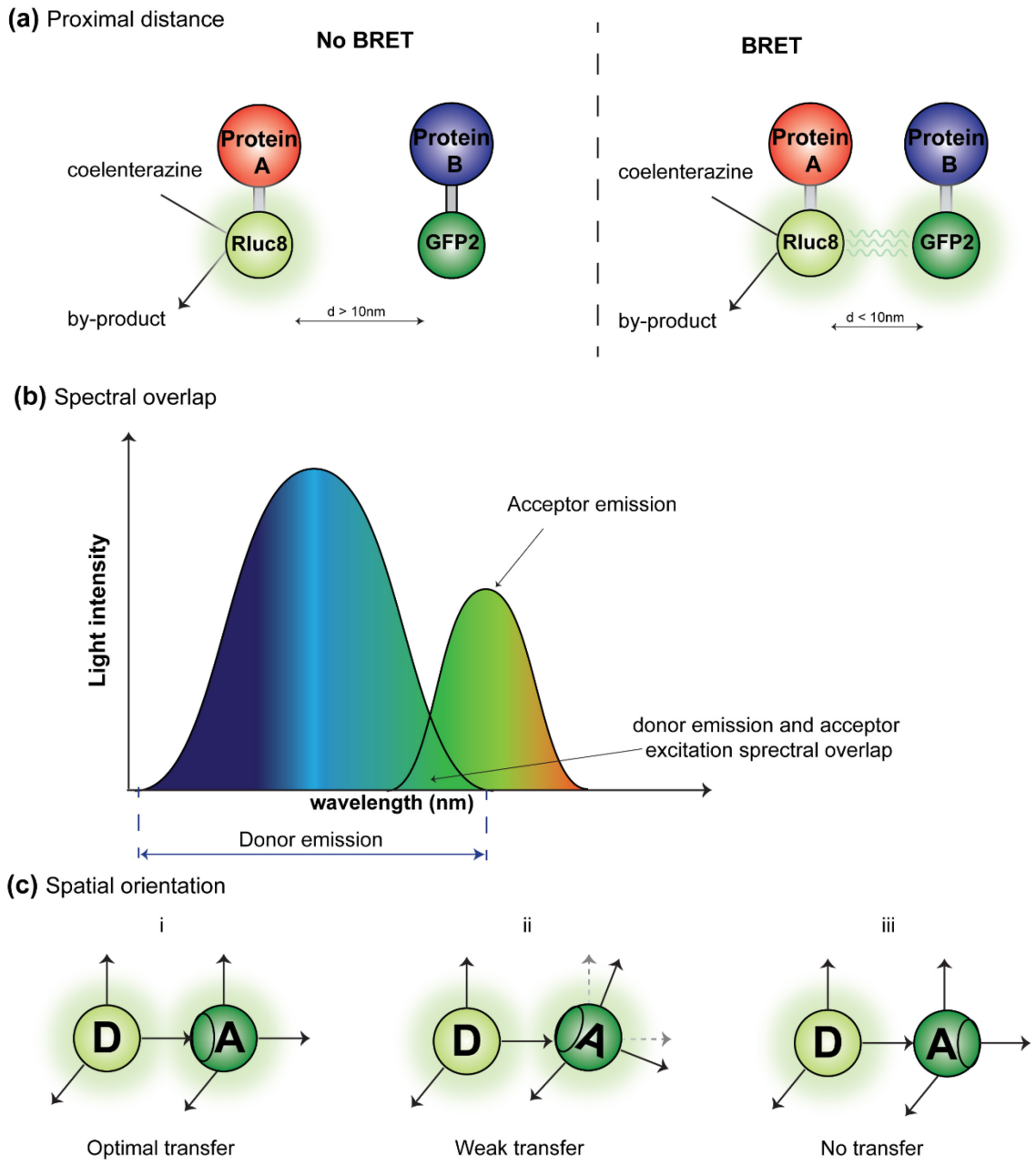

Figure 19. Schematic illustration of the conditions for BRET

Schematic illustrations of critical conditions for BRET based energy transfer. ***(a)*** *Donor luminophore (Rluc8) must be within a 10nm proximal distance to the acceptor fluorophore (GFP2).* ***(b)*** *The donor emission spectral wavelength must overlap with the acceptor excitation wavelength for BRET to occur.* ***(c)*** *Donor and acceptor must maintain an aligned spatial orientation for BRET to occur due to the dipole-dipole nature of the resonance energy transfer process.*

Multiple BRET systems including BRET1, BRET2, eBRET2, BRET3 and quantum dots (QDs) BRET have been developed (Bacart et al., 2008). Each system is compatible with different donor-acceptors pairs and diverse experimental applications including, live cell imaging, in vivo imaging, drug screening etc. (Bacart et al., 2008). The BRET 1 system uses coelenterazine h (benzyl-coelenterazine) as a substrate for the luciferase. The maximum emission of Rluc was observed at 480nm and this wavelength is particularly suited for the excitation of a yellow fluorescent protein (YFP) variant named enhanced YFP (EYFP) at 530nm. This system have been applied for the screening of compounds as well as for cell imaging experiments (Bacart et al., 2008). The BRET2 system which improves upon BRET1 uses DeepBlueC™ (Coelenterazine 400a), a chemical derivative of coelenterazine h which shifts the emission maximum of Rluc to 395nm. The optimal acceptors for this system are GFP2 and GFP10 with excitation and emission maxima of 400 and 510nm respectively. BRET2 offers the advantage of having a better separation of the spectra of the donor and acceptor emission peaks (Bacart et al., 2008). Consequently, BRET2 is superior to BRET1 particularly in compound screening applications where low signal to background ratios are desired (Bacart et al., 2008). However, DeepBlueC™ exhibits a 300-fold lower capacity for light emission thus requiring the overexpression of a conjugated luciferase protein (Hamdan et al., 2006). To overcome this limitation, an enhance version of Rluc named Rluc8 (containing 8 amino acid substitutions) (Pfleger and Eidne, 2006). This new eBRET2 system achieves a 32-fold increase in quantum yield when DeepBlueC™, and leads to a 5.5-fold improvement in the BRET signal in addition to the strong spectral resolution of the standard BRET2 system (Pfleger and Eidne, 2006, Bacart et al., 2008). eBRET2 is widely used in compound screening and drug discovery projects, live cell imaging and in vivo experiments due to the advantages pointed out (De et al., 2007, Xu et al., 2007, Massoud et al., 2007, Bacart et al., 2008). The application of BRET in Ras protein-protein interaction studies have recently led to the identification of Ras-Raf interface inhibitors (Bery et al., 2018, Bery and Rabbitts, 2019). Indeed, these new tools will allow for the identification of small molecules capable of disrupting Ras isoform specific interactions. In this thesis, we have generated Ras isoform biosensors as well as biosensors for the assessment of the K-Ras/CaM interaction based on the eBRET2 system. We validated their suitability for the screening of small molecules and found the technique to be robust and high-throughput amenable.

3.2.3 BRET assay

BRET assays were extensively used in this thesis for the evaluation of protein-protein interactions and the effects of inhibitors on the stated interactions. The BRET experiments were essentially performed as described by others (Bery et al., 2018, Lavoie et al., 2013). About 100,000 to 150,000 HEK293-EBNA cells were seeded per well of a 12-well plate in 1 mL of DMEM containing 10% FBS and 2 mM L-glutamine and were grown for 24 h. Next day, Rluc8-tagged donor and GFP2-tagged acceptor constructs were transfected into cells using jetPRIME transfection reagent. Each well was transfected with about 1 µg of plasmid DNA using 3 µL of jetPRIME reagent. For BRET donor saturation titration experiments, the concentration of donor plasmid (25 ng) was kept constant and the concentration of acceptor plasmid was increased from 0 to 500 ng for Ras-G12V BRET pairs and 0 to 1000 ng for K-Ras/ CaM BRET pairs. The empty pcDNA3.1(-) plasmid was used to top-up the total DNA load per transfection. After 24 h of transfection, cells were treated with compounds or vehicle control (DMSO 0.2% v/v in growth medium) at the specified concentration for 24 h or the stipulated time period in case of the time-course experiments.

The cells from one well of a 12-well plate were collected, washed, and re-plated in PBS on flat bottom, white 96-well plates as four technical replicates containing 90 µL of cell suspension per well. Then fluorescence intensity followed by BRET readings were carried out on Clariostar plate reader at 25 °C. The fluorescence intensity (RFU) of GFP2 was measured with excitation at 405 ± 10 nm and emission 515 ± 10 nm; it is proportional to the acceptor concentration [acceptor]. BRET readings were taken well by well by adding 10 µL of 100 µM coelenterazine 400a, the Rluc8 substrate to each well using the injector present in the plate reader. Luminescence emission intensities were simultaneously recorded at 410 ± 40 nm (RLU, proportional to [donor]) and 515 ± 15 nm (BRET signal).

The raw BRET ratio was calculated as the BRET signal measured at 515 nm divided by emission signal measured at 410 nm (RLU). The BRET ratio was obtained by subtracting the raw BRET ratio by a background BRET signal measured for cells expressing only the donor (Bacart et al., 2008) as indicated in the formula below,

$$BRET\ ratio = \frac{\lambda em\ 515\ nm_{(donor+acceptor)}}{\lambda em\ 410\ nm_{(donor+acceptor)}} - \frac{\lambda em\ 515\ nm_{(donor\ only)}}{\lambda em\ 410\ nm_{(donor\ only)}}$$

With *donor+acceptor* denoting cells transfected with the BRET pair and *donor only* being cells expressing only the donor.

The expression of acceptor relative to donor ([acceptor]/[donor]) was determined as, $relative\ expression = \frac{RFU}{RLU}$

For BRET donor saturation titration experiments, the BRET ratio was plotted against the ratio of acceptor to donor plasmid amounts (A/D plasmid ratio) that were transfected or the relative expression. The A/D plasmid ratio at which the BRET ratio changes most linearly with the relative expression was determined for each BRET sensor and then used for testing compound treatments. The BRET ratio vs relative expression data were fit into a binding saturation equation in the Prism (GraphPad) software to obtain the $BRET_{max}$ and $BRET_{50}$ using the equation, $y = \frac{BRET_{max} \times x}{BRET_{50}+x}$, where x is the relative expression and y is the BRET ratio. The $BRET_{max}$ represents the maximum saturation BRET signal and depends on structural parameters (distance, orientation) of the BRET complex. $BRET_{50}$ corresponds to the ratio of acceptor construct over donor construct required to attain 50% of the maximum BRET signal and is a measure of the effective relative affinity between the interacting BRET pair (Marullo and Bouvier, 2007).

3.2.4 Drug sensitivity score (DSS) analysis

The quantitative profiling of the drug sensitivities of the various cell lines used in this thesis was evaluated with the drug sensitivity score (DSS) analysis. DSS values are essentially normalized area under the curve (AUC) measures of dose-response inhibition data which provide a more robust representation of drug activity compared to the classic EC_{50} and IC_{50} curvess (Yadav et al., 2014). Drug response data files (in Excel) ready for online analysis were prepared according to the example file obtained from the DSS pipeline website, called Breeze (https://breeze.fimm.fi/) (Potdar et al., 2020). Either raw fluorescence intensity measurements or normalized % inhibition data (for BRET assay analysis) were uploaded.

The output file provides several drug sensitivity measures including EC_{50} and AUC. We plotted the DSS_3 value (Yadav et al., 2014), which was calculated as

$$DSS_3 = DSS_2 \frac{x_2 - x_1}{C_{max} - C_{min}}$$

Where DSS_2 is given by the equation $DSS_2 = \frac{DSS_1}{\log a}$

and DSS_1 is given by the equation $DSS_1 = \frac{AUC - t(x_2 - x_1)}{(100-t)(C_{max} - C_{min})}$

DSS_3 was employed to emphasize drugs that obtain their response area over a relatively wide dose window, as compared to drugs that show increased response only at the higher end of the concentration range. After logistic fitting of the dose-response inhibition data, the area under the curve (AUC) was determined as exact solution. A 10% minimal activity threshold (t) was set. The

maximum (C_{max}) and minimum (C_{min}) concentrations were used for screening of the inhibitors, with $C_{max} = x_2$ and x_1 concentration with minimal activity t. The parameter a is the value of the top asymptote, which is different from 100% inhibition as obtained from 100 µM benzethonium chloride treatment.

3.2.5 Synergism experiments and Bliss scoring

To access the synergistic potential of our compounds, we performed a full dose response analysis of one agent (calmidazolium) and maintained a fixed concentration of the other inhibitor (DT-061, either 1 or 2 µM). The drug response profiles obtained for the various combinations in the cell lines were then compared against the profiles of each single agent using the SynergyFinder platform. SynergyFinder (https://synergyfinder.fimm.fi) is a stand-alone web-application for interactive analysis and visualization of drug combination screening data (Ianevski et al., 2020). We employed the Bliss model (Bliss, 1939). Which generates the multiplicative effects of single agents as if they acted independently in scoring our pairwise combinations

$S_{BLISS} = E_{A,B,\ldots,N} - (E_A + E_B + \ldots + E_N - E_A E_b - E_A E_N - E_B E_N - \ldots - E_A E_B \ldots E_N)$.

Here, $E_A, E_B, \ldots, E_N$ are the measured responses of the single drugs, while *b* are the doses of the single drugs required to produce the combination effect $E_{A,B,\ldots,N}$.

3.2.6 Western blotting

MiaPaCa-2 cells were lysed cell lysis buffer (50 mM Tris, 150 mM NaCl, 0.1% SDS, 1% triton, 1% NP40 and a Roche tablet for 10 ml lysis buffer volume) and incubated on ice for 30 min. Cell lysates were mixed with Laemmli buffer with 0.1% bromophenol blue heated for 5 min at 95°C and resolved on a 12% home-made gel. Proteins were subsequently transferred to a membrane using the Trans®-Blot® Turbo® Transfer system (BIO-RAD). The blotted membranes were incubated for 1 h in blocking buffer (5% BSA in Tris-buffered saline (TBS)–T (Tween 0.1%) and treated with primary antibodies for pERK 1:400 (Santa cruz, sc-81503), ERK 1:1000 (Cell Signaling, 9102) A mouse antibody against GAPDH 1:2000 (Sigma, G8795) was used for housekeeping gene control. After overnight incubation, the membrane was washed 3× 5 min in TBS–T buffer the following day and then treated with the corresponding anti-rabbit and anti-mouse secondary antibodies (1:10000 dilutions). The proteins were detected using a LI-COR ODYSSEY CLx system (Westburg). The level of proteins was densitometrically quantified from western blot membranes using ImageLab software (BIO-RAD).

RESULTS

4.0 RESULTS

4.1 PDE6D inhibitor with a new design principle selectively block K-Ras activity

Farid A. Siddiqui, Catharina Alam, Petja Rosenqvist, Mikko Ora, Ahmed Sabt, Ganesh babu Manoharan, Lakshman Bindu, **Sunday Okutachi,** Marie Catillon, Troy Taylor, Omaima M. Abdelhafez, Harri Lönnberg, Andrew G. Stephen, Anastassios C. Papageorgiou, Pasi Virta and Daniel Abankwa.

4.1.1 Manuscript 1: Summary

Ras mutations are present in about 19% of all solid malignancies worldwide (Prior et al., 2020). Despite the recent successes with covalent direct K-RasG12C inhibitors, a majority of K-Ras mutated malignancies remain undrugged. PDE6D is a trafficking chaperone of K-Ras and other prenylated proteins capable of modulating the dynamic localization of K-Ras to the plasma membrane where it is required for signaling (Chandra et al., 2011). Small molecules developed against PDE6D have shown promise in in vitro and in vivo studies (Papke et al., 2016, Zimmermann et al., 2013, Martin-Gago et al., 2017). However, the PDE6D cargo ejection process mediated by Arl2 also results in the undesirable removal of these compounds from PDE6D (Martin-Gago et al., 2017). By increasing the hydrogen-bonding capabilities of these compounds, some improvements were made but the lingering challenge of ejection still persists (Martin-Gago et al., 2017).

In this study, our goal was to develop PDE6D inhibitors with improved resilience to the Arl2-mediated unloading whilst improving cell penetration and overall anti-cancer activity. To this end, we proffered an alternative design strategy for PDE6D inhibitors. We engineered a “chemical spring” consisting of a flexible hexyl linker into these new inhibitors to minimize prenyl pocket ejection and attached a cell penetrating group to improve cellular uptake and cellular potency. A small collection of compounds was generated and assessed in assays such as surface plasmon resonance (SPR) and fluorescence polarization for evaluating compound binding to PDE6D. Flourescence life-time imaging based FRET (FLIM-FRET) was used for the evaluation of isoform specific inhibitory properties of the compounds whilst target engagement of the compounds was

evaluated in a K-Ras/PDE6D FRET assay. The 3D spheroid assay was utilized for evaluating their effects on K-Ras driven stemness characteristics.

Collectively, our results identified **Deltaflexin 1** and **Deltaflexin 2** as selective disruptors of K-Ras but not H-Ras membrane organization. These compounds also showed anti-cancer effects on K-Ras driven cancer cell lines of lung, breast and colon origins. Importantly, our compounds showed selectivity for inhibiting K-Ras driven stemness characteristics as compared to the B-Raf-V600E mutant melanoma cell line. Although this generation of our compounds showed low overall cellular potency to proceed as viable drug candidates, the novel design principle proves to be useful in minimizing Arl2-mediated ejection and will form the basis for our next generation Deltaflexins drug development efforts.

4.1.2 Manuscript 1: Personal contributions of Sunday Okutachi

- Designed, performed and analysed the sphere formation and cell proliferation experiments
- Designed and generated figure 4E
- Analysed and generated the ATARiS gene dependency profiling of the cell lines (SI figure 3G)
- Involved in discussions and drafting of corresponding data contribution

The personal contributions of all authors to the manuscript are listed in the *Authors' contributions* Section at the end of the corresponding manuscript.

ACS OMEGA

Article

Cite This: ACS Omega 2020, 5, 832−842

http://pubs.acs.org/journal/acsodf

PDE6D Inhibitors with a New Design Principle Selectively Block K-Ras Activity

Farid A. Siddiqui,[†] Catharina Alam,[†] Petja Rosenqvist,[§] Mikko Ora,[§] Ahmed Sabt,[§,∥] Ganesh babu Manoharan,[‡] Lakshman Bindu,[⊥] Sunday Okutachi,[‡] Marie Catillon,[‡] Troy Taylor,[⊥] Omaima M. Abdelhafez,[∥] Harri Lönnberg,[§] Andrew G. Stephen,[⊥] Anastassios C. Papageorgiou,[†] Pasi Virta,[§] and Daniel Abankwa*[,†,‡]

[†]Turku Bioscience Centre, University of Turku and Åbo Akademi University, 20520 Turku, Finland

[‡]Cancer Cell Biology and Drug Discovery Group, Life Sciences Research Unit, University of Luxembourg, 4362 Esch-sur-Alzette, Luxembourg

[§]Department of Chemistry, University of Turku, 20014 Turku, Finland

[∥]Chemistry of Natural Compounds Department, National Research Centre, Dokki, 12622 Giza, Egypt

[⊥]NCI RAS Initiative, Cancer Research Technology Program, Frederick National Laboratory for Cancer Research, 21702 Frederick, Maryland, United States

Supporting Information

ABSTRACT: The trafficking chaperone PDE6D (also referred to as PDEδ) has been nominated as a surrogate target for K-Ras4B (hereafter K-Ras). Arl2-assisted unloading of K-Ras from PDE6D in the perinuclear area is significant for correct K-Ras localization and therefore activity. However, the unloading mechanism also leads to the undesired ejection of PDE6D inhibitors. To counteract ejection, others have recently optimized inhibitors for picomolar affinities; however, cell penetration generally seems to remain an issue. To increase resilience against ejection, we engineered a "chemical spring" into prenyl-binding pocket inhibitors of PDE6D. Furthermore, cell penetration was improved by attaching a cell-penetration group, allowing us to arrive at micromolar in cellulo potencies in the first generation. Our model compounds, Deltaflexin-1 and -2, selectively disrupt K-Ras, but not H-Ras membrane organization. This selectivity profile is reflected in the antiproliferative activity on colorectal and breast cancer cells, as well as the ability to block stemness traits of lung and breast cancer cells. While our current model compounds still have a low in vitro potency, we expect that our modular and simple inhibitor redesign could significantly advance the development of pharmacologically more potent compounds against PDE6D and related targets, such as UNC119 in the future.

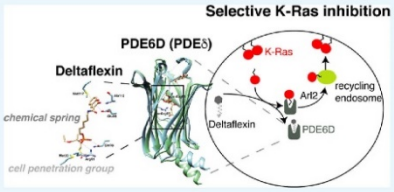

INTRODUCTION

The oncogene Ras is one of the best-established cancer targets without an approved inhibitor. Ras drug development efforts in the 1990s were thwarted by the failure of farnesyltransferase inhibitors (FTI) in clinical trials.[1] At that time, it was underappreciated that the highly mutated K-Ras and N-Ras can be alternatively prenylated by geranylgeranyltransferase I, reinstating Ras plasma membrane localization and thus activity, even in the presence of FTIs.[2]

Recently, there has been a resurgence in Ras drug development, with both direct and indirect targeting approaches.[3] The Shokat group has pioneered direct, covalent inhibitors that target a switch II pocket in GDP-bound K-RasG12C.[4] Efficacy of these compounds relies on the intrinsic GTPase activity of that mutant and trapping of an inhibitor-bound inactive state.[5] Therefore, inhibitor efficacy can be increased by enriching the cellular pool of GDP-bound K-RasG12C, such as through inhibition of upstream receptor tyrosine kinases (e.g., EGFR, FGFR1, AXL) or Ras/Sos1 inhibitors, such as BAY-293.[6]

Switch II pocket inhibitors have rapidly evolved[7] and are now in clinical trials.[8] Thus, it is for the first time possible to assess the effect of selectively targeting a driver oncogene. While lung cancer patient data are encouraging, the durable responses and adaptive immunity that is seen in animal models are striking and may indicate the significance of K-Ras inhibition for curing cancer.

Given that other mutant K-Ras alleles are not targeted by these covalent inhibitors, different K-Ras inhibition approaches are still needed. Therefore, other noncovalent Ras binders with inhibitory potential remain interesting. They were typically discovered by computational approaches, such as the Kobe-compounds or pyrazolopyrimidine allosteric compounds, which block Ras-effector interaction and have micromolar cellular potencies.[9,10]

Received: October 29, 2019
Accepted: December 9, 2019
Published: December 23, 2019

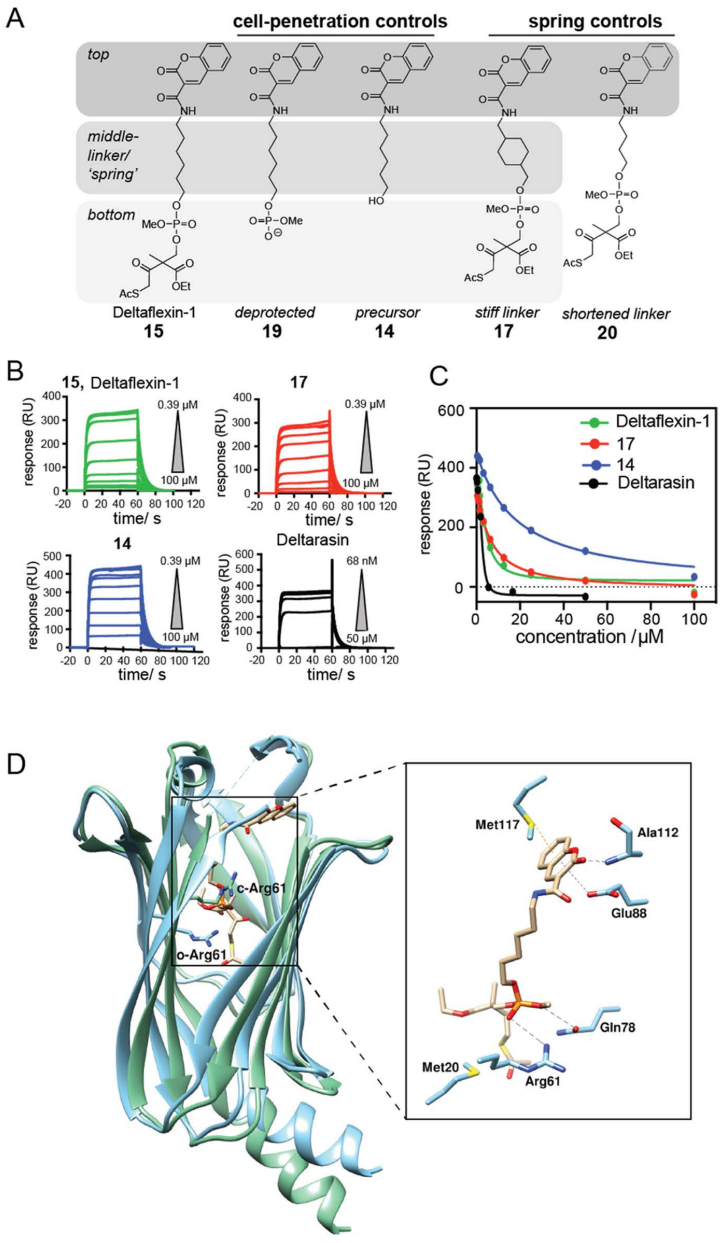

Figure 1. Newly designed inhibitors compete with K-Ras for PDE6D in vitro. (A) Design of Deltaflexin compounds, where in the first generation a generic heterocycle "top" was linked via a flexible hexyl "spring" to the protected phosphodiester "bottom". (B) SPR data of Deltarasin and compounds **15** (Deltaflexin-1), **14** and **17**; $n = 3$. N-terminal avi-tagged K-RasFMe was captured on a neutravidin sensor chip and the inhibitory activity of compounds for the PDE6D/avi-K-RasFMe interaction was measured. (C) Dose−response curve of Deltarasin and compounds **15** (Deltaflexin-1), **14** and **17** from the SPR data. (D) Docked structure of Deltaflexin-1 into the crystal structure of PDE6D in the open (cyan, PDB code 4JV8) and Arl2-GTP-bound, closed state (green, PDB code 1KSJ). Right shows details of PDE6D (open) residues in proximity of docked Deltaflexin-1.

The indirect target PDE6D is a trafficking chaperone of farnesylated proteins, which may suggest that its inhibition affects the same clients as inhibition of farnesyltransferase. However, PDE6D has a different client profile than farnesyltransferase, as it cannot facilitate intracellular diffusion of proteins that are also palmitoylated.[11,12] Moreover, PDE6D has the potential to accommodate geranyl-geranylated clients.[12] Thus, PDE6D inhibition selectively affects K-Ras4B (hereafter

DOI: 10.1021/acsomega.9b03639
ACS Omega 2020, 5, 832−842

K-Ras) trafficking but has much less effect on trafficking of dual-palmitoylated H-Ras.[11,13]

In order to relay signaling, K-Ras needs to be localized predominantly to the plasma membrane. This requires energy-dependent vesicular transport of K-Ras to the plasma membrane from the recycling endosome, where it is collected after PDE6D-assisted diffusion from internal cellular membranes.[11,13] Unloading of K-Ras from PDE6D in the perinuclear compartment requires the binding of GTP-Arl2 to PDE6D, which results in an allosteric conformational change in PDE6D that effectively releases its cargo.[14] Unfortunately, this ejection mechanism also applies to the first two generations of PDE6D inhibitors Deltarasin[15] and Deltazinone,[16] developed by the Waldmann group. Only their third generation of PDE6D inhibitors, the Deltasonamides, can largely withstand Arl2-mediated ejection, as they were highly optimized for sub-nanomolar affinity. However, these compounds have a low partitioning coefficient, suggesting low cell penetration.[17] Unfortunately, this theme of micromolar cellular potency, despite nanomolar affinity to the target in vitro, also continues with more recent PDE6D inhibitors that emerged through substantial fragment-based discovery and structure-based virtual screening efforts by the Xiong and Sheng groups.[18]

In order to advance PDE6D inhibitor development, it may therefore be necessary to change the overall concept, as the discovery of various chemotypes with high in vitro affinity has been well demonstrated. We here present Deltaflexins, which have only micromolar in vitro, yet also micromolar in cellulo potencies. We have overcome the approximately 1000-fold in vitro to in cellulo potency gap, by employing an innovative compound engineering approach.

RESULTS AND DISCUSSION

Generic Design of PDE6D Inhibitors with a Flexible Hexyl-Linker and Cleavable Cell Penetration Group. In order to improve the resilience of inhibitors against Arl2-mediated ejection from the PDE6D prenyl-binding pocket, a flexible hexyl linker that was envisaged to act like a buffering spring, was attached to a moiety that would provide major contacts to the "top" of the pocket. The design was completed by a simple phosphodiester "bottom" moiety, which was protected with a previously developed cell penetration group that was tunable for pharmacological stability.[19,20] In our first-generation model compound, Deltaflexin-1 (**15**), the generic, heterocylic coumarin was chosen as "top"-moiety, as it would allow for H-bonding and π-stacking (Figure 1A). In addition, a panel of seven control compounds was synthesized that allowed us to assess the contribution of each of the design elements (Figures 1A, S1A).

In order to validate the inhibitory activity of the compounds on the PDE6D/K-Ras interaction, we established a surface plasmon resonance (SPR) assay. Farnesylated and carboxymethylated K-Ras (K-RasFMe) were captured on the sensor chip surface via an avi-tag, and the binding of PDE6D was measured (K_d PDE6D/avi-K-RasFMe = 3.6 ± 0.1 μM) (Figure S1B, Table 1). Deltaflexin-1 (**15**) bound with a surprisingly good, low micromolar K_d that was only 2.6-fold higher than what we determined for Deltarasin (Figure 1B,C, Table 1). This was encouraging given that this was the first generation of compounds. Importantly, the control compound **17** with a "stiff", methyl cyclohexylmethyl linker had essentially the same affinity to PDE6D as compound **15** and therefore represented an excellent control for testing the significance of the flexible hexyl linker later on in cells (Figure 1C, Table 1). The relatively hydrophobic **14**, which lacked the cell-penetration bottom-moiety exhibited a reduced binding activity (Figure 1C, Table 1). Surprisingly, compound **19** the phosphorylated (charged) derivative of **14** showed an increase in the SPR response, suggesting stabilization of the PDE6D/avi-K-RasFMe complex. Direct target binding data were corroborated by a previously published fluorescence anisotropy (FA) assay, which detects displacement of a fluorescently labeled, farnesylated peptide derived from the PDE6D client Rheb (F-Rheb)[14] (Figure S1C, Table S1).

Table 1. Inhibitory Activities of Deltaflexins and Control Compounds on Binding of PDE6D to avi-K-RasFMe as Determined by SPR

	inhibition of PDE6D/avi-K-RasFMe	
compound	IC_{50} ± SEM/μM	K_d ± SEM/μM
Deltarasin	1.9 ± 0.1	1.4 ± 0.1
15 (Deltaflexin-1)	4.87 ± 0.03	3.61 ± 0.02
19	inconclusive	
14	18.9 ± 0.2	14.1 ± 0.2
17	6.7 ± 0.1	4.97 ± 0.07
22	10.27 ± 0.03	7.62 ± 0.02
23 (Deltaflexin-2)	3.94 ± 0.03	2.92 ± 0.02

Computational docking of Deltaflexin-1 into the PDE6D crystal structure suggested that similar to the Deltasonamide derivatives, the phosphotriester bottom moiety of Deltaflexin-1 forms hydrogen bonds with Arg61 and Gln78, at the base of the PDE6D pocket (Figures 1D, S1D,E).[16,17] In addition, the top-moiety contacted Glu88, Ala112, and Met117. Therefore, three out of the seven contacts that were also engaged by the most optimized deltasonamide derivative (compound **8**[17]) were utilized by Deltaflexin-1, consistent with the overall similar positioning of the compound (Figure S1E). A comparison of Deltaflexin-1 docked into PDE6D in the open and closed (Arl2-bound) state illustrates that the potential steric clash between the protected phosphodiester at the bottom of the pocket and Arg61 would likewise persist (Figure 1D). However, the presence of the adjacent flexible hexyl linker may enable the protected phosphodiester bottom moiety of Deltaflexin-1 to evade this clash.

Deltaflexin-1 Disrupts K-Ras/PDE6D Interaction and K-Ras Membrane Organization in Cells. Next, we tested for on-target activity in cells, using a FRET-assay, which directly detects the interaction between K-RasG12V and PDE6D. Deltaflexin-1 significantly reduced the FRET to a level comparable to that of Deltarasin (Figure 2A). This activity was also seen with three derivatives that employed different chemical coupling between top and linker moieties, suggesting a notable degree of flexibility for compound synthesis (Figure S2A). By contrast, the control compound, **17**, with a "stiff" methyl-cyclohexylmethyl linker moiety, lacked in cellulo activity (Figure 2A), despite identical in vitro activity (Table 1). Likewise, **14** and **19** without the cell-penetration bottom-moiety did not block the interaction (Figure 2A). In support of the middle moiety requiring a specific length, shortening of the methylen-linker to four carbons abrogated the inhibitory activity in **20** (Figure 2A). Similar results were obtained using the previously described FRET-pair of PDE6D and another client, the farnesylated Ras-like GTPase Rheb (Figure S2B).[11]

PDE6D inhibition is expected to suppress K-Ras localization and activity more than H-Ras.[13] We therefore employed an

DOI: 10.1021/acsomega.9b03639
ACS Omega 2020, 5, 832−842

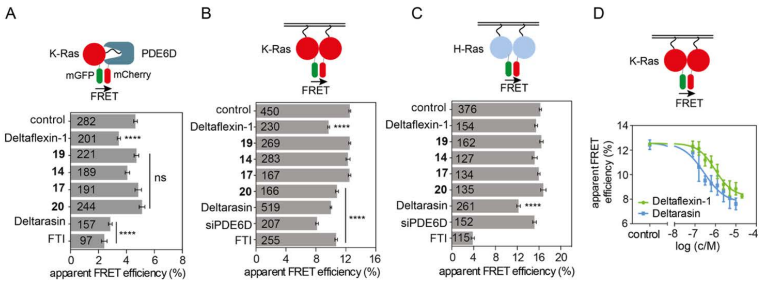

Figure 2. Deltaflexin-1 inhibits K-Ras/PDE6D interaction and selectively disrupts K-Ras membrane organization (A) PDE6D/K-Ras interaction by FLIM-FRET. HEK cells were co-transfected with mGFP tagged K-RasG12V and mCherry tagged PDE6D. Transfected cells were treated with 0.1% dimethyl sulfoxide (DMSO) control or 5 μM Deltaflexin-1, **17**, **14**, Deltarasin, or 500 nM FTI-277 for 24 h; $n = 3$. (B,C) Ras membrane organization measured with nanoclustering-FRET in HEK cells coexpressing mGFP or mCherry tagged K-RasG12V (B) or mGFP or mCherry tagged H-RasG12V (C). Cells were cotransfected with siRNA-PDE6D for 48 h or treated with 0.1% DMSO control, 5 μM Deltaflexin-1, **17**, **14**, Deltarasin, or 0.2 μM FTI-277 for 24 h; $n = 3$. (D) K-Ras nanoclustering-FRET dose response curve of Deltaflexin-1 or Deltarasin. Cells were treated for 24 h; $n = 3$. The numbers on the bars indicate numbers of analyzed cells. Graphs show mean values ± SEM. Statistical significance levels are annotated as ****$p < 0.0001$; ns, not significant.

additional cellular FRET-assay that detects FRET due to nanoscale clustering (nanoclustering-FRET) of Ras oligomers, including dimers, on the membrane.[21] We previously demonstrated that nanoclustering-FRET can quantify subcellular distribution changes that may be difficult to establish by confocal imaging (Figure S2C).[22,23] Thus, we confirmed that FTI selectively affects H-Ras membrane anchorage more than that of K-Ras, as the latter can be alternatively prenylated by geranylgeranyltransferase I[2,24] (Figure 2B,C). Given that rate-limiting steps of the PDE6D-mediated trafficking cycle selectively facilitate plasma membrane anchorage of K-Ras, but not H-Ras, knockdown of PDE6D selectively reduced the K-Ras but not H-Ras nanoclustering-FRET (Figures 2B,C and S2D). By contrast, the reference PDE6D-inhibitor, Deltarasin, reduced FRET of both Ras isoforms about equally. This indicates pan-Ras-directed, off-target effects of Deltarasin that may underlie its relatively high general toxicity.[16] Deltaflexin-1 on the other hand selectively reduced K-RasG12V but not H-RasG12V FRET as expected (Figure 2B,C). This was confirmed with the three linkage derivatives, further corroborating the flexibility at this position in our generic design (Figure S2E,F). Importantly, Deltaflexin-1 demonstrated an in cellulo potency in this FRET-assay [IC_{50}(**15**) = 1.65 ± 0.95 μM (mean ± standard error of the mean (SEM))] that was comparable to the in vitro affinity (K_d = 3.61 ± 0.02 μM), although it was not as potent as Deltarasin in cellulo [Figure 2D, IC_{50}(Deltarasin) = 0.7 ± 0.4 μM (mean ± SEM)].

Previous work suggested that the pharmacological stability of the cell penetration group can be tuned within the esterase cleavable *S*-acyl moiety by the electronegativity of the 2-substituent, such as ethoxycarbonyl (relatively labile) or methyl (more stable).[20] Indeed, heating of Deltaflexin-1 before application to cells decreased its cellular activity to a level similar to that of **14** or **19**, which both do not have the cell penetration group (Figure S2G).

In conclusion, these results demonstrate that the hexyl-spring and cell penetration group enable a similar in cellulo potency of Deltaflexin-1 as observed in vitro. Importantly, Deltaflexin-1 acts on-target in cells allowing for a selective inhibition of K-Ras activity, whereas the reference compound Deltarasin affects equally K-Ras and H-Ras.

Deltaflexin-1 Selectively Inhibits Oncogenic K-Ras Driven Cell Proliferation and Tumorosphere Formation. In order to further validate the K-Ras selectivity in cells, we examined the effect of Deltaflexin-1 and derivatives on 2D proliferation of colorectal cancer cell lines. Deltaflexin-1 inhibited the K-RasG13D mutated HCT116 (IC_{50} = 11 μM, CI 95% 8.1−16 μM) significantly more than the Ras wt HT-29 cell line (IC_{50} = 40 μM, CI 95% CI 25−72 μM, $p < 0.0001$) (Figure 3A,B). Similar micromolar activities and oncogenic K-Ras selectivity ($p < 0.0001$) were also seen in the K-RasG13D-mutated and -dependent MDA-MB-231 (IC_{50} = 7.2 μM, CI 95% 5.1−9.7 μM) and H-RasG12D-mutated and -dependent Hs 578T (IC_{50} = 21 μM, CI 95% 13−35 μM) breast cancer cell lines (Figure S3A,B,G). Both activity and K-Ras selectivity in colon and breast cancer cells were corroborated by Deltaflexin-1 linkage derivatives (Figure S3C−F).

Thus, half-maximal inhibition of K-Ras-mutant cancer cell viability by Deltaflexin-1 occurred at approximately 7- to 11-fold higher concentrations than in the cellular K-Ras nanoclustering-FRET assay, which also means that the in vitro and cancer cell inhibitory activities were very similar. By contrast, the difference between cellular inhibition and in cellulo on-target activity of the bis-sulfonamide inhibitor Deltasonamide 2 was 12- to 25-fold, while an even greater difference is apparent for this compound when compared to the in vitro affinity (650- to 1300-fold).[17] It is plausible to assume that the better in vitro/cell inhibition activity relation of Deltaflexin-1 compared to Deltasonamide 2 is due to its spring moiety.

While these results demonstrate selectivity for cancer cells expressing mutant K-Ras, the comparison of proliferation in 2D is not as discriminatory as the nanoclustering-FRET assay. However, in the past, we established that compounds which selectively decrease K-Ras-, but not H-Ras-nanoclustering-FRET, have a high potential as inhibitors of stemness properties of cancer cells, as measured by the formation of tumorospheres.[22,25] Accordingly, the selective effect of PDE6D on K-Ras but not H-Ras (Figure 2B,C) makes PDE6D a good target to enable such anticancer stemness activity. Indeed, tumorosphere formation of K-RasG12V, but not H-RasG12V transfected or control HEK cells,[26] was selectively decreased after knockdown of PDE6D (Figure S3H−J). Similarly, mammospheres derived from K-Ras mutant MDA-MB-231 were inhibited by Delta-

DOI: 10.1021/acsomega.9b03639
ACS Omega 2020, 5, 832−842

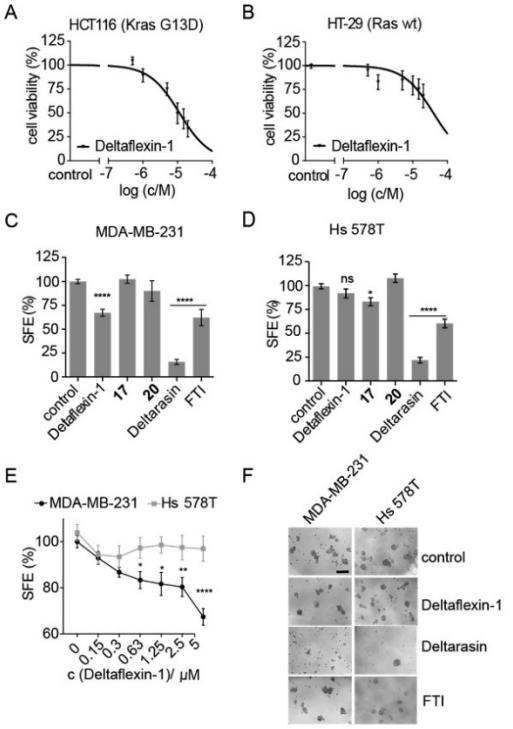

Figure 3. Deltaflexin-1 selectively inhibits oncogenic K-Ras-driven cell proliferation and mammosphere formation. (A,B) Dose-dependent cell viability in response to 72 h treatment with Deltaflexin-1 at concentrations ranging from 0 to 20 μM in HCT116 cells (A) and HT-29 cells (B). Graphs show mean values ± SEM, $n = 4$. (C,D) Sphere formation efficiency (SFE) of MDA-MB-231 cells (C), $n = 11$, and Hs 578T cells (D), $n = 7$, cultured in suspension culture for 6 days, followed by a 72 h incubation with 5 μM Deltaflexin-1 or Deltarasin, 0.5 μM FTI or 0.1% DMSO control. Graphs show mean values ± SEM. (E) Deltaflexin-1 dose-dependent effect on SFE with the same protocol as in (C,D). Graphs show mean values ± SEM, $n = 4$. The SFE is significantly different between MDA-MB-231 and Hs 578T above 0.63 μM. (C−E) Statistical significance levels are annotated as ns, not significant; $*p < 0.05$; $**p < 0.01$; $****p < 0.0001$; ns, not significant. (F) Representative images of MDA-MB-231 and Hs 578T spheroids at day 10 of suspension culture, after indicated treatments as in (C,D). Scale bar of 200 μm is representative for all images.

flexin-1 more significantly than those of H-Ras mutant Hs 578T (Figure 3C−F). Control compounds **17** and **20** with a stiff or shortened linker, respectively, had no significant effect (Figure 3C,D). This K-Ras-mutant mammosphere selectivity was largely confirmed with the Deltaflexin-1 linkage derivatives (Figure S3K,L), nevertheless suggesting some off-target effects on tumorosphere growth by the different linkages.

Second Generation Deltaflexins with Improved Chemotype. Encouraged by these results, a second generation of inhibitors was developed based on Deltaflexin-1. We replaced the potentially toxic coumarin moiety with a substituted terephthalic acid moiety, thus generating a partial hybrid with a bis-sulfonamide Deltasonamide inhibitor (compound **8**[17]) (Figure 4A). In addition, the bottom moiety was varied to characterize the activity of the pharmacologically more stable 2-methyl-substituent on the S-acyl cell penetration group. While compound **23** with the more stable bottom-moiety had a comparable affinity to **15**, its analogue **22** bound with a 2.6-fold lower affinity (Figure 4B, Table 1, Figure S4A, Table S1).

Computational docking supported these data, as overall similar positioning and similar contacts as for Deltaflexin-1 were observed for the second-generation compounds in the PDE6D pocket (Figure S4B). It appeared though that the substitution of the top moiety from an aromatic two-ring system to one aromatic ring allowed for more flexibility of the top moiety orientation. Moreover, the potential for a new hydrogen bond with Ser115 was identified for both **22** and **23**. In addition, the bending of **23** could contribute to the formation of an additional hydrogen bond with Glu88, which is not observed in **22** (Figure S4B). The relative strength of these interactions may contribute to the observed differences in the binding affinities.

In agreement with the in vitro data, second-generation compound **23** performed as well as **15** and somewhat better than **22** in disrupting the K-RasG12V/PDE6D interaction as assessed by FRET-experiments in cells (Figure 4C). Similarly, amongst the 4*n*-methylen-linker counterparts of **22** and **23**, **25** performed better than **24** (Figure 4A,C). These data further support that the replacement of the relatively labile 2-ethoxycarbonyl with the more stable 2-methyl on the S-acyl cell penetration group is beneficial. Finally, **22** and **23** (hereafter named Deltaflexin-2) led to a significant dose-dependent reduction of the K-RasG12V nanoclustering-FRET compared with **24** and **25** (Figure 4D). No effect on H-RasG12V FRET was observed (Figure S4C).

Recently, exquisite K-RasG12C selectivity was demonstrated for the covalent inhibitor ARS-1620.[7] In agreement with a significant overall activity, quantitative scoring of the chemical inhibition of PDE6D with Deltaflexin-2 revealed that it had 70% activity of ARS-1620 in KRAS-G12C mutant NCI-H358 lung cancer cells grown as tumorospheres. Moreover, Deltaflexin-2 was inactive in the B-RafV600E mutant A375 lung metastasis melanoma cell line, as was ARS-1620 (Figure 4E). These data confirm that Deltaflexins significantly inhibit cell spheroid growth in a K-Ras selective manner. By contrast, no such selectivity was found for Deltarasin, which showed equally high activity in both cell lines, again suggesting a general off-target toxicity.

Similarly, K-RasG13D-mutant MDA-MB-231- but not H-RasG12V-mutant Hs 578T-mammosphere formation was selectively decreased by Deltaflxin-2, while the counterpart with the shorter flexible linker **25** was inactive (Figure S4D,E). In line with the Ras-mutation status, the mammosphere formation of MDA-MB-231 and Hs 578T was selectively abrogated by the knockdown only of the mutated Ras isoform (Figure S4F−I), confirming that this assay can report on the selectivity for oncogenic K-Ras (MDA-MB-231) or H-Ras (Hs 578T). However, knockdown of PDE6D strongly affected sphere formation of both cell lines (Figure S4F,G).

We therefore conclude that Deltaflexins can block stemness traits of cancer cells and have a clear in cellulo selectivity for K-Ras as compared to H-Ras. However, our data also suggest that the stemness inhibiting activity of PDE6D inhibitors depends at least in breast cancer cell lines on other clients or activities of PDE6D.

In this work, we have demonstrated that the attachment of a "chemical spring" and cell penetration group to a generic heterocycle enables the de novo design of low micromolar PDE6D inhibitors in the first generation. This redesign approach is strikingly simple and together with the flexible

DOI: 10.1021/acsomega.9b03639
ACS Omega 2020, 5, 832−842

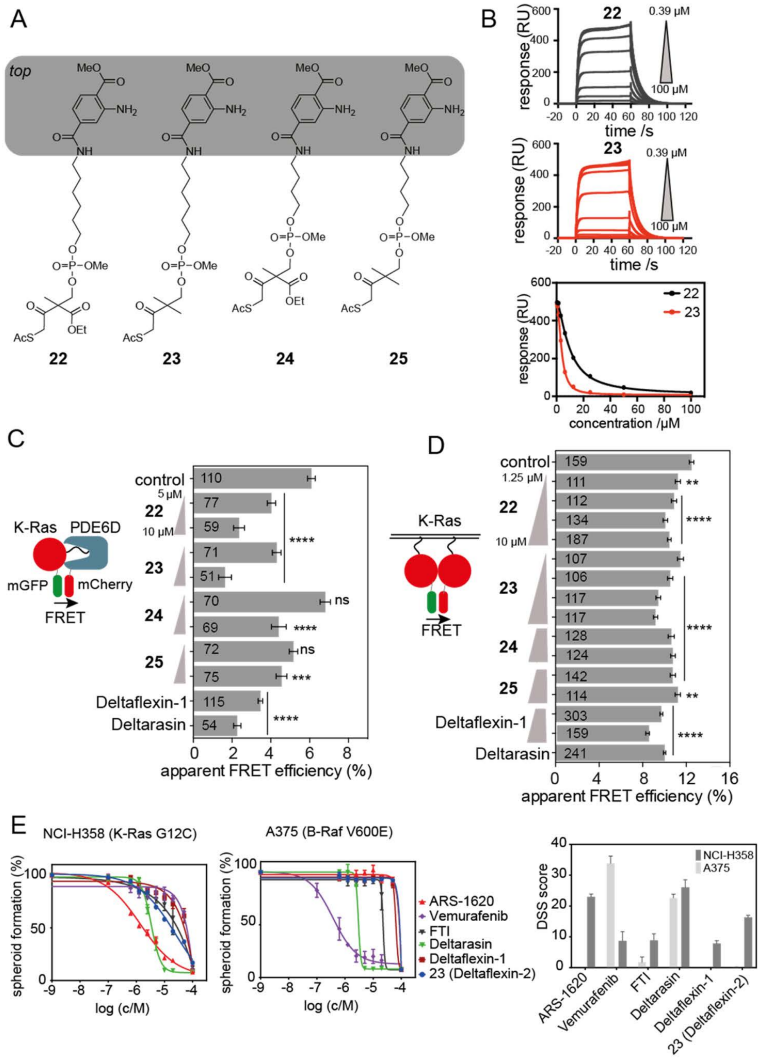

Figure 4. Partial scaffold hybridization creates second-generation inhibitors. (A) Second-generation compounds have an altered "top" moiety taken from a previously published PDE6D inhibitor. Note the variation of the protecting group between **22** and **23**, as well as **24** and **25**. Linker length is varied between the **22**, **23** vs **24**, **25**. (B) SPR data of avi-K-RasFMe/PDE6D treated with **22** and **23** (Deltaflexin-2) and dose response curves constructed from SPR kinetic data; $n = 3$. (C) PDE6D/K-Ras interaction by FLIM-FRET. HEK cells were cotransfected with mGFP-tagged K-RasG12V and mCherry-tagged PDE6D. Transfected cells were treated with 0.1% DMSO control or 5 μM ($n = 3$) and 10 μM ($n = 1$) compounds **22**, **23**, **24**, **25**, or 5 μM Deltaflexin-1, Deltarasin for 24 h;. (D) K-Ras membrane organization measured with nanoclustering-FRET in HEK cells coexpressing mGFP or mCherry tagged K-RasG12V for 48 h or treated with 0.1% DMSO control, and various concentrations of compounds **22**, **23**, **24**, **25**, or 5 μM Deltaflexin-1, Deltarasin for 24 h; $n = 3$. For all FRET-data, the numbers on the bars indicate the number of analyzed cells. (E) Dose-dependent cell viability of lung cancer cell lines, NCI-H358 and A375 grown as spheroids under low attachment and serum free conditions in response to 72 h treatment with ARS-1620, Vemurafenib, FTI-277, Deltarasin, Deltaflexin-1, and Deltaflexin-2 at concentrations ranging from 0 to 20 μM; $n \geq 3$. Higher efficacy results in a higher drug sensitivity score (DSS), an area under the curve (AUC) metric. Graphs show mean values ± SEM. Statistical significance levels are annotated as $^{**}p < 0.01$; $^{****}p < 0.0001$; ns, not significant.

coupling chemistry should allow for improvements of existing PDE6D inhibitors. As validated by the second-generation compounds, our approach is compatible with compound-scaffold hybridization of existing PDE6D compounds. Thus, we expect to quickly advance the development of more potent derivatives in the near future. Moreover, our strategy may apply to inhibitors of closely related targets, such as UNC119,[27] in addition to PDE6D inhibitors.

Past generations of PDE6D inhibitors underwent substantial structure-based optimization to arrive at sub and low nanomolar in vitro activities, but surprisingly they exhibited ~1000-fold less antiproliferative potential in cancer cells. Thus, the relation of

DOI: 10.1021/acsomega.9b03639
ACS Omega 2020, 5, 832−842

Deltaflexin-2 in vitro and in cellulo potencies is ~60- to 180-times better than that of Deltasonamide-2. Moreover, as compared to Deltarasin, Deltaflexins demonstrated the expected selectivity for K-Ras over H-Ras in cells. Therefore, the current Deltaflexins can serve as valuable tool compounds to investigate the PDE6D associated anticancer mechanisms. While we demonstrate the K-Ras selectivity of Deltaflexins, the comparison of PDE6D- and KRAS-knockdown data suggests K-Ras-independent effects of PDE6D inactivation on stemness traits of cancer cells. Other activities of PDE6D or clients other than K-Ras could be important in this context. For example, the PDE6D client INPP5E (inositol polyphosphate-5-phosphatase E) localizes to the primary cilium in a PDE6D-dependent manner.[28−30] In line with a potential contribution of INPP5E inhibition to the antistemness effect, primary ciliogenesis and associated Hedgehog signaling have recently been linked to epithelial−mesenchymal transition and stemness promotion in triple negative breast cancer.[31]

Nonetheless, K-Ras overactivity appears to be an important biomarker for the efficacy of PDE6D inhibitors.[32] In order to establish the exact therapeutic spectrum of the single-agents, a broader panel of cancer cells should be tested with PDE6D inhibitors in the future. Given that carboxymethylation of the prenylated C-termini of small GTPase clients provides additional affinity, it is foreseeable that concurrent inhibition of isoprenylcysteine carboxyl methyltransferase, by inhibitors such as cysmethynil, will be synergistic with PDE6D inhibitors.[12,32]

While targeting of signaling or trafficking hubs, such as PDE6D, could intuitively lead to more side effects, this approach may in the end be advantageous from the drug development point of view. Given that different cancer types and subtypes have diverse sets of drivers,[33,34] drugs that target a hub may affect several cancer drivers at once. Such hub inhibitors may therefore be more easily applicable to several types of cancer. This strategy is, for example, pursued for inhibitors of Hsp90, which is a major hub of kinases.[35,36] Irrespective of their exact mechanism of action, PDE6D inhibitors therefore remain attractive as potential cancer drugs.

METHODS

DNA Constructs and siRNA. Plasmids pmGFP/mCherry-H-RasG12V and pmGFP/mCherry-K-RasG12V were previously described.[22,23] Plasmids for mCit-Rheb and mCherry-PDE6D were previously described.[11] The human gene-directed siRNAs were purchased from Dharmacon as ON-TARGET plus SMART siRNA pools. The catalogue numbers are as follows: scrambled siRNA (cat. no. D-001810-10-05), human KRAS (cat. no. L-005069-00, lot 170710), human HRAS (cat. no. L-004142-00, lot 160414), and human PDE6D (cat. no. L-004310-00). Opti-MEM and transfection reagents Lipofectamine 3000 (cat. no. L3000001) and RNAiMAX (cat. no. 13778030) were purchased from Thermo Fisher Scientific. JetPrime (cat. no. 114-75) was obtained from Polyplus, Illkrich-Graffenstaden, France. FuGENE HD (cat. no. E2311) was purchased from Promega Biotech AB, Nacka, Sweden.

Cell Culture. HEK293 EBNA cells were kind gift of Prof. Florian M Wurm, EPFL, Lausanne, Switzerland. MDA-MB-231, Hs 578T, HCT116, HT-29, NCI-H358, and A-375 cell lines were obtained from ATCC. HEK293 EBNA, Hs 578T, HCT116, and HT-29 cell lines were maintained in Dulbecco's modified Eagle's medium (DMEM, cat. no. D6171, Sigma-Aldrich, Helsinki, Finland), supplemented with 10% fetal bovine serum (FBS) (cat. no. S1810, Biowest, Nuaille, France) and 2 mM L-glutamine (cat. no. G7513, Sigma-Aldrich). MDA-MB-231, NCI-H358, and A375 cells were cultured in Roswell Park Memorial Institute medium (RPMI, cat. no. R5886, Sigma-Aldrich), containing 10% FBS and 2 mM L-glutamine. All cells were incubated at 37 °C, with 5% CO_2, in a humidified cell incubator. Cells were subcultured twice a week.

Fluorescence Lifetime Imaging Microscopy-FRET. HEK293 EBNA cells were seeded in 12-well plates onto sterile coverslips. The next day, cells were transfected using FuGENE HD or jetPRIME transfection reagent with a total of 800 ng of plasmids. For donor samples, cells were transfected with mGFP or mCitrine-tagged plasmid. In FRET pairs, donors and acceptors were transfected at a 1:3 ratio. Acceptors were mCherry-tagged Ras plasmids in the nanoclustering-FRET experiments for membrane organization studies. For interaction studies, pmGFP-K-RasG12V and pmCherry-PDE6D, or pmCitrine-Rheb and pmCherry-PDE6D, were used all at the same 1:3 ratios with a total of 800 ng plasmids being used in each experiment. After 24 h of transfection, cells were treated with either 0.1% DMSO control or various concentrations of test compound or Deltarasin (cat. no. 9001536, Cayman Chemical, Tallinn, Estonia), or FTI-277 (cat. no. Sc-215058, Santa Cruz Biotechnology, Dallas, USA) or FTI-2628 (cat. no. sc-221635, Santa Cruz Biotechnology) for 24 h and fixed in 4% paraformaldehyde (PFA) before mounting with Mowiol 4-88 (cat. no. 81381, Sigma-Aldrich). The donor fluorescence lifetime was measured using a fluorescence microscope (Zeiss AXIO Observer D1) with a fluorescence lifetime imaging attachment (Lambert Instruments, Groningen, The Netherlands), as previously described in refs 37, 38. The fluorescence lifetime of at least 40 cells per treatment was measured in each experiment. The percentage of the apparent FRET efficiency (E_{app}) was determined using the measured lifetimes of donor−acceptor pairs (τ_{DA}) of samples and the average donor lifetime (τ_D), based on the equation: $E_{app} = (1 - \tau_{DA}/\tau_D) \times 100\%$.

Tumorosphere Assays. Mammosphere formation assays were performed in F-bottom 96-well suspension culture plates (cat. no. 655185, Cellstar, Greiner Bio-One, Frickenhausen, Germany). 1500 cells per well were seeded in 50 μL DMEM or RPMI medium containing 1× B27 (cat. no. 17504044, Gibco, Thermo Fisher Scientific), 25 ng/mL EGF (cat. no. E9644, Sigma-Aldrich), and 25 ng/mL FGF (cat. no. RP-8628, Thermo Fisher Scientific). Cells were cultured for 6 days and then treated with test compounds or DMSO control (0.1% v/v) for additional 3 days. The cells were resupplemented with fresh growth medium every 2 days. For knockdown experiments and for K-Ras and H-Ras transfections, cells were seeded in 6-well plates and treated with either 50 nM scrambled siRNA or siRNA targeting PDE6D KRAS or HRAS or with mGFP-K-RasG12V or mGFP-H-RasG12V plasmids, using jetPRIME transfection reagent or Lipofectamine 3000. On the next day, cells were replated into 96-well plates for suspension cell culture. Mammosphere formation was analyzed under an EVOS FL microscope (Thermo Fisher Scientific) and spheres exceeding 50 μm in diameter were counted. The SFE was expressed as percentage normalized to vehicle-treated control. In protein overexpression or knockdown experiments, SFE was normalized to the empty vector or scrambled siRNA-transfected controls, respectively.

Tumorospheres of lung cancer cells were generated by seeding NCI-H358 or A-375 cells (1500 cells per well) as a suspension culture in F-bottom 96-well suspension culture plates (cat. no. 655185, Cellstar, Greiner Bio-One) in 50 μL

DOI: 10.1021/acsomega.9b03639
ACS Omega 2020, 5, 832−842

RPMI medium supplemented with 0.5% methylcellulose, 25 ng/mL EGF, 25 ng/mL FGF, 1× B-27 supplement, and 2 mM L-glutamine. Cells were initially grown for 72 h and treated with freshly thawed compounds. After another 72 h of incubation, the cell viability was assessed using the alamarBlue assay (cat. no. DAL1100, Invitrogen, Carlsbad, CA, USA). A 10% final volume of alamarBlue reagent was added to each well of the plate and incubated for 4 h at 37 °C. Then, the fluorescence intensity was measured using a FLUOstar OPTIMA plate reader (BMG Labtech, Germany) with an excitation wavelength of 560 ± 5 nm and emission wavelength of 590 ± 5 nm. The obtained fluorescence intensity data were normalized to DMSO control. To quantitatively profile the drug sensitivity from the dose–response data, the DSS algorithm was employed.[39] The DSS score was calculated according to the formula

$$\mathrm{DSS} = \frac{100 \times \mathrm{AUC}}{\mathrm{TA} \times \log a}$$

The curve fitting parameters were used to calculate the AUC relative to the total area (TA) between the 10% threshold (DMSO at 0.1%) and 100% inhibition (benzethonium chloride at 100 μM). The integrated response is divided by the logarithm of the top asymptote (log *a*).

2D Cell Viability Assay. Hs 578T, HCT-116, and HT29 cells were plated onto 96-well cell culture plates at a density of 500 cells/well and allowed to attach for 24 h. Freshly thawed aliquots of test compounds were then added ice-cold at indicated concentrations. DMSO (0.1% v/v) was used as control. Plates were further incubated for 72 h. The cell viability was assessed using the alamarBlue reagent, according to manufacturer's instructions. The fluorescence intensity was read with the excitation wavelength of 530 ± 10 nm and emission wavelength of 590 ± 10 nm using a Synergy H1 plate reader (BioTek, Winooski, VT, USA).

Western Blotting. Cells were lysed in RIPA buffer (cat. no. 89900, Thermo Scientific) containing protease (cat. no. 88666, Thermo Scientific) and phosphatase inhibitors (cat. no. 0496845001, Roche, Mannheim, Germany) and then sonicated for 5 min in ice-cold water. Proteins were separated on 10% sodium dodecyl sulfate polyAcrylamide gel electrophoresis (SDS-PAGE) gels and transferred to nitrocellulose membranes (cat. no. NBA 083C001EA, Protran, Waltham, USA) using a Transferblot Turbo Transfer System (Bio-Rad, Hercules, CA, USA). Briefly, the membranes were blocked in 1xTBS containing 0.1% Tween-20 and 5% w/v nonfat dry milk for 30 min and incubated with primary antibodies PDE6D (cat. no. sc-166854, Santa Cruz Biotechnology, Paso Robles, CA, USA.) or β-actin (cat. no. A1978, Sigma-Aldrich) overnight, at 4 °C. The membranes were then incubated with secondary antibodies antimouse (cat. no. sc-2954, Santa Cruz Biotechnology) for 1 h at room temperature. Protein bands were detected using a ChemiDoc MP instrument (Bio-Rad) after treatment with ECL reagent (cat. no. 170-5061, BioRad). The protein-band intensities were measured using Image Lab software (Bio-Rad).

RT-qPCR Analysis for Gene Knockdowns. MDA-MB-231 and Hs 578T cells were seeded in 6-well plates and transfected with 50 nM of siRNA KRAS or HRAS or scrambled, negative control siRNA (QIAGEN, cat. no. 1022076, QIAGEN, Hilden, Germany) using Lipofectamine. After 24 h of transfection, total RNA was isolated using NucleoZol according to the manufacturer's protocol (cat. no.: 7040404, Macherey-Nagel, Hoerdt, France). Reverse transcription was performed with 1 μg of total RNA using SuperScript III Reverse Transcriptase (cat. no.: 18080093, Invitrogen). The knockdowns of KRAS and HRAS gene transcripts were analyzed by real-time qPCR using SsoAdvanced Universal SYBR Green Supermix (Bio-Rad), on the CFX-connect real-time PCR instrument (Bio-Rad). The transcripts were selectively amplified using specific primers producing amplicons for KRAS (total) and HRAS. The gene β-actin was used as reference. The following primers were used: for KRAS (total), forward 5′-tacagtgcaatgagggacca-3′, reverse 5′-tcctgagcctgttttgtgtct-3′ (amplicon 206 bp); for HRAS, forward 5′-ctgaccatccagctgatcca-3′, reverse 5′-tggcaaacacacaggaag-3′ (amplicon 196 bp); for ACTB (β-actin), forward 5′-ggggtgttgaaggtctcaaa-3′; reverse 5′-ggcatcctcaccctgaagta-3′.[40]

Confocal Imaging. MDCK cells, stably overexpressing mGFP-KRasG12V, were seeded onto coverslips in 12-well cell culture plates. The cells were treated with 0.1% DMSO control or 5 μM Deltarasin or Deltaflexin-1. After 24 h cells were fixed in 4% PFA and mounted with Mowiol, cells were imaged using a laser scanning microscope (LSM 780) Carl Zeiss Microscopy, Jena, Germany.

Compound Syntheses. Purchased compounds were used without further purifications. Chemicals and solvents were purchased from the companies Sigma-Aldrich, VWR, and Thermo Fisher Scientific. Solvents were dried over 3 or 4 Å molecular sieves. Commercially available solvents for semi-preparative high-performance liquid chromatography (HPLC) (acetonitrile HPLC grade) were used. Solvent mixtures are understood as volume/volume. Extended information on the complete compound syntheses and analytics are described in Supporting Information S1.

Molecular Modeling. Docking studies were carried out by the GOLD module[41] of Discovery Studio 4.5 (Accelrys Inc. San Diego, USA, http://www.accelrys.com/) using the crystal structure of PDE6D determined at 1.45 Å resolution (PDB code 4JV8)[15] as the receptor molecule. Water molecules and the bound ligand were removed from the structure prior to the docking. Binding sites were identified by using the binding site identification tool in Discovery Studio. The binding site that matched also the binding site identified by the crystal structure was selected for docking. The ligands were generated with ChemDraw Professional 15.1 (PerkinElmer Informatics, www.cambridgesoft.com) and exported as *.mol files to the Discovery Studio. Hydrogen atoms were added to the protein and the ligand. The Goldscore fitness function was used to score the poses.

SPR Binding and Inhibition Assays. SPR binding experiments were performed on a Biacore S200 instrument (GE Healthcare Life Sciences, Marlborough, MA, USA) as described previously.[42] Farnesylated and methylated K-Ras-GDP (K-RasFMe), with an N-terminal avi-tag, was captured on neutravidin-coupled CM5 sensor chips (capture density 500–1500 RU). PDE6D (2-fold serial dilution, 20–0.039 μM) was injected over the K-RasFMe surface in 20 mM *N*-(2-hydroxyethyl)piperazine-*N*′-ethanesulfonic acid (HEPES) (pH 7.5), 150 mM NaCl, 0.01%, Tween 20, 5 mM $MgCl_2$, and 5% DMSO at 30 μL/min and with a contact time of 60 s. The inhibitory activity of compounds for PDE6D/K-RasFMe interaction was measured using 1.25 μM PDE6D and a serial dilution of compound (2-fold, 100–0.39 μM) using the same buffer and flow rate. PDE6D (1.25 μM) was diluted with Deltarasin (3-fold, 50 μM to 68 nM) was used as a positive control. All titrations were run over three flow cells with variable surface densities of K-RasFMe. The data were processed by

DOI: 10.1021/acsomega.9b03639
ACS Omega 2020, 5, 832–842

subtracting binding responses on the reference flow cells as well as the buffer subtraction. The samples were also corrected for DMSO mismatches using a DMSO standard curve. The equilibrium binding constant and IC_{50} values were calculated using the Biacore S200 Evaluation software. The IC_{50} value obtained from SPR and FA assay was converted into K_d using a modified Cheng−Prusoff equation

$$K_d = \frac{IC_{50}}{1 + \frac{[L]}{K_D}}$$

where K_D is the dissociation constant between PDE6D/K-RasFMe and $[L]$ is the concentration of PDE6D used in SPR experiments.[44]

FA Assay. The binding of compounds to PDE6D was assessed in an FA assay using fluorescein-tagged farnesylated Rheb (F-Rheb) peptide as the probe.[14,43] PDE6D was produced as described below. FA assays were performed on a black low volume, round-bottom, non-binding surface 384-well plate (Corning, #4514) in an assay buffer composed of 30 mM Tris, 150 mM NaCl, and 3 mM dithiothreitol. To a three-fold dilution of compounds in assay buffer (300 μM to 1.7 nM), a complex of 0.25 μM F-Rheb peptide and 2 μM PDE6D was added, and the reaction mix was incubated for 15 min at RT. Then, the FP was recorded on a Synergy H1 hybrid plate reader (BioTek) equipped with a polarization cube with an excitation wavelength of 485 ± 10 nm and emission wavelength of 528 ± 10 nm. The FP data were plotted against the logarithmic concentration of compounds and fit to log inhibitor vs response−variable slope (four parameters) equation in Prism (GraphPad), and the IC_{50} was determined.

Cloning, Expression, and Purification of Recombinant Proteins. PDE6D was recombinantly produced in *Escherichia coli* BL21 (DE3) transformed with pDest-His6-MBP-PDE6D grown at 37 °C until OD of 0.6−0.8 and then induced with 0.5 mM of β-D-1-thiogalactopyranoside overnight at 16 °C.[12] The bacterial lysate was prepared in a binding buffer (20 mM HEPES, pH 7.6, 300 mM NaCl, 5 mM $MgCl_2$, 1 mM TCEP (Tris(2-carboxyethyl)phosphine hydrochloride), and protease inhibitor tablet from Roche) containing 0.5 mg/mL of lysozyme. Soluble proteins were isolated after sonication and centrifugation steps. The protein His6-MBP-TEV-PDE6D was purified on HisTrap HP column (GE Healthcare) in binding buffer containing imidazole and eluted with a 20 column-volume gradient from 35 to 500 mM imidazole. The eluted fractions were analyzed on SDS-PAGE. The fractions containing His6-MBP-TEV-PDE6D were treated with tobacco etch virus (TEV) protease (cat. no.: T4455, Sigma-Aldrich) (1:25 w/w, TEV/fusion protein) for 1 h at room temperature and then dialyzed overnight in binding buffer without protease inhibitor. The cleavage product containing His6-MBP and PDE6D was loaded a second time on a HisTrap HP column in binding buffer. The peak fractions (OD280) corresponding to the nonbound protein PDE6D were collected, pooled, concentrated using Amicon Ultra Centrifugal Filters (Merck Millipore, Molsheim, France), and analyzed on a SDS-PAGE gel with Coomassie blue. The presence of purified PDE6D was confirmed by Western blotting using a monoclonal anti-PDE6D antibody (cat. no.: sc-376724, Santa Cruz Biotechnology; dilution ratio 1:200).

The baculovirus expression vector for production of processed K-Ras4B has been previously described.[44] An avi-tagged full-length K-Ras4B clone was generated by introducing an avi sequence (LNDIFEAQKIEWG) between the TEV protease cleavage site (ENLYFQG) sequence and amino acids 2−188 of K-Ras4B. The baculovirus expression vector for the production of processed avi-K-Ras4B was produced using the methods described previously.[44] Expression of farnesylated and carboxymethylated K-Ras4B (K-RasFMe) and avi-K-Ras-FMe followed the methods as described.[42] Purification of processed avi-tagged full-length K-Ras4B was as described[44] with modifications. Protein isolated after the removal of the N-terminal His6-MBP tag (21.5 μM avi-K-Ras-FMe) was biotinylated by incubating for 2 h at room temperature with 2.8 μM His6-BirA, 3.6 mM ATP, 215 μM biotin in a buffer of 20 mM HEPES, pH 7.3, 300 mM NaCl, 5 mM $MgCl_2$, 1 mM TCEP (Tris(2-carboxyethyl)phosphine hydrochloride), and 1:1000 v/v protease inhibitor (P8849 Sigma-Aldrich). The reaction was then dialyzed at 4 °C for 16 h against 20 mM HEPES, pH 7.3, 300 mM NaCl, 5 mM $MgCl_2$, and 1 mM TCEP. The dialyzed reaction was passed over a HisTrap FF column (GE Healthcare), equilibrated with dialysis buffer, to remove His6-BirA. The biotinylated avi-K-Ras-FMe has a slight affinity for the column and elutes from the column at low (<50 mM) imidazole concentrations. Fractions were analyzed by coomassie-stained SDS-PAGE, and positive fractions were pooled and dialyzed against 20 mM HEPES, pH 7.3, 300 mM NaCl, 1 mM $MgCl_2$, and 1 mM TCEP for 3 h at room temperature. The protein concentration was determined by absorbance at 280 nm, and aliquots were snap frozen in liquid nitrogen and stored at −80 °C.

Statistical Analysis. GraphPad Prism software was used for the statistical analysis. The sample size n for each data set is provided in the relevant figure legends and represents independent experiments. Unless otherwise stated, statistical significance was evaluated with the Student's *t*-test or One-way ANOVA complemented by multiple comparison post hoc tests, as appropriate. A *p*-value of <0.05 is considered statistically significant, and the statistical significance levels are annotated as * = $p < 0.05$; ** = $p < 0.01$; *** = $p < 0.001$; **** = $p < 0.0001$, or ns = not significant.

■ ASSOCIATED CONTENT

Supporting Information

The Supporting Information is available free of charge at https://pubs.acs.org/doi/10.1021/acsomega.9b03639.

Compound affinities by anisotropy; linkage derivatives and binding data; linkage derivative cell activity and heat passivation data; linkage derivative antiproliferation effect and genetic dependencies; additional second generation Deltaflexin data and knockdown controls; and compound synthesis and characterization (PDF)

■ AUTHOR INFORMATION

Corresponding Author

*E-mail: daniel.abankwa@uni.lu.

ORCID

Ganesh babu Manoharan: 0000-0001-7305-9845

Pasi Virta: 0000-0002-6218-2212

Daniel Abankwa: 0000-0003-2769-0745

Author Contributions

F.A.S. designed, performed, and analyzed all FLIM-FRET and WB experiments. C.A. and S.O. designed, performed, and analyzed sphere formation and cell proliferation experiments. A.S., O.M.A., H.L., M.O., and P.V. collaboratively designed the

DOI: 10.1021/acsomega.9b03639
ACS Omega 2020, 5, 832−842

compounds **5**, **9**, **13**, and **15**. M.O., P.V., P.R., and D.A. collaboratively designed the compounds **17**, **19**, **20**, **22**, **23**, **24**, and **25**. A.S. and P.R. prepared the compounds under supervision of M.O. M.C. prepared PDE6D protein. G.b.M. performed and analyzed FA experiments. L.B. and A.G.S. designed, performed, and analyzed SPR experiments. TT prepared avi-KRasFMe. A.C.P. performed computational docking and prepared graphs of structures. M.O. and P.V. wrote the chemical synthesis description. D.A. conceived the study, designed experiments, interpreted results, and wrote the manuscript together with F.A.S. All authors commented on the manuscript.

Funding

This work was supported by a CIMO fellowship to A.S. and F.A.S. P.V. received the support from the Academy of Finland Project (#308931). D.A. received the support from the Academy of Finland Key Project (#304638) grant, the Sigrid Juselius Foundation, and the Cancer Society of Finland.

Notes

The authors declare the following competing financial interest(s): We have filed a patent around second generation inhibitor Deltaflexin-2.

■ ACKNOWLEDGMENTS

The authors are grateful for the support from the cell imaging core (CIC, Turku Bioscience Centre, Turku, Finland). The infrastructure support from Biocenter Finland is acknowledged. We thank Prof. Philippe I. H. Bastiaens (Max-Planck Institute Dortmund, Germany) for providing the mCitrine-Rheb and mCherry-PDEδ constructs. We thank Lange Yakubu Saleh for the synthesis of compound **20** and Anuer Al-Rammahi for the synthesis of compound **17**. We thank Eyad K. Fansa (Max-Planck Institute Dortmund, Germany) for providing the F-Rheb peptide. We acknowledge the protein production support for avi-KRAS-FMe and KRasFMe from Vanessa Wall, Matt Drew, and Jennifer Mehalko and Dominic Esposito for providing the pDest-His6-MBP-PDE6D plasmid (NCI-RAS Initiative, Frederick National Laboratory for Cancer Research, USA). This project was funded in whole or in part with federal funds from National Cancer Institute, NIH Contract HHSN261200800001E. The content of this publication does not necessarily reflect the views or policies of the Department of Health and Human Services, and the mention of trade names, commercial products, or organizations does not imply endorsement by the US Government.

■ REFERENCES

(1) Papke, B.; Der, C. J. Drugging RAS: Know the enemy. *Science* **2017**, *355*, 1158−1163.

(2) Lerner, E. C.; Zhang, T.-T.; Knowles, D. B.; Qian, Y.; Hamilton, A. D.; Sebti, S. M. Inhibition of the Prenylation of K-Ras, but Not H- or N-Ras, Is Highly Resistant to CAAX Peptidomimetics and Requires Both a Farnesyltransferase and a Geranylgeranyltransferase I Inhibitor in Human Tumor Cell Lines. *Oncogene* **1997**, *15*, 1283−1288.

(3) Spiegel, J.; Cromm, P. M.; Zimmermann, G.; Grossmann, T. N.; Waldmann, H. Small-Molecule Modulation of Ras Signaling. *Nat. Chem. Biol.* **2014**, *10*, 613−622.

(4) Ostrem, J. M.; Peters, U.; Sos, M. L.; Wells, J. A.; Shokat, K. M. K-Ras(G12C) Inhibitors Allosterically Control GTP Affinity and Effector Interactions. *Nature* **2013**, *503*, 548−551.

(5) Lito, P.; Solomon, M.; Li, L.-S.; Hansen, R.; Rosen, N. Allele-Specific Inhibitors Inactivate Mutant KRAS G12C by a Trapping Mechanism. *Science* **2016**, *351*, 604−608.

(6) Hillig, R. C.; Sautier, B.; Schroeder, J.; Moosmayer, D.; Hilpmann, A.; Stegmann, C. M.; Werbeck, N. D.; Briem, H.; Boemer, U.; Weiske, J.; Badock, V.; Mastouri, J.; Petersen, K.; Siemeister, G.; Kahmann, J. D.; Wegener, D.; Böhnke, N.; Eis, K.; Graham, K.; Wortmann, L.; Nussbaum von, F.; Bader, B. Discovery of Potent SOS1 Inhibitors That Block RAS Activation via Disruption of the RAS-SOS1 Interaction. *Proc. Natl. Acad. Sci. U.S.A.* **2019**, *116*, 2551.

(7) Janes, M. R.; Zhang, J.; Li, L.-S.; Hansen, R.; Peters, U.; Guo, X.; Chen, Y.; Babbar, A.; Firdaus, S. J.; Darjania, L.; Feng, J.; Chen, J. H.; Li, S.; Li, S.; Long, Y. O.; Thach, C.; Liu, Y.; Zarieh, A.; Ely, T.; Kucharski, J. M.; Kessler, L. V.; Wu, T.; Yu, K.; Wang, Y.; Yao, Y.; Deng, X.; Zarrinkar, P. P.; Brehmer, D.; Dhanak, D.; Lorenzi, M. V.; Hu-Lowe, D.; Patricelli, M. P.; Ren, P.; Liu, Y. Targeting KRAS Mutant Cancers with a Covalent G12C-Specific Inhibitor. *Cell* **2018**, *172*, 578−589.e17.

(8) Canon, J.; Rex, K.; Saiki, A. Y.; Mohr, C.; Cooke, K.; Bagal, D.; Gaida, K.; Holt, T.; Knutson, C. G.; Koppada, N.; Lanman, B. A.; Werner, J.; Rapaport, A. S.; Miguel, T. S.; Ortiz, R.; Osgood, T.; Sun, J.-R.; Zhu, X.; McCarter, J. D.; Volak, L. P.; Houk, B. E.; Fakih, M. G.; O'Neil, B. H.; Price, T. J.; Falchook, G. S.; Desai, J.; Kuo, J.; Govindan, R.; Hong, D. S.; Ouyang, W.; Henary, H.; Arvedson, T.; Cee, V. J.; Lipford, J. R. The Clinical KRAS(G12C) Inhibitor AMG 510 Drives Anti-Tumour Immunity. *Nature* **2019**, *575*, 217−223.

(9) Shima, F.; Yoshikawa, Y.; Ye, M.; Araki, M.; Matsumoto, S.; Liao, J.; Hu, L.; Sugimoto, T.; Ijiri, Y.; Takeda, A.; Nishiyama, Y.; Sato, C.; Muraoka, S.; Tamura, A.; Osoda, T.; Tsuda, K.-I.; Miyakawa, T.; Fukunishi, H.; Shimada, J.; Kumasaka, T.; Yamamoto, M.; Kataoka, T. In Silico Discovery of Small-Molecule Ras Inhibitors That Display Antitumor Activity by Blocking the Ras-Effector Interaction. *Proc. Natl. Acad. Sci. U.S.A.* **2013**, *110*, 8182.

(10) McCarthy, M. J.; Pagba, C. V.; Prakash, P.; Naji, A. K.; van der Hoeven, D.; Liang, H.; Gupta, A. K.; Zhou, Y.; Cho, K.-J.; Hancock, J. F.; Gorfe, A. A. Discovery of High-Affinity Noncovalent Allosteric KRAS Inhibitors That Disrupt Effector Binding. *ACS Omega* **2019**, *4*, 2921−2930.

(11) Chandra, A.; Grecco, H. E.; Pisupati, V.; Perera, D.; Cassidy, L.; Skoulidis, F.; Ismail, S. A.; Hedberg, C.; Hanzal-Bayer, M.; Venkitaraman, A. R.; Wittinghofer, A.; Bastiaens, P. I. H. The GDI-like solubilizing factor PDEδ sustains the spatial organization and signalling of Ras family proteins. *Nat. Cell Biol.* **2011**, *14*, 148−158.

(12) Dharmaiah, S.; Bindu, L.; Tran, T. H.; Gillette, W. K.; Frank, P. H.; Ghirlando, R.; Nissley, D. V.; Esposito, D.; McCormick, F.; Stephen, A. G.; Simanshu, D. K. Structural basis of recognition of farnesylated and methylated KRAS4b by PDEδ. *Proc. Natl. Acad. Sci. U.S.A.* **2016**, *113*, E6766−E6775.

(13) Schmick, M.; Vartak, N.; Papke, B.; Kovacevic, M.; Truxius, D. C.; Rossmannek, L.; Bastiaens, P. I. H. KRas Localizes to the Plasma Membrane by Spatial Cycles of Solubilization, Trapping and Vesicular Transport. *Cell* **2014**, *157*, 459−471.

(14) Ismail, S. A.; Chen, Y.-X.; Rusinova, A.; Chandra, A.; Bierbaum, M.; Gremer, L.; Triola, G.; Waldmann, H.; Bastiaens, P. I. H.; Wittinghofer, A. Arl2-GTP and Arl3-GTP Regulate a GDI-Like Transport System for Farnesylated Cargo. *Nat. Chem. Biol.* **2011**, *7*, 942−949.

(15) Zimmermann, G.; Papke, B.; Ismail, S.; Vartak, N.; Chandra, A.; Hoffmann, M.; Hahn, S. A.; Triola, G.; Wittinghofer, A.; Bastiaens, P. I. H.; Waldmann, H. Small molecule inhibition of the KRAS-PDEδ interaction impairs oncogenic KRAS signalling. *Nature* **2013**, *497*, 638−642.

(16) Papke, B.; Murarka, S.; Vogel, H. A.; Martín-Gago, P.; Kovacevic, M.; Truxius, D. C.; Fansa, E. K.; Ismail, S.; Zimmermann, G.; Heinelt, K.; Schultz-Fademrecht, C.; Saabi, Al; Baumann, M.; Nussbaumer, P.; Wittinghofer, A.; Waldmann, H.; Bastiaens, P. I. H. Identification of Pyrazolopyridazinones as PDEδ Inhibitors. *Nat. Commun.* **2016**, *7*, 11360.

(17) Martín-Gago, P.; Fansa, E. K.; Klein, C. H.; Murarka, S.; Janning, P.; Schürmann, M.; Metz, M.; Ismail, S.; Schultz-Fademrecht, C.; Baumann, M.; Bastiaens, P. I. H.; Wittinghofer, A.; Waldmann, H. A PDE6δ-KRas Inhibitor Chemotype with up to Seven H-Bonds and

DOI: 10.1021/acsomega.9b03639
ACS Omega 2020, 5, 832−842

Picomolar Affinity that Prevents Efficient Inhibitor Release by Arl2. *Angew. Chem., Int. Ed.* **2017**, *56*, 2423−2428.
(18) Chen, D.; Chen, Y.; Lian, F.; Chen, L.; Li, Y.; Cao, D.; Wang, X.; Chen, L.; Li, J.; Meng, T.; Huang, M.; Geng, M.; Shen, J.; Zhang, N.; Xiong, B. Fragment-based drug discovery of triazole inhibitors to block PDEδ-RAS protein-protein interaction. *Eur. J. Med. Chem.* **2019**, *163*, 597−609.
(19) Hecker, S. J.; Erion, M. D. Prodrugs of Phosphates and Phosphonates. *J. Med. Chem.* **2008**, *51*, 2328−2345.
(20) Kiuru, E.; Ahmed, Z.; Lönnberg, H.; Beigelman, L.; Ora, M. 2,2-Disubstituted 4-Acylthio-3-Oxobutyl Groups as Esterase- and Thermolabile Protecting Groups of Phosphodiesters. *J. Org. Chem.* **2013**, *78*, 950−959.
(21) Prakash, P.; Sayyed-Ahmad, A.; Cho, K.-J.; Dolino, D. M.; Chen, W.; Li, H.; Grant, B. J.; Hancock, J. F.; Gorfe, A. A. Computational and Biochemical Characterization of Two Partially Overlapping Interfaces and Multiple Weak-Affinity K-Ras Dimers. *Sci. Rep.* **2017**, *7*, 40109.
(22) Posada, I. M. D.; Lectez, B.; Siddiqui, F. A.; Oetken-Lindholm, C.; Sharma, M.; Abankwa, D. Opposite Feedback From mTORC1 to H-Ras and K-ras4B Downstream of SREBP1. *Sci. Rep.* **2017**, *7*, 8944.
(23) Posada, I. M. D.; Lectez, B.; Sharma, M.; Oetken-Lindholm, C.; Yetukuri, L.; Zhou, Y.; Aittokallio, T.; Abankwa, D. Rapalogs Can Promote Cancer Cell Stemness in Vitro in a Galectin-1 and H-Ras-Dependent Manner. *Oncotarget* **2017**, *8*, 44550−44566.
(24) Sun, J.; Blaskovich, M. A.; Knowles, D.; Qian, Y.; Ohkanda, J.; Bailey, R. D.; Hamilton, A. D.; Sebti, S. M. Antitumor Efficacy of a Novel Class of Non-Thiol-Containing Peptidomimetic Inhibitors of Farnesyltransferase and Geranylgeranyltransferase I. *Cancer Res.* **1999**, *59*, 4919.
(25) Najumudeen, A. K.; Jaiswal, A.; Lectez, B.; Oetken-Lindholm, C.; Guzmán, C.; Siljamäki, E.; Posada, I. M. D.; Lacey, E.; Aittokallio, T.; Abankwa, D. Cancer Stem Cell Drugs Target K-Ras Signaling in a Stemness Context. *Oncogene* **2016**, *35*, 5248−5262.
(26) Debeb, B. G.; Zhang, X.; Krishnamurthy, S.; Gao, H.; Cohen, E.; Li, L.; Rodriguez, A. A.; Landis, M. D.; Lucci, A.; Ueno, N. T.; Robertson, F.; Xu, W.; Lacerda, L.; Buchholz, T. A.; Cristofanilli, M.; Reuben, J. M.; Lewis, M. T.; Woodward, W. A. Characterizing Cancer Cells with Cancer Stem Cell-Like Features in 293T Human Embryonic Kidney Cells. *Mol. Cancer* **2010**, *9*, 180.
(27) Mejuch, T.; Garivet, G.; Hofer, W.; Kaiser, N.; Fansa, E. K.; Ehrt, C.; Koch, O.; Baumann, M.; Ziegler, S.; Wittinghofer, A.; Waldmann, H. Small-Molecule Inhibition of the UNC119-Cargo Interaction. *Angew. Chem., Int. Ed.* **2017**, *129*, 6277−6282.
(28) Humbert, M. C.; Weihbrecht, K.; Searby, C. C.; Li, Y.; Pope, R. M.; Sheffield, V. C.; Seo, S. ARL13B, PDE6D, and CEP164 Form a Functional Network for INPP5E Ciliary Targeting. *Proc. Natl. Acad. Sci. U.S.A.* **2012**, *109*, 19691−19696.
(29) Thomas, S.; Wright, K. J.; Corre, S. L.; Micalizzi, A.; Romani, M.; Abhyankar, A.; Saada, J.; Perrault, I.; Amiel, J.; Litzler, J.; Filhol, E.; Elkhartoufi, N.; Kwong, M.; Casanova, J.-L.; Boddaert, N.; Baehr, W.; Lyonnet, S.; Munnich, A.; Burglen, L.; Chassaing, N.; Encha-Ravazi, F.; Vekemans, M.; Gleeson, J. G.; Valente, E. M.; Jackson, P. K.; Drummond, I. A.; Saunier, S.; Attié-Bitach, T. A HomozygousPDE6D-Mutation in Joubert Syndrome Impairs Targeting of Farnesylated INPP5E Protein to the Primary Cilium. *Hum. Mutat.* **2013**, *35*, 137−146.
(30) Fansa, E. K.; Kösling, S. K.; Zent, E.; Wittinghofer, A.; Ismail, S. PDE6δ-Mediated Sorting of INPP5E Into the Cilium Is Determined by Cargo-Carrier Affinity. *Nat. Commun.* **2016**, *7*, 11366.
(31) Guen, V. J.; Chavarria, T. E.; Kröger, C.; Ye, X.; Weinberg, R. A.; Lees, J. A. EMT Programs Promote Basal Mammary Stem Cell and Tumor-Initiating Cell Stemness by Inducing Primary Ciliogenesis and Hedgehog Signaling. *Proc. Natl. Acad. Sci. U.S.A.* **2017**, *114*, E10532−E10539.
(32) Winter-Vann, A. M.; Baron, R. A.; Wong, W.; dela Cruz, J.; York, J. D.; Gooden, D. M.; Bergo, M. O.; Young, S. G.; Toone, E. J.; Casey, P. J. A Small-Molecule Inhibitor of Isoprenylcysteine Carboxyl Methyltransferase with Antitumor Activity in Cancer Cells. *Proc. Natl. Acad. Sci. U.S.A.* **2005**, *102*, 4336−4341.
(33) Robinson, D. R.; Wu, Y.-M.; Lonigro, R. J.; Vats, P.; Cobain, E.; Everett, J.; Cao, X.; Rabban, E.; Kumar-Sinha, C.; Raymond, V.; Schuetze, S.; Alva, A.; Siddiqui, J.; Chugh, R.; Worden, F.; Zalupski, M. M.; Innis, J.; Mody, R. J.; Tomlins, S. A.; Lucas, D.; Baker, L. H.; Ramnath, N.; Schott, A. F.; Hayes, D. F.; Vijai, J.; Offit, K.; Stoffel, E. M.; Roberts, J. S.; Smith, D. C.; Kunju, L. P.; Talpaz, M.; Cieślik, M.; Chinnaiyan, A. M. Integrative Clinical Genomics of Metastatic Cancer. *Nature* **2017**, *548*, 297−303.
(34) Garraway, L. A.; Lander, E. S. Lessons From the Cancer Genome. *Cell* **2013**, *153*, 17−37.
(35) Butler, L. M.; Ferraldeschi, R.; Armstrong, H. K.; Centenera, M. M.; Workman, P. Maximizing the Therapeutic Potential of HSP90 Inhibitors. *Mol. Cancer Res.* **2015**, *13*, 1445−1451.
(36) Taipale, M.; Krykbaeva, I.; Koeva, M.; Kayatekin, C.; Westover, K. D.; Karras, G. I.; Lindquist, S. Quantitative Analysis of Hsp90-Client Interactions Reveals Principles of Substrate Recognition. *Cell* **2012**, *150*, 987−1001.
(37) Guzmán, C.; Oetken-Lindholm, C.; Abankwa, D. Automated High-Throughput Fluorescence Lifetime Imaging Microscopy to Detect Protein-Protein Interactions. *J. Lab. Autom.* **2016**, *21*, 238−245.
(38) Guzmán, C.; Šolman, M.; Ligabue, A.; Blaževitš, O.; Andrade, D. M.; Reymond, L.; Eggeling, C.; Abankwa, D. The Efficacy of Raf Kinase Recruitment to the GTPase H-Ras Depends on H-Ras Membrane Conformer-Specific Nanoclustering. *J. Biol. Chem.* **2014**, *289*, 9519−9533.
(39) Yadav, B.; Pemovska, T.; Szwajda, A.; Kulesskiy, E.; Kontro, M.; Karjalainen, R.; Majumder, M. M.; Malani, D.; Murumägi, A.; Knowles, J.; Porkka, K.; Heckman, C.; Kallioniemi, O.; Wennerberg, K.; Aittokallio, T. Quantitative Scoring of Differential Drug Sensitivity for Individually Optimized Anticancer Therapies. *Sci. Rep.* **2014**, *4*, 5193.
(40) Tsai, F. D.; Lopes, M. S.; Zhou, M.; Court, H.; Ponce, O.; Fiordalisi, J. J.; Gierut, J. J.; Cox, A. D.; Haigis, K. M.; Philips, M. R. K-Ras4A splice variant is widely expressed in cancer and uses a hybrid membrane-targeting motif. *Proc. Natl. Acad. Sci. U.S.A.* **2015**, *112*, 779−784.
(41) Jones, G.; Willett, P.; Glen, R. C.; Leach, A. R.; Taylor, R. Development and validation of a genetic algorithm for flexible docking 1 1Edited by F. E. Cohen. *J. Mol. Biol.* **1997**, *267*, 727−748.
(42) Agamasu, C.; Ghirlando, R.; Taylor, T.; Messing, S.; Tran, T. H.; Bindu, L.; Tonelli, M.; Nissley, D. V.; McCormick, F.; Stephen, A. G. KRAS Prenylation Is Required for Bivalent Binding with CaM in a Nucleotide Independent Manner. *Biophys. J.* **2019**, *116*, 1049−1063.
(43) Blaževitš, O.; Mideksa, Y. G.; Solman, M.; Ligabue, A.; Ariotti, N.; Nakhaeizadeh, H.; Fansa, E. K.; Papageorgiou, A. C.; Wittinghofer, A.; Ahmadian, M. R.; Abankwa, D. Galectin-1 Dimers Can Scaffold Raf-Effectors to Increase H-Ras Nanoclustering. *Sci. Rep.* **2016**, *6*, 24165.
(44) Gillette, W. K.; Esposito, D.; Blanco, M. A.; Alexander, P.; Bindu, L.; Bittner, C.; Chertov, O.; Frank, P. H.; Grose, C.; Jones, J. E.; Meng, Z.; Perkins, S.; Van, Q.; Ghirlando, R.; Fivash, M.; Nissley, D. V.; McCormick, F.; Holderfield, M.; Stephen, A. G. Farnesylated and Methylated KRAS4b: High Yield Production of Protein Suitable for Biophysical Studies of Prenylated Protein-Lipid Interactions. *Sci. Rep.* **2015**, *5*, 15916.

DOI: 10.1021/acsomega.9b03639
ACS Omega 2020, 5, 832−842

SUPPORTING INFORMATION

PDE6D inhibitors with a new design principle selectively block K-Ras activity

Farid A. Siddiqui [1], Catharina Alam [1], Petja Rosenqvist [3], Mikko Ora [3], Ahmed Sabt [3,4], Ganesh babu Manoharan [2], Lakshman Bindu [5], Sunday Okutachi [2], Marie Catillon [2], Troy Taylor [5], Omaima M. Abdelhafez [4], Harri Lönnberg [3], Andrew G. Stephen [5], Anastassios C. Papageorgiou[1], Pasi Virta [3], Daniel Abankwa [1,2*]

[1] Turku Bioscience, University of Turku and Åbo Akademi University, 20520 Turku, Finland; [2] Cancer Cell Biology and Drug Discovery Group, Life Sciences Research Unit, University of Luxembourg, 4362 Esch-sur-Alzette, Luxembourg; [3] Department of Chemistry, University of Turku, 20014 Turku, Finland; [4] Chemistry of Natural Compounds Department, National Research Centre, Dokki, 12622 Giza, Egypt; [5] NCI RAS Initiative, Cancer Research Technology Program, Frederick National Laboratory for Cancer Research, Frederick, MD, USA

[*] Corresponding author: daniel.abankwa@uni.lu

SUPPORTING INFORMATION to Siddiqui *et al.* PDE6D inhibitors with a new design

Supplementary Table 1. Affinity of Deltaflexin compounds and Deltarasin determined in a fluorescence anisotropy assay (data from Figures S1C and S4A)

Compound	FP (PDE6D/ F-Rheb)	
	IC_{50} (95% CI) /μM	K_d /μM
Deltarasin	0.45 (0.26 – 0.9)	0.13
15 (Deltaflexin-1)	25.4 (22 – 29)	7.27
19	No binding	
14	855 (337 – 19540)	244.2
17	27.1 (22 – 33)	7.73
22	234 (180 – 336)	68.5
23 (Deltaflexin-2)	25.1 (17 – 37)	7.17

SUPPORTING INFORMATION to Siddiqui *et al.* PDE6D inhibitors with a new design

Supplementary Figure S1. Related to Figure 1 - Newly designed inhibitors compete with K-Ras for PDE6D in vitro.

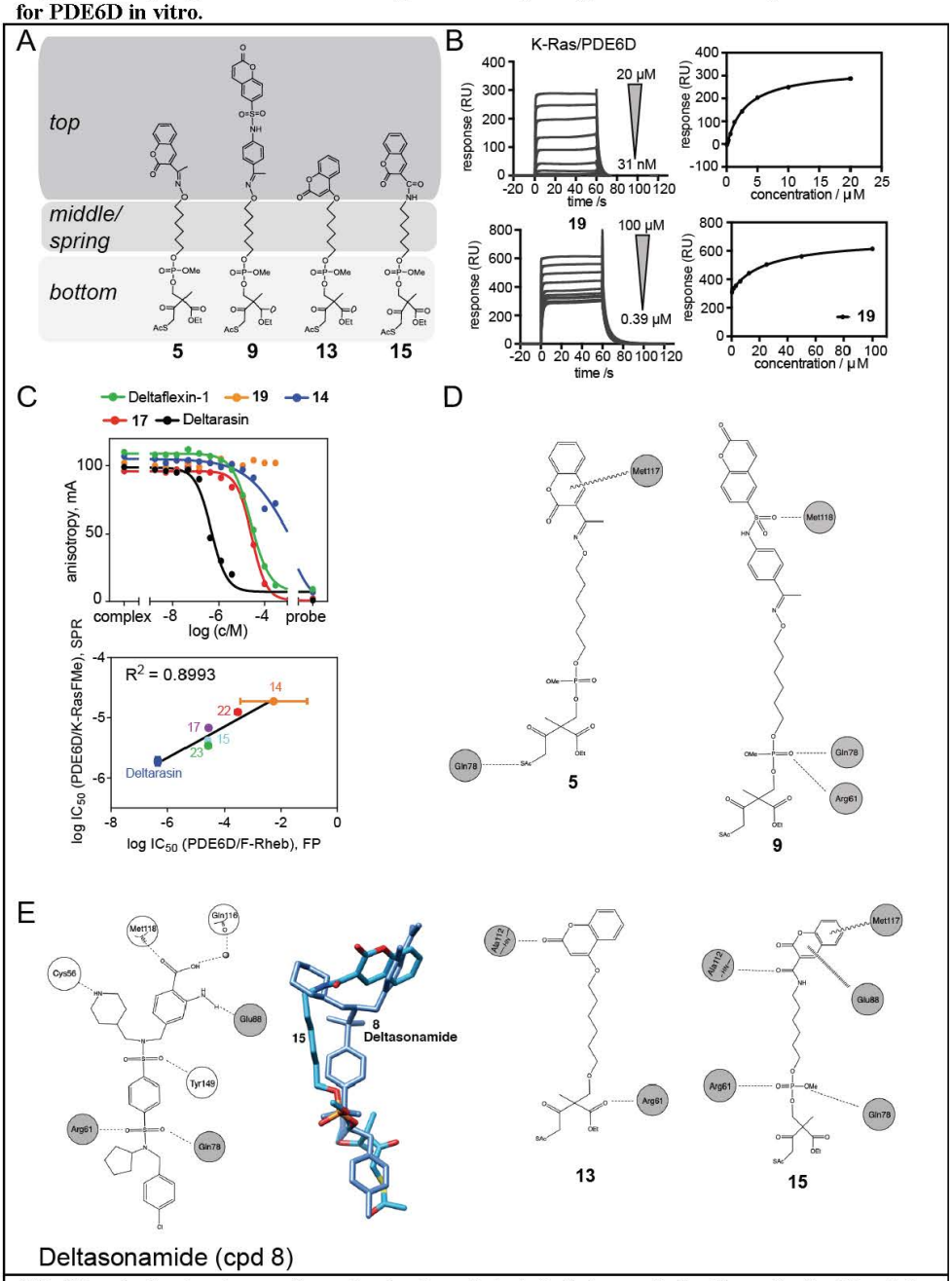

(A) Chemical structures of synthesized and tested linkage derivatives **5**, **9**, **13** of the Deltaflexin-series, as compared to **15** (Delataflexin-1). (B) SPR binding kinetics of PDE6D

with N-terminal avi-tagged K-RasFMe captured on a neutravidin chip (top left) and SPR binding kinetics of compound **19** in competition with PDE6D/ K-RasFMe interaction. n=3 (**C**) Binding of Deltarasin, Deltaflexin-1 and compounds **14, 17** and **19** to PDE6D determined in the fluorescence anisotropy assay; n=1. The correlation between IC_{50} values of compounds obtained by SPR analysis and fluorescence anisotropy assay is presented (right). (**D**) Schematic binding mode of compounds **5**, **9**, **13** and **15** to PDE6D based on computational docking results. (**E**) Comparison of the PDE6D binding mode (left) of the Deltasonamide (compound **8** in Martin-Gago et al. 2017, PDB code 5ML6) and **15** (Deltaflexin-1). (D) Residues involved in interactions similar to those of the depicted Deltasonamide (E) are shown in grey. Hydrogen bonds are depicted with dashed lines. Aromatic stacking interactions are shown with squiggled lines.

SUPPORTING INFORMATION to Siddiqui *et al.* PDE6D inhibitors with a new design

Supplemental Figure S2. Related to Figure 2 - Deltaflexin-1 suppresses K-Ras/ PDE6D interaction and selectively K-Ras membrane organization.

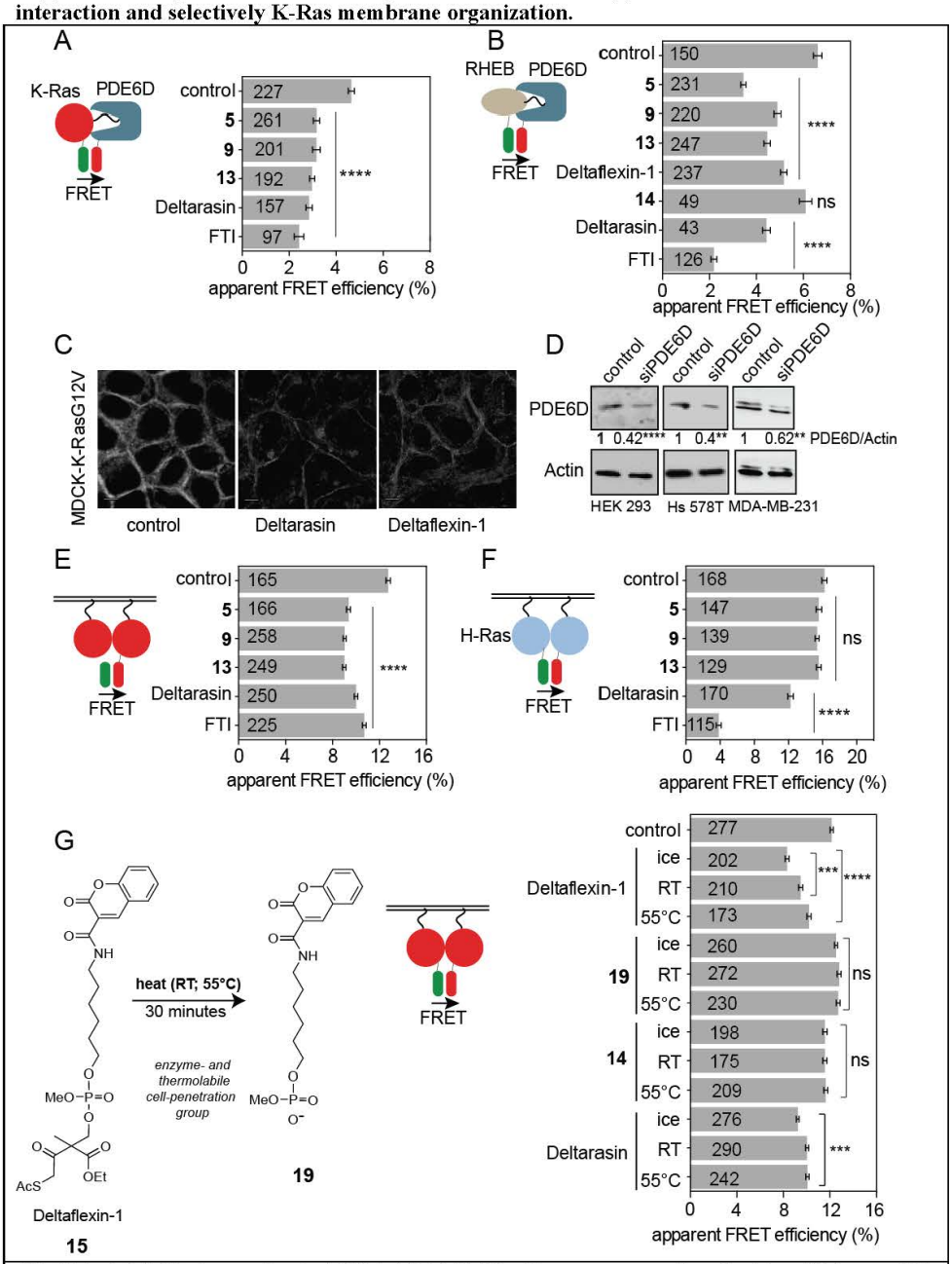

(**A**) K-Ras/ PDE6D interaction by FLIM-FRET. HEK cells were co-transfected with mGFP tagged K-RasG12V and mCherry tagged PDE6D and treated with 0.1% DMSO control or 5 µM of **5, 9, 13**, Deltarasin or 0.5 µM of FTI-277 for 24 h, n = 4. (**B**) PDE6D-Rheb interaction by FLIM-FRET. HEK

cells were co-transfected with mCitrine tagged Rheb and mCherry tagged PDE6D. Transfected cells were treated with 0.1% DMSO control or 5 μM of compounds **5**, **9**, **13**, Deltaflexin-1, **14** (Deltaflexin-1 precursor lacking the cell penetration moiety), Deltarasin or 0.5 μM FTI-2628 for 24 h, n = 3. The overall higher FRET of this latter reporter agreed with the higher soluble fraction of Rheb and a more efficient FRET-fluorophore pair. (**C**) Confocal imaging of MDCK cells expressing mGFP-K-RasG12V at 5 μM of indicated compounds treatments. Scale bar = 100 μm, n = 2. **(D)** Representative Western blot data showing the knock-down efficacy for PDE6D in siPDE6D-transfected cells, n ≥ 3. Cells were treated with 50 nM of siRNA for 48 h. (**E, F**) Ras membrane organization by nanoclustering-FRET in HEK cells co-expressing mGFP and mCherry tagged K-RasG12V (E) or H-RasG12V (F). Cells were co-transfected with siRNA PDE6D for 48 h or treated with 0.1% DMSO control or 5 μM of **5**, **9** **13**, Deltarasin or 0.5 μM FTI-277 for 24 h, n = 3. **(G)** K-Ras nanoclustering-FRET in HEK cells co-expressing mGFP or mCherry tagged K-RasG12V. The cells were treated with 2.5 μM Deltaflexin-1, **14**, **19**, or Deltarasin. Freshly thawed compound aliquots were immediately diluted in ice cold medium (ice) and then added to cells or incubated for 1 h at room temperature (RT), or for 30 minutes at 55°C (55°C) before addition to cells, n = 3. The latter two conditions led to the premature, thermal deprotection of the compounds from their cell-penetration groups. For all FRET-data the numbers on the bars indicate the number of analysed cells and the bars represent mean values ± SEM. (**A,B,D,F,G**) Statistical significance levels are annotated as ns, not significant; *p < 0.05; **p < 0.01; ***p < 0.001; ****p < 0.0001; ns, not significant..

Supplemental Figure S3. Related to Figure 3 - Deltaflexin-1 selectively inhibits oncogenic K-Ras driven cell proliferation and mammosphere formation.

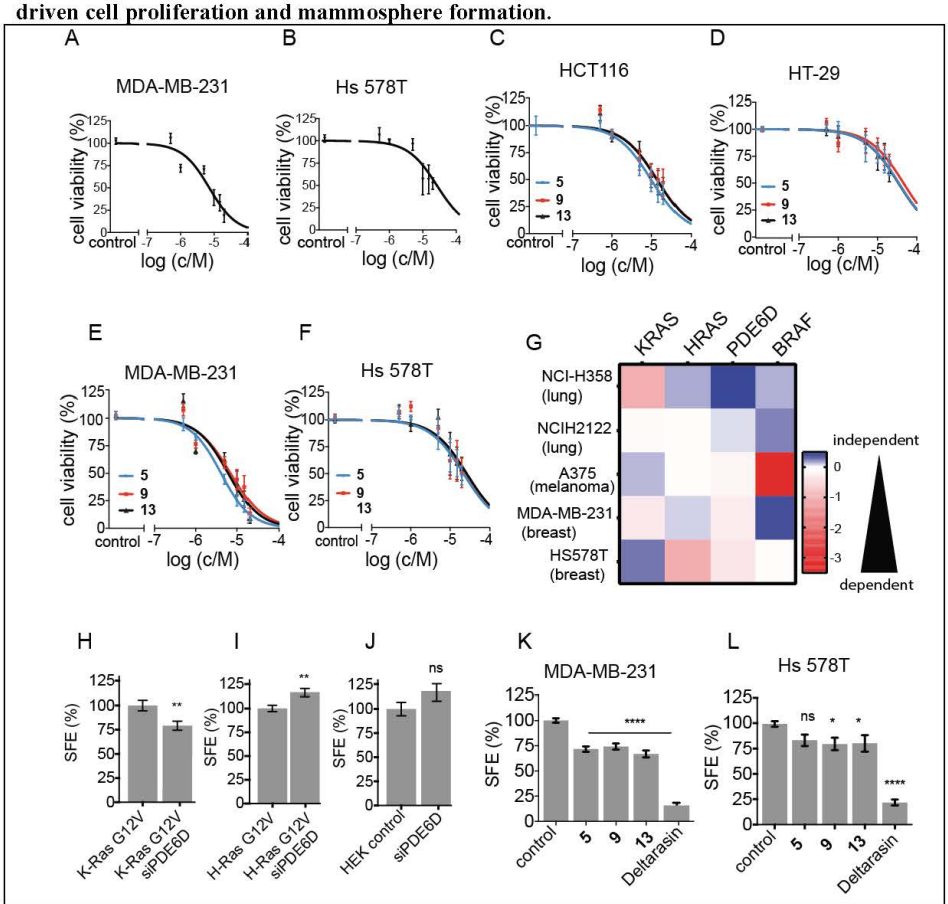

(**A, B**) Cell viability of MDA-MB-231 cells (A) and Hs578T cells (B) in response to Deltaflexin-1; n=3. (**C-F**) Cell viability of HCT116 (C), HT-29 (D), MDA-MB-231 (E) and Hs578T (F) cells in response to Deltaflexin derivatives. Cell viability curves (A-F) are expressed as % cell viability relative to 0.1% DMSO-treated control plotted against the log-transformed drug concentrations; n=3. (**G**) ATARis gene sensitivity profile of indicated cell lines and genes. Gene dependency/sensitivity data wer collected from the Project drive (ATARis) database at https://oncologynibr.shinyapps.io/drive/. The ATARis study is a large-scale RNAi screen in which viability effects of mRNA knockdown were assessed for 7,837 genes using an average of 20 shRNAs per gene in 398 cancer cell lines. The study outlines the classes of cancer dependency genes and their relationships to genetic, expression and lineage features. (**H,I,J**) Tumorosphere forming efficiency (SFE) after knockdown of PDE6D in HEK cells transiently transfected with K-RasG12V (H), H-

RasG12V (I) with or without 50 nM of scrambled siRNA or siPDE6D for 48 h (J). SFE is calculated as percent relative to scrambled siRNA control. Statistical comparison was done against the scrambled siRNA control. (**K,L**) SFE in MDA-MB-231 (K) and Hs 578T (L) cells in response to treatment with 5 µM Deltaflexin derivatives or Deltarasin for 72 h. All values are mean values ± SEM, n = 4. (**H-L**) Statistical significance levels are annotated as ns, not significant; *p < 0.05; **p < 0.01; ***p < 0.001; ****p < 0.0001; ns, not significant.

SUPPORTING INFORMATION to Siddiqui *et al.* PDE6D inhibitors with a new design

Supplemental Figures S4. Related to Figure 4 - Partial scaffold hybridization creates second generation inhibitors.

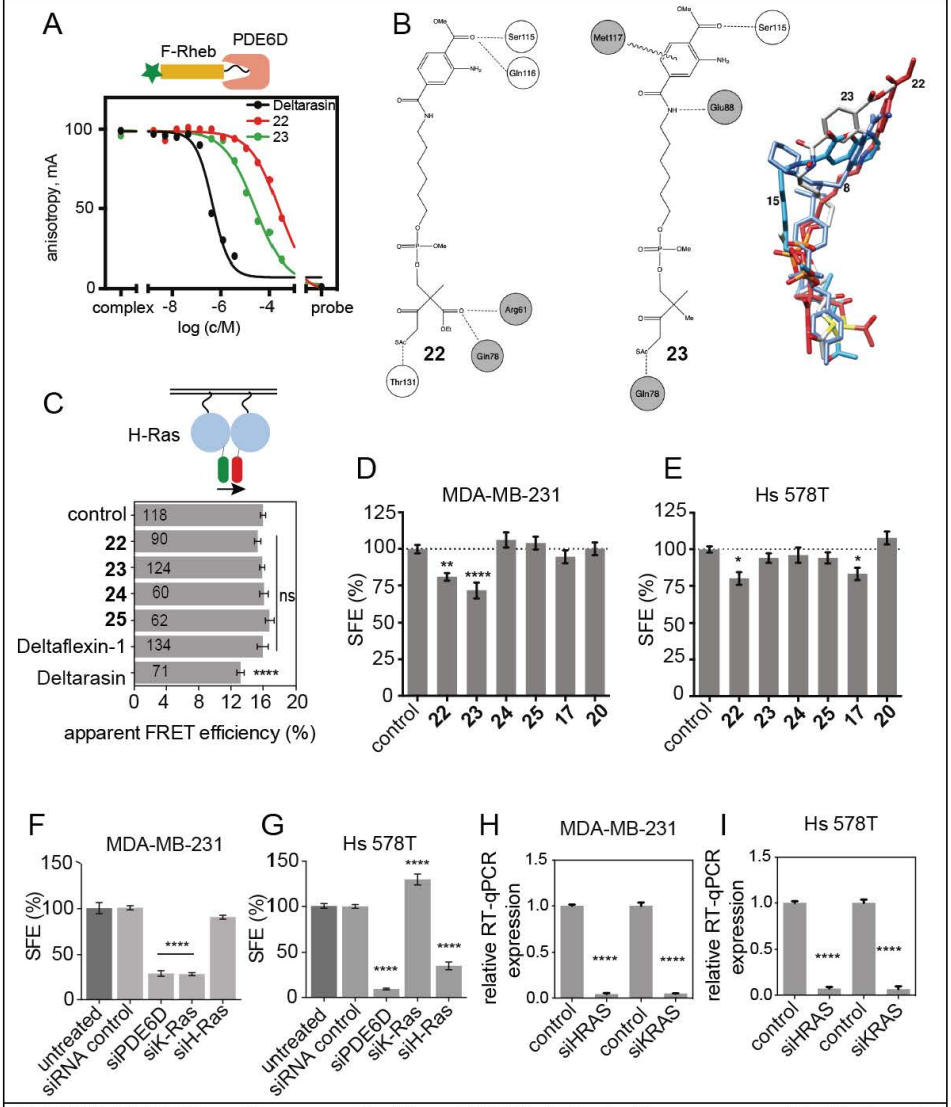

(**A**) PDE6D binding of compounds **22** and **23** (Deltaflexin-2) as compared to Deltarasin determined in fluorescence anisotropy assay; n = 1. (**B**) Schematic binding mode of compounds **22** and **23** to PDE6D based on computational docking results. New contacts as compared to the Deltasonamide compound 8 (Figure S1E) are shown with white background. Superposition of **23**, **23**, Deltasonamide compound 8, and **15** is shown on the right in stick representation. (**C**) H-Ras membrane organization by nanoclustering-FRET in

HEK cells co-expressing mGFP or mCherry tagged H-RasG12V. After 24 h of transfection, cells were treated with 5 μM of indicated compounds, n = 2. (**D,E**) Sphere formation efficiency (SFE) of MDA-MB-231 cells (D), n ≥ 4, and Hs 578T cells (E) n ≥ 4, cultured in suspension culture followed by a 72 h incubation with 5 μM of indicated compounds. (**F,G**) SFE of MDA-MB-231 cells (F) and Hs 578T cells (G) either untreated or transfected with 50 nM of scrambled siRNA, siPDE6D, siKRAS or siHRAS. (**H,I**) RT-qPCR analysis of knockdown efficiency of siKRAS and siHRAS in MDA-MB-231 cells (H) and Hs578T cells (I); n = 1. The figures represent mean values ± SEM. Statistical significance levels are annotated as ns, not significant; *p < 0.05; **p < 0.01; ***p < 0.001; ****p < 0.0001; ns, not significant.

Supplementary Data S1: Related to "Compound synthesis" in the Methods section. Chemical synthesis and analytical data

Table of Contents

SYNTHESES

Seven different coumarin-phosphate derivatives (**5**, **9**, **13**, **15**, **17**, **19** and **20**, Figure S4 and Scheme 1) and four terepthalic acid-phosphate derivatives (**22**, **23**, **24** and **25,** Figure S4), bearing a bioactivatable and thermolabile phosphate protecting groups (4-acetylthio-2-ethoxycarbonyl-3-oxo-2-methylbutyl, **26**[1] or 4-acetylthio-2,2-dimethyl-3-oxobutyl, **27**[1]), were prepared as outlined in Schemes 2-8. The coumarin or terepthalic acid and phosphate moieties are connected to each other through the *O*-hexyl oxime (**5**), *N*-arylsulfonamide-*O*-hexyl oxime (**9**), *O*-hexyl (**13**), hexylamide (**15, 22** and **23**), butylamide (**20**, **24** and **25**) and methyl cyclohexylmethylamide (**17**) linkers. The 2,2-disubstituted 4-acylthio-3-oxobutyl group is an esterase- and thermolabile phosphate protecting group that enhances cellular uptake of the drug candidates. The enzymatic and nonenzymatic deprotection of 4-acetylthio-2-ethoxycarbonyl-3-oxo-2-methylbutyl and 4-acetylthio-2,2-dimethyl-3-oxobutyl group takes place by intramolecular cyclization to give the negatively charged phosphodiester and a substituted tetrahydrothiophenone (deprotection for **15** given as an example in Scheme 1).[1] Additionally, the 4,4-disubstituted dihydrothiophen-3(2H)-one byproduct is not markedly alkylating, confirmed by glutathione adduct experiments in our earlier studies.[1] If the enzymatic reaction becomes retarded, the thermolytic removal takes a place.[2]

REFERENCES

1. Kiuru, E., Ahmed, Z., Lönnberg, H., Beigelman, L. & Ora, M. 2,2-Disubstituted 4-acylthio-3-oxobutyl groups as esterase- and thermo-labile protecting groups of phosphodiesters. *J. Org. Chem.* **78**, 950-959 (2013).

2. Leisvuori, A. Lönnberg, H. & Ora, M. Acetylthio-2,2-dimethyl-3-oxobutyl group as an esterase- and thermo-labile protecting group for oligomeric phosphodiesters *Eur. J. Org. Chem.* 5816-5826 (2014).

3. Defrancq, E & Lhomme, J. Use of an aminooxy linker for the functionalization of oligodeoxyribonucleotides. *Bioorg. Med. Chem. Lett.* **11**, 931-933 (2001).

4. Cebon, B., Lambert, J. N., Leung, D., Mackie, H., McCluskey, K. L., Nguyen, X. & Tassone, C. New DNA modification strategies involving oxime formation. *Aust. J. Chem.* **53**, 333-339 (2000).

5. Siddiqui, N., Arshad, M. F. & Khan, S. A. Synthesis of some new coumarin incorporated thiazolyl semicarbazones as anticonvulsants. *Acta Pol. Pharm. Drug Res.* **66**, 161-167 (2009).

6. Abdel-Wahab B. F., Mohamed, H. A. & Farhat, A. A. Ethyl coumarin-3-carboxylate: synthesis and chemical properties. *Org. Commun.* 7, 1-27 (2014).

7. Al-Kindy, S. M. Z. & Miller, J. N. Coumarin-6-sulphonyl chloride: A novel label in fluorimetry and phosphorimetry. *Anal. Chim. Acta* **227**, 145-153 (1989).

8. Bahekar, S. P., Sarode, P. B. Agrawal, N. R. & Chandak, H. S. Synthesis of some sulfonamide chalcones of biological interest. *IJCPS* 2015, **4**, 99-104.

9. Kolaczek, A., Fusiarz, I., Lawecka, J. & Branowska, D. Biological activity and synthesis of sulfonamide derivatives: a brief review. *CHEMIK* **68**, 620–628 (2014).

10. Joshi, P., Tripathi, M. & Rawat, D. S. Synthesis and characterization of novel 1,2,3-triazole-linked theophylline and coumarin *s*-triazines. *Ind. J. Chem.* **53B**, 311-318 (2014).

4.2 A covalent calmodulin inhibitor as a tool to study cellular mechanisms of K-Ras driven stemness

Sunday Okutachi, Ganesh Babu Manoharan, Alexandros Kiriazis, Christina Laurini, Marie Catillon, Frank McCormick, Jari Yli-Kauhaluoma, Daniel Abankwa.

4.2.1 Manuscript 2: Summary

CaM is a universal calcium signal regulatory protein that is known to play a key role in cell cycle regulation (LaBaer et al., 1997). It is also highly expressed in malignant tissues and cancer cell lines (Berchtold and Villalobo, 2014). It was therefore pursued as a cancer drug target in the 1980s. Current data suggest that Ca^{2+}/CaM is a K-Ras trafficking chaperone, able to facilitate the dynamic distribution of K-Ras in the cell (Agamasu et al., 2019, Grant et al., 2020b, Sperlich et al., 2016). Recent studies have implicated CaM in the promotion of K-Ras driven cancer stemness through the suppression of frizzled-8 mediated non-canonical Wnt signaling (Wang et al., 2015b). Indeed, our group previously showed that OphA disrupts the membrane organization of K-Ras4B in a CaM dependent manner and blocked the growth of cancer stem cell enriched spheroids (Najumudeen et al., 2016). However, the application of OphA as an inhibitor of CaM or a tool compound is limited by its high cellular toxicity (Chidley et al., 2016). Furthermore, studying CaM cell biology continues to be an interesting subject due to the vast implication of CaM in many cellular processes (Berchtold and Villalobo, 2014). However, the presence of 3 genes coding for this protein makes knockout and knockdown studies difficult. To this end, a major interest of this thesis is to develop novel CaM inhibitors that could be applied as potential chemical knock-down tools in cell biological studies.

In this study, we describe the identification and characterization of a novel covalent OphA-like CaM inhibitor named **Calmirasone1**. Calmirasone1 is a formyl-benzazulenone, which can be synthetized in a six-stepped reaction from guaiazulene. Initially, a small library of benzazulenones was synthesized and analyzed in cellular toxicity/viability assays, spheroid formation assays and a fluorescence polarization assay. Ras isoform specificity and on-target activity of the compounds in cells was determined using a newly developed BRET assay. Calmirasone1 showed a 4-fold higher affinity to CaM than OphA, it displayed a 7-fold faster reactivity with CaM in vitro whilst maintaining a similar K-Ras versus H-Ras cellular anticancer selectivity as OphA. Similarly, Calmirasone1 more selectively reduced the K-Ras BRET sensor signal than their H-Ras counterparts as did OphA but reached an over 38% K-Ras BRET inhibition within minutes as compared to the hours it took OphA. Furthermore, we showed that Calmirasone1 exhibited a clear

on-target activity by blocking the BRET between our K-Ras/CaM biosensors and confirmed its ability to selectively blocked K-Ras driven sphere formation whilst maintaining low unspecific cytotoxicity on the H-Ras mutated cancer cell lines. Likewise, in conformity with the central role of CaM in cell cycle regulation, we observed that Calmirasone1 induces a multipolar and an acentrosomal phenotype in HeLa cells. Conclusively, our results indicate that Calmirasone1 can serve as a novel tool compound for the elucidation of the cell biology of K-Ras/CaM associated cancer cell stemness characteristics.

4.2.2 Manuscript 2: Personal contributions of Sunday Okutachi

- Designed, performed and analysed the 3D spheroid assays as well as the 2D cell viability and toxicity assays
- Designed, performed and analysed all BRET assay data
- Performed all RT-qPCR experiments together with Marie Catillon and analysed all data
- Performed the DSS and composite drug activity score analysis
- Analysed and generated the ATARiS gene dependency profiling of the cell lines
- Generated and compiled all figures submitted for this manuscript
- Contributed to writing parts of the manuscript with guidance from Daniel Abankwa and Ganesh Manoharan

The personal contributions of all authors to the manuscript are listed in the *Authors' contributions* Section at the end of the corresponding manuscript.

frontiers

A covalent calmodulin inhibitor as a tool to study cellular mechanisms of K-Ras-driven stemness

Sunday Okutachi[1], Ganesh Babu Manoharan[1], Alexandros Kiriazis[2], Christina Laurini[1], Marie Catillon[1], Frank McCormick[3, 4], Jari Yli-Kauhaluoma[2], Daniel Abankwa[1*]

[1]University of Luxembourg, Luxembourg, [2]University of Helsinki, Finland, [3]University of California, San Francisco, United States, [4]Frederick National Laboratory for Cancer Research (NIH), United States

Submitted to Journal:
Frontiers in Cell and Developmental Biology

Specialty Section:
Cellular Biochemistry

Article type:
Original Research Article

Manuscript ID:
665673

Received on:
08 Feb 2021

Revised on:
18 May 2021

Journal website link:
www.frontiersin.org

frontiers

Conflict of interest statement

The authors declare that the research was conducted in the absence of any commercial or financial relationships that could be construed as a potential conflict of interest

Author contribution statement

S.O. designed and performed 3D spheroid assay, 2D cell viability and toxicity studies, BRET assays, DSS analysis, performed the RT-qPCR experiments and cloning together with M.C. G.M. developed the BRET assay, designed, and performed FP assays, and performed cloning. A.K. synthesized the compounds and curated the analytical data. C.L. performed microscopy. M.C. together with G.M. implemented the gateway cloning system, performed cloning, protein purification and RT-qPCR. F.M. contributed reagents and funding support. J.Y-K collaboratively designed the compounds with A.K. S.O. and G.M analyzed all the data. D.A. conceived the study, designed experiments, interpreted results, and wrote the manuscript together with S.O., G.M., A.K. and J.Y-K. All authors commented on the manuscript.

Keywords

K-ras, Calmodulin, covalent inhibitor, Cancer Stem Cell (CSC), BRET

Abstract

Word count: 219

Recently, the highly mutated oncoprotein K-Ras4B (hereafter K-Ras) was shown to drive cancer cell stemness in conjunction with calmodulin (CaM). We previously showed that the covalent CaM inhibitor ophiobolin A (OphA), can potently inhibit K-Ras stemness activity. However, OphA a fungus derived natural product, exhibits an unspecific, broad toxicity across all phyla.
Here we identified a less toxic, functional analogue of OphA that can efficiently inactivate CaM by covalent inhibition. We analyzed a small series of benzazulenones, which bear some structural similarity to OphA and can be synthesized in only six steps. We identified the formyl aminobenzazulenone 1, here named Calmirasone1, as a novel and potent covalent CaM inhibitor. Calmirasone1 has a 4-fold increased affinity for CaM as compared to OphA and was active against K-Ras in cells within minutes, as compared to hours required by OphA. Calmirasone1 displayed a 2.5 - 4.5-fold higher selectivity for KRAS over BRAF mutant 3D spheroid growth than OphA, suggesting improved relative on-target activity. Importantly, Calmirasone1 has a 40 - 260-fold lower unspecific toxic effect on HRAS mutant cells, while it reaches almost 50% of the activity of novel K-RasG12C specific inhibitors in 3D spheroid assays. Our results suggest that Calmirasone1 can serve as a new tool compound to further investigate the cancer cell biology of the K-Ras and CaM associated stemness activities.

Contribution to the field

The interplay between the most frequently mutated oncogene KRAS and calmodulin (CaM) has been suggested as a drug target for cancer stem cells. While a critical role for KRAS in driving stemness is consistent with its high mutation rate, CaM was so far pursued as a cancer drug target because of its multiple roles during cell division. Both KRAS and CaM have been independently explored as drug targets for many years in the early 1990s. Recently, KRAS has gained significant interest again, which led to clinical stage covalent inhibitors targeting specifically the KRAS-G12C allele. It is currently not well understood how KRAS and CaM collaborate on the molecular cell biological level to drive stemness. We have here developed the first synthetic covalent CaM inhibitor, which has a significantly reduced toxicity as compared to its natural product counterpart Ophiobolin A. Our best inhibitor named Calmirasone1 now offers the opportunity to perform a 'chemical knockdown' of CaM, which is transcribed from three genes. This tool compound will allow to investigate the cellular interactions and activities of KRAS and CaM in driving cancer cell stemness.

Funding statement

This work was supported by the Finnish Funding Agency for Innovation, Tekes, 3iRegeneration, project 40395/13) and Jane and Aatos Erkko Foundation to JYK. DA received funding from the Academy of Finland (Key Project # 304638) and core funding support by the University of Luxembourg.

A covalent calmodulin inhibitor as a tool to study cellular mechanisms of K-Ras-driven stemness

Sunday Okutachi[1], Ganesh babu Manoharan[1], Alexandros Kiriazis[2], Christina Laurini[1], Marie Catillon[1], Frank McCormick[3,4], Jari Yli-Kauhaluoma[2], Daniel Abankwa[1,*]

[1]Cancer Cell Biology and Drug Discovery Group, Department of Life Sciences and Medicine, University of Luxembourg, 4362 Esch-sur-Alzette, Luxembourg
[2]Drug Research Program, Division of Pharmaceutical Chemistry and Technology, Faculty of Pharmacy, University of Helsinki, FI-00014 Helsinki, Finland
[3]Helen Diller Family Comprehensive Cancer Center, University of California San Francisco, San Francisco, CA, USA
[4] National Cancer Institute RAS Initiative, Cancer Research Technology Program, Frederick National Laboratory for Cancer Research, Leidos Biomedical Research, Inc., Frederick, MD 21702

*** Correspondence:**
Daniel Abankwa
daniel.abankwa@uni.lu

1 Abstract

Recently, the highly mutated oncoprotein K-Ras4B (hereafter K-Ras) was shown to drive cancer cell stemness in conjunction with calmodulin (CaM). We previously showed that the covalent CaM inhibitor ophiobolin A (OphA), can potently inhibit K-Ras stemness activity. However, OphA a fungus derived natural product, exhibits an unspecific, broad toxicity across all phyla.

Here we identified a less toxic, functional analogue of OphA that can efficiently inactivate CaM by covalent inhibition. We analyzed a small series of benzazulenones, which bear some structural similarity to OphA and can be synthesized in only six steps. We identified the formyl aminobenzazulenone **1**, here named Calmirasone1, as a novel and potent covalent CaM inhibitor. Calmirasone1 has a 4-fold increased affinity for CaM as compared to OphA and was active against K-Ras in cells within minutes, as compared to hours required by OphA. Calmirasone1 displayed a 2.5 – 4.5-fold higher selectivity for KRAS over BRAF mutant 3D spheroid growth than OphA, suggesting improved relative on-target activity. Importantly, Calmirasone1 has a 40 – 260-fold lower unspecific toxic effect on HRAS mutant cells, while it reaches almost 50% of the activity of novel K-RasG12C specific inhibitors in 3D spheroid assays.

Our results suggest that Calmirasone1 can serve as a new tool compound to further investigate the cancer cell biology of the K-Ras and CaM associated stemness activities.

Keywords: K-Ras, calmodulin, covalent inhibitor, cancer stem cell (CSC), BRET

2 Introduction

Calmodulin (CaM) is a small (17 kDa) dumbbell-shaped signaling adapter, with hundreds of protein interactions and widespread functions in cellular signaling (Tidow and Nissen, 2013). Its two N- and C-terminal lobes each contain two EF-hands that can coordinate altogether four Ca^{2+} ions. Ca^{2+}/CaM classically recognizes with high, nanomolar affinity approximately 20-residue long peptides with bulky hydrophobic and basic residues that become encased in the hydrophobic pocket formed by the two lobes. This leads to a significant conformational change of CaM with loss of the central helical structure (Tidow and Nissen, 2013). Non-canonical CaM binders typically possess a polybasic N- or C-terminus with a single lipid-modification, which can bind to either or both of the hydrophobic pockets on the N- and C-lobes (Grant et al., 2020b).

CaM has been pursued as a cancer drug target in the 1980s, due to its significant role in activating CDKs in the cell cycle (Hait and Lazo, 1986). CaM levels increase during the cell cycle, peaking at G2/M, with a drop-off thereafter (Berchtold and Villalobo, 2014). In addition, CaM seems to be indirectly important for the activation of CDKs that are active in G1 (Taules et al., 1998). CaM distribution is furthermore tightly associated with cell division, as it co-distributes with major structures of the mitotic machinery, such as the central spindle, centrosomes and the cleavage furrow (Li et al., 1999;Yu et al., 2004). In line with this, CaM inhibitors have been demonstrated to block tumor growth, such as for example in multiple myeloma cell line xenografts (Yokokura et al., 2014).

Several non-covalent CaM inhibitors have been developed including frequently used calmidazolium (Sunagawa et al., 1999) and the highly water soluble and cell penetrating naphthalenesulfonamides, such as W-7 (Hidaka et al., 1981;Sengupta et al., 2007). However, the latter can also inhibit CaM targets, such as Ca^{2+}/CaM-dependent cyclic nucleotide phosphodiesterase at concentrations > 100 µM (Itoh and Hidaka, 1984;Zimmer and Hofmann, 1984).

Ophiobolin A (OphA) is a potent, covalent CaM inhibitor (Leung et al., 1984). It is a naturally occurring fungal 5-8-5 tricyclic sesterterpene metabolite with broad toxicity against plants, microbes and cancer cells (Au et al., 2000). It forms an irreversible covalent adduct via C5, C21-dicarbonyl functionalities after intermediate Schiff base formation with Lys 75 or Lys 77 and Lys 148 of CaM (**Scheme S1**). Thus, OphA can react with CaM at a 2:1 ratio, similar to covalent phenothiazine derivatives, which also react with the same lysines (Faust et al., 1987). Despite its potency against CaM, OphA appears to have several other targets, such as phosphatidylethanolamine (Chidley et al., 2016). Together with its broad toxicity across most phyla this suggests a problematic toxicity spectrum of OphA.

We previously identified OphA as a K-Ras4B (hereafter K-Ras), but not H-Ras selective inhibitor (Najumudeen et al., 2016). OphA disrupts membrane organization of K-Ras in a CaM dependent manner and blocked the growth of cancer stem cell enriched spheroids derived from breast cancer cell lines. Up to two K-Ras proteins can directly bind to the two lobes of Ca^{2+}/CaM (Agamasu et al., 2019;Grant et al., 2020a). Interestingly, K-Ras has a higher affinity to the C-terminal lobe (K_D = 0.5 µM) than to the N-terminal lobe (K_D = 4 µM). Complementary to this, the C-terminal lobe of CaM binds Ca^{2+} with higher affinity compared to the N-terminal lobe (Teleman et al., 1986). This affinity constellation may underpin a Ca^{2+}-mediated K-Ras release mechanism. Binding of K-Ras is nucleotide-independent, but dependent on the farnesylated C-terminus, while also geranylgeranylation mediates binding albeit with an almost 10-fold lower affinity (Wu et al., 2011;Agamasu et al., 2019;Grant et al., 2020a). In addition, basic residues of the hypervariable region of K-Ras may contribute to the interaction, however, interaction with the prenyl moiety provides the core affinity (Jang et al., 2019;Grant et al., 2020a). In contrast to these more recently established binding determinants, a preference of CaM binding to GTP-K-Ras was previously observed (Villalonga et al., 2001;Abraham et al., 2009).

Experimental data show that palmitoylated Ras isoforms do not interact with CaM (Villalonga et al., 2001), probably because the palmitoyl-moiety would hinder binding to CaM sterically. Thus its client selectivity could resemble that of PDE6D (PDEδ), a trafficking chaperone that is important for K-Ras plasma membrane localization (Chandra et al., 2011). Indeed, evidence suggests that Ca^{2+}/CaM can act as a trafficking chaperone for K-Ras (Fivaz and Meyer, 2005;Grant et al., 2020a), which at high concentration could sequester K-Ras from the membrane as it binds with a lower affinity (K_D = 4 µM) to nanodiscs than to Ca^{2+}/CaM (Gillette et al., 2015). Given that Ca^{2+}/CaM has a different K-Ras affinity, release mechanism, cellular distribution and probably client spectrum than PDE6D, it can be expected that these proteins have overlapping, yet non-redundant chaperone functions. The interaction of CaM with K-Ras is inhibited by phosphorylation of Ser181 in the C-terminus of K-Ras, while vice versa CaM binding prevents phosphorylation (Alvarez-Moya et al., 2010). Intriguingly, the phosphomimetic S181D has a reduced stemness potential (Wang et al., 2015b). Consistently, the atypical PKC agonist prostratin reduced the growth in several murine tumor models, including pancreatic cancer cell line derived xenografts (Wang et al., 2015b).

Thus, a novel rationale for the development of CaM inhibitors has emerged, which is tied to the K-Ras dependent induction of cancer cell stemness. While this K-Ras and cancer stemness association may rekindle CaM inhibitor drug development, further dissection of the molecular mechanism is hampered by the fact that three transcribed copies of CaM genes exist (*CALM1-3*) in the human genome (Toutenhoofd and Strehler, 2000). CaM cell biology is therefore difficult to dissect genetically.

Here we describe the identification of the formyl aminobenzazulenone **1**, later named Calmirasone1, as a novel, covalent CaM inhibitor. The compound is synthetically readily accessible in a six-step synthesis from commercially available guaiazulene. Its higher CaM affinity, fast K-Ras directed cellular activity and > 40-fold reduced unspecific cell toxicity as compared to OphA allow utilization of Calmirasone1 in acute cell biological experiments.

3 Results

3.1 Phenotypic assessment of amino benzazulenones versus ophiobolin A

OphA is a potent CaM inhibitor that covalently inactivates its target. We previously showed that it selectively inhibits the functional membrane organization of oncogenic K-Ras. This enabled inhibition of cancer stem cell features by an as yet not fully defined cellular mechanism (Najumudeen et al., 2016). However, the broad toxicity of OphA limits its application (Chidley et al., 2016).

In order to identify a less toxic functional analogue of OphA for application in cell biological studies, we chose the azulene-derived aromatic benzazulen-3-one scaffold, which is distantly related to the nonaromatic 5-8-5 tricyclic ring framework of OphA. This choice was based only on the chemical similarity and no additional compound-design or -screening efforts were made. We prepared two series of synthetically easily accessible compounds, formylated and matching non-formylated aminobenzazulenones, containing two or one electrophilic functionalities for covalent binding (**Scheme 1**). The *ortho*-quinone methide electrophile is part of the ring structure and was shown to react readily with primary amines in a nucleophilic aromatic substitution reaction (Kiriazis et al., 2017) (**Data S1**), however, other nucleophiles could also react with it. In addition, formyl aminobenzazulenones can undergo a typical Schiff base reaction with amines via their C1-formyl, similar to OphA.

Given that toxicity was the major obstacle to overcome, we first characterized the effects of the compounds in phenotypic assays. Clonogenic growth of breast cancer cell derived 3D tumor spheroids under low adherent conditions, is a well-established assay for cancer stem cell properties (Dontu et al., 2003). We were interested in compounds with high K-Ras selectivity in 3D spheroid assays, but low general toxicity in 2D proliferation assays. Consistent with their Ras mutation status, MDA-MB-231

(K-RasG13D) and Hs 578T (H-RasG12D) spheroids were selectively sensitive to KRAS and HRAS knockdown, respectively (**Figure S1 A-D**), as shown previously (Siddiqui et al., 2020).
Compounds showed varying potencies in 3D spheroids with IC_{50} values between 12 µM and > 40 µM in MDA-MB-231, and 5.2 µM and > 40 µM in Hs 578T, as compared to 0.3 µM and 1.8 µM, respectively, for OphA (**Table 1; Figure S1 E-H**). In order to have a more robust descriptor of the compound effect on the clonogenic sphere forming ability of these cells, we used the drug sensitivity score, DSS_3, which is a normalized area under the dose-response curve value with superior accuracy over IC_{50} determination (**Figure 1 A,B)** (Yadav et al., 2014). Thus, it became clear that some compounds had a selectivity for the KRAS-dependent MDA-MB-231 spheroids that was similar to or better than that of OphA.
Next we compared the general cytotoxicity (**Figure 1 C,D)** and anti-proliferative activity in cells grown in 2D at 10 µM compound concentration (**Figure S1 I,J)**. Higher toxicities and anti-proliferative effects with selectivity for MDA-MB-231 were generally observed for the formyl aminobenzazulenones. However, none of the compounds tested at 10 µM was as non-specifically toxic as OphA at only 1 µM against HRAS-dependent Hs 578T cells.

3.2 Several benzazulenones have a higher affinity to CaM than OphA

High affinity to the target typically reduces off-target toxicities (Bedard et al., 2020). We therefore next determined the in vitro affinity of the 14 compounds to the intended target CaM using a fluorescence polarization assay previously developed by us (Manoharan et al., 2019). This assay measures the displacement of a fluorescein-labelled CaM-binding peptide, here derived from plasma membrane calcium-ATPase (PMCA), from purchased CaM by the inhibitors (**Table 2; Figure S2 A,B**).
Compounds **2** and **3** showed the highest affinity (15-fold higher affinity than OphA) and **1** being third best (4-fold higher affinity) after 24 h incubation. The fact that OphA had a significantly higher cytotoxic- and antiproliferative activity (**Figure 1 C-D; Figure S1 I,J**), despite lower affinity than six of the compounds, confirms its problematic off-target toxicity (Chidley et al., 2016).
Based on these in vitro and the phenotypic data, we calculated a customized **composite drug activity score** to select compounds with most favorable properties in each series i.e. high overall activity in the 3D spheroid assay, high MDA-MB-231 KRAS-mutant cell line selectivity in 3D spheroid assays, low relative 2D growth toxicity against Hs 578T cells relatively to MDA-MB-231 and high affinity (**Figure S2 E,F**). Thus, we selected **1**, **2, 3, 8, 9** and **11** for further analysis.
Of note, the binding affinity of OphA increased over several hours, consistent with the slow covalent Schiff base bond formation and the additional pyrrole adduct formation (**Figure 2 A,B; Scheme S1**). By contrast, most benzazulenones immediately showed high IC_{50} ranging from sub-micromolar to tens of micromolar.
The potency and selectivity of covalent inhibitors are governed by two parameters namely K_i, the affinity constant of initial non-covalent complexand k_2, the rate of subsequent covalent bond-formation (Singh et al., 2011). The latter cannot be too high to avoid non-specific reactivity. Analysis of the reactivity of the top six compounds, revealed that formyl aminobenzazulenonens had lower K_i as compared to non-formylated compounds, suggesting that the formyl moiety decreases the non-covalent affinity component (**Table 3; Figure S2 G,H**). This is consistent with the hydrophobic binding sites on CaM. However, k_2 increased for **1** and **2**, as well as **8** and **9**, with both **2** and **9** having a covalent bond rate constant as high as that of OphA, which also showed and intermediate K_i value.

3.3 Cellular BRET experiments confirm K-Ras selectivity of top compound 1

Ras proteins are tightly packed into proteo-lipid membrane signaling complexes called nanoclusters (Abankwa et al., 2007). Fluorescent tagging of Ras proteins with a pair of FRET-enabling fluorophores thus leads to the emergence of nanoclustering-dependent FRET. Loss of this FRET signal reports however not only on the loss of nanoclustering, but also on any upstream processes, i.e. proper Ras plasma membrane trafficking or lipid modifications (Kohnke et al., 2012).

Here we established an analogous nanoclustering-BRET assay by tagging RasG12V proteins with Rluc8, enabling donor emission, and GFP2 as acceptor. As expected, treatment with mevastatin, which blocks prenyl-synthesis, reduced nanoclustering-BRET of both Ras isoforms fairly indiscriminately, while treatment with a farnesyl transferase inhibitor (FTI-277) selectively (1.4-fold) decreased H-Ras nanoclustering-BRET (**Figure 3 A,B**), due to the alternative prenylation of K-Ras, as described before (Kohnke et al., 2012).

Inhibition of the trafficking chaperone PDE6D, which facilitates plasma membrane trafficking in particular of K-Ras, decreases selectively K-Ras nanoclustering-FRET (Siddiqui et al., 2020). In agreement with CaM acting as a trafficking chaperone that can likewise promote forward trafficking to the plasma membrane, we observed a K-Ras selective reduction of nanoclustering-BRET after CaM inhibition with calmidazolium (1.5-fold) and OphA (1.2-fold). The atypical PKC agonist prostratin, which would stimulate K-Ras-Ser181 phosphorylation and thus block CaM binding, had a similar selectivity (1.5-fold) as the CaM inhibitors.

We then tested the top six compounds in this assay in order to directly assess their in cellulo K-Ras selectivity. While most compounds appeared to show some level of K-Ras selectivity (all < 1.3-fold) when compared at 20 µM and 24 h exposure (**Figure 3 A,B**), testing over a wider concentration range revealed distinct potencies and selectivities (**Figure S3 A,B**). We employed the DSS analysis adapted to BRET-data (BRET-DSS_3) to quantify these activities (**Figure 3 C**). While again overall BRET-activity was highest for OphA, K-Ras-selectivity was highest for **1**. All other compounds had lower and non-significant selectivities. By doing a BRET donor saturation titration analysis, we further confirmed that **1** has a similar K-Ras vs. H-Ras selectivity as OphA (**Figure 3 D,E; Figure S3 C-F**).

Compound **1** affinity to CaM changes less over time than that of OphA, suggesting it assumes its full activity faster (**Figure 2**), which could be advantageous if true also in cellular applications. We therefore tested this property in cells using the K-Ras BRET biosensor. In order to see clear effects at short exposure times, all compound concentrations were increased. OphA showed no significant BRET change during the 2 h treatment timeframe, consistent with the significant time it requires for high affinity binding (**Figure 2**). Likewise, mevastatin did not cause any reduction in the BRET signal, as it has to block metabolic pathways for farnesyl- and geranylgeranyl-pyrophosphate synthesis and therefore acts slowly after protein turnover. In agreement with the in vitro data, **1** showed a 38% reduction in BRET signal within 10 minutes of treatment (**Figure 3 F**). It was therefore even more active acutely in cells than the non-covalent CaM inhibitors trifluoperazine (K_d = 1.35 µM) or calmidazolium (K_d = 13.5 nM) (Manoharan et al., 2019).

3.4 BRET experiments confirm K-Ras/ CaM disrupting on-target activity in cells

Previously a preference of CaM binding to active, GTP-K-Ras was observed (Villalonga et al., 2001;Abraham et al., 2009). In agreement with these data, we observed in cells a higher BRET of N-terminally Rluc8-tagged K-RasG12V with GFP2-CaM, than of non-oncogenic K-Ras (**Figure 4 A; Figure S4**). Likewise higher BRET levels were confirmed with three additional oncogenic mutants of K-Ras (**Figure 4 B; Figure S4 A,B**). Furthermore, in line with previous reports (Villalonga et al., 2001), K-RasG12V ($BRET_{max}$ = 0.35 ± 0.02) displayed a significantly (p = 0.001, upaired t test) higher cellular BRET ratio with GFP2-CaM than H-RasG12V did ($BRET_{max}$ = 0.20 ± 0.02), which remained at or below control levels (**Figure 4 C; Figure S4**). This could explain the preferential effect on K-Ras nanoclustering-BRET by CaM inhibitors (**Figure 3**).

In order to have a high dynamic range of the BRET-signal, we used the Rluc8-K-RasG12V/ GFP2-CaM BRET pair to directly assess the effect of modulators of the K-Ras/ CaM interaction. Both CaM inhibitor calmidazolium and OphA significantly reduced the BRET signal. Surprisingly, prostratin did not have an effect at the tested concentration (**Figure 4 D**).
To further delineate the structural requirements for the on-target, K-RasG12V/ CaM disrupting activity, we tested formyl aminobenzazulenone **1** in comparison to the closely related, but less active aminobenzazulenone derivative **8**, which lacks the C1-formyl group. Compound **1** (IC_{50} = 31 ± 2 µM) was significantly more active than **8** (IC_{50} = 70 ± 11 µM; p = 0.03), also when tested over a wider concentration range (**Figure 4 E**). Yet, OphA remained the most effective compound in this cellular assay after a 24 h long exposure (IC_{50} = 12 ± 2 µM).

3.5 Dependence of the activity of top compound 1 on lysines 75, 77 and 148 of CaM

We previously showed that the K-Ras directed effect of OphA is abolished if a lysine-mutant of CaM is expressed to rescue the knockdown of endogenous CaM (Najumudeen et al., 2016). In this mutant CaM (mutCaM) lysines 75, 77 and 148 were replaced by glutamine, i.e. those residues that were reported to be modified by OphA (Kong Au and Chow Leung, 1998). To assess the dependence of compound **1** binding to CaM on these lysine residues, we again employed a fluorescence polarization assay using in house purified, His-tagged CaM or mutCaM. Both variants bound to the fluorescein-labelled peptide of Ca^{2+}/calmodulin dependent kinase II (CaMKII) (Manoharan et al., 2019). As observed before (**Figure 2**), the affinity of OphA to wild-type (wt) CaM increased over several hours, while no binding was observed to mutCaM (**Figure 5 A; Figure S5 A,B**), as reported previously (Najumudeen et al., 2016;Manoharan et al., 2019). By contrast, compound **1** also displayed binding to mutCaM, however, as compared to wt CaM, the affinity did not increase over time (**Figure 5 B; Figure S5 E,F**). This was different for the non-formylated counterpart **8**, which showed the same binding affinity for wt CaM and mutCaM over time (**Figure 5C; Figure S5 E,F**). The comparison of the activities of all three compounds suggests that the K75Q, K77Q, and K148Q mutations in the mutCaM has rendered CaM partially insensitive to **1** and **8** binding. It furthermore shows that the lysine-dependent increase in affinity over time of compound **1** depends on the C1-formyl, which could form a Schiff base bond in a slow reaction.

3.6 Activity in cell proliferation assays correlates with the K-Ras dependence of cancer cell lines

Unspecific, broad toxicity against KRAS (MDA-MB-231, MIA PaCa-2) and HRAS mutant (Hs 578T, T24) cancer cell lines, as well as HEK293-EBNA cells is a major issue of OphA (**Figure 6A**). This broad toxicity appears to greatly contribute to the high 'anti-cancer cell activity' that is observed with this compound, and clearly contrasts to the KRAS mutant cancer cell line selectivity seen with calmidazolium and **1** (**Figure 6 B; Figure S6 A-E**). Of note, the latter has a background activity against HRAS mutant cancer cells that was as low as that of the covalent K-RasG12C inhibitor AMG-510.
When compounds were compared in 3D spheroid growth assays, the significant potency difference between clinical compounds and **1** became however more obvious than in 2D assays. Both AMG-510 and vemurafenib selectively and potently abolished growth of the K-RasG12C- and BRAF-V600E-mutant cancer cell 3D spheroids, respectively, with basically no activity against other cancer cell spheroids (**Figure 6 C; Figure S6 F-I**). Compound **1** had a visibly lower activity, yet the activity profile seemed to correlate with the KRAS dependence of the cancer cell lines (**Figure 6 C,D**). Again, OphA appeared highly potent, yet clearly at the cost of its broad toxicity (**Figure 6 A,C**). These data are in line with a much improved on target activity of **1** as compared to OphA.

3.7 The best tool compound 1 can be utilized in cell biological experiments

Given the significantly reduced unspecific toxicity of **1** as compared to OphA, we tested its application in cell biological experiments. CaM dynamically localizes to centrosomes, spindle and other structures during mitosis, and its inhibition is known to affect proper cleavage furrow formation, which can lead to multipolarity (Yu et al., 2004;Wu et al., 2010).
In order to track this phenotype and the CaM distribution, we transfected HeLa cells with a mCherry-CaM construct, which primarily localized to centrosomes in mitotic cells (**Figure 7 A**). When these cells were synchronized and treated with the potent, non-covalent CaM inhibitor calmidazolium, an increased fraction of multipolar cells with multiple mCherry-CaM-positive centrosomes was observed. As expected from the faster in cell activity observed in BRET experiments (**Figure 3 F**), this phenotype was significantly pronounced with **1** (**Figure 7 B**), confirming its utility in cell biological experiments. Finally, we named compound **1**, the best performing tool compound, **Calmirasone1**.

4 Discussion

We have here identified compound **1**, which we named **Calmirasone1,** a synthetically well accessible, high affinity covalent CaM inhibitor with fast cellular K-Ras selectivity and significantly lower toxicity than the natural product counterpart OphA. While the current potency and properties of **Calmirasone1** do not fit for a compound with future medical applications, our data support its intended utility as a tool compound in cell biological applications to study CaM dependent cellular processes. Such tool compounds are important also for drug development, as they can foreshadow some on-target issues and reveal crucial mechanistic features of actual drug candidates.
Several of our compounds bound to CaM with submicromolar affinity, with **Calmirasone1** binding 4-times better than OphA. Comparison of **Calmirasone1** and **8** affinities with purified wt and mutant CaM suggests that the affinity binding component that remained constant over time was independent of the C1-formyl (**Figure 5**). This immediate high affinity could have been of non-covalent or actually also of covalent nature. Given that a second reactive group with covalent binding potential (ortho quinone-methide, *o*-QM) is present in both **Calmirasone1** and **8**, it is possible that this electrophile mediates additional covalent binding to lysine residues other than those three mutated lysines in mutCaM (**Data S1**), or alternatively cysteines. However, nucleophilic cysteines are not present in the studied CaM variants. Based on previous synthetic studies the *o*-QM reactivity towards nucleophiles (amine or thiol) can be very fast (within minutes) and proceeds via a nucleophilic aromatic substitution (S_NAr-type) reaction (Kiriazis et al., 2017). We currently lack evidence, whether this second electrophile is also engaged covalently.
Our rate analysis (**Table 3**) shows that the compound with the highest second order rate constant was **2**, followed by **3**. However, as our cellular BRET-data in **Figure 3 C** indicate, this increased reactivity appears to come at the cost of selectivity. We see a maximal selectivity for K-RasG12V vs. H-RasG12V for **1**, which has intermediate parameters, in agreement with a balance between sufficient affinity and a moderate reactivity.
We speculate that the formyl-independent binding component significantly improves the unspecific toxicity of compounds **Calmirasone1** and **8** (**Figure 1 C,D**). However, the major, slower affinity increase stems from the C1-formyl and depends on mutated lysines 75,77 and 148. This is consistent with the formyl as a hard electrophile reacting with lysine as a hard nucleophile. The typically slow Schiff base formation may therefore explain the slow increase in the effective affinity (**Figure 5 B**). The formyl substituent is furthermore beneficial, as it lowers the relatively high clogP, thus potentially increasing water solubility of these not very drug-like molecules.
Currently, the structural basis for CaM inhibition by OphA is not known. However, similar to other non-covalent inhibitors, such as trifluoperazine, the conformational dynamics of CaM may change dramatically upon inhibitor binding, collapsing the original dumbbell shaped molecule into a compact globular structure (Vandonselaar et al., 1994). We speculate that covalent inhibitors, such as OphA and

the here tested compounds would have a similar effect on the conformation and therefore activity of CaM to bind its canonical and non-canonical clients, such as K-Ras.

The Ras nanoclustering-dependent BRET-assay that we used before successfully in the FRET-format to assess the Ras-selectivity close to the mechanistic target K-Ras (Najumudeen et al., 2016;Posada et al., 2016), is sensitive to disruption of Ras membrane anchorage and correct plasma membrane trafficking. CaM was recently established as a K-Ras trafficking chaperone which can essentially act as a solubilizing factor to shield the farnesyl tail from the aqueous environment of the cytoplasm (Grant et al., 2020a). Therefore, the drop in K-Ras nanoclustering-BRET with CaM inhibitors is consistent with CaM being a trafficking chaperone for K-Ras (Grant et al., 2020b).

We have previously demonstrated similar changes in membrane anchorage of K-Ras with the inhibition of PDE6D, another prominent trafficking chaperone of K-Ras (Siddiqui et al., 2020). For PDE6D, clients such as H-Ras that are in addition palmitoylated, cannot bind as long as they are palmitoylated (Chandra et al., 2011;Dharmaiah et al., 2016). This establishes an effective K-Ras over H-Ras selectivity for PDE6D inhibition induced cell growth effects (Siddiqui et al., 2020). Grant et al. recently derived singly lipidated polybasic termini of proteins as non-canonical CaM interaction sequences (Grant et al., 2020a). Consistently, K-Ras but not H-Ras or N-Ras bind to CaM (Villalonga et al., 2001). It can be speculated that any additional palmitoylation would sterically hinder access to CaM, making palmitoylated Ras isoforms clients only if they are in their non-palmitoylated state (Agamasu et al., 2019). This would explain why the potent CaM inhibitor calmidazolium decreased the BRET-signal of H-Ras, albeit to a lesser extent than that of K-Ras (**Figure 3 A,B**).

The highly potent calmidazolium, as well as the covalent inhibitors OphA and **Calmirasone1** significantly disrupted K-Ras/ CaM-BRET in cells. By contrast, the PKC agonist prostratin had no effect on K-Ras/ CaM-BRET, but on K-RasG12V nanoclustering BRET. It may therefore be that prostratin exerts its K-Ras selectivity by a different mechanistic route than inhibition of K-Ras/ CaM interaction. Interestingly, prostratin had almost no effect on cell growth in 3D spheroid assays (**Figure 6 C**).

Clonogenic 3D spheroid growth depends on stemness associated asymmetric and symmetric division processes of cancer cells with stemness traits (Cicalese et al., 2009). Accordingly, **Calmirasone1** demonstrates an efficacy against 3D spheroid growth that correlates with the KRAS-dependence of the tested cell lines. In this regard it is noteworthy that the DSS_3-potency of **Calmirasone1** reaches already approximately 50% of AMG-510, the K-RasG12C inhibitor that is currently being evaluated in the clinic (Hong et al., 2020). However, a much larger number of cell lines would have to be tested to demonstrate a correlation between compound activity and anticipated K-Ras/ CaM targeting mechanism. For instance, both cell lines that were employed here also carry mutations in BRAF (MDA-MB-231) or in TP53 (both MDA-MB-231 and Hs578T). For both B-Raf and p53 connections to CaM signaling have been reported (Ren et al., 2008;Taylor et al., 2020), hence the cell killing activity may relate to multiple pathways that are affected downstream of CaM.

In addition, we could demonstrate the benefits of using **Calmirasone1** as a tool compound in cell biological experiments, which are not possible with OphA due to its high toxicity. We observed the induction of multipolar cells by CaM inhibitor treatment. Inhibition of CaM affects multiple processes during cell division, notably cleavage furrow formation (Yu et al., 2004). While failure of cytokinesis can lead to chromosomal instability and therefore a hallmark of cancer cells, the exact nature of the multipolar phenotype and additional effects could also play a role in the ultimately cell growth inhibiting effect of CaM inhibition (Wu et al., 2010). Interestingly, a different compound that induces multipolar acentrosomal spindles was found to selectively kill tumor cells (Wang et al., 2015a). In our cell biological experiments **Calmirasone1** (K_d = 0.87 ± 0.02 µM) can be considered more effective than non-covalent calmidazolium (K_d = 13.5 nM) (**Figures 3 F** and **7 B**). While **Calmirasone1** was used at 2.5-fold higher concentration, the 64-fold affinity difference between these two compounds suggests a > 25-fold higher effectivity of **Calmirasone1**. Therefore, **Calmirasone1** can be used to

acutely (within 30 – 60 minutes) perform a chemical knock-down of CaM in cells in a more efficient manner than with the most potent non-covalent inhibitor calmidazolium.
Covalent inhibitors have experienced a renaissance in the past few years (Singh et al., 2011). Our novel covalent CaM inhibitor **Calmirasone1** will add to the arsenal of covalent tool compounds to study in particular the cell biology of K-Ras/ CaM driven stemness processes.

5 Methods

5.1 Compound synthesis

Synthesis of chemical compounds and their analytical information are given in **Supplementary Material Data S1**.

5.2 Expression constructs and siRNA

Most expression constructs described in the study were produced by multi-site gateway cloning as described (Wall et al., 2014) (**SI Table 1**). For plasmids used in BRET assay, three entry clones, with compatible LR recombination sites, encoding the CMV promoter, Rluc8 or GFP2 tag and the gene of interest were recombined with a destination vector, pDest-305 or pDest-312 using Gateway LR Clonase II enzyme mix (cat. no. 11791020, ThermoFisher Scientific). The reaction mix was transformed into ccdB sensitive *E. coli* strain DH10B (cat. no. EC0113, ThermoFisher Scientific) and positive clones were selected using ampicillin. pDest527-His-wtCaM and pDest527-His-mutCaM were produced from the LR reaction between pDest-527 vector with either entry clone pDONR221-wtCaM or pDONR221-mutCaM. The N-terminally GFP2-tagged CaM plasmid, pDest-CMV-GFP2-CaM was cloned at Genecust (France) and amplified in *E. coli* CopyCutter EPI-400 strain (cat. no. C400CH10, Lucigen) according to the manufacturer's instruction. All the plasmids were verified by sequencing. Expression and localization of the Ras and CaM fusion proteins were confirmed by confocal microscopy (**SI Figure 7**). Protein sequences of all expression constructs are given in the Supplementary Material section. pmCherry-wtCaM was previously described (Manoharan et al., 2019).
Knockdown of CALM1 was done using a master mix of multiple siRNA against the CALM1 transcript (QIAGEN Hs_CALM1, siRNAs: SI00092925 (CALM1_4), SI02224215 (CALM1_5), SI02224222 (CALM1_6) and SI03649268 (CALM1_8)). For knockdown of specific Ras isoforms, we used for KRAS (K-Ras4A + K-Rras4B- L-005069-00) and HRAS (L-004142-00) Dharmacon On-Target plus siRNA SMARTpools. Scrambled siRNA control was from QIAGEN (cat. no. 102276).

5.3 Commercial chemical inhibitors

Fluorescein-labeled CaMKII and PMCA peptide were from Pepmic, China, and Genscript, USA respectively (Manoharan et al., 2019). DMSO was from PanReac-AppliChem (cat. no. A3672, ITW Reagents). Sources of the inhibitors used in the study are listed below.

Compound	Source	Catalogue Number
ophiobolin A	Santa Cruz	sc-202266
mevastatin	Alfa Aesar	J61357
FTI-277	BioVision	2874
prostratin	Sigma-Aldrich	P0077
calmidazolium	Santa Cruz	sc-201494
AMG-510	MedChem Express	HY-114277
vemurafenib	Selleckchem	S1267
trifluoperazine	Cayman	15068

benzethonium chloride	Sigma-Aldrich	53751

392

393 **5.4 RT-qPCR analysis of gene transcript knockdown**

394 MDA-MB-231 and Hs 578T cells were seeded in 12-well plates and transfected with indicated amounts
395 of siRNAs. Where required, siRNA was transfected into cells using Lipofectamine RNAiMAX (cat.
396 no. 13778075, ThermoFisher Scientific) reagent according to manufacturer's instruction. After 24 h of
397 transfection, total RNA was isolated using NucleoZol (cat. no. 7040404, Macherey-Nagel) according
398 to the manufacturer protocol. Reverse transcription was performed with 1 µg of total RNA using
399 SuperScript III Reverse Transcriptase (cat. no. 18080093, ThermoFisher Scientific). The knockdowns
400 of KRAS, HRAS and CALM1 gene transcripts were analyzed by real-time qPCR using SsoAdvanced
401 Universal SYBR Green Supermix (cat. no. 1725274, BIO-RAD), on the CFX-connect real-time PCR
402 instrument (BIO-RAD). The transcripts were selectively amplified using specific primers producing
403 amplicons for total KRAS (both KRAS4A and KRAS4B), HRAS and CALM1. The gene transcript
404 ACTB encoding for β-actin was used as reference. The following primers were used (Tsai et al., 2015):
405 for total KRAS, forward 5'- tacagtgcaatgagggacca-3', reverse 5'- tcctgagcctgttttgtgtct-3' (amplicon
406 206 bp); for HRAS, forward 5'- ctgaccatccagctgatcca-3', reverse 5'-tggcaaacacacacaggaag-3'
407 (amplicon 196 bp); For ACTB , forward 5'-ggggtgttgaaggtctcaaa-3'; reverse 5'- ggcatcctcaccctgaagta-
408 3' (amplicon 203 bp); For CALM1, forward 5'- gctcgcaccatggctgat-3' , reverse 5'-
409 tgttgggttctgacccagtg-3' (amplicon 144 bp).

410 **5.5 3D Spheroid Assays**

411 3D spheroid formation assays were performed in 96-well low-attachment, suspension culture plates
412 (cat. no. 655185, Cellstar, Greiner Bio-One) under serum free condition. About 1000 (MDA-MB-231,
413 NCI-H358 and MIA PaCa-2) or 2500 (Hs 578T) cells per well were seeded in 50 µL of either RPMI
414 medium (cat. no. 52400-025, Gibco, ThermoFisher Scientific) (MDA-MB-231, A375 and NCI-H358)
415 or DMEM (cat. no. 41965-039, Gibco, ThermoFisher Scientific) (Hs 578T and MIA PaCa-2),
416 containing 0.5% MethoCult (cat. no. SF H4636, Stemcell technologies), 1x B27 (cat. no. 17504044,
417 Gibco, ThermoFisher Scientific), 25 ng/mL EGF (cat. no. E9644, Sigma-Aldrich) and 25 ng/mL FGF
418 (cat. no. RP-8628, ThermoFisher Scientific). Cells were cultured for 3 days and then treated with
419 compounds or vehicle control (DMSO 0.1% v/v in growth medium) for another 3 days. The cells were
420 supplemented with fresh growth medium on the third day together with the drug treatment. For
421 knockdown experiments, cells were seeded in 12-well plates and treated with either 50 nM scrambled
422 siRNA (cat. no. 1022076, QIAGEN) or indicated concentrations of siRNAs. Next day, cells were
423 collected by trypsinization and re-plated into 96-well plates for 3D spheroid suspension culture.
424 Spheroid formation efficiency was analyzed by alamarBlue assay reagent (cat. no. DAL1100,
425 ThermoFisher Scientific). A 10% final volume of alamarBlue reagent was added to each well of the
426 plate and incubated for 4 h at 37 °C. Then the fluorescence intensity was measured using the FLUOstar
427 OPTIMA plate reader (BMG Labtech, Germany) with an excitation wavelength of 560 ± 5 nm and
428 emission wavelength of 590 ± 5 nm. The obtained fluorescence intensity data were normalized to
429 vehicle control corresponding to 100% sphere formation and the signal after 100 µM benzethonium
430 chloride treatment, which killed all cells (i.e. maximum inhibition of sphere formation).

431 **5.6 Drug sensitivity score (DSS) analysis**

432 To quantitatively profile the drug sensitivity with a more robust parameter than the IC_{50} or EC_{50} values,
433 the drug sensitivity score (DSS) analysis was employed. DSS values are essentially normalized area
434 under the curve (AUC) measures of dose-response inhibition data (Yadav et al., 2014). Drug response

data files (in Excel) ready for online analysis were prepared according to the example file obtained from the DSS pipeline website, called Breeze (https://breeze.fimm.fi/) (Potdar et al., 2020). Either raw fluorescence intensity measurements or normalized % inhibition data (for BRET assay analysis) were uploaded.

The output file provides several drug sensitivity measures including EC_{50} and AUC. We plotted the DSS_3 value (Yadav et al., 2014), which was calculated as

$$DSS_3 = DSS_2 \frac{x_2 - x_1}{C_{max} - C_{min}}$$

Where DSS_2 is given by the equation $DSS_2 = \frac{DSS_1}{\log a}$

and DSS_1 is given by the equation $DSS_1 = \frac{AUC - t(x_2 - x_1)}{(100 - t)(C_{max} - C_{min})}$

DSS_3 was employed to emphasize drugs that obtain their response area over a relatively wide dose window, as compared to drugs that show increased response only at the higher end of the concentration range. After logistic fitting of the dose-response inhibition data, the area under the curve (AUC) was determined as exact solution. A 10% minimal activity threshold (t) was set. The maximum (C_{max}) and minimum (C_{min}) concentrations were used for screening of the inhibitors, with $C_{max} = x_2$ and x_1 concentration with minimal activity t. The parameter a is the value of the top asymptote, which can be different from 100% inhibition as obtained from 100 µM benzethonium chloride treatment.

5.7 2D cell toxicity and viability assays

Hs 578T and MDA-MB-23 cells cultured in complete DMEM and RPMI medium (i.e supplemented with 10% FBS (cat. no. 10270-098, Gibco, ThermoFisher Scientific), 2 mM L-glutamine (cat. no. 25030-024, ThermoFisher Scientific)), respectively, were plated onto 96-well F-bottom cell culture plates (cat. no. 655180, Cellstar, Greiner Bio-One) at a density of 1000 cells (MDA-MB-231, MIA-PaCa-2, T24 and HEK293-EBNA) and 2500 cells (Hs 578T) per well grown for 24 h. Freshly thawed aliquots of test compounds were then added at indicated concentrations. DMSO 0.2% v/v in growth medium was used as vehicle control. Plates were further incubated for 72 h. The cell viability and cell toxicity effects were analyzed by alamarBlue and CellTox Green (cat. no. G8743, Promega) assays, respectively. A 10% final volume of alamarBlue reagent was added to each well of the plate and incubated for 4 h at 37 °C. Then the fluorescence intensity was measured using the FLUOstar OPTIMA plate reader (BMG Labtech) with an excitation wavelength of 560 ± 5 nm and emission wavelength of 590 ± 5 nm. The obtained fluorescence intensity data were normalized to vehicle control (100% viability).

For the CellTox Green assay, 100 µL of 2x CellTox Green reagent was added to each well of 96-well plate containing 100 µL of medium. The plate was protected from light and incubated for 15 min at 37 °C, then orbitally shaken for 1 min at 700 – 900 rpm. The fluorescence intensity was measured using the Clariostar plate reader (BMG Labtech) with an excitation wavelength of 485 ± 4 nm and emission wavelength of 530 ± 4 nm. The obtained fluorescence intensity data were normalized to vehicle control (0% toxicity).

5.8 Protein purification

Our numbering of CaM follows (Kong Au and Chow Leung, 1998) with Ala being the first amino acid in human CaM, as the N-terminal methionine of CaM is removed in most organisms (Halling et al., 2016). His-wtCaM and His-mutCaM were expressed in *E. coli* BL21 Star (DE3)pLysS (cat. no. C602003, ThermoFisher Scientific). pDest527-His-wtCaM and pDest527-His-mutCaM plasmids encoding wild-type human CaM and CaM with K75Q, K77Q and K148Q mutations respectively, were transformed into *E. coli* BL21 Star (DE3)pLysS and grown in Luria Broth medium supplemented with

ampicillin (100 µg/mL). At A_{600} of 0.6 – 0.8, the culture was induced with 0.5 mM of isopropyl β-D-thiogalactopyranoside and expressed for 16 h at 25 °C. Cells were collected by centrifugation and incubated on ice for 30 min. The cell suspension was sonicated in lysis buffer (20 mM HEPES, pH 7.6, 150 mM NaCl, 5 mM $MgCl_2$, 0.5 mg/mL lysozyme, and DNase I). The lysates were clarified by centrifugation at 18000 *g* for 30 min at 4 °C. The soluble factions were subjected to protein purification. The His-tagged proteins were purified on HisTrap™ HP Prepacked Columns (GE Healthcare) using the chromatography system ÄKTAprime plus (GE Healthcare). The columns were equilibrated in a buffer composed of 50 mM Tris HCl, pH 7.5, 150 mM NaCl, and 35 mM imidazole, and the His-tagged proteins were eluted in elution buffer containing 250 mM of imidazole. The eluted fractions were dialyzed for 16 h at 4 °C in buffer composed of 50 mM Tris HCl, pH 7.5, 150 mM NaCl, and 2 mM $CaCl_2$. Protein concentration was measured using NanoDrop 2000c Spectrophotometer (ThermoFisher Scientific) and purified proteins were analyzed on a 4 – 12% NuPAGE gel (cat. no. NP0321, ThermoFisherScientific) (**SI Figure 8**).

5.9 Fluorescence polarization assay

Fluorescence polarization (FP) assays were performed as described (Manoharan et al., 2019). The IC_{50} of compounds were determined in a binding/ displacement assay using fluorescein-labelled PMCA peptide (derived from plasma membrane Ca^{2+} transporting ATPase, a CaM binding protein) as the probe and recombinant bovine calmodulin (cat. no. 208690, Merck), which has an amino acid sequence identical to the human isoform. The F-CaMKII peptide was used at 5 nM concentration with 50 nM of His-tagged wt and mutCaM. FP assays were carried out in black low volume round bottom 384-well plate (cat. no. 4514, Corning) with a reaction volume of 20 µL. Compounds were three-fold diluted in assay buffer (20 mM Tris Cl pH 7.5, 50 mM NaCl, 1 mM $CaCl_2$ and 0.005% Tween 20) and a complex of 100 nM CaM and 10 nM F-PMCA peptide was added. The FP signals were recorded on the Clariostar (BMG labtech) plate reader with excitation at 482 ± 8 nm and emission at 530 ± 20 nm at 25 °C, after 30 min to 60 min interval for up to 5 h. Then the plate was incubated overnight at 4 °C and the next day final readings were taken after a total of 24 h incubation. The fluorescence anisotropy was calculated and plotted against the logarithm of the compound concentration and fit to log inhibitor *vs.* response – variable slope (four parameters) equation in Prism (GraphPad). The IC_{50} of the inhibitor was converted into K_d as described in (Sinijarv et al., 2017) using the equation,

$$K_d = \frac{[I]_{50}}{1 + \frac{[P]_{50}}{K_{D,probe}} + \frac{[E]_0}{K_{D,probe}}}$$

where $[I]_{50}$ is the concentration of free inhibitor at 50% displacement, given as $[I]_{50} = IC_{50} - [EI]_{50}$, where $[EI]_{50}$ is the concentration of CaM:inhibitor complex in case of 50% displacement, $[P]_{50}$ is concentration of free probe at 50% displacement, $[E]_0$ is concentration of free CaM at 0% displacement, $K_{D,probe}$ is the dissociation constant of the complex of probe and CaM. The K_D of the probe, F-PMCA to CaM is 6 nM (Manoharan et al., 2019).

The potency of the irreversible covalent inhibitors were assessed as described in (Singh et al., 2011). The potency and selectivity of a covalent inhibitor are governed by two parameters namely, the K_i, the affinity constant of the initial non-covalent complex and k_2, the rate of subsequent covalent bond-forming reaction as given in the chemical equation,

$$E + I \underset{}{\overset{K_i}{\rightleftharpoons}} E \cdot I \overset{k_2}{\rightleftharpoons} E - I \quad (k_{-2})$$

E and I denote a protein target and its covalent inhibitor, respectively. E · I is the initial non-covalent complex and E – I is the final covalent complex. To obtain the K_i and k_2 rates, the fluorescence polarization signal after inhibitor treatment was plotted against the incubation time and fit using a one

phase decay function to obtain the observed rate constant, k_{obs}. This was repeated for several inhibitor concentrations. Then, k_{obs} was plotted against the concentration of inhibitor and the data were fit to a hyperbolic equation, $k_{obs} = \frac{k_2 \times [I]}{K_i + [I]}$ to obtain K_i and k_2. The ratio of k_2/K_i represents the second order rate constant of the reaction of covalent inhibitor with the target.

5.10 Composite drug activity score

The composite drug activity score was obtained by computing the activity of the compounds across various assays performed. The desired properties taken into consideration are, a high activity in spheroid assay, higher selectivity for MDA-MB-231 over Hs 578T in spheroid assay, lower toxicity in 2D assay against Hs 578T as compared to MDA-MB-231 cells and higher affinity to CaM. The final score is obtained using the equation below,

$$composite\ drug\ activiy\ score = \frac{DSS_{(MDA-MB-231)}{}^{2}}{DSS_{(Hs\ 578T)}} \times \frac{2D_{toxicity(Hs\ 578T)}}{2D_{toxicity(MDA-MB-231)}} \times \frac{1}{K_d}$$

5.11 BRET assays

BRET assays were essentially performed as described by others (Lavoie et al., 2013;Bery et al., 2018). About 100,000 to 150,000 HEK293-EBNA (Meissner et al., 2001) cells were seeded per well of a 12-well plate in 1 mL of DMEM containing 10% FBS and 2 mM L-glutamine and were grown for 24 h. Next day, Rluc8-tagged donor and GFP2-tagged acceptor constructs were transfected into cells using jetPRIME transfection reagent (cat. no. 114-75, Polyplus). Each well was transfected with about 1 µg of plasmid DNA using 3 µL of jetPRIME reagent. For BRET donor saturation titration experiments, the concentration of donor plasmid (25 ng) was kept constant, and the concentration of acceptor plasmid was increased from 0 to 500 ng for RasG12V BRET pairs and 0 to 1000 ng for K-Ras/ CaM BRET pairs. The empty pcDNA3.1(-) plasmid was used to top-up the total DNA load per transfection. After 24 h of transfection, cells were treated with compounds or vehicle control (DMSO 0.2% v/v in growth medium) at the specified concentration for 24 h or the stipulated time period in case of the time-course experiments. The cells from one well of a 12-well plate were collected, washed, and re-plated in PBS (cat. no. 14190-094, Gibco, ThermoFisher Scientific) on flat bottom, white 96-well plates (cat. no. 236108, Nunc, ThermoFisher Scientific) as four technical replicates containing 90 µL of cell suspension per well. Then fluorescence intensity followed by BRET readings were carried out on a Clariostar (BMG Labtech) plate reader at 25 °C. The fluorescence intensity (RFU) of GFP2 was measured with excitation at 405 ± 10 nm and emission 515 ± 10 nm; it is proportional to the acceptor concentration [acceptor]. BRET readings were taken well by well by adding 10 µL of 100 µM coelenterazine 400a (cat. no. C-320, GoldBio), the Rluc8 substrate to each well (final concentration of 10 µM) using the injector present in the plate reader. Luminescence emission intensities were simultaneously recorded at 410 ± 40 nm (RLU, proportional to [donor]) and 515 ± 15 nm (BRET signal).

The raw BRET ratio was calculated as the BRET signal measured at 515 nm divided by emission signal measured at 410 nm (RLU). The BRET ratio was obtained by subtracting the raw BRET ratio by a background BRET signal measured for cells expressing only the donor (Bacart et al., 2008) as indicated in the formula below,

$$BRET\ ratio = \frac{\lambda em\ 515\ nm_{(donor+acceptor)}}{\lambda em\ 410\ nm_{(donor+acceptor)}} - \frac{\lambda em\ 515\ nm_{(donor\ only)}}{\lambda em\ 410\ nm_{(donor\ only)}}$$

With *donor+acceptor* denoting cells transfected with the BRET pair and *donor only* being cells expressing only the donor.

The expression of acceptor relative to donor ([acceptor]/[donor]) was determined as, $relative\ expression = \frac{RFU}{RLU}$

For BRET donor saturation titration experiments, the BRET ratio was plotted against the [acceptor]/[donor] ratio. Technical repeat data points were averaged and data points from all biological repeats were collected into one graph for subsequent fitting. The BRET ratio vs relative expression data were fitted using a binding saturation equation in the Prism (GraphPad) software to obtain the $BRET_{max}$ and $BRET_{50}$ using the equation, $y = \frac{BRET_{max} \times x}{BRET_{50}+x}$, where x is the relative expression and y is the BRET ratio. The $BRET_{max}$ represents the maximum saturation BRET signal and depends on structural parameters (distance, orientation) of the BRET complex. $BRET_{50}$ corresponds to the ratio of acceptor construct over donor construct required to attain 50% of the maximum BRET signal and is a measure of the effective relative affinity between the interacting BRET pair (Marullo and Bouvier, 2007).

When applying the DSS analysis to nanoclustering-BRET data, we used mevastatin (10 µM) to obtain the asymptote parameter (a) for maximal inhibition effect, as it prevents prenylation of Ras proteins, their plasma membrane trafficking and therefore nanoclustering. Otherwise, normalized BRET ratio data were converted to % inhibition and then subsequently uploaded onto the Breeze site (https://breeze.fimm.fi/).

Using BRET donor saturation data, the A/D plasmid ratio at which the BRET ratio changes most linearly with the relative expression was determined for each BRET sensor and then used for testing compound treatments.

5.12 ATARiS gene dependence score

To generate the ATARiS sensitivity plots, excel files corresponding to the normalized viability data for the siRNA knockdown of each gene of interest were downloaded from the publicly available database of the project DRIVE (https://oncologynibr.shinyapps.io/drive/) (McDonald et al., 2017). The Project DRIVE study is a large-scale RNAi screen in which 2D viability effects of mRNA knockdown were assessed (McDonald et al., 2017). The ATARiS algorithm was used in this study to aggregate consistent shRNA activity to gene level activity (Shao et al., 2013). From the excel files of each gene of interest, the sensitivity score data were extracted and a double gradient heatmap plot was generated using Prism (GraphPad). A higher gene dependence (of 2D viability) is indicated by a negative score, while scores zero or above represent no or neutral effects.

5.13 Confocal imaging

The localization of Ras and CaM fusion proteins were visualized by confocal microscopy. For imaging MDCK cells were cultured in DMEM supplemented with 10% FBS and 2 mM L-glutamine at 37 °C with 5% CO_2. Cells were seeded on glass coverslips 1.5H (cat. no. LH22.1, Carl Roth) in six-well plates (cat. no. 657160, Cellstar, Greiner Bio-One) and plasmids were transiently transfected with jetPRIME. Cells were fixed 48 h after the transfection with 4% paraformaldehyde (cat. no. 43368, Alfa Aesar) in PBS for 10 min at ambient temperature. After washing with PBS-Tween 0.05% (cat. no. 9127.1, Carl Roth), DNA was stained with a 1 µg/mL solution of DAPI (cat. no. D1306, ThermoFisher Scientific) diluted in PBS for 10 min. The coverslips were mounted onto glass slides using Vectashield (cat. no. H-1000, Vector Laboratories). Images were captured on a spinning disk confocal microscope (Andor, Oxford Instruments), fitted with a Zyla 5.5 sCMOS camera (Andor, Oxford Instruments), using a plan APO 60×/1.40 Ph3 DM oil immersion objective (Nikon) and NIS-Elements Imaging Software (Nikon).

To evaluate the effect of compounds on centrosome numbers during mitosis, HeLa cells were seeded in 6-well plates onto sterile coverslips and co-transfected with 0.5 µg of pmCherry-CaM and 1.5 µg pEGFP-Centrin1 plasmids using 4 µL of jetPRIME. 24 h after the transfection, cells were synchronized with 60 ng/mL of nocodazole for 16 h. After the removal of nocodazole, the cells were treated with the protease inhibitor MG132 (10 µM) to block the cells in metaphase and either calmidazolium (20 µM), **1** (50 µM) or DMSO (0.5%) for 2 h. Cells were then fixed with 4% paraformaldehyde in PBS for 10 min at ambient temperature. After washing with PBS-Tween 0.05%, DNA was stained with a 1 µg/mL solution of DAPI diluted in PBS for 10 min. Coverslips were mounted on glass slides using Vectashield and images were captured on a spinning disk confocal microscope. Images were analysed with the ImageJ software and the number of transfected mitotic cells with multipolar and normal bipolar phenotypes were counted (between 35 to 70 cells per test condition). The percentage multipolar versus bipolar cells was computed to generate the plot using the Prism software.

5.14 Data analysis

All data analysis was performed using Prism (GraphPad) version 9, unless otherwise indicated. The number of independent biological repeats, n, for each data set is provided in the relevant figure legend. Unless otherwise stated, statistical significance was evaluated using one-way ANOVA. A p-value of < 0.05 is considered statistically significant and the statistical significance levels are annotated as: * = $p < 0.05$; ** = $p < 0.01$; *** = $p < 0.001$; **** = $p < 0.0001$, or ns = not significant.

6 Figure and Scheme legends

Scheme 1. Structures of OphA and the synthetic formyl aminobenzazulenones (**1**-**7**) and matching aminobenzazulenones (**8**-**14**).

Figure 1. Phenotypic assessment of anti-clonogenic and cytotoxic activities of compounds. (**A,B**) A higher DSS_3 reflects a more potent effect of formyl aminobenzazulenones (A) and aminobenzazulenones (B) tested at a concentration range of 0.6 µM – 40 µM on KRAS-mutant MDA-MB-231 and HRAS-mutant Hs 578T 3D spheroid formation in low attachment condition without serum. Data represent mean values ± SD, $n \geq 3$. Numbers above the bars indicate the KRAS/HRAS mutant cell line DSS_3 ratios (**C,D**) The relative toxicity of formyl aminobenzazulenones (C) and aminobenzazulenones (D) was assessed in the CellTox Green assay. Cells were grown as 2D adherent monolayers overnight and then treated for 72 h with 1 µM OphA or 10 µM of the indicated benzazulenones. Data represent mean values ± SD, $n \geq 2$.

Figure 2. Benzazulenones have higher IC_{50} with less change over time as compared to OphA. Change of effective CaM-binding affinity over time of OphA and formyl aminobenzazulenones (**A**) and aminobenzazulenones (**B**) as measured in the fluorescence polarization assay using F-PMCA peptide as the fluorescent probe. Data represent mean values ± SD, n = 2. Binding curves are plotted in **Figure S2 A,B**. Derived rate analysis plots are in **Figure S2 G,H**.

Figure 3. Nanoclustering-BRET assays confirm K-Ras selectivity and fast intracellular activity of compound 1 in cells. (**A,B**) Testing of top six benzazulenones at 20 µM and 24 h exposure in K-RasG12V (A) and H-RasG12V (B) nanoclustering-BRET assays. Controls are FTI-277 (1 µM), OphA (2.5 µM), mevastatin (10 µM), calmidazolium (20 µM) and prostratin (10 µM). The acceptor/donor (A/D) plasmid ratio of GFP2- and Rluc8-tagged RasG12V was 4/1. Data represent mean values ± SD, n = 3. (**C**) BRET-DSS_3 values for selected six benzazulenones and OphA, derived from dose response analysis of benzazulenones (0.1 µM – 80 µM) and OphA (0.3 µM – 20 µM) on K-RasG12V and H-

RasG12V nanoclustering-BRET data (**SI Figure 3A-B**). Numbers above the bars indicate the K-RasG12V/H-RasG12V BRET-DSS_3 ratios. The A/D plasmid ratio was 4/1. Data represent mean values ± SD, n ≥ 3. (**D**) K-RasG12V and (**E**) H-RasG12V nanoclustering-BRET donor saturation titration curves showing the effect of OphA (2.5 μM), **1** (20 μM) and vehicle control. Data represent mean values ± SD, n = 2. Note, error bars are very small and may not be recognizable. $BRET_{max}$ data represent mean values ± SD, n = 2. (**F**) Time-dependent change of K-RasG12V nanoclustering-BRET signal after treatment with **1** (50 μM), OphA (10 μM), mevastatin (10 μM), trifluoperazine (20 μM) and calmidazolium (20 μM). The A/D plasmid ratio was 4/1. Data represent mean values ± SD, n ≥ 2.

Figure 4. Cellular K-RasG12V/ CaM interaction BRET confirms on-target activity of compound 1 in cells. (**A**) BRET donor saturation titration curves between Rluc8-K-Ras or Rluc8-K-RasG12V and N-terminally GFP2-tagged CaM. (**B**) BRET donor saturation titration curves between the Rluc8-tagged K-Ras oncogenic mutants (K-RasG12C, K-RasG13D and K-RasQ61H) with GFP2-CaM. The $BRET_{max}$ data represent mean values ± SD, n ≥ 2. (**C**) BRET donor saturation titration curves between Rluc8-K-RasG12V or Rluc8-H-RasG12V and GFP2-CaM. Plasmids expressing Rluc8 and GFP2 proteins alone were used as controls for non-specific interaction. (**D**) Compounds calmidazolium (20 μM), prostratin (20 μM) or OphA (5 μM), as well as formyl aminobenzazulenone **1** (20 μM) or non-formylated counterpart aminobenzazulenone **8** (20 μM) were tested using the Rluc8-K-RasG12V/ GFP2-CaM BRET reporter. The A/D plasmid ratio was 9/1. Data represent mean values ± SD, n ≥ 2. (**E**) Dose-response analysis of compound **1** and its non-formylated derivative **8** as compared to OphA using Rluc8-K-RasG12V/ GFP2-CaM BRET signal. The A/D plasmid ratio was 9/1. Data represent mean values ± SD, n ≥ 2.

Figure 5. Assessment of lysine-dependent CaM-binding activity of OphA, formyl aminobenzazulenone 1 and aminobenzazulenone 8. Time-course of lysine-dependent CaM-binding activity of OphA (**A**), compound **1** (**B**) and compound **8** (**C**) as measured in the fluorescence polarization assay using F-CaMKII peptide as the fluorescent probe. OphA displayed negligible binding with mutCaM compared to wtCaM, hence no IC_{50} values could be derived (**SI Figure 5 A,B**).

Figure 6. Benchmarking of top compound 1 in several cancer cell lines. (**A**) The relative 2D viability of various cell lines following single dose treatment with AMG-510 (1 μM), calmidazolium (2.5 μM), OphA (1 μM) and **1** (10 μM) was assessed using the alamarBlue assay. Cells were grown as 2D adherent monolayers overnight and then treated for 72 h with indicated compounds. Data represent mean values ± SD, n ≥ 3. (**B**) DSS_3 measuring the effects of AMG-510 (0.003 – 40 μM), calmidazolium (0.3 – 40 μM), OphA (0.3 – 40 μM) and **1** (0.6 – 80 μM). Cells were grown as 2D adherent monolayers overnight and then treated for 72 h. Results represent mean values ± SD, n = 3. (**C**) DSS_3 measuring the effects of AMG-510 (0.6 – 40 μM), vemurafenib (0.3 – 20 μM), prostratin (0.6 – 80 μM), OphA (0.3 – 20 μM) and **1** (1.3 – 80 μM). Cells were grown as 3D spheroids for 72 h then treated with compounds for another 72 h before alamarBlue viability measurements. Data represent mean values ± SD, n ≥ 2. (**D**) Heatmap of ATARiS gene sensitivity scores obtained from the project DRIVE database for KRAS dependent cell lines (MIA PaCa-2, NCI H358 and MDA-MB-231) and HRAS dependent cell lines (Hs 578T and T24). Negative values (red) indicate sensitivity of the cell line proliferation to the knockdown of shown genes, while positive (blue) indicates the opposite.

Figure 7. Phenotypic effects of CaM inhibitors on centrosome numbers. (**A**) Representative images for bipolar normal (DMSO 0.5%, top) and multipolar centrosomes in HeLa cells after acute treatment for 2 h with calmidazolium (20 μM, middle) **1** (50 μM, bottom). Hela cells expressing mCherry-wtCaM (red) cells were synchronized with nocodazole to G2/M phase for 16 h. Then cells were treated with compounds and simultaneously with the protease inhibitor MG132 (10 μM). Arrows indicate

699 predominant localization of mCherry-wtCaM on the centrosomes during mitosis. DNA was stained
700 with DAPI (blue). Scale bar, 5 µm. (**B**) The multipolar phenotype was quantified for each treatment
701 from images containing 35 to 70 cells per condition. Data represent mean values ± SD, n = 3. Statistical
702 significance was evaluated with Fisher's exact test.

703 **7 Tables**

704 **Table 1. IC_{50} values of benzazulenones tested on 3D tumorosphere assay.** Data represent mean of
705 3 biological repeats (**Figure S1 E-H**).

	MDA-MB-231		Hs 578T	
Compound	*IC_{50} / µM*	*$logIC_{50}$ ± SD*	*IC_{50} / µM*	*$logIC_{50}$ ± SD*
1	12	-4.92 ± 0.03	22.5	-4.65 ± 0.04
2	22.8	-4.64 ± 0.06	24.9	-4.61 ± 0.05
3	35	-4.46 ± 0.05	25.8	-4.6 ± 0.1
4	> 40	inconclusive	> 40	inconclusive
5	34.5	-4.46 ± 0.05	13.2	-4.88 ± 0.04
6	> 40	inconclusive	> 40	inconclusive
7	> 40	inconclusive	> 40	inconclusive
8	32.4	-4.5 ± 0.5	10.6	-4.98 ± 0.03
9	19.6	-4.71 ± 0.03	17.4	-4.76 ± 0.01
10	> 40	inconclusive	23.1	-4.64 ± 0.04
11	15.4	-4.81 ± 0.05	5.2	-5.23 ± 0.04
12	> 40	inconclusive	8.5	-5.1 ± 0.1
13	> 40	inconclusive	> 40	inconclusive
14	> 40	inconclusive	> 40	inconclusive
OphA	0.3	-6.54 ± 0.02	1.8	-5.75 ± 0.02

706
707 **Table 2. CaM-binding affinity of compounds after 24 h incubation.** A fluorescence polarization
708 assay with the fluorescently labelled PMCA peptide as probe was performed. For comparison
709 K_d(OphA) = 3.5 ± 0.2 µM. While some compounds showed faint autofluorescence under the
710 polarization assay conditions, their emission was too weak as compared to that of fluorescein to
711 interfere with the measurements (**Figure S2 C,D**).

Formyl aminobenzazulenones		Aminobenzazulenones	
Compound	*K_d ± SD / µM*	*Compound*	*K_d ± SD / µM*
1	0.87 ± 0.02	**8**	3.1 ± 0.3
2	0.23 ± 0.01	**9**	1.44 ± 0.03
3	0.25 ± 0.02	**10**	inconclusive
4	39 ± 12	**11**	0.81 ± 0.03
5	29 ± 7	**12**	6.1 ± 0.3
6	31 ± 10	**13**	62 ± 26
7	45 ± 4	**14**	21.4 ± 0.6

712
713 **Table 3. Analysis of K_i and k_2 and the second order rate constant k_2/K_i from data plotted in**
714 **Figure 2 and processed as described.**

Compound	*k_2 ± SD / h^{-1}*	*K_i ± SD / µM*	*k_2/K_i / $h^{-1}µM^{-1}$*

OphA	1.09 ± 0.04	79 ± 8	0.0140
1	0.51 ± 0.09	52 ± 29	0.0097
2	1.18 ± 0.09	13 ± 4	0.0930
3	0.45 ± 0.07	11 ± 6	0.0424
8	0.35 ± 0.03	39 ± 10	0.0091
9	1.3 ± 0.2	229 ± 67	0.0059
11	0.29 ± 0.05	78 ± 34	0.0037

8 Conflict of Interest

The authors declare that the research was conducted in the absence of any commercial or financial relationships that could be construed as a potential conflict of interest.

9 Author contributions

S.O. designed and performed 3D spheroid assay, 2D cell viability and toxicity studies, BRET assays, DSS analysis, performed the RT-qPCR experiments and cloning together with M.C. G.M. developed the BRET assay, designed, and performed FP assays, and performed cloning. A.K. synthesized the compounds and curated the analytical data. C.L. performed microscopy. M.C. together with G.M. implemented the gateway cloning system, performed cloning, protein purification and RT-qPCR. F.M. contributed reagents and funding support. J.Y-K collaboratively designed the compounds with A.K. S.O. and G.M analyzed all the data. D.A. conceived the study, designed experiments, interpreted results, and wrote the manuscript together with S.O., G.M., A.K. and J.Y-K. All authors commented on the manuscript.

10 Funding

This work was supported by the Finnish Funding Agency for Innovation, Tekes, 3iRegeneration, project 40395/13) and Jane and Aatos Erkko Foundation to JYK. DA received funding from the Academy of Finland (Key Project # 304638) and core funding support by the University of Luxembourg.

11 Acknowledgements

We are thankful to Dr. Dominic Esposito and Vanessa Wall (Frederick National Laboratory for Cancer Research Frederick, MD USA) for providing the entry clones and destination vectors for multi-site gateway cloning. Nina Sipari from Viikki Metabolomics Unit (Helsinki Institute of Life Science, University of Helsinki; Biocenter Finland) is thanked for her expertise with the LC-MS analyses.

12 Supplementary Material

The Supplementary Material files for this article can be found online.

13 References

Abankwa, D., Gorfe, A.A., and Hancock, J.F. (2007). Ras nanoclusters: molecular structure and assembly. *Semin Cell Dev Biol* 18, 599-607.

744 Abraham, S.J., Nolet, R.P., Calvert, R.J., Anderson, L.M., and Gaponenko, V. (2009). The
745 hypervariable region of K-Ras4B is responsible for its specific interactions with calmodulin.
746 *Biochemistry* 48, 7575-7583.
747 Agamasu, C., Ghirlando, R., Taylor, T., Messing, S., Tran, T.H., Bindu, L., Tonelli, M., Nissley, D.V.,
748 Mccormick, F., and Stephen, A.G. (2019). KRAS Prenylation Is Required for Bivalent Binding
749 with Calmodulin in a Nucleotide-Independent Manner. *Biophys J* 116, 1049-1063.
750 Alvarez-Moya, B., Lopez-Alcala, C., Drosten, M., Bachs, O., and Agell, N. (2010). K-Ras4B
751 phosphorylation at Ser181 is inhibited by calmodulin and modulates K-Ras activity and
752 function. *Oncogene* 29, 5911-5922.
753 Au, T.K., Chick, W.S., and Leung, P.C. (2000). The biology of ophiobolins. *Life Sci* 67, 733-742.
754 Bacart, J., Corbel, C., Jockers, R., Bach, S., and Couturier, C. (2008). The BRET technology and its
755 application to screening assays. *Biotechnol J* 3, 311-324.
756 Bedard, P.L., Hyman, D.M., Davids, M.S., and Siu, L.L. (2020). Small molecules, big impact: 20 years
757 of targeted therapy in oncology. *Lancet* 395, 1078-1088.
758 Berchtold, M.W., and Villalobo, A. (2014). The many faces of calmodulin in cell proliferation,
759 programmed cell death, autophagy, and cancer. *Biochim Biophys Acta* 1843, 398-435.
760 Bery, N., Cruz-Migoni, A., Bataille, C.J., Quevedo, C.E., Tulmin, H., Miller, A., Russell, A., Phillips,
761 S.E., Carr, S.B., and Rabbitts, T.H. (2018). BRET-based RAS biosensors that show a novel
762 small molecule is an inhibitor of RAS-effector protein-protein interactions. *Elife* 7.
763 Chandra, A., Grecco, H.E., Pisupati, V., Perera, D., Cassidy, L., Skoulidis, F., Ismail, S.A., Hedberg,
764 C., Hanzal-Bayer, M., Venkitaraman, A.R., Wittinghofer, A., and Bastiaens, P.I. (2011). The
765 GDI-like solubilizing factor PDEdelta sustains the spatial organization and signalling of Ras
766 family proteins. *Nat Cell Biol* 14, 148-158.
767 Chidley, C., Trauger, S.A., Birsoy, K., and O'shea, E.K. (2016). The anticancer natural product
768 ophiobolin A induces cytotoxicity by covalent modification of phosphatidylethanolamine. *Elife*
769 5, e14601.
770 Cicalese, A., Bonizzi, G., Pasi, C.E., Faretta, M., Ronzoni, S., Giulini, B., Brisken, C., Minucci, S., Di
771 Fiore, P.P., and Pelicci, P.G. (2009). The tumor suppressor p53 regulates polarity of self-
772 renewing divisions in mammary stem cells. *Cell* 138, 1083-1095.
773 Dharmaiah, S., Bindu, L., Tran, T.H., Gillette, W.K., Frank, P.H., Ghirlando, R., Nissley, D.V.,
774 Esposito, D., Mccormick, F., Stephen, A.G., and Simanshu, D.K. (2016). Structural basis of
775 recognition of farnesylated and methylated KRAS4b by PDEdelta. *Proc Natl Acad Sci U S A*
776 113, E6766-E6775.
777 Dontu, G., Abdallah, W.M., Foley, J.M., Jackson, K.W., Clarke, M.F., Kawamura, M.J., and Wicha,
778 M.S. (2003). In vitro propagation and transcriptional profiling of human mammary
779 stem/progenitor cells. *Genes Dev* 17, 1253-1270.
780 Faust, F.M., Slisz, M., and Jarrett, H.W. (1987). Calmodulin is labeled at lysine 148 by a chemically
781 reactive phenothiazine. *The Journal of biological chemistry* 262, 1938-1941.
782 Fivaz, M., and Meyer, T. (2005). Reversible intracellular translocation of KRas but not HRas in
783 hippocampal neurons regulated by Ca2+/calmodulin. *J Cell Biol* 170, 429-441.
784 Gillette, W.K., Esposito, D., Abreu Blanco, M., Alexander, P., Bindu, L., Bittner, C., Chertov, O.,
785 Frank, P.H., Grose, C., Jones, J.E., Meng, Z., Perkins, S., Van, Q., Ghirlando, R., Fivash, M.,
786 Nissley, D.V., Mccormick, F., Holderfield, M., and Stephen, A.G. (2015). Farnesylated and
787 methylated KRAS4b: high yield production of protein suitable for biophysical studies of
788 prenylated protein-lipid interactions. *Sci Rep* 5, 15916.
789 Grant, B.M.M., Enomoto, M., Back, S.I., Lee, K.Y., Gebregiworgis, T., Ishiyama, N., Ikura, M., and
790 Marshall, C.B. (2020a). Calmodulin disrupts plasma membrane localization of farnesylated
791 KRAS4b by sequestering its lipid moiety. *Sci Signal* 13, eaaz0344.

792 Grant, B.M.M., Enomoto, M., Ikura, M., and Marshall, C.B. (2020b). A Non-Canonical Calmodulin
793 Target Motif Comprising a Polybasic Region and Lipidated Terminal Residue Regulates
794 Localization. *Int J Mol Sci* 21.
795 Hait, W.N., and Lazo, J.S. (1986). Calmodulin: a potential target for cancer chemotherapeutic agents.
796 *J Clin Oncol* 4, 994-1012.
797 Halling, D.B., Liebeskind, B.J., Hall, A.W., and Aldrich, R.W. (2016). Conserved properties of
798 individual Ca2+-binding sites in calmodulin. *Proc Natl Acad Sci U S A* 113, E1216-1225.
799 Hidaka, H., Sasaki, Y., Tanaka, T., Endo, T., Ohno, S., Fujii, Y., and Nagata, T. (1981). N-(6-
800 aminohexyl)-5-chloro-1-naphthalenesulfonamide, a calmodulin antagonist, inhibits cell
801 proliferation. *Proc Natl Acad Sci U S A* 78, 4354-4357.
802 Hong, D.S., Fakih, M.G., Strickler, J.H., Desai, J., Durm, G.A., Shapiro, G.I., Falchook, G.S., Price,
803 T.J., Sacher, A., Denlinger, C.S., Bang, Y.J., Dy, G.K., Krauss, J.C., Kuboki, Y., Kuo, J.C.,
804 Coveler, A.L., Park, K., Kim, T.W., Barlesi, F., Munster, P.N., Ramalingam, S.S., Burns, T.F.,
805 Meric-Bernstam, F., Henary, H., Ngang, J., Ngarmchamnanrith, G., Kim, J., Houk, B.E.,
806 Canon, J., Lipford, J.R., Friberg, G., Lito, P., Govindan, R., and Li, B.T. (2020). KRAS(G12C)
807 Inhibition with Sotorasib in Advanced Solid Tumors. *N Engl J Med* 383, 1207-1217.
808 Itoh, H., and Hidaka, H. (1984). Direct interaction of calmodulin antagonists with Ca2+/calmodulin-
809 dependent cyclic nucleotide phosphodiesterase. *J Biochem* 96, 1721-1726.
810 Jang, H., Banerjee, A., Marcus, K., Makowski, L., Mattos, C., Gaponenko, V., and Nussinov, R.
811 (2019). The Structural Basis of the Farnesylated and Methylated KRas4B Interaction with
812 Calmodulin. *Structure* 27, 1647-1659 e1644.
813 Kiriazis, A., Aumuller, I.B., Arnaudova, R., Brito, V., Ruffer, T., Lang, H., Silvestre, S.M., Koskinen,
814 P.J., and Yli-Kauhaluoma, J. (2017). Nucleophilic Substitution of Hydrogen Facilitated by
815 Quinone Methide Moieties in Benzo[cd]azulen-3-ones. *Org Lett* 19, 2030-2033.
816 Kohnke, M., Schmitt, S., Ariotti, N., Piggott, A.M., Parton, R.G., Lacey, E., Capon, R.J., Alexandrov,
817 K., and Abankwa, D. (2012). Design and application of in vivo FRET biosensors to identify
818 protein prenylation and nanoclustering inhibitors. *Chem Biol* 19, 866-874.
819 Kong Au, T., and Chow Leung, P. (1998). Identification of the binding and inhibition sites in the
820 calmodulin molecule for ophiobolin A by site-directed mutagenesis. *Plant Physiol* 118, 965-
821 973.
822 Lavoie, H., Thevakumaran, N., Gavory, G., Li, J.J., Padeganeh, A., Guiral, S., Duchaine, J., Mao, D.Y.,
823 Bouvier, M., Sicheri, F., and Therrien, M. (2013). Inhibitors that stabilize a closed RAF kinase
824 domain conformation induce dimerization. *Nat Chem Biol* 9, 428-436.
825 Leung, P.C., Taylor, W.A., Wang, J.H., and Tipton, C.L. (1984). Ophiobolin A. A natural product
826 inhibitor of calmodulin. *J Biol Chem* 259, 2742-2747.
827 Li, C.J., Heim, R., Lu, P., Pu, Y., Tsien, R.Y., and Chang, D.C. (1999). Dynamic redistribution of
828 calmodulin in HeLa cells during cell division as revealed by a GFP-calmodulin fusion protein
829 technique. *Journal of Cell Science* 112, 1567-1577.
830 Manoharan, G.B., Kopra, K., Eskonen, V., Härmä, H., and Abankwa, D. (2019). High-throughput
831 amenable fluorescence-assays to screen for calmodulin-inhibitors. *Anal Biochem* 572, 25-32.
832 Marullo, S., and Bouvier, M. (2007). Resonance energy transfer approaches in molecular
833 pharmacology and beyond. *Trends Pharmacol Sci* 28, 362-365.
834 Mcdonald, E.R., 3rd, De Weck, A., Schlabach, M.R., Billy, E., Mavrakis, K.J., Hoffman, G.R., Belur,
835 D., Castelletti, D., Frias, E., Gampa, K., Golji, J., Kao, I., Li, L., Megel, P., Perkins, T.A.,
836 Ramadan, N., Ruddy, D.A., Silver, S.J., Sovath, S., Stump, M., Weber, O., Widmer, R., Yu, J.,
837 Yu, K., Yue, Y., Abramowski, D., Ackley, E., Barrett, R., Berger, J., Bernard, J.L., Billig, R.,
838 Brachmann, S.M., Buxton, F., Caothien, R., Caushi, J.X., Chung, F.S., Cortes-Cros, M.,
839 Debeaumont, R.S., Delaunay, C., Desplat, A., Duong, W., Dwoske, D.A., Eldridge, R.S.,
840 Farsidjani, A., Feng, F., Feng, J., Flemming, D., Forrester, W., Galli, G.G., Gao, Z., Gauter, F.,

Gibaja, V., Haas, K., Hattenberger, M., Hood, T., Hurov, K.E., Jagani, Z., Jenal, M., Johnson, J.A., Jones, M.D., Kapoor, A., Korn, J., Liu, J., Liu, Q., Liu, S., Liu, Y., Loo, A.T., Macchi, K.J., Martin, T., Mcallister, G., Meyer, A., Molle, S., Pagliarini, R.A., Phadke, T., Repko, B., Schouwey, T., Shanahan, F., Shen, Q., Stamm, C., Stephan, C., Stucke, V.M., Tiedt, R., Varadarajan, M., Venkatesan, K., Vitari, A.C., Wallroth, M., Weiler, J., Zhang, J., Mickanin, C., Myer, V.E., Porter, J.A., Lai, A., Bitter, H., Lees, E., Keen, N., Kauffmann, A., Stegmeier, F., Hofmann, F., Schmelzle, T., and Sellers, W.R. (2017). Project DRIVE: A Compendium of Cancer Dependencies and Synthetic Lethal Relationships Uncovered by Large-Scale, Deep RNAi Screening. *Cell* 170, 577-592 e510.

Meissner, P., Pick, H., Kulangara, A., Chatellard, P., Friedrich, K., and Wurm, F.M. (2001). Transient gene expression: recombinant protein production with suspension-adapted HEK293-EBNA cells. *Biotechnol Bioeng* 75, 197-203.

Najumudeen, A.K., Jaiswal, A., Lectez, B., Oetken-Lindholm, C., Guzman, C., Siljamaki, E., Posada, I.M., Lacey, E., Aittokallio, T., and Abankwa, D. (2016). Cancer stem cell drugs target K-ras signaling in a stemness context. *Oncogene* 35, 5248-5262.

Posada, I.M., Serulla, M., Zhou, Y., Oetken-Lindholm, C., Abankwa, D., and Lectez, B. (2016). ASPP2 Is a Novel Pan-Ras Nanocluster Scaffold. *PLoS One* 11, e0159677.

Potdar, S., Ianevski, A., Mpindi, J.P., Bychkov, D., Fiere, C., Ianevski, P., Yadav, B., Wennerberg, K., Aittokallio, T., Kallioniemi, O., Saarela, J., and Ostling, P. (2020). Breeze: an integrated quality control and data analysis application for high-throughput drug screening. *Bioinformatics* 36, 3602-3604.

Ren, J.G., Li, Z., and Sacks, D.B. (2008). IQGAP1 integrates Ca2+/calmodulin and B-Raf signaling. *J Biol Chem* 283, 22972-22982.

Sengupta, P., Ruano, M.J., Tebar, F., Golebiewska, U., Zaitseva, I., Enrich, C., Mclaughlin, S., and Villalobo, A. (2007). Membrane-permeable calmodulin inhibitors (e.g. W-7/W-13) bind to membranes, changing the electrostatic surface potential: dual effect of W-13 on epidermal growth factor receptor activation. *J Biol Chem* 282, 8474-8486.

Shao, D.D., Tsherniak, A., Gopal, S., Weir, B.A., Tamayo, P., Stransky, N., Schumacher, S.E., Zack, T.I., Beroukhim, R., Garraway, L.A., Margolin, A.A., Root, D.E., Hahn, W.C., and Mesirov, J.P. (2013). ATARiS: computational quantification of gene suppression phenotypes from multisample RNAi screens. *Genome Res* 23, 665-678.

Siddiqui, F.A., Alam, C., Rosenqvist, P., Ora, M., Sabt, A., Manoharan, G.B., Bindu, L., Okutachi, S., Catillon, M., Taylor, T., Abdelhafez, O.M., Lonnberg, H., Stephen, A.G., Papageorgiou, A.C., Virta, P., and Abankwa, D. (2020). PDE6D Inhibitors with a New Design Principle Selectively Block K-Ras Activity. *ACS Omega* 5, 832-842.

Singh, J., Petter, R.C., Baillie, T.A., and Whitty, A. (2011). The resurgence of covalent drugs. *Nat Rev Drug Discov* 10, 307-317.

Sinijarv, H., Wu, S., Ivan, T., Laasfeld, T., Viht, K., and Uri, A. (2017). Binding assay for characterization of protein kinase inhibitors possessing sub-picomolar to sub-millimolar affinity. *Anal Biochem* 531, 67-77.

Sunagawa, M., Yokoshiki, H., Seki, T., Nakamura, M., Laber, P., and Sperelakis, N. (1999). Direct block of Ca2+ channels by calmidazolium in cultured vascular smooth muscle cells. *J Cardiovasc Pharmacol* 34, 488-496.

Taules, M., Rius, E., Talaya, D., Lopez-Girona, A., Bachs, O., and Agell, N. (1998). Calmodulin is essential for cyclin-dependent kinase 4 (Cdk4) activity and nuclear accumulation of cyclin D1-Cdk4 during G1. *J Biol Chem* 273, 33279-33286.

Taylor, A.M., Macari, E.R., Chan, I.T., Blair, M.C., Doulatov, S., Vo, L.T., Raiser, D.M., Siva, K., Basak, A., Pirouz, M., Shah, A.N., Mcgrath, K., Humphries, J.M., Stillman, E., Alter, B.P., Calo, E., Gregory, R.I., Sankaran, V.G., Flygare, J., Ebert, B.L., Zhou, Y., Daley, G.Q., and

Zon, L.I. (2020). Calmodulin inhibitors improve erythropoiesis in Diamond-Blackfan anemia. *Sci Transl Med* 12.

Teleman, A., Drakenberg, T., and Forsen, S. (1986). Kinetics of Ca2+ binding to calmodulin and its tryptic fragments studied by 43Ca-NMR. *Biochim Biophys Acta* 873, 204-213.

Tidow, H., and Nissen, P. (2013). Structural diversity of calmodulin binding to its target sites. *FEBS J* 280, 5551-5565.

Toutenhoofd, S.L., and Strehler, E.E. (2000). The calmodulin multigene family as a unique case of genetic redundancy: multiple levels of regulation to provide spatial and temporal control of calmodulin pools? *Cell Calcium* 28, 83-96.

Tsai, F.D., Lopes, M.S., Zhou, M., Court, H., Ponce, O., Fiordalisi, J.J., Gierut, J.J., Cox, A.D., Haigis, K.M., and Philips, M.R. (2015). K-Ras4A splice variant is widely expressed in cancer and uses a hybrid membrane-targeting motif. *Proc Natl Acad Sci U S A* 112, 779-784.

Vandonselaar, M., Hickie, R.A., Quail, J.W., and Delbaere, L.T. (1994). Trifluoperazine-induced conformational change in Ca(2+)-calmodulin. *Nat Struct Biol* 1, 795-801.

Villalonga, P., Lopez-Alcala, C., Bosch, M., Chiloeches, A., Rocamora, N., Gil, J., Marais, R., Marshall, C.J., Bachs, O., and Agell, N. (2001). Calmodulin binds to K-Ras, but not to H- or N-Ras, and modulates its downstream signaling. *Mol Cell Biol* 21, 7345-7354.

Wall, V.E., Garvey, L.A., Mehalko, J.L., Procter, L.V., and Esposito, D. (2014). Combinatorial assembly of clone libraries using site-specific recombination. *Methods Mol Biol* 1116, 193-208.

Wang, J., Li, J., Santana-Santos, L., Shuda, M., Sobol, R.W., Van Houten, B., and Qian, W. (2015a). A novel strategy for targeted killing of tumor cells: Induction of multipolar acentrosomal mitotic spindles with a quinazolinone derivative mdivi-1. *Mol Oncol* 9, 488-502.

Wang, M.T., Holderfield, M., Galeas, J., Delrosario, R., To, M.D., Balmain, A., and Mccormick, F. (2015b). K-Ras Promotes Tumorigenicity through Suppression of Non-canonical Wnt Signaling. *Cell* 163, 1237-1251.

Wu, L.J., Xu, L.R., Liao, J.M., Chen, J., and Liang, Y. (2011). Both the C-terminal polylysine region and the farnesylation of K-RasB are important for its specific interaction with calmodulin. *PLoS One* 6, e21929.

Wu, Q., Sahasrabudhe, R.M., Luo, L.Z., Lewis, D.W., Gollin, S.M., and Saunders, W.S. (2010). Deficiency in myosin light-chain phosphorylation causes cytokinesis failure and multipolarity in cancer cells. *Oncogene* 29, 4183-4193.

Yadav, B., Pemovska, T., Szwajda, A., Kulesskiy, E., Kontro, M., Karjalainen, R., Majumder, M.M., Malani, D., Murumagi, A., Knowles, J., Porkka, K., Heckman, C., Kallioniemi, O., Wennerberg, K., and Aittokallio, T. (2014). Quantitative scoring of differential drug sensitivity for individually optimized anticancer therapies. *Sci Rep* 4, 5193.

Yokokura, S., Yurimoto, S., Matsuoka, A., Imataki, O., Dobashi, H., Bandoh, S., and Matsunaga, T. (2014). Calmodulin antagonists induce cell cycle arrest and apoptosis in vitro and inhibit tumor growth in vivo in human multiple myeloma. *BMC Cancer* 14, 882.

Yu, Y.Y., Chen, Y., Dai, G., Chen, J., Sun, X.M., Wen, C.J., Zhao, D.H., Chang, D.C., and Li, C.J. (2004). The association of calmodulin with central spindle regulates the initiation of cytokinesis in HeLa cells. *Int J Biochem Cell Biol* 36, 1562-1572.

Zimmer, M., and Hofmann, F. (1984). Calmodulin antagonists inhibit activity of myosin light-chain kinase independent of calmodulin. *Eur J Biochem* 142, 393-397.

Figure 1.JPEG

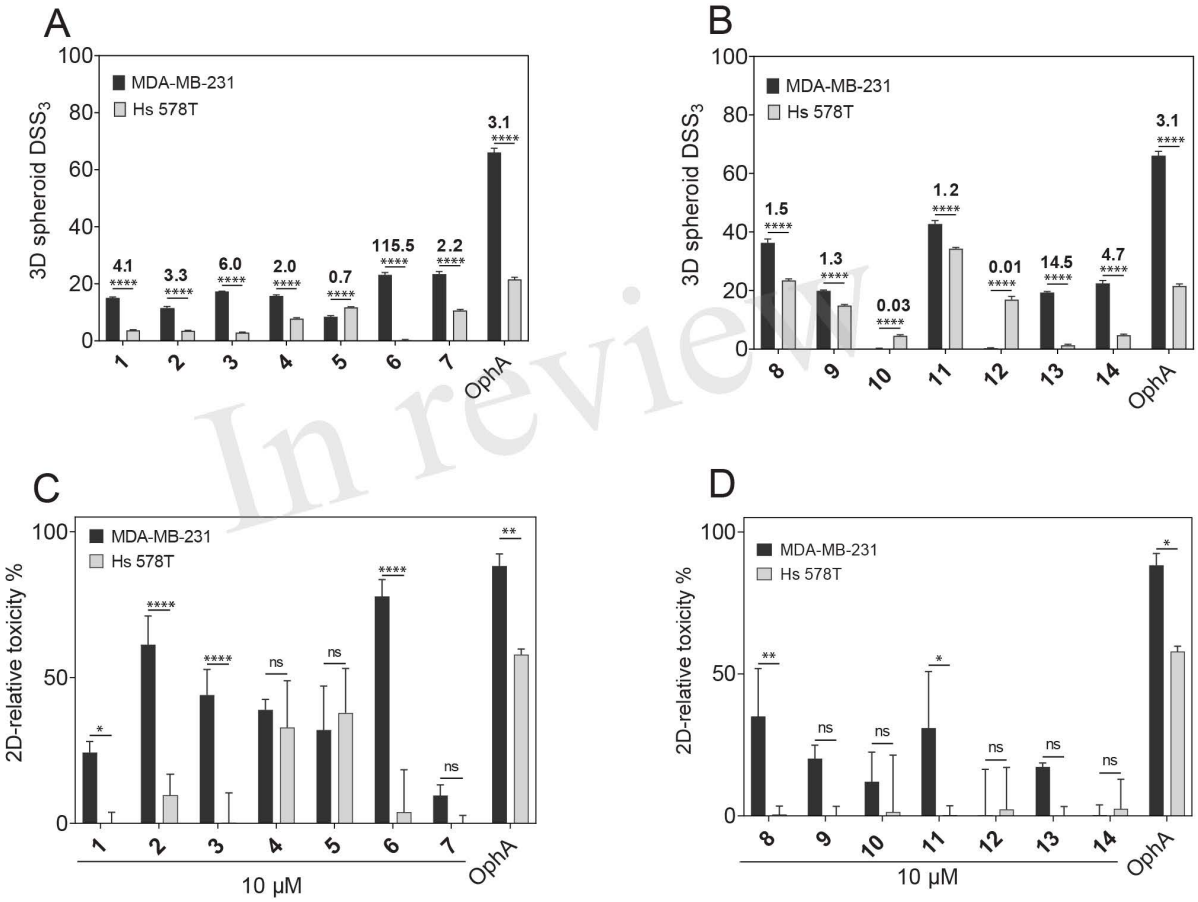

Figure 2.JPEG

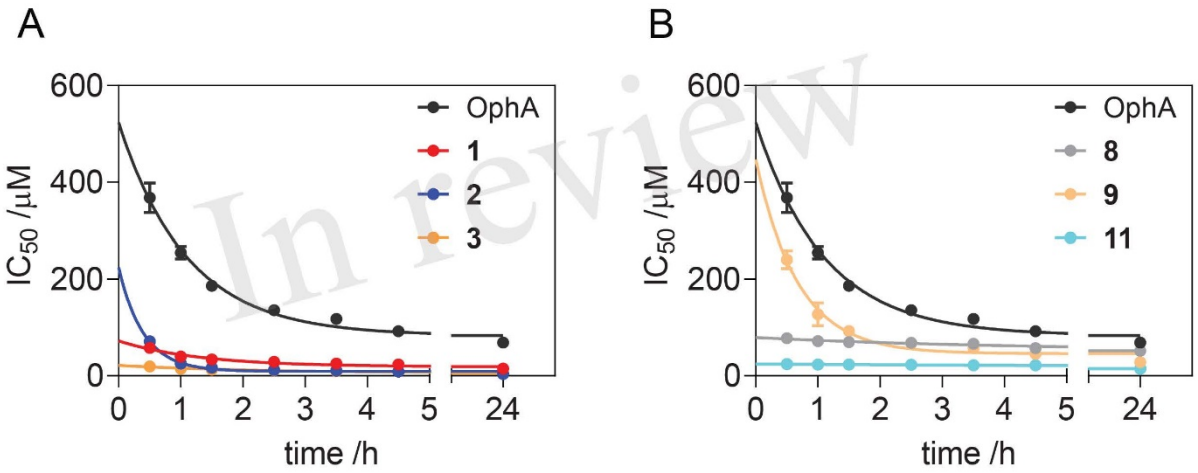

Figure 3.JPEG

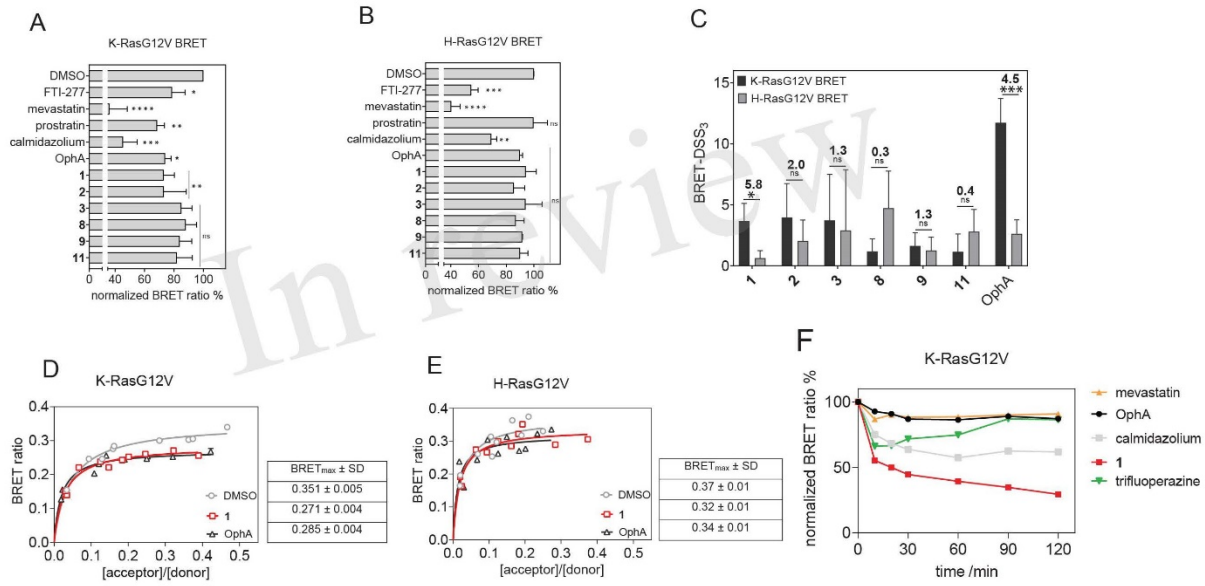

Figure 4.JPEG

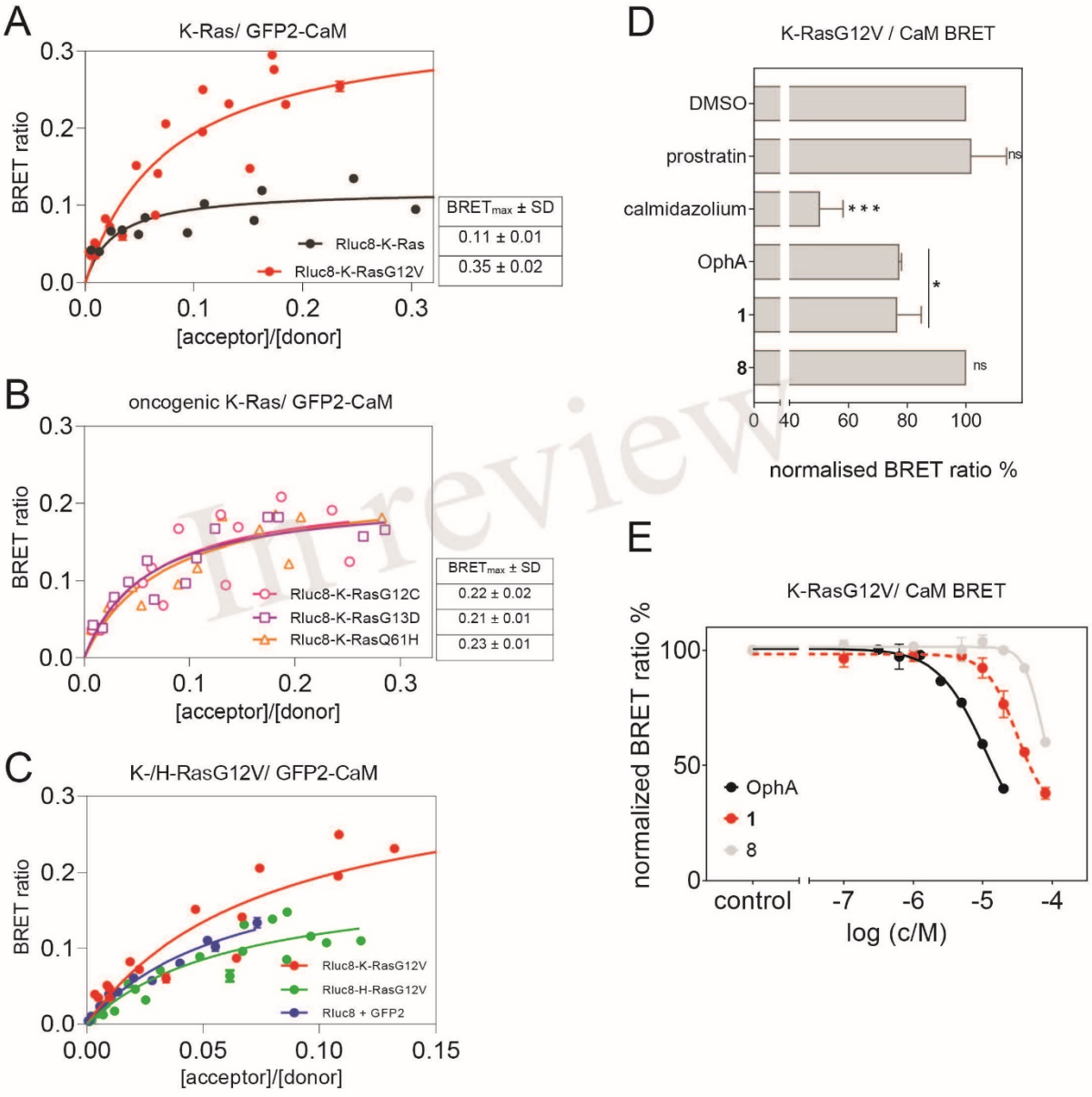

Figure 5.JPEG

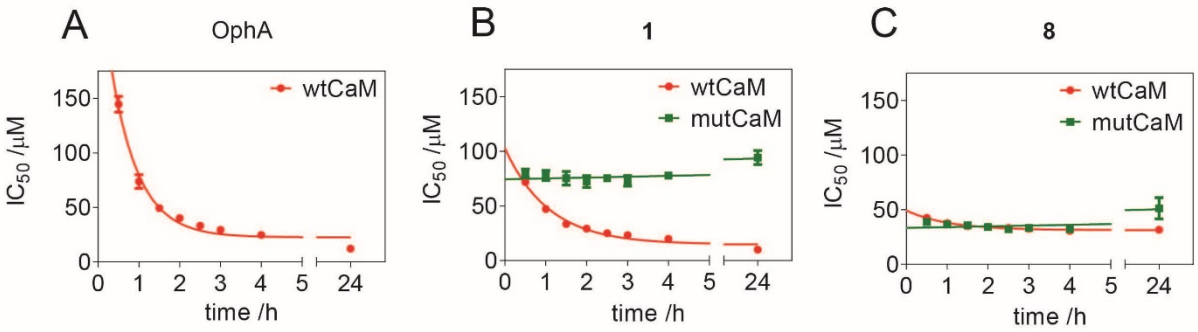

Figure 6.JPEG

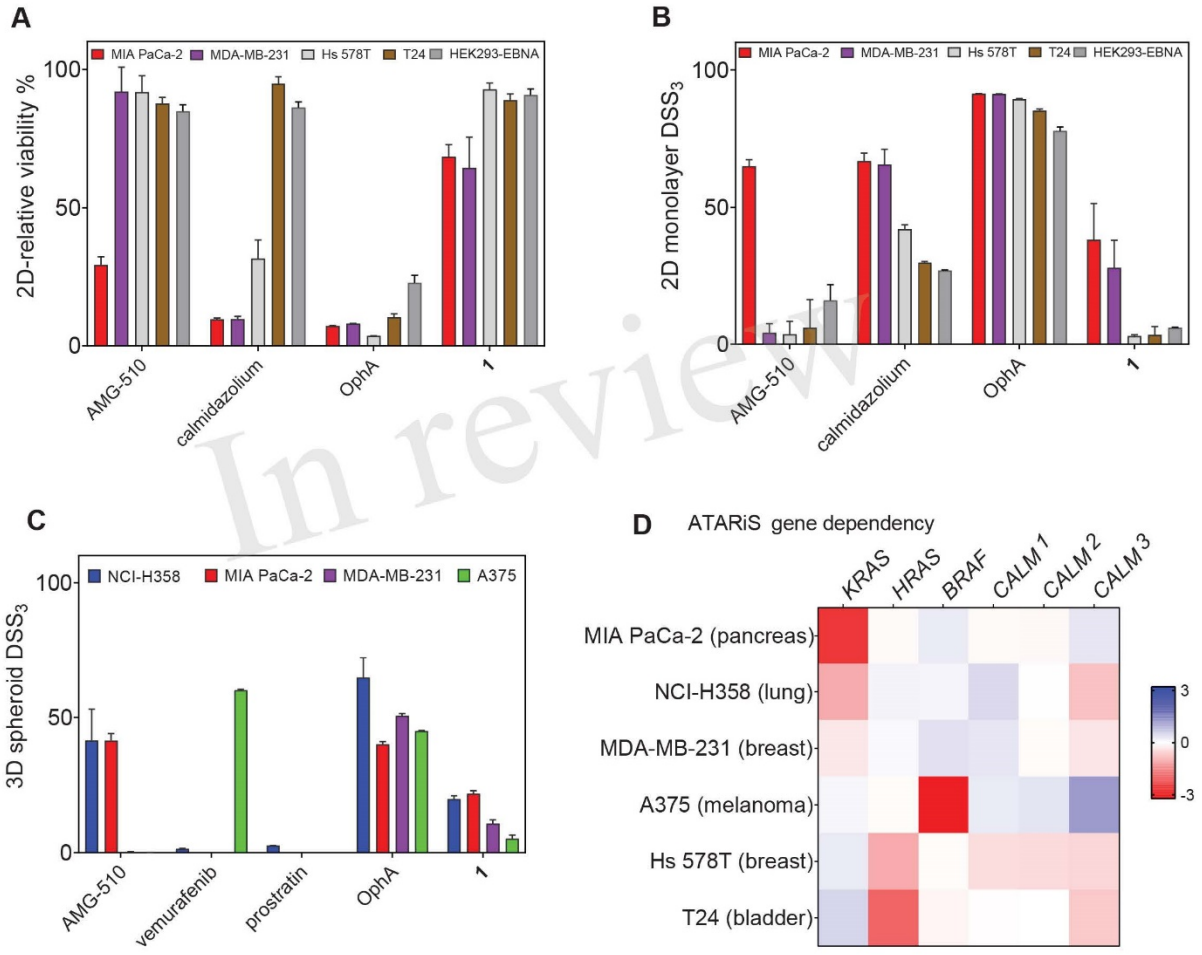

Figure 7.JPEG

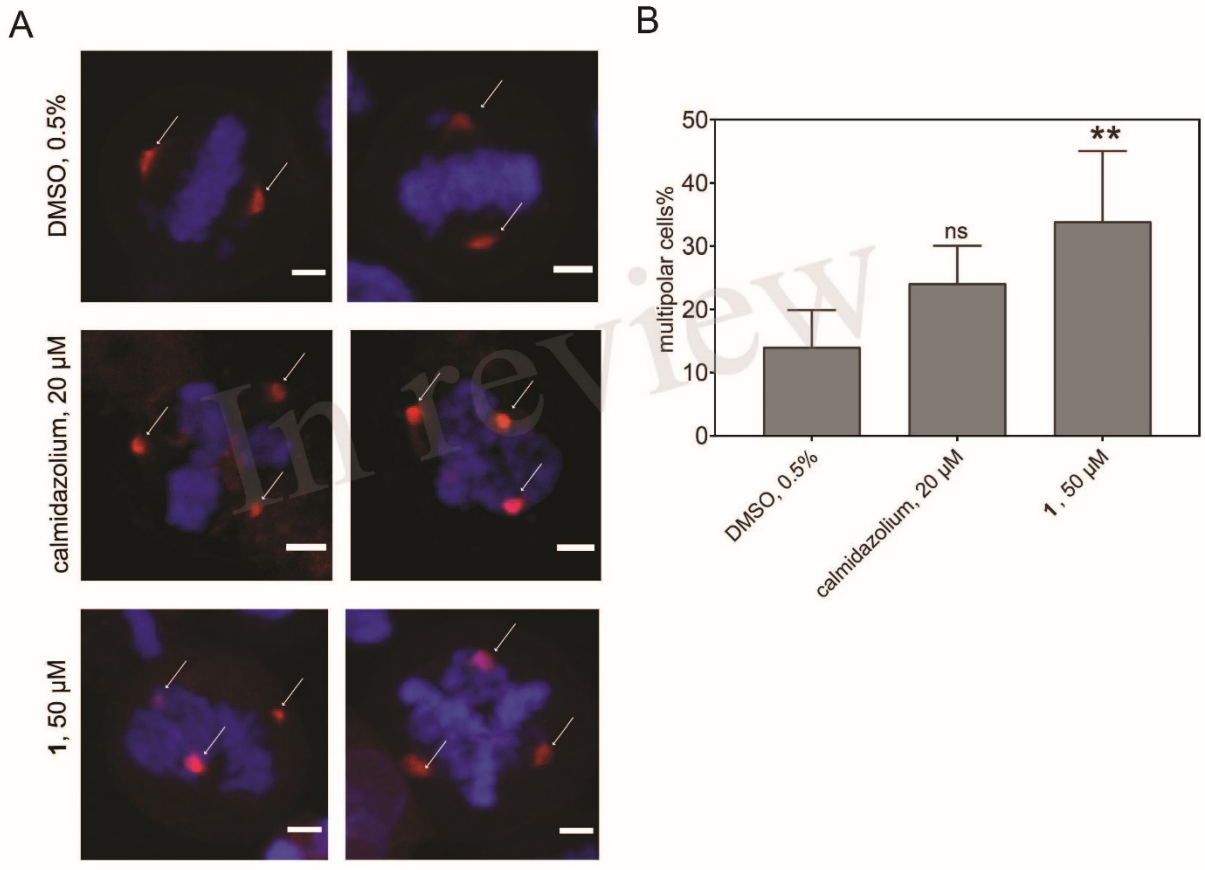

Figure 8.JPEG

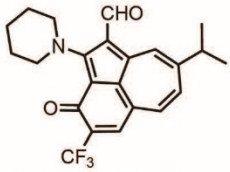

1 (Calmirasone1)

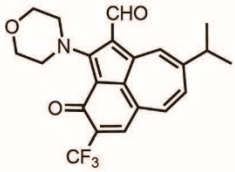

2

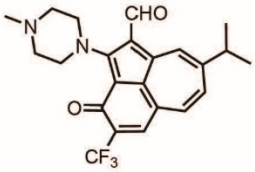

3

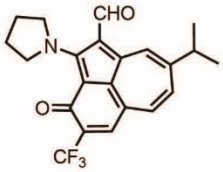

4

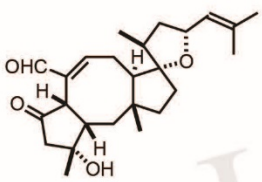

Ophiobolin A

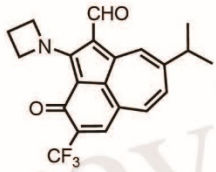

5

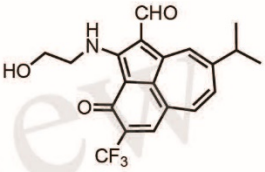

6

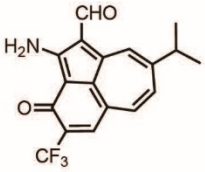

7

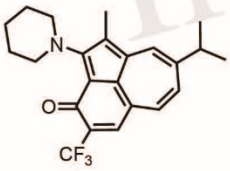

8

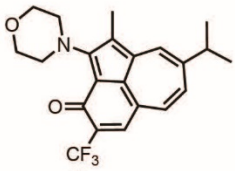

9

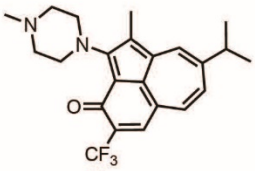

10

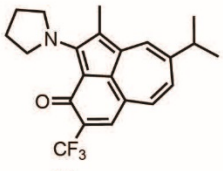

11

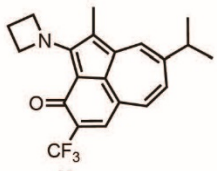

12

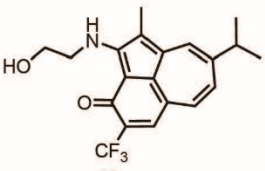

13

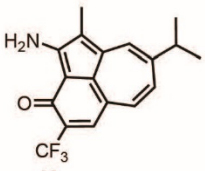

14

frontiers

Supplementary Material

1 Supplementary Figures

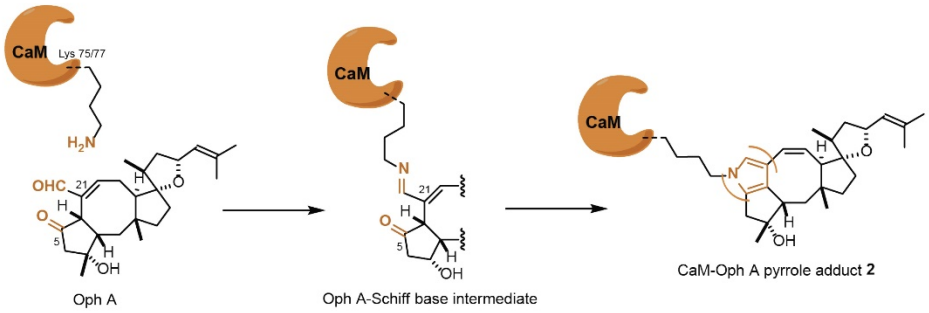

Scheme S1. Schematic drawing of covalent reaction of OphA with lysines of CaM. The irreversible pyrrole adduct **2** is formed from the Schiff base intermediate.

Supplementary Material

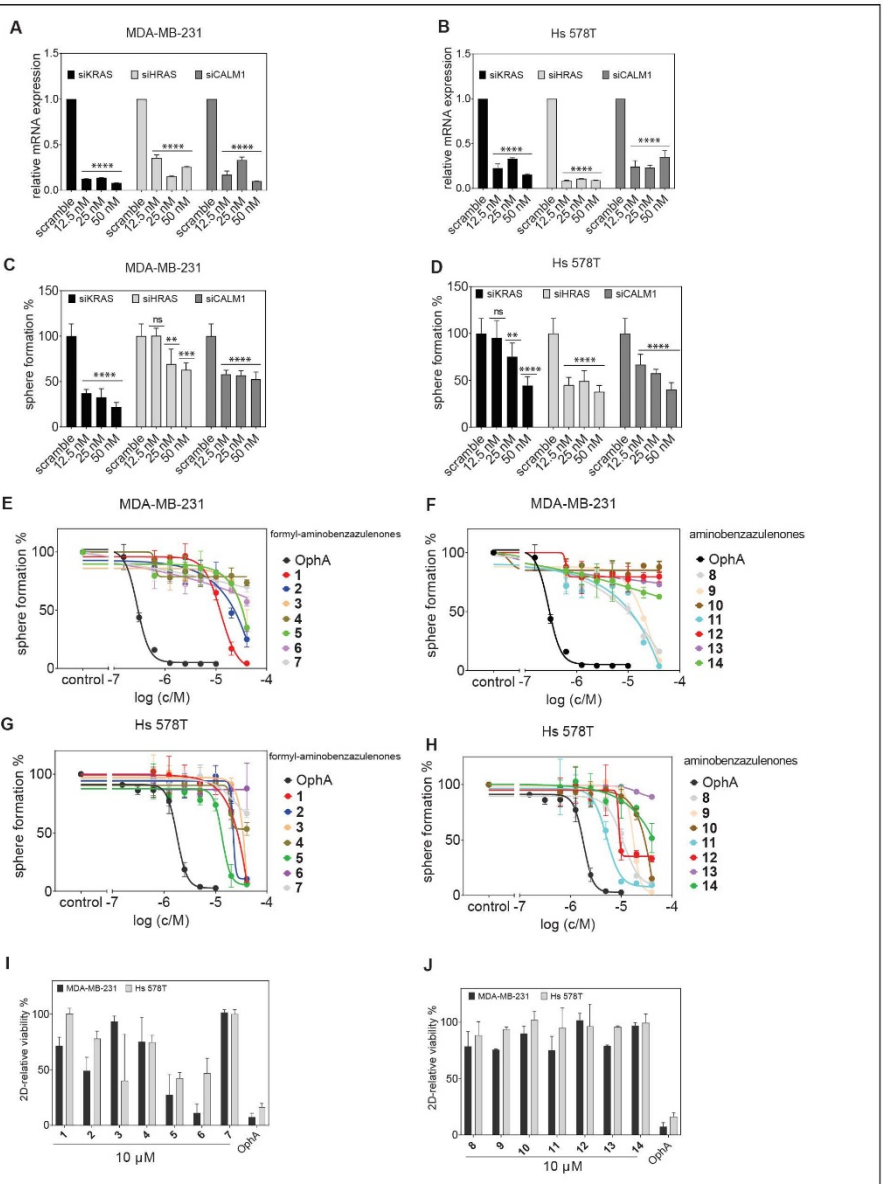

Figure S1. 3D spheroid formation data and knockdown controls. (A,B) RT-qPCR based evaluation of the relative mRNA expression of KRAS, HRAS or CALM1 upon siRNA mediated knockdown in MDA-MB-231 (A) and Hs 578T (B) cells. The siRNA against the KRAS gene (siKRAS), HRAS (siHRAS) and a mix of four siRNAs Targeting the CALM1 gene (siCALM1)

were used for this experiment. Data represent mean values ± SD, n = 2. **(C,D)** Effect of the knockdown of KRAS, HRAS or CALM1 genes on the 3D spheroid formation of MDA-MB-231 (C) and Hs 578T (D) cells in low attachment plates without serum. Data represent mean values ± SD, n = 2. **(E-H)** Dose response curves showing the effect of formyl aminobenzazulenones (0.6 – 40 μM), aminobenzazulenones (0.6 – 40 μM) and OphA (0.2 – 10 μM) on 3D spheroid formation of MDA-MB-231 (E, F) and Hs 578T (G, H) cells, as indicated. Cells were grown as 3D spheroids under low attachment and serum free conditions and then treated 3 days with compounds. The data were fit to log (inhibitor) vs response – variable slope (four parameters) equation using the Prism (GraphPad) software. Note that the actual curve fitting for DSS calculations was done on the breeze-site (https://breeze.fimm.fi/). Data represent mean values ± SD, n ≥ 3. **(I,J)** The relative viability of the compounds were assessed in alamarBlue assay. Cells were grown as 2D adherent monolayers overnight and then treated for 72 h with 1 μM OphA or 10 μM of the indicated benzazulenones. Data represent mean values ± SD, n ≥ 2.

3

Supplementary Material

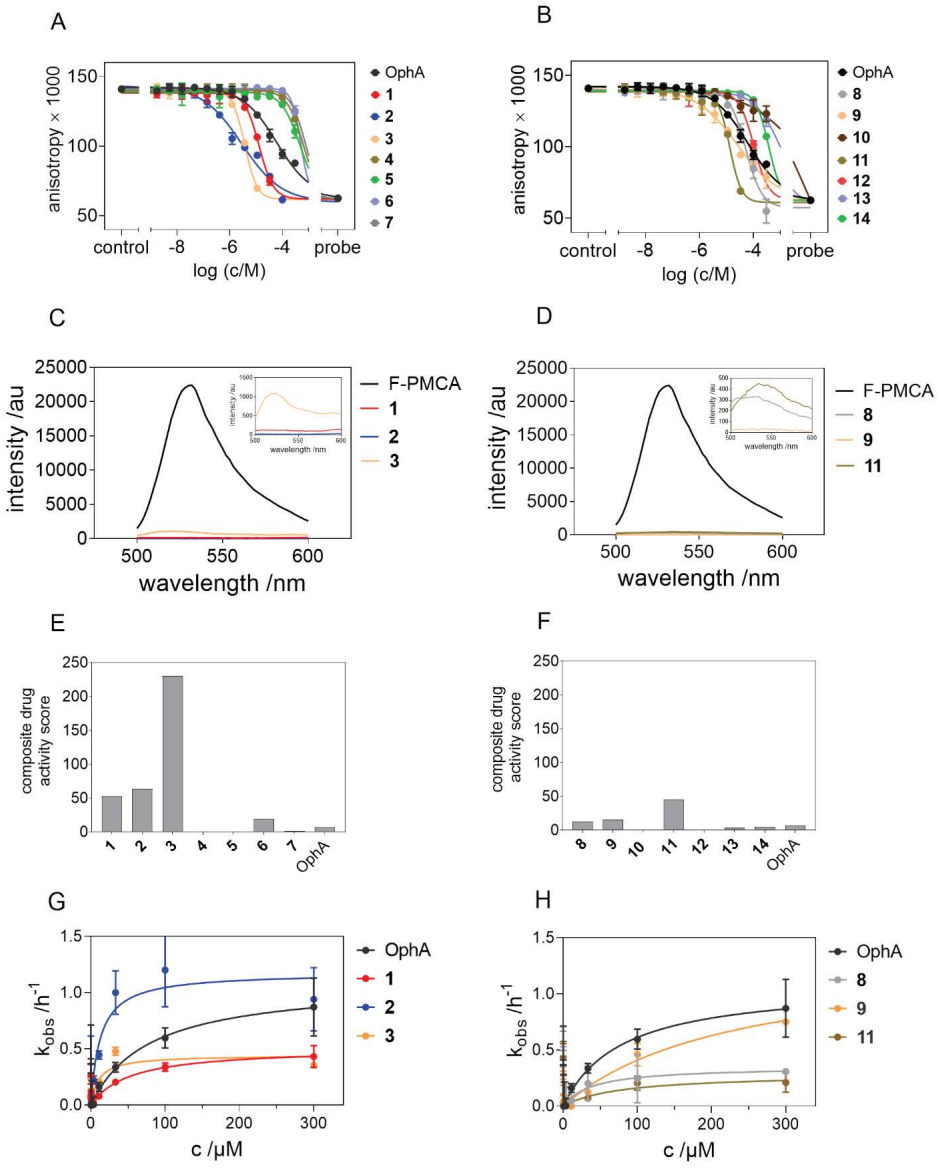

Figure S2. Assessment of binding affinity of benzazulenones to CaM by a fluorescence polarization assay and composite drug activity score. (**A**,**B**) Displacement of complex of 100 nM

CaM and 10 nM F-PMCA peptide by formyl aminobenzazulenones (A) and aminobenzazulenones (B) after 24 h incubation. Data represent mean values ± SD, n = 2. (**C, D**) Comparison of autofluorescence of compounds with that of F-PMCA. Fluorescence emission spectra were recorded with excitation at 475 ± 10 nm for benzazulenone compounds at 5 mM concentration and 10,000× lower concentration of 0.5 µM for F-PMCA peptide using a Clariostar plate reader. **(E,F)** Visualization of composite drug activity scores for formyl aminobenzazulenones (E) and aminobenzazulenones (F). Note that **3** was chemically not as stable and therefore deprioritized. **(G,H)** Hyperbolic fit to observed rate constants in order to derive the covalent step rate constant k_2 and the affinity constant for the non-covalent intermediate K_i.

5

Supplementary Material

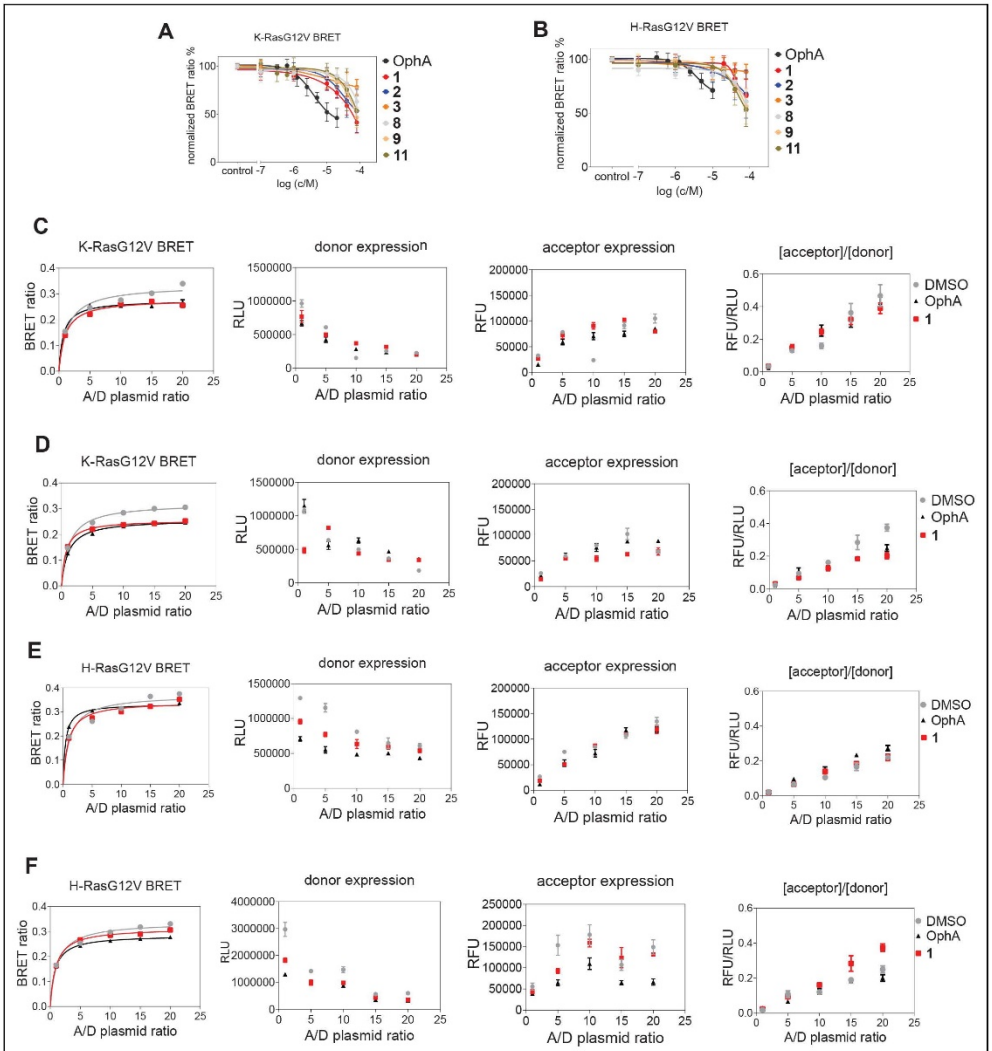

Figure S3. Nanoclustering-BRET assays confirm K-Ras selectivity and faster reactivity of 1 in cells. (**A,B**) Dose response curves of top six benzazulenones (0.1 – 80 µM) and OphA (0.3 – 20 µM) on K-RasG12V (A) and H-RasG12V (B) nanoclustering BRET. The A/D plasmid ratio was 4/1. Data represent mean values ± SD, n ≥ 3. The data were fit into log(inhibitor) vs. variable response (four parameters) function was used in the Prism (GraphPad) software to obtain the dose response curve. The actual curve fitting for DSS_3 calculation was done on the breeze-site (https://breeze.fimm.fi/). (**C-F**) BRET ratio vs. acceptor/donor plasmid ratio (A/D plasmid ratio), donor and acceptor expression data of BRET donor saturation titration experiments. Data from BRET pairs of Rluc8- and GFP2-tagged K-RasG12V (E,F) and corresponding H-RasG12V (G,H)

after 24h treatment with DMSO (0.2% v/v in growth medium), OphA (2.5 μM) or **1** (20 μM). Each figure group represents individual biological repeats with (left to right) BRET ratio plotted against acceptor/donor plasmid ratio (A/D plasmid ratio), and then donor expression (RLU), acceptor expression (RFU) and relative expression of the two (RFU/RLU) plotted against acceptor/donor plasmid ratio (A/D plasmid ratio). Each biological repeat is the mean of four technical replicates (± SD). The BRET ratio vs. relative expression data were fit with a hyperbolic function in Prism to obtain the $BRET_{max}$ and $BRET_{50}$ values.

Supplementary Material

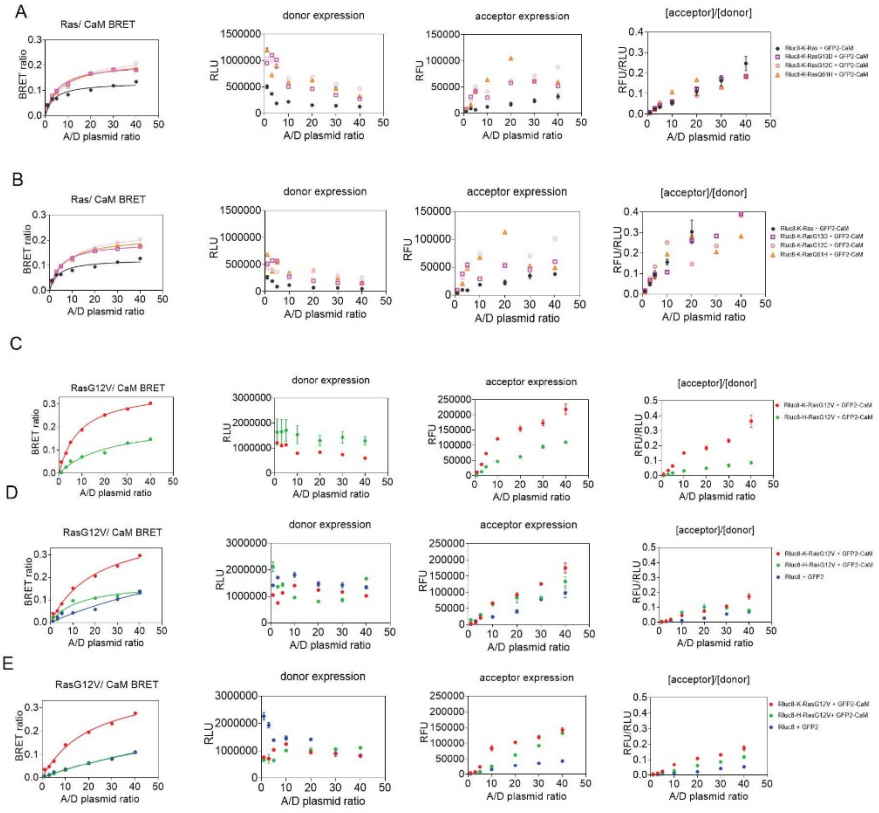

Figure S4. Repeat data of Ras/ CaM BRET experiments. The above figure represents BRET ratio vs. acceptor/donor plasmid ratio (A/D plasmid ratio), donor and acceptor expression data of BRET donor saturation titration experimental repeats for various Ras/ CaM titration curves. **(A,B)** Shows donor saturation titration curves for Rluc8-tagged wild type K-Ras and various G-domain mutants (G12C, G13D, and Q61H) with GFP2-CaM. **(C,D,E)** Shows donor saturation titration curves for Rluc8-K-RasG12V and Rluc8-H-RasG12V with GFP2-CaM. Rluc8 vs GFP2 alone were used to control for unspecific interactions. Each figure group represents individual biological repeats with (left to right) BRET ratio plotted against acceptor/donor plasmid ratio (A/D plasmid ratio), and then donor expression (RLU), acceptor expression (RFU) and relative expression of the two (RFU/RLU) plotted against acceptor/donor plasmid ratio (A/D plasmid ratio). Each biological repeat is the mean of four technical replicates (± SD). The BRET ratio vs. relative expression data were fit with a hyperbolic function in Prism to obtain the $BRET_{max}$ and $BRET_{50}$ values.

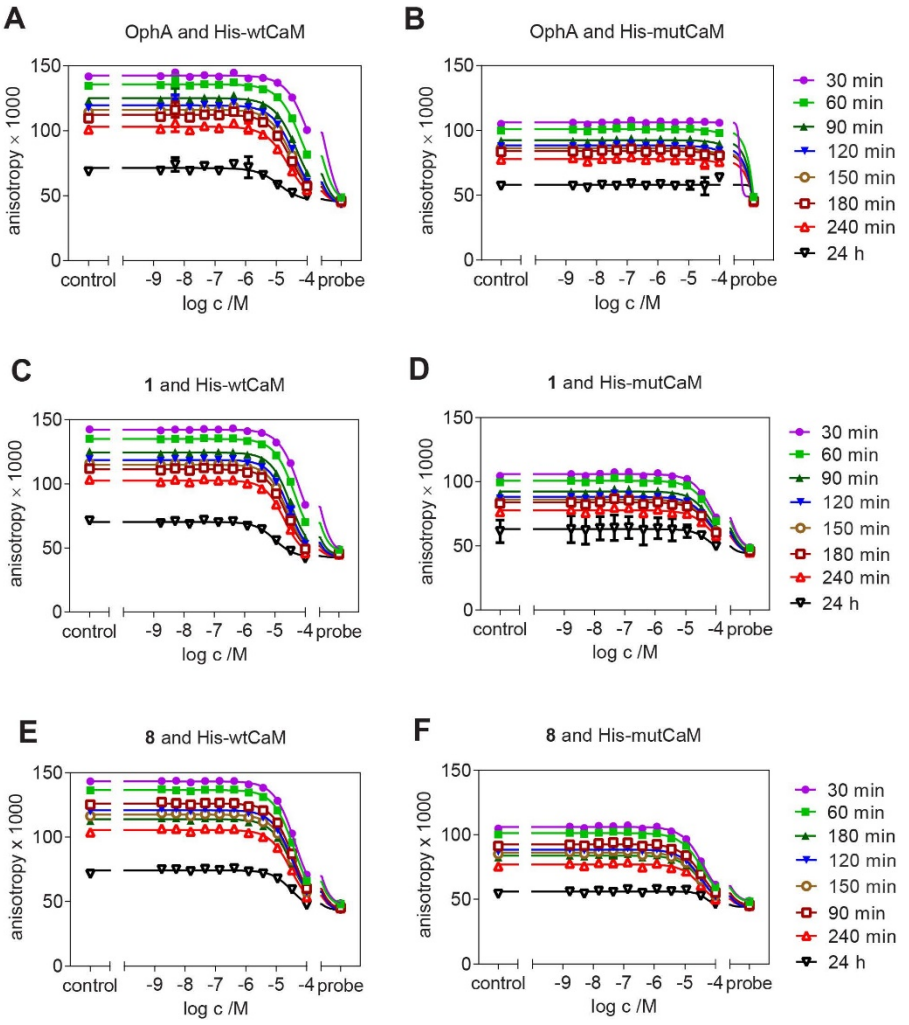

Figure S5. Lysine-dependent CaM-binding activity of OphA, 1 and 8. Displacement of complex of 50 nM His-wtCaM or His-mutCaM and 5 nM F-CaMKII peptide by OphA (**A, B**), **1** (**C, D**) and **8** (**E, F**) at various incubation times. Data represent mean values ± SD, n = 3. The IC_{50} value calculated at each time point was plotted against the time of incubation on **Figure 5**.

Supplementary Material

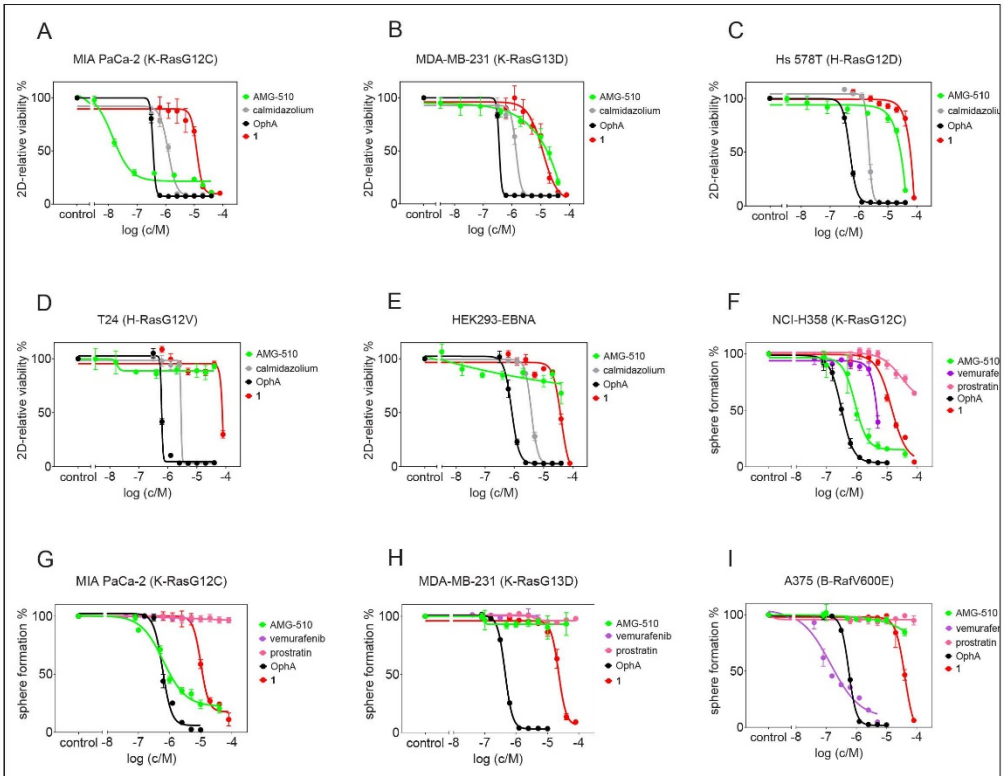

Figure S6. Dose-response curves of benchmarking of 1. (**A-E**) Comparison of effects of compounds on 2D monolayers derived from MDA-MB-231 (A), MIA PaCa-2 (B), Hs 578T (C), T24 (D) and HEK293-EBNA (E). Cells were treated with concentration range of 0.6 µM – 80 µM (**1**), 0.3 µM – 40 µM (calmidazolium and OphA) and 0.003 µM – 40 µM (AMG-510). Data represent mean values ± SD, n = 3. **(F-I)** Assessment of the effects of compound on 3D spheroids derived from NCI-H358 (F), MIA PaCa-2 (G), MDA-MB-231 (H) and, A375 (I). Cells were treated with indicated compounds. **1** was tested at 1.3 – 80 µM. K-RasG12C inhibitor AMG-510 was tested at 0.6 – 40 µM. Additional compounds tested were vemurafenib (0.3 – 20 µM), OphA (0.3 – 20 µM) and prostratin (0.6 – 80 µM). The data were fit to log (inhibitor) vs response – variable slope (four parameters) equation using the Prism (GraphPad) software. Note that the actual curve fitting for DSS calculations was done on the breeze-site (https://breeze.fimm.fi/). Data represent mean values ± SD, n ≥ 2.

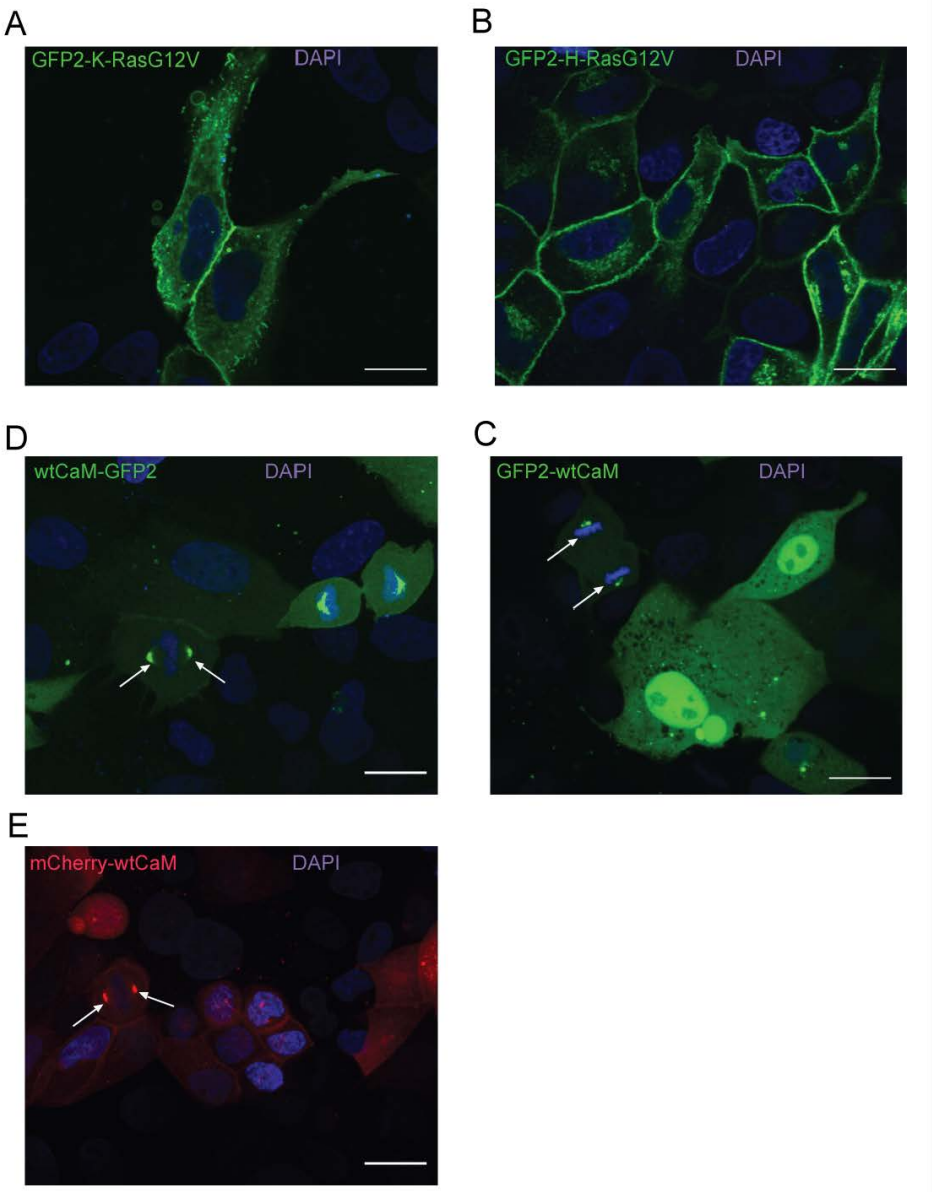

Figure S7. Validation of cellular localization of tagged Ras- and CaM constructs. (**A,B**) Predominant plasma membrane localization of GFP2-K-RasG12V (A), GFP2-H-RasG12V (B). (**D-E**) All CaM constructs, GFP2-wtCaM (C), wtCaM-GFP2 (D) and mCherry-wtCaM (E),

showed characteristic localization to the centrosomes (pointed arrows) and spindles in mitotic cells. Cell nuclei were stained with DAPI (blue). Scale bars, 20 µm.

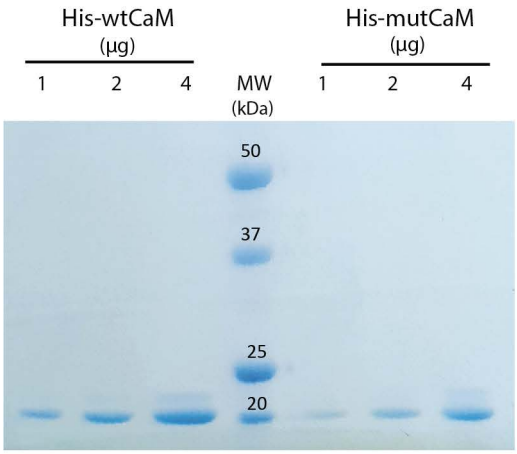

Figure S8. Analysis of purified proteins His-wtCaM and His-mutCaM by SDS PAGE. The gel was stained with ROTI Blue quick. Different amounts (1, 2 and 4 µg) of recombinant proteins were loaded on the gel.

2 Supplementary Tables

Table S1: Expression constructs generated by multi-site Gateway cloning

#	Recombinant plasmid	Entry clone 1	Entry clone 2	Entry clone 3	Destination vector
1	pDest305-CMV-Rluc8-K-RasG12V	CMV51p (C453-E04)	Rluc8 (C511-E03)	Hs. K-RasG12V	pDest-305
2	pDest305-CMV-Rluc8-H-RasG12V	CMV51p (C453-E04)	Rluc8 (C511-E03)	Hs. H-RasG12V	pDest-305
3	pDest305-CMV-GFP2-K-RasG12V	CMV51p (C453-E04)	pDONR235-GFP2-no stop	Hs. K-RasG12V	pDest-305
4	pDest305-CMV-GFP2-H-RasG12V	CMV51p (C453-E04)	pDONR235-GFP2-no stop	Hs. H-RasG12V	pDest-305
5	pDest305-CMV-Rluc8-K-Ras	CMV51p (C453-E04)	Rluc8 (C511-E03)	Hs. K-Ras	pDest-305
6	pDest305-CMV-Rluc8-H-Ras	CMV51p (C453-E04)	Rluc8 (C511-E03)	Hs. H-Ras	pDest-305
7	pDest305-CMV-Rluc8-K-RasG12C	CMV51p (C453-E04)	Rluc8 (C511-E03)	Hs. K-RasG12C	pDest-305
8	pDest305-CMV-Rluc8-K-RasQ61H	CMV51p (C453-E04)	Rluc8 (C511-E03)	Hs. K-RasQ61H	pDest-305
9	pDest305-CMV-Rluc8-K-RasG13D	CMV51p (C453-E04)	Rluc8 (C511-E03)	Hs. K-RasG13D	pDest-305
10	pDest305-CMV-Rluc8	CMV51p (C453-E04)	Rluc8 (C511-E03)	Stuffer (C125-E01)	pDest-305
11	pDest312-CMV-GFP2	CMV51p (C413-E36)	Stuffer (C125-E01)	pDONR257-GFP2-stop	pDest-307
12	pDest527-His-wtCaM	pDONR221-wtCaM	-	-	pDest-527
13	pDest527-His-mtCaM	pDONR221-mutCaM	-	-	pDest-527

Sources:

- All entry clones listed in the table with a code number in parenthesis and destination vectors were obtained from the RAS initiative, FNLCR-NCI, USA
- pDONR257-GFP2-stop (R2-L3) and pDONR235-GFP2-no stop (R5-R1) were commercially cloned at Genewiz Inc., USA. The GFP2 gene was synthesized and cloned into pDONR-235 and pDONR-257 vectors
- The wild type K-Ras4B and H-Ras and the mutant genes were from the RAS mutant collection V2.0 library (kit #1000000089), obtained from Addgene
- pDONR221-wtCaM and pDONR221-mutCaM were commercially obtained from Genecust, France. The wtCaM and mutCaM (containing K75Q, K77Q, and 148Q mutations) were gene synthesized and cloned into pDONR-221 vector using 5' and 3' BsrGI sites

Sequences of proteins encoded by plasmids used in the BRET experiments

Supplementary Material

Legend: Rluc8, GFP2, RAS, CaM

1. pDest305-CMV-Rluc8-K-RasG12V

MASKVYDPEQRKRMITGPQWWARCKQMNVLDSFINYYDSEKHAENAVIFLHGNATSSYLW
RHVVPHIEPVARCIIPDLIGMGKSGKSGNGSYRLLDHYKYLTAWFELLNLPKKIIFVGHDWG
AALAFHYAYEHQDRIKAIVHMESVVDVIESWDEWPDIEEDIALIKSEEGEKMVLENNFFVET
VLPSKIMRKLEPEEFAAYLEPFKEKGEVRRPTLSWPREIPLVKGGKPDVVQIVRNYNAYLRA
SDDLPKLFIESDPGFFSNAIVEGAKKFPNTEFVKVKGLHFLQEDAPDEMGKYIKSFVERVLKN
EQTTLYKKVGTMTEYKLVVVGAVGVGKSALTIQLIQNHFVDEYDPTIEDSYRKQVVIDGET
CLLDILDTAGQEEYSAMRDQYMRTGEGFLCVFAINNTKSFEDIHHYREQIKRVKDSEDVPM
VLVGNKCDLPSRTVDTKQAQDLARSYGIPFIETSAKTRQGVDDAFYTLVREIRKHKEKMSK
DGKKKKKKSKTKCVIM

2. pDest305-CMV-Rluc8-H-RasG12V

MASKVYDPEQRKRMITGPQWWARCKQMNVLDSFINYYDSEKHAENAVIFLHGNATSSYLW
RHVVPHIEPVARCIIPDLIGMGKSGKSGNGSYRLLDHYKYLTAWFELLNLPKKIIFVGHDWG
AALAFHYAYEHQDRIKAIVHMESVVDVIESWDEWPDIEEDIALIKSEEGEKMVLENNFFVET
VLPSKIMRKLEPEEFAAYLEPFKEKGEVRRPTLSWPREIPLVKGGKPDVVQIVRNYNAYLRA
SDDLPKLFIESDPGFFSNAIVEGAKKFPNTEFVKVKGLHFLQEDAPDEMGKYIKSFVERVLKN
EQTTLYKKVGMTEYKLVVVGAVGVGKSALTIQLIQNHFVDEYDPTIEDSYRKQVVIDGETC
LLDILDTAGQEEYSAMRDQYMRTGEGFLCVFAINNTKSFEDIHQYREQIKRVKDSDDVPMV
LVGNKCDLAARTVESRQAQDLARSYGIPYIETSAKTRQGVEDAFYTLVREIRQHKLRKLNPP
DESGPGCMSCKCVLS

3. pDest305-GFP2-K-RasG12V

MVSKGEELFTGVVPILVELDGDVNGHKFSVSGEGEGDATYGKLTLKFICTTGKLPVPWPTLV
TTLSYGVQCFSRYPDHMKQHDFFKSAMPEGYVQERTIFFKDDGNYKTRAEVKFEGDTLVNR
IELKGIDFKEDGNILGHKLEYNYNSHNVYIMADKQKNGIKVNFKIRHNIEDGSVQLADHYQQ
NTPIGDGPVLLPDNHYLSTQSALSKDPNEKRDHMVLLEFVTAAGITLGMDELYKTSLYKKV
GTMTEYKLVVVGAVGVGKSALTIQLIQNHFVDEYDPTIEDSYRKQVVIDGETCLLDILDTAG
QEEYSAMRDQYMRTGEGFLCVFAINNTKSFEDIHHYREQIKRVKDSEDVPMVLVGNKCDLP
SRTVDTKQAQDLARSYGIPFIETSAKTRQGVDDAFYTLVREIRKHKEKMSKDGKKKKKKSK
TKCVIM

4. pDest305-GFP2-H-RasG12V

MVSKGEELFTGVVPILVELDGDVNGHKFSVSGEGEGDATYGKLTLKFICTTGKLPVPWPTLV
TTLSYGVQCFSRYPDHMKQHDFFKSAMPEGYVQERTIFFKDDGNYKTRAEVKFEGDTLVNR
IELKGIDFKEDGNILGHKLEYNYNSHNVYIMADKQKNGIKVNFKIRHNIEDGSVQLADHYQQ
NTPIGDGPVLLPDNHYLSTQSALSKDPNEKRDHMVLLEFVTAAGITLGMDELYKTSLYKKV
GMTEYKLVVVGAVGVGKSALTIQLIQNHFVDEYDPTIEDSYRKQVVIDGETCLLDILDTAGQ
EEYSAMRDQYMRTGEGFLCVFAINNTKSFEDIHQYREQIKRVKDSDDVPMVLVGNKCDLA
ARTVESRQAQDLARSYGIPYIETSAKTRQGVEDAFYTLVREIRQHKLRKLNPPDESGPGCMS
CKCVLS

5. pDest305-CMV-Rluc8-K-Ras

MASKVYDPEQRKRMITGPQWWARCKQMNVLDSFINYYDSEKHAENAVIFLHGNATSSYLW
RHVVPHIEPVARCIIPDLIGMGKSGKSGNGSYRLLDHYKYLTAWFELLNLPKKIIFVGHDWG
AALAFHYAYEHQDRIKAIVHMESVVDVIESWDEWPDIEEDIALIKSEEGEKMVLENNFFVET
VLPSKIMRKLEPEEFAAYLEPFKEKGEVRRPTLSWPREIPLVKGGKPDVVQIVRNYNAYLRA
SDDLPKLFIESDPGFFSNAIVEGAKKFPNTEFVKVKGLHFLQEDAPDEMGKYIKSFVERVLKN
EQTTLYKKVGTMTEYKLVVVGAGGVGKSALTIQLIQNHFVDEYDPTIEDSYRKQVVIDGET
CLLDILDTAGQEEYSAMRDQYMRTGEGFLCVFAINNTKSFEDIHHYREQIKRVKDSEDVPM
VLVGNKCDLPSRTVDTKQAQDLARSYGIPFIETSAKTRQGVDDAFYTLVREIRKHKEKMSK
DGKKKKKKSKTKCVIM

6. pDest305-CMV-Rluc8-H-Ras

MASKVYDPEQRKRMITGPQWWARCKQMNVLDSFINYYDSEKHAENAVIFLHGNATSSYLW
RHVVPHIEPVARCIIPDLIGMGKSGKSGNGSYRLLDHYKYLTAWFELLNLPKKIIFVGHDWG
AALAFHYAYEHQDRIKAIVHMESVVDVIESWDEWPDIEEDIALIKSEEGEKMVLENNFFVET
VLPSKIMRKLEPEEFAAYLEPFKEKGEVRRPTLSWPREIPLVKGGKPDVVQIVRNYNAYLRA
SDDLPKLFIESDPGFFSNAIVEGAKKFPNTEFVKVKGLHFLQEDAPDEMGKYIKSFVERVLKN
EQTTLYKKVGMTEYKLVVVGAGGVGKSALTIQLIQNHFVDEYDPTIEDSYRKQVVIDGETC
LLDILDTAGQEEYSAMRDQYMRTGEGFLCVFAINNTKSFEDIHQYREQIKRVKDSDDVPMV
LVGNKCDLAARTVESRQAQDLARSYGIPYIETSAKTRQGVEDAFYTLVREIRQHKLRKLNPP
DESGPGCMSCKCVLS

7. pDest305-CMV-Rluc8-K-RasG12C

MASKVYDPEQRKRMITGPQWWARCKQMNVLDSFINYYDSEKHAENAVIFLHGNATSSYLW
RHVVPHIEPVARCIIPDLIGMGKSGKSGNGSYRLLDHYKYLTAWFELLNLPKKIIFVGHDWG
AALAFHYAYEHQDRIKAIVHMESVVDVIESWDEWPDIEEDIALIKSEEGEKMVLENNFFVET
VLPSKIMRKLEPEEFAAYLEPFKEKGEVRRPTLSWPREIPLVKGGKPDVVQIVRNYNAYLRA
SDDLPKLFIESDPGFFSNAIVEGAKKFPNTEFVKVKGLHFLQEDAPDEMGKYIKSFVERVLKN
EQTTLYKKVGTMTEYKLVVVGACGVGKSALTIQLIQNHFVDEYDPTIEDSYRKQVVIDGET
CLLDILDTAGQEEYSAMRDQYMRTGEGFLCVFAINNTKSFEDIHHYREQIKRVKDSEDVPM
VLVGNKCDLPSRTVDTKQAQDLARSYGIPFIETSAKTRQGVDDAFYTLVREIRKHKEKMSK
DGKKKKKKSKTKCVIM

8. pDest305-CMV-Rluc8-K-RasQ61H

MASKVYDPEQRKRMITGPQWWARCKQMNVLDSFINYYDSEKHAENAVIFLHGNATSSYLW
RHVVPHIEPVARCIIPDLIGMGKSGKSGNGSYRLLDHYKYLTAWFELLNLPKKIIFVGHDWG
AALAFHYAYEHQDRIKAIVHMESVVDVIESWDEWPDIEEDIALIKSEEGEKMVLENNFFVET
VLPSKIMRKLEPEEFAAYLEPFKEKGEVRRPTLSWPREIPLVKGGKPDVVQIVRNYNAYLRA
SDDLPKLFIESDPGFFSNAIVEGAKKFPNTEFVKVKGLHFLQEDAPDEMGKYIKSFVERVLKN
EQTTLYKKVGTMTEYKLVVVGAGGVGKSALTIQLIQNHFVDEYDPTIEDSYRKQVVIDGET
CLLDILDTAGHEEYSAMRDQYMRTGEGFLCVFAINNTKSFEDIHHYREQIKRVKDSEDVPM
VLVGNKCDLPSRTVDTKQAQDLARSYGIPFIETSAKTRQGVDDAFYTLVREIRKHKEKMSK
DGKKKKKKSKTKCVIM

9. pDest305-CMV-Rluc8-K-RasG13D

MASKVYDPEQRKRMITGPQWWARCKQMNVLDSFINYYDSEKHAENAVIFLHGNATSSYLW
RHVVPHIEPVARCIIPDLIGMGKSGKSGNGSYRLLDHYKYLTAWFELLNLPKKIIFVGHDWG

AALAFHYAYEHQDRIKAIVHMESVVDVIESWDEWPDIEEDIALIKSEEGEKMVLENNFFVET
VLPSKIMRKLEPEEFAAYLEPFKEKGEVRRPTLSWPREIPLVKGGKPDVVQIVRNYNAYLRA
SDDLPKLFIESDPGFFSNAIVEGAKKFPNTEFVKVKGLHFLQEDAPDEMGKYIKSFVERVLKN
EQTTLYKKVGTMTEYKLVVVGAGDVGKSALTIQLIQNHFVDEYDPTIEDSYRKQVVIDGET
CLLDILDTAGQEEYSAMRDQYMRTGEGFLCVFAINNTKSFEDIHHYREQIKRVKDSEDVPM
VLVGNKCDLPSRTVDTKQAQDLARSYGIPFIETSAKTRQGVDDAFYTLVREIRKHKEKMSK
DGKKKKKKSKTKCVIM

10. pDest305-CMV-Rluc8

MASKVYDPEQRKRMITGPQWWARCKQMNVLDSFINYYDSEKHAENAVIFLHGNATSSYLW
RHVVPHIEPVARCIIPDLIGMGKSGKSGNGSYRLLDHYKYLTAWFELLNLPKKIIFVGHDWG
AALAFHYAYEHQDRIKAIVHMESVVDVIESWDEWPDIEEDIALIKSEEGEKMVLENNFFVET
VLPSKIMRKLEPEEFAAYLEPFKEKGEVRRPTLSWPREIPLVKGGKPDVVQIVRNYNAYLRA
SDDLPKLFIESDPGFFSNAIVEGAKKFPNTEFVKVKGLHFLQEDAPDEMGKYIKSFVERVLKN
EQTTLYKKVG

11. pDest312-CMV-GFP2

MVSKGEELFTGVVPILVELDGDVNGHKFSVSGEGEGDATYGKLTLKFICTTGKLPVPWPTLV
TTLSYGVQCFSRYPDHMKQHDFFKSAMPEGYVQERTIFFKDDGNYKTRAEVKFEGDTLVNR
IELKGIDFKEDGNILGHKLEYNYNSHNVYIMADKQKNGIKVNFKIRHNIEDGSVQLADHYQQ
NTPIGDGPVLLPDNHYLSTQSALSKDPNEKRDHMVLLEFVTAAGITLGMDELYK

12. pDest305-CMV-GFP2-CaM

MVSKGEELFTGVVPILVELDGDVNGHKFSVSGEGEGDATYGKLTLKFICTTGKLPVPWPTLV
TTLSYGVQCFSRYPDHMKQHDFFKSAMPEGYVQERTIFFKDDGNYKTRAEVKFEGDTLVNR
IELKGIDFKEDGNILGHKLEYNYNSHNVYIMADKQKNGIKVNFKIRHNIEDGSVQLADHYQQ
NTPIGDGPVLLPDNHYLSTQSALSKDPNEKRDHMVLLEFVTAAGITLGMDELYKKVGMADQ
LTEEQIAEFKEAFSLFDKDGDGTITTKELGTVMRSLGQNPTEAELQDMINEVDADGNGTIDFP
EFLTMMARKMKDTDSEEEIREAFRVFDKDGNGYISAAELRHVMTNLGEKLTDEEVDEMIRE
ADIDGDGQVNYEEFVQMMTAK

Sequences of purified proteins

Legend: His6, CaM

1. pDest527-His-wtCaM

MRSGSHHHHHHRSDITSLYKKVGMADQLTEEQIAEFKEAFSLFDKDGDGTITTKELGTVMR
SLGQNPTEAELQDMINEVDADGNGTIDFPEFLTMMARKMKDTDSEEEIREAFRVFDKDGNG
YISAAELRHVMTNLGEKLTDEEVDEMIREADIDGDGQVNYEEFVQMMTAK

2. pDest527-His-mutCaM

MRSGSHHHHHHRSDITSLYKKVGMADQLTEEQIAEFKEAFSLFDKDGDGTITTKELGTVMR
SLGQNPTEAELQDMINEVDADGNGTIDFPEFLTMMARQMQDTDSEEEIREAFRVFDKDGNG
YISAAELRHVMTNLGEKLTDEEVDEMIREADIDGDGQVNYEEFVQMMTAQ

4.3 Potential of phenothiazines to synergistically block calmodulin and reactivate PP2A in cancer cells

Sunday Okutachi, Ganesh babu Manoharan, Daniel Abankwa*

4.3.1 Manuscript 3: Summary

Phenothiazines (PTZs) are a group of clinically approved antipsychotic drugs that in addition to their classical neuroleptic functions, have been implicated as potential anti-cancer agents (Gutierrez et al., 2014, Wu et al., 2016, Jiang et al., 2018). Their ability to pass through the blood-brain barrier as well as their ability to block multiple oncogenic signaling proteins have resulted in great interest in their potential use in managing cancer. Several studies have shown that PTZs inhibit the growth of various cancer types including glioblastomas, melanoma, colorectal cancer and acute lymphoblastic leukemia (Gutierrez et al., 2014, Wu et al., 2016, Jiang et al., 2018). Previous evidence have identified CaM and PP2A within the target spectrum of PTZs (Hait et al., 1987, Gutierrez et al., 2014). Thus, we were interested in assessing the synergistic potential of combining CaM inhibition and PP2A reactivation as a viable anti-cancer therapeutic strategy in Ras driven cancers due to the fact that both CaM and PP2A have been implicated in the regulation of Ras signaling pathways (Villalonga et al., 2001, Wlodarchak and Xing, 2016, Kuo et al., 2008).

Here we showed through a battery of cellular and in vitro assays including 3D spheroids, fluorescence anisotropy assays, BRET assays and western blotting that synergistic inhibition of CaM and PP2A-reactivation has some potential in mitigating Ras driven cancer proliferation and signaling. Importantly, we showed that the PTZ derivative fluphenazine mustard is a potent inhibitor of Ras driven spheroid growth, an inhibitor of Ras membrane organization and confirmed its CaM directed activity through a K-Ras/CaM BRET assay we previously developed. We also show that fluphenazine mustard significantly reduces MAPK signaling output by up to 60% in MIA PaCa-2 pancreatic cancer cell line after just 2 h of treatment. Taken together, our results suggest that fluphenazine mustard is a potent anti-cancer agent with a CaM and potentially PP2A-directed activity in Ras driven cancer cell lines.

4.3.2 Personal contributions of Sunday Okutachi

- Designed, performed and analysed the synergy experiments, 3D spheroid assays as well as the 2D cell viability and toxicity assays
- Designed and generated all BRET assay data
- Performed the DSS analysis on cellular phenotype data and BRET data

- Designed, performed and anlysed the western blot experimental data
- Analysed and generated the ATARiS gene dependency profiling of the cell lines

Results

Assessment of the synergistic potential of CaM inhibition and PP2A reactivation in 3D spheroids of Ras-MAPK driven cancer cell lines

It is well established that CaM directly interacts with K-Ras and acts a trafficking chaperone of K-Ras membrane localization and signalling (Alvarez-Moya et al., 2010, Grant et al., 2020b). PP2A on the other hand modulates signalling of kinases by promoting their dephosphorylation through its phosphatase activity (Sangodkar et al., 2016). The inhibition of CaM and the reactivation of PP2A have been independent shown to block the growth and proliferation of Ras mutated cancer cell lines (Najumudeen et al., 2016, Sangodkar et al., 2017).

PTZs have been reported to show both CaM inhibitory and PP2A activating properties (Hait et al., 1987, Gutierrez et al., 2014). We therefore evaluated the effectiveness of CaM inhibitor calmidazolium (CMZ) and the PP2A agonist DT-061 either as single agents or in combination and compared their activities to that of the PTZ trifluoperazine in a 3D spheroid synergy assay **(Figure 20A,C).** The K-RasG12C specific inhibitor ARS-1620 was used as a test control compound. In this synergy experiment, the full dose response analysis of inhibitors was determined in three Ras/MAPK mutated cancer cell lines MDA-MB-231 (K-RasG13D), NCI-H358 (K-RasG12C) and A 375 (B-RafV600E). The ATARiS gene dependency database was used to profile the cell lines on the basis of their unique genetic dependencies on critical genes of interest (K-Ras, B-Raf, CaM, SET, PPME1) **(Figure 20B)** (McDonald et al., 2017, Ogris et al., 1999, Cristobal et al., 2012).

When we tested a combination of CMZ and DT-061 in 3D spheroid synergism assays, we observed a 2 to 8-fold increased anti-cancer activity relative to the single agent treatments in three Ras/MAPK mutated cancer cell lines **(Figure 20A).** Interestingly, we observed a similar level of activity for the tricyclic neuroleptic agent trifluoperazine (i.e between 2-7 folds lower than the single agent IC_{50} values across all 3 cell lines) **(Figure 20A).** The synergy between the two compounds was quantitatively validated with the Bliss synergy scoring algorithm **(Figure 20C; SI Figure 1D)** (Ianevski et al., 2020).

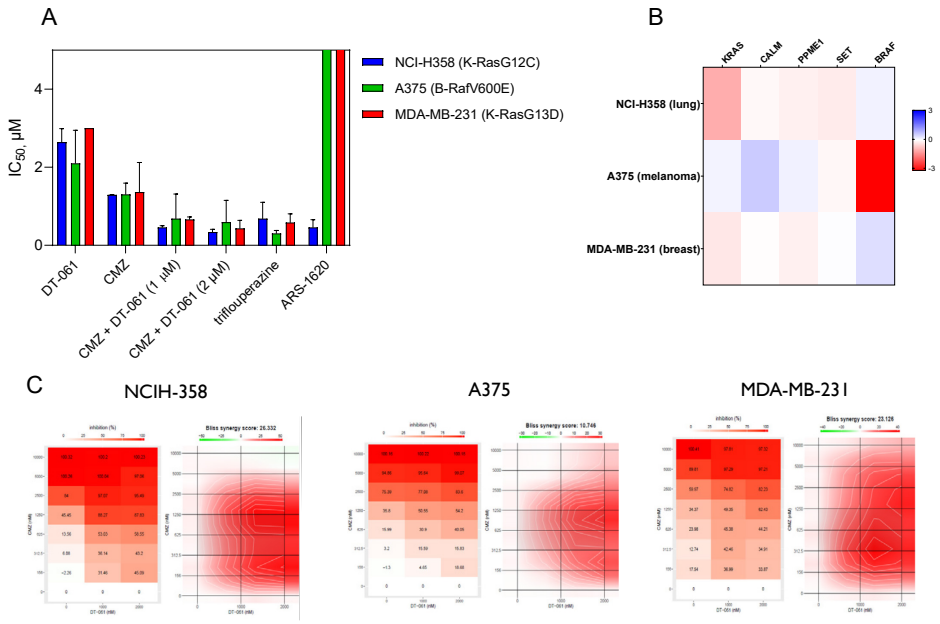

Figure 20. Cellular assessment of CaM inhibition and PP2A activation reveal synergistic potential against Ras pathway dependent cancer cell lines.

(A) *IC50 values for various inhibitors in Ras pathway mutant cell lines NCIH-358, MDA-MB-231 and A375 grown in serum free 3D spheroid suspensions. Compounds were tested as either single agents at concentration ranges of 0.2 µM – 10 µM (calmidazolium), 0.6 µM – 40 µM (DT-061), 0.2 µM – 40 µM (trifluoperazine) and 0.6 µM – 40 µM (ARS-1620) or in combination at a full dose response range of 0.2 µM – 10 µM for calmidazolium plus 1 or 2 µM of DT-061 added to all test conditions. Data represent mean values ± SEM, n = 2.* ***(B)*** *Heatmaps of ATARiS sensitivity scores of KRAS dependent cell lines (NCI H358 and MDA-MB-231) and BRAF dependent cell lines (A375). Heatmap with negative values (shaded red) indicate sensitivity of the cell line proliferation to the knockdown of shown genes whereas, heatmaps with positive scores (shaded blue) indicates insensitivity of the cell line to the shown gene.* ***(C)*** *Representative Bliss synergism heatmaps for combinatorial calmidazolium and DT-061 effects in Ras mutant cancer cell lines. Heatmaps with positive scores (shaded red) indicate synergistic drug interaction whereas, heatmaps with negative scores (green shade on heatmap indicator) indicates antagonistic drug interaction.*

Together, these initial findings prompted us to explore in more details the activity of phenothiazines in Ras driven cancers with a primary interest in delineating the potential contributions of covalent modifications to the observed Ras and CaM-directed activity due to our previous work on covalent calmodulin inhibitors (Okutachi et al., under review). Two analogous phenothiazines; the covalent fluphenazine-N-2-chloroethane (hereafter, fluphenazine mustard) and its non-covalent relative fluphenazine hydrochloride (hereafter, fluphenazine) were selected.

In vitro binding studies show improved CaM binding properties of fluphenazine mustard derivative.

We next used a fluorescence anisotropy assay for the determination of the binding affinities of compounds to CaM **(Figure 21B,C)** (Manoharan et al., 2019). The method measures the displacement of fluorescein labelled plasma membrane calcium-ATPase-derived peptide from CaM, compounds with high CaM binding affinities cause a displacement of the peptide resulting in a lower fluorescence anisotropy readout **(Figure 21A).**

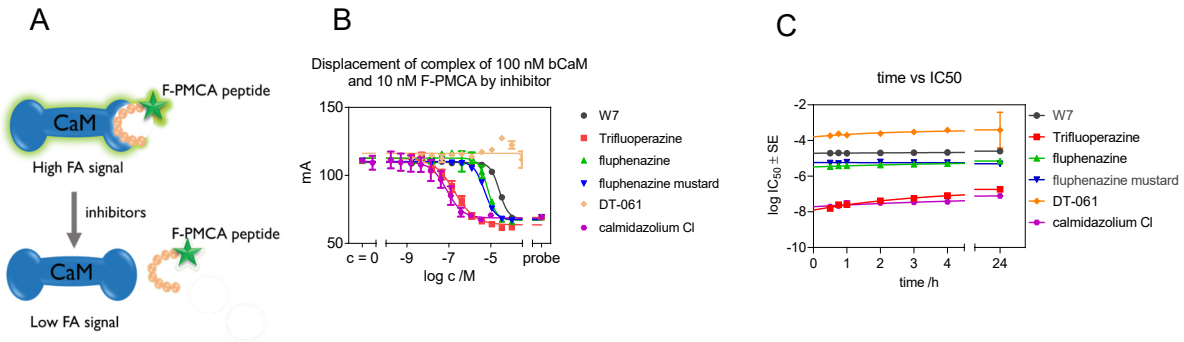

Figure 21. Assessment of binding affinity of compounds to CaM by a fluorescence polarization assay

(A) *Schematic model depicting the mechanism of loss of fluorescence anisotropy signal due to the displacement of fluorescein labelled PMCA peptide by CaM binding small molecules* ***(B)*** *Displacement of complex of 100 nM bovine CaM and 10 nM F-PMCA peptide by inhibitors. Fluorescence anisotropy measured after 24 h of incubation. Data represent mean values ± SEM, n = 2.* ***(C)*** *Dependency of IC_{50} of the inhibitors on time of incubation. In both the figures average of two replicate data with SEM as error is presented. Data represent mean values ± SE, n = 2.*

In comparison to calmidazolium (K_d = 1.09 ± 0.09 nM), W-7 (K_d = 1.51 ± 0.08 µM) appeared to bind at a lesser extent to CaM as demonstrated by the over 1000-fold difference in binding affinity between calmidazolium and W-7. Consistent with its mode of action as a PP2A agonist, we observed that DT-061 binds weakly to CaM (K_d = 219 ± 119 µM). We observed that trifluoperazine binds with high affinity commensurate to that of calmidazolium (K_d = 6 ± 4 nM) **(Figure 21B).** Interestingly, we observed an over 4-fold improved potency of the covalent fluphenazine mustard to CaM (K_d = 0.09 ± 0.02 µM) compared with its non-covalent structural relative fluphenazine (K_d = 0.4 ± 0.1 µM) over a 24 h period of incubation indicating that covalent modification is relevant in improving binding affinity to CaM **(Figure 21B).** Overall, the binding activity of the tested

inhibitors did not significantly change over a 24 hour incubation period when we plotted the IC50 values against time. Hence, none of the tested compounds may be considered to possess a slow CaM reactivity profile **(Figure 21C).**

Cellular BRET assay identify Ras isoform inhibitory properties of covalent fluphenazine mustard.

Using our recently established BRET assay for the identification of compounds capable of selectively inhibiting Ras isoforms specific membrane organization (Okutachi et al., under review), we assessed the effects of DT-061, fluphenazine and fluphenazine mustard on K-Ras vs H-Ras BRET signal output. Inhibitors of Ras membrane organization, Ras chaperone activity inhibitors and post translational modification inhibitors facilitate a measurable loss in the BRET signal which is detected in our assay **(Figure 22A)**. In addition to our test compounds, CaM inhibitors calmidazolium, OphA as well as the farnesyl transferase inhibitor FTI-277 were used as controls **(Figure 22B,C,D; SI Figure 2A)**.

Consistent with our previous observations, the CaM inhibitors calmidazolium and OphA more selectively decreased the BRET signal of the K-Ras biosensor pairs both at a single concentration and when tested in the full dose response concentration range **(Figure 22B,C,D; SI Figure 2A).** Indeed, we observed a 4-folds selective decrease of K-Ras BRET signal by ophiobolin A and a 2-fold selectivity by calmidazolium in our DSS-BRET analysis **(Figure 22D; SI Figure 2A).** Treatment with the farnesyl transferase inhibitor FTI-277 more selectively decreased H-Ras nanoclustering-BRET (**Figure 22B,C**) due to the alternative prenylation mechanism available to K-Ras4b (Kohnke et al., 2012). However, we fail to observe any significant effect of DT-061 on the BRET signal for both K-Ras and H-Ras biosensor pairs either at a single dose or over several concentration ranges (**Figure 22B,C,D**). Interestingly, whilst fluphenazine did not decrease the BRET signal of either Ras isoform biosensor constructs, the covalently reacting mustard derivative showed a clear effect on both K-RasG12V and H-RasG12V BRET biosensor signalling output albeit without any indication of isoform specific selectivity (**Figure 22B,C,D; SI Figure 2A**).

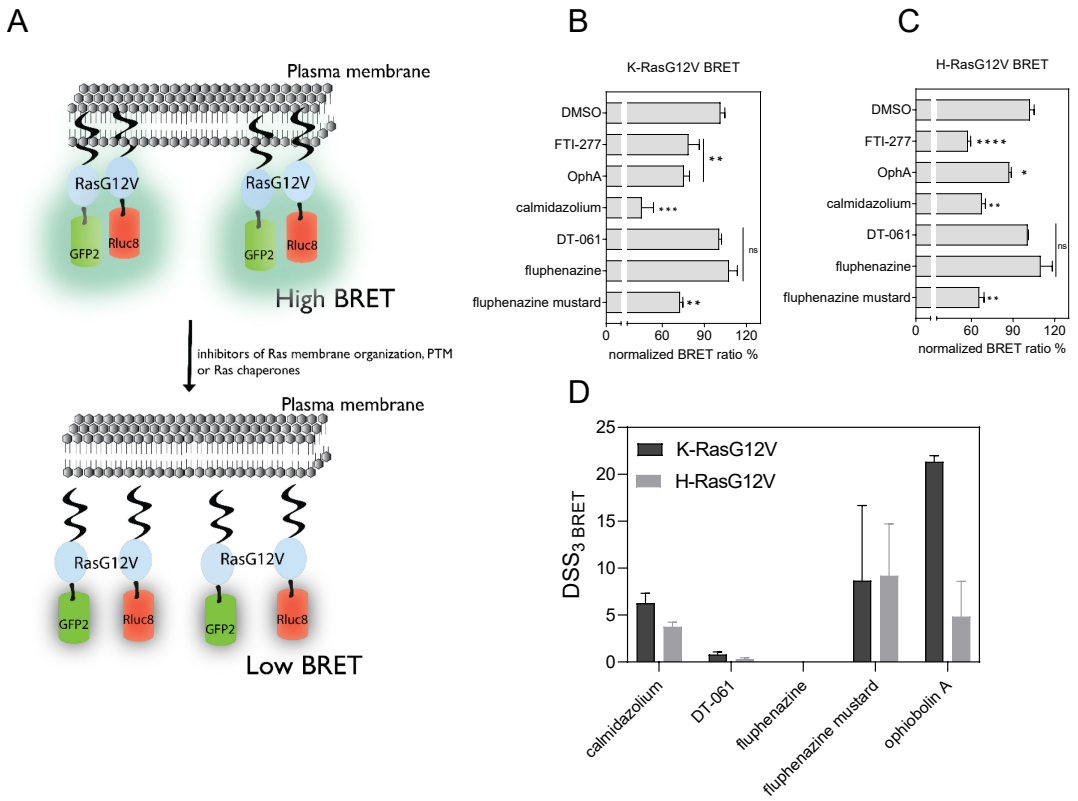

Figure 22. BRET assays identifies fluphenazine mustard as an inhibitor of Ras isoform signaling in cells.

(A) *Schematic representation of the mechanism of Ras nanoclustering BRET signal loss due to small molecule perturbation. Compounds capable of disrupting Ras membrane organization, prenyl moiety biosynthesis inhibitors or inhibitors of Ras chaperone activity cause a decrease in Ras BRET signal output.* ***(B,C)*** *Testing of inhibitors at 20 µM and 24 h exposure in K-RasG12V (A) and H-RasG12V (B) nanoclustering-BRET assays. Controls are FTI-277 (1 µM), OphA (2.5 µM), calmidazolium (20 µM) and DT-061 (20 µM) (The acceptor/donor (A/D) plasmid ratio of GFP2- and Rluc8-tagged RasG12V was 4/1. Data represent mean values ± SEM, n ≥2. Statistical differences to vehicle control are annotated as *p < 0.05; **p < 0.01; ****p < 0.0001; ns, not significant. (**D**) BRET-DSS$_3$ values for calmidazolium, DT-061 and fluphenazines derived from dose response analysis (0.1 µM – 80 µM) and OphA (0.3 µM – 20 µM) on K-RasG12V and H-RasG12V nanoclustering-BRET. The A/D plasmid ratio was 4/1. Data represent mean values ± SEM, n ≥ 2.*

K-Ras/CaM BRET assays confirms the target engagement activity of fluphenazines in cells.

In order to properly delineate the on-target activity of the fluphenazine derivatives, we assessed their direct effects on the K-Ras/CaM interaction using our Rluc8-K-RasG12V/GFP2-CaM BRET pairs (Okutachi et al., under review). Consistent with our previous observations, CaM inhibitors

ophiobolin A and calmidazolium clearly decreased the BRET signal at single concentrations and over a full dose-response range **(Figure 23B,C; SI Figure 3A).** Similarly, fluphenazine and fluphenazine mustard decreased the BRET signal output thus confirming their CaM on-target activity **(Figure 23B,C; SI Figure 3A).** Interestingly, fluphenazine mustard exhibited a much stronger effect in decreasing the K-Ras/CaM BRET signal as demonstrated by its 3-fold higher DSS-BRET score over fluphenazine **(Figure 23B)**. This once again suggests that covalent modification is critical to the improved CaM-directed activity **(Figure 23C).** Further assessment of fluphenazine mustard along with OphA in a donor titration saturation experiment showed that both compounds are effective at decreasing the K-RasG12V/CaM BRET signal over a wide range of increasing acceptor concentrations **(Figure 23D; SI Figure 3B,C,D).**

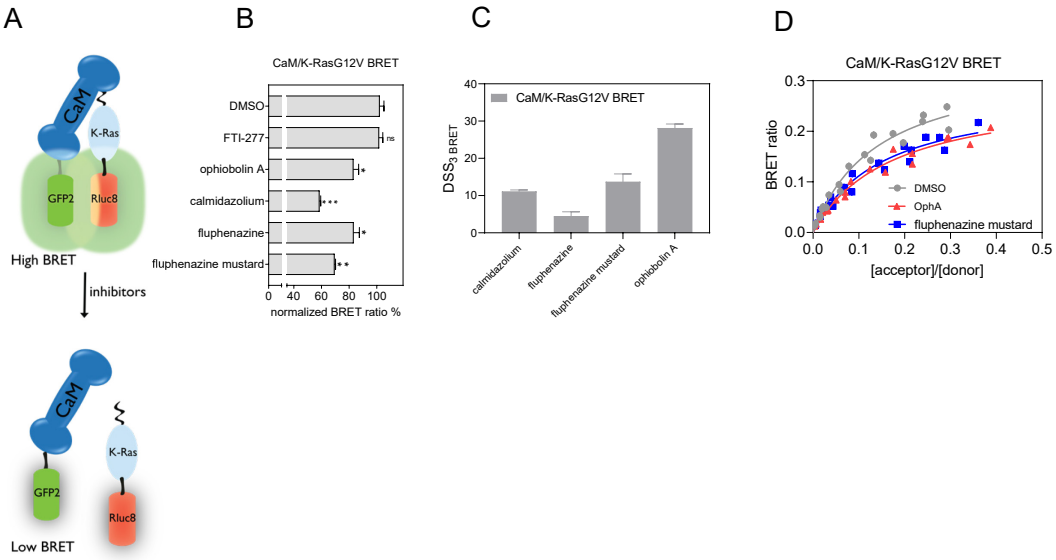

Figure 23. Cellular CaM/K-RasG12V interaction BRET confirms on-target activity of fluphenazines in cells.

(A) *Schematic model depicting the hypothetical binding of Rluc8-K-RasG12V to the C-terminus of GFP2-CaM. This interacts produces a high BRET signal which is significantly lower upon small molecule interruption of the complex.* ***(B)*** *Compounds FTI-277 (1 µM), OphA (5 µM) or calmidazolium (20 µM), as well as fluphenazine (20 µM) and covalent derivative fluphenazine mustard (20 µM) were tested using the Rluc8-K-RasG12V/ GFP2-CaM BRET reporter. The A/D plasmid ratio was 9/1. Data represent mean values ± SEM, n = 2. Statistical differences to vehicle control are annotated as *p < 0.05; **p < 0.01; ****p < 0.0001; ns, not significant.* ***(C)*** *DSS_3–BRET values for calmidazolium, DT-061 and fluphenazines derived from dose response analysis and OphA (0.1 µM – 80 µM) on Rluc8-K-RasG12V/ GFP2-CaM BRET signal. The A/D plasmid ratio was 9/1. Data represent mean values ± SEM, n = 2. (**D**) K-RasG12V/CaM BRET donor saturation titration curves showing the effect of OphA (2.5 µM), fluphenazine mustard (10 µM) and vehicle control. Data represent mean values ± SEM, n = 3. Note, error bars are small and may not be recognizable.*

Synergistic inhibition of CaM and PP2A activation blocks Ras mediated tumor growth and Ras pathway signaling output.

Upon confirming the on-target activity of the phenothiazine derivatives in our cellular BRET assays, we were next interested in characterizing their phenotypic and signaling effects on Ras driven cancer cells. To this end, we performed 2D cell viability experiments using two K-Ras mutated cancer cell lines; MIA PaCa-2 (K-RasG12C) and MDA-MB-231 (K-RasG13D) and the non-malignant human embryonic kidney cell line (HEK-293 EBNA) **(Figure 24A,B; SI Figure 4A,B,C).** We observed that the phenothiazine compounds more selectively inhibited the proliferation of the cancer cell lines by a factor of about 3 to 12-folds higher than HEK-293 EBNA **(Figure 24B; SI Figure 4A,B,C).** Interestingly, we observed that the selectivity was more pronounced in the pancreatic cancer cell line MIA PaCa-2 which we have previously identified to be more dependent on K-Ras based on the data from the ATARiS gene dependency database **(Figure 24B; SI Figure 4A,B,C)** (McDonald et al., 2017). Indeed, this is consistent with our previous findings where we showed that the inhibitory activity of the novel covalent CaM inhibitor Calmirasone1 correlated with the K-Ras dependency of cancer cell lines (Okutachi et al., under review).

The evaluation of ERK phosphorylation status is well established as an indicator of Ras/MAPK mediated signaling output (Guo et al., 2020). Therefore, in order to determine the signaling consequences of CaM inhibition and PP2A reactivation, we performed western blot analysis on serum starved and EGF stimulated MIA PaCa-2 cells after a 2 h incubation period with the inhibitors **(Figure 24C,D; SI Figure 4D)**. We employed the MEK inhibitor trametinib and the K-RasG12C covalent inhibitor sotorasib (AMG-510) as compound controls whilst DMSO was used as vehicle control. Predictably, both trametinib and sotorasib reduced phospho-ERK signaling output by more than 70% after the 2 h period. DT-061 and calmidazolium both achieved ~30% pERK signal reduction as single agents. However, we only observed a slightly improved (~40%) reduction in pERK output in the combinatorial setup. Interestingly and consistent with its overall activity as a potent CaM inhibitor and potential PP2A agonist, fluphenazine mustard achieved over 60% reduction in pERK signaling output in our western blot experiments thus validating the compound as an effective inhibitor of Ras mediated MAPK signaling output **(Figure 24C,D; SI Figure 4D)**.

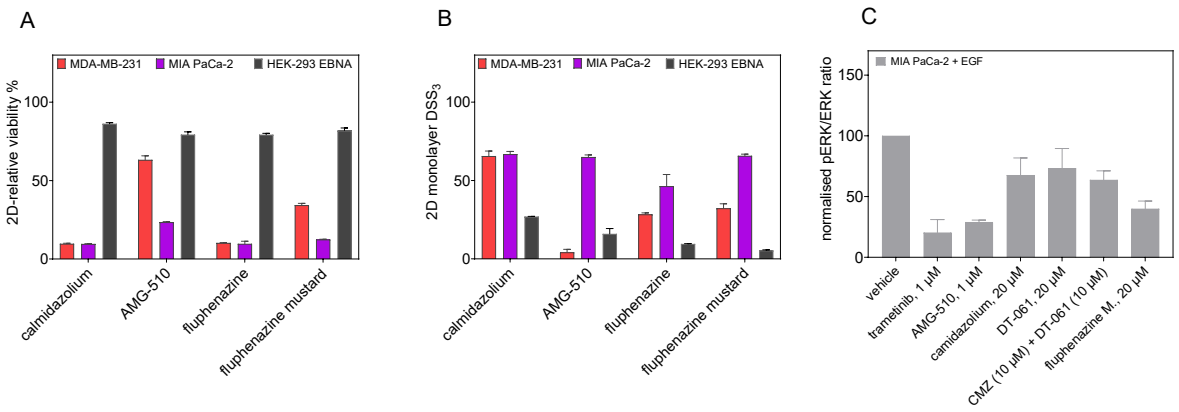

Figure 24. Phenotypic and signaling effects of synergistic targeting of CaM and PP2A.

(A) *The relative 2D viability of MDA-MB-231, MIA PaCa-2 and HEK-293 EBNA following single dose treatment with AMG-510 (10 µM), calmidazolium (2.5 µM), fluphenazine (10 µM) and fluphenazine mustard (10 µM) was assessed using the alamarBlue assay. Cells were grown as 2D adherent monolayers overnight and then treated for 72 h with indicated compounds. Data represent mean values ± SEM, n = 3.* ***(B)*** *DSS_3 measuring the effects of AMG-510 (0.003 – 40 µM), calmidazolium (0.3 – 40 µM), fluphenazine (0.6 – 80 µM) and fluphenazine mustard (0.6 – 80 µM). Cells were grown as 2D adherent monolayers overnight and then treated for 72 h. Results represent mean values ± SEM, n = 3.* ***(C)*** *Densitometric quantification of the pERK/ERK ratio analysis.* *MAPK signaling output was measured in MIA PaCa-2 upon treatment with control compounds trametinib (1 µM) and AMG-510 (1 µM), single agent treatment with camidazolium (20 µM) and DT-061 (20 µM) or in combination (DT-061 10 µM + CMZ 10 µM) as well as fluphenazine mustard (20 µM). pERK/ERK levels were assessed using a mouse monoclonal antibody against pERK and a rabbit polyclonal antibody against ERK. GAPDH was used as endogenous control for protein expression. Cells were seeded in 6-well plates for 24hrs, serum starved, treated with indicated concentrations of inhibitors for 2 h and then stimulated with EGF for 10 min before lysis. Data represent mean values ± SD, n =3.*

DISCUSSION

5.0 DISCUSSION

5.1 Novel PDE6D inhibitors with a new design principle show K-Ras selective anti-cancer activity

Two major challenges have hampered efforts to develop PDE6D inhibitors namely; the Arl2 mediated ejection mechanism of PDE6D inhibitors and the poor cellular penetration of current PDE6D inhibitors (Martin-Gago et al., 2017). In this study we developed Deltaflexin 1 and Deltaflexin 2 as proof of concept PDE6D binding molecules able to selectively inhibit K-Ras nanocluster formation in addition to selectively inhibiting the growth of K-Ras driven cancer cell proliferation.

We were able to show that our first generation PDE6D inhibitor Deltaflexin 1 selectively blocked K-Ras membrane organization and selectively inhibited the growth of K-Ras mutated cancer cell lines from different tissue backgrounds including breast, lung and colon. Through structural optimization efforts by replacing the coumarin ring with a terephthalic acid moiety which is similar to deltasonamide (compound 8), and the replacement of the bottom moiety with 2a pharmacologically more stable 2-methyl-substituent on the S-acyl cell penetration group, we improved the overall performance of this new design in the second generation with Deltaflexin 2. Consistently, Deltaflexin 2 showed improved binding and K-Ras selectivity relative to Deltaflexin-1. In general, our Deltaflexins selectively inhibited K-Ras mediated oncogenesis and stemness properties in lung cancer. Similarly, Our new design principle significantly improved the over 1000-fold difference between in vitro and cellular anti-cancer activity of previous PDE6D inhibitors as we could achieve micromolar activity in cells even though our compounds possess micromolar in vitro binding affinity to PDE6D.

Importantly, the siRNA knockdown data for PDE6D and K-Ras in this study suggests that PDE6D downregulation may have K-Ras independent effects on the stemness characteristics of cancer cells. Indeed, inositol polyphosphate-5-phosphatase-E (INPP5E) is a client of PDE6D which is known to localize in the primary cilium via a PDE6D-dependent process (Humbert et al., 2012, Fansa et al., 2016). Mutations in PDE6D have been implicated in Joubert syndrome, a developmental disorder characterized by distinctive cerebellar structural defects (Thomas et al., 2014). The potential contribution of INPP5E to the stemness associated anti-cancer activity of PDE6D inhibition is plausible given that ciliogenesis and associated Hedgehog signaling have been recently implicated in the epithelial to mesenchymal transition process and the promotion of

the stemness phenotype in triple negative breast cancer (Guen et al., 2017). It is also plausible that PDE6D inhibition affects the activity and localization of other client proteins as is the case with drug inhibition strategies against major trafficking hub proteins. Hence, the possibility of alternative-target effects cannot be excluded. Consistently, a recent study with PDE6D inhibitors deltasonamide 1 and 2 conjugated in a PROTAC system showed that the PDE6D degradation increased the sterol regulatory binding protein (SREBP)-mediated gene expression of lipid metabolism enzymes which was accompanied by an increase in the level of cholesterol biosynthesis precursors (Winzker et al., 2020). This finding highlights the much broader spectrum of functional effects associated with PDE6D inhibition and degradation. Likewise, recent observations that a PROTAC construct of the clinical B-Raf inhibitor sorafenib targets PDE6D emphasizes the relevance of multi-target activity of some approved small molecules in providing clinical benefit. (Yang Li, 2020). Consequently, off-target and/or multi-target effects might become advantageous particularly in cancers with multiple and diverse sets of driver mutations where the need to drug more than one protein target is desirable.

Although our current Deltaflexins are not suitable to be considered as viable drug candidates, it is important to note that our design approach is compatible with compound-scaffold hybridization of existing PDE6D inhibitors and will consequently be advantageous for the rapid advancement of improved PDE6D derivatives. This strategy may also be adopted for the development of inhibitors for similar lipid binding chaperone proteins such as UNC119, an N-Terminally myristoylated chaperone that facilitates the trafficking of Src Kinases (Mejuch et al., 2017).

5.2 A novel CaM covalent inhibitor blocks K-Ras/CaM interaction and K-Ras driven cancers

Recent evidence suggests a stemness context specific collaboration of CaM and K-Ras (Wang et al., 2015b). Disruption of this interaction through prostratin mediated S181 phosphorylation as well as the direct inhibition of CaM by OphA demonstrated anti-cancer activity (Wang et al., 2015b, Najumudeen et al., 2016). Taken together, these earlier studies indicated that targeting CaM in K-Ras driven cancers may offer a new window of opportunity for CaM drug development (Najumudeen et al., 2016, Wang et al., 2015b, Saito et al., 2017).

From a small collection of compounds, we have identified **Calmirasone1**, an OphA-like formyl benzazulenenone which binds to CaM with a 4-fold higher affinity relative to OphA. Upon comparison of Calmirasone1 and its non-formylated relative compound 8 in our in vitro CaM binding experiments, we observed that the binding affinity characteristics of the compound that remained unchanged over time was independent of the C-1 formylation since the non-formylated

compound 8 also exhibits this characteristic. We therefore posit that the *ortho* quinone-methide electrophilic reactivity group which possess covalent binding potential is responsible for the unchanged CaM binding characteristic.

Based on the similar selectivity observed for Calmirasone1 and compound 8 in our 2D K-Ras vs H-Ras selectivity experiments, we speculate that the formyl-independent binding of our compounds is also responsible for the unspecific toxicity component of Calmirasone1 activity. However, the over 4-fold increased CaM binding potency observed for Calmirasone1 over compound 8 clearly stems from the C1-formyl group. Importantly, we show that the C1-formyl-dependent activity is lost upon mutations to the Lys 75, 77 and 148 residues of CaM.

Given that the potent CaM inhibitor calmidazolium significantly decreased the BRET-signal of both K-Ras and H-Ras, it is plausible that CaM inhibition affects the membrane anchorage, trafficking and/or nanoclustering of both K-Ras and H-Ras, Indeed, like K-Ras, H-Ras is farnesylated and may potentially employ CaM for trafficking (Agamasu et al., 2019).

Importantly, cyclic amino group appears to combine several beneficial structural and reactivity properties in Calmirasone1. This is also reflected in cell activity data, where in both 2D and 3D growth experiments, a significant selectivity for KRAS-mutant cells was observed. This suggests a formyl-dependent CaM/K-Ras-directed mechanism of action of these formyl aminobenzazulenones.

Whilst calmidazolium, as well as the covalent inhibitors OphA and Calmirasone1 significantly disrupted K-Ras/ CaM-BRET in cells, we observed that the PKC agonist prostratin did not inhibit the cellular BRET between K-RasG12V and CaM at the tested concentrations. Therefore, prostratin may exert its K-Ras nanocluster inhibition selectivity by a different mechanistic route than inhibition of K-Ras/CaM interaction. Consistent with the BRET data, prostratin also elicited no effect on tumor cell proliferation in the spheroid assays. Although, the structural implication of OphA inhibition of CaM is not yet resolved, the structural evidence from the non-covalent phenothiazine trifluoperazine in complex with CaM shows that binding of trifluoperazine induces a collapse of the original dumbbell shape of CaM into a compact globular structure (Vandonselaar et al., 1994). It is therefore reasonable to speculate that covalent inhibitors like Calmirasone1 and OphA may elicit a similar effect on CaM conformation and functionality. Indeed, in its collapsed form, the hydrophobic pocket may become inaccessible to both canonical and non-canonical targets including K-Ras (Vandonselaar et al., 1994).

Clonogenic 3D spheroid growth depends on stemness associated asymmetric and symmetric division processes of cancer cells (Cicalese et al., 2009). Accordingly, Calmirasone1 demonstrates an efficacy against 3D spheroid growth that correlates with the KRAS-dependence

of the tested cell lines as defined by the ATARiS gene dependency plots. Likewise, it is important to note that the DSS_3-potency of Calmirasone1 reaches about 50% of the clinical K-RasG12C inhibitor sotorasib (AMG-510) (Hong et al., 2020).

Taken together, we have identified Calmirasone1 as a high affinity and easily synthesizable covalent inhibitor of CaM. We showed that Calmirasone1 has a significantly lower unspecific toxicity compared to the natural product OphA. We demonstrated the ability of this compound to selectively and rapidly disrupt K-Ras membrane organization in our BRET assays whilst also showing its ability to directly interrupt the K-Ras/CaM interaction in cells. Importantly, we showed that Calmirasone1 selectively inhibits the growth of K-Ras dependent cancer cells under both 2D monolayer and 3D spheroid conditions.

CaM has been implicated in several biological processes including cell cycle regulation, cell division, apoptosis, invasion and migration etc. (Berchtold and Villalobo, 2014). The inhibition of CaM is known to affect cell division processes including cleavage furrow formation (Yu et al., 2004). Indeed, the quinazolinone compound mdivi-1 which induces multipolar acentrosomal spindles was shown to kill cancer cells (Wang et al., 2015a). Our cell biological experiments with Calmirasone1 (K_d = 0.87 ± 0.02 µM) and the potent non-covalent CaM inhibitor calmidazolium (K_d = 13.5 nM) indicated that only Calmirasone1 significantly induced a multipolar phenotype despite the ~80-fold higher in vitro binding affinity of calmidazolium to CaM.

Conclusively, although Calmirasone1 does not possess desirable characteristics for progression into a viable clinical agent, its utility as a tool compound for further studies into the mechanism of the K-Ras/CaM associated cancer stemness mechanism will be insightful. Similarly, Calmirasone1 may be applied to acutely and rapidly achieve a chemical knock-down of all CaM in cells in a more efficient manner than with the most potent non-covalent inhibitor calmidazolium. This application may find relevance in many aspects of CaM biology beyond cancer research due to the central role of CaM in modulating cellular processes across species (Berchtold and Villalobo, 2014).

5.3 Synergistic targeting of CaM and PP2A in K-Ras driven cancers

To effectively suppress K-Ras driven cancers, the use of inhibitor combinations and/or the development of inhibitors capable of blocking several signalling proteins relevant to Ras activation is pertinent. Here, we show that fluphenazine mustard, a potent tricyclic PTZ containing an alkylating chloroethylamine chain possesses improved anti-CaM activity through a variety of assays. Unlike fluphenazine dihydrochloride, fluphenazine mustard irreversibly inhibits CaM (Hait et al., 1987). We show an over 4-fold higher affinity for CaM by the mustard derivative compared

to fluphenazine thus suggesting that the chloroethyamine moiety is central for improved anti-CaM directed covalent activity in vitro since this is the only structural difference between the two compounds. We could also show that DT-061 failed to bind effectively to CaM consistent with its mechanism of action as a PP2A Aα scaffold subunit binder and stabilizer of the B56a-PP2A holoenzyme.

Consistent with the earlier mentioned importance of the alkylating chloroethyamine group for improved anti-CaM effects, our Ras nanoclustering BRET assays confirm that fluphenazine mustard reduced both K-Ras and H-Ras membrane interaction. Indeed, this significant decrease the BRET signal of both K-Ras H-Ras by a covalent CaM inhibitor highlights our previous observation that membrane anchorage, trafficking and/or nanoclustering of both K-Ras and H-Ras are susceptible to CaM inhibition (Okutachi et al., under review). Interestingly, DT-061 did not show any appreciable effect on the membrane anchorage of both Ras isoforms. This indicates that the compound's mechanistic binding to the PP2A Aα scaffold subunit and subsequent stabilization of the B56a-PP2A holoenzyme has no direct impact on Ras membrane dynamics (Leonard et al., 2020). In the same vein, fluphenazine mustard maintained a 3-fold higher DSS-BRET score over fluphenazine in our on-target K-Ras/CaM experiments, thus further validating the relevance of the chloroethyamine alkylating modification for improved CaM activity.

Upon western blot assessment, we show that fluphenazine mustard already achieves an over 60% reduction in pERK signalling output, an important indicator for cellular Ras activity. The effect of fluphenazine mustard was higher than those of single agent CMZ and DT-061 over the 2 h treatment period. Further phenotypic assessment by 2D proliferation assays also confirms the ability of the compound to inhibit the growth of Ras mutated cancer cell lines.

Although we were unable to directly assess the binding of the phenothiazines to PP2A as a result of the difficulty in establishing an in vitro binding assay with the fully functional PP2A protein, the use of indirect approaches to measure PP2A effects may become relevant in this study. The tumor suppressor activity of PP2A is known to be mediated through its ability to dephosphorylate diverse targets implicated in cancer (Gutierrez et al., 2014). Therefore, by assessing the dephosphorylation status of PP2A targets such as AKT, p70S6K, MYC, ERK and BAD upon fluphenazine mustard treatment, an indirect measure of PP2A activity can be achieved. However, notwithstanding the current experimental limitation, the highly similar structure of DT-061 to phenothiazines which differs essentially by the replacement of the basic amine group of the phenothiazines with a polar functional group, allows us to speculate that fluphenazine mustard may also bind to PP2A (Kastrinsky et al., 2015). Consistently, it has been documented that

perphenazine, another structurally similar phenothiazine elicits its anti-tumor activity by PP2A reactivation (Gutierrez et al., 2014).

While our study is quite limited, it suggests that preservation of the CaM inhibitory activity of PTZ derivatives that can also activate PP2A is desirable. Our data show however, that DT-061 does not bind to CaM and would therefore have lost the synergistic potential. We propose that the preservation of the investigated polypharmacology of PTZ could allow for a higher, yet selective cancer cell killing activity.

CONCLUSIONS AND PERSPECTIVES

6.0 CONCLUSIONS AND PERSPECTIVES

Renewed interest in Ras drug development, potentiated by the development of the covalent G12C inhibitors has led to a significant increase in the body of knowledge on Ras therapeutic targeting. Since entering clinical trials, some studies have already identified resistance mechanisms against these inhibitors (Tanaka et al., 2021, Dunnett-Kane et al., 2021). Indeed, the differences in Ras isoform tumorigenic abilities brought about by the interplay between multiple factors such as Ras gene dosage, differential isoform specific signaling as well as the contribution of tissue or cellular contexts that dictate genetic, epigenetic and proteomic landscapes, makes the effective targeting of Ras driven cancers a daunting challenge (Prior et al., 2020). Therefore, to effectively treat K-Ras mutated and/or K-Ras driven cancers, the need to pursue multiple direct and indirect therapeutic strategies including the targeting of K-Ras trafficking chaperones as well as the synergistic targeting of different nodes in K-Ras mediated signaling pathways will be crucial.

In my PhD thesis, the overarching aim was to identify novel small molecules that can interfere with K-Ras membrane localization through the inhibition of K-Ras trafficking chaperones by both covalent and non-covalent binding. To this end, we designed and developed relevant assays for the in vitro and in cellulo characterization of small molecules against the trafficking chaperone proteins CaM and PDE6D. Collectively, the findings of this thesis show that the inhibition of the K-Ras trafficking chaperones clearly interferes with proper K-Ras membrane localization, and signaling. Consistently, we established that blocking the K-Ras chaperone activity of PDE6D and CaM with Deltaflexins and Calmirasone1 blocked 2D and 3D proliferation of K-Ras mutated cancer cell lines. Consequently, the compounds Deltaflexin 1, Deltaflexin 2 and Calmirasone1 identified in this thesis may become useful tool in the further interrogation of the activities of PDE6D and CaM particularly in the context of the K-Ras associated cancer stemness phenotype. Among the Ras isoforms, K-Ras has the greatest potential to induce stemness traits (Quinlan et al., 2008, Chippalkatti and Abankwa, 2021). To properly unravel the mechanistic details of this K-Ras associated cancer stemness phenomena, it may be insightful to look beyond the canonical K-Ras plasma membrane localization/ functions and explore other activities and localizations implicated in cell fate decision making. This K-Ras stemness traits potentially enabled by the activity of trafficking chaperones CaM and PDE6D due to both proteins being dynamically localized and relevant for the organization and functions of cell fate linked cellular machineries like the centrosome and primary cilium highlights the importance of having useful tool compounds to study this process.

Beyond K-Ras specific anti-cancer effects, drugging PDE6D has the potential to provide therapeutic benefit for disease conditions where other PDE6D clients are relevant. For instance, PDE6D have been implicated in the development of Joubert syndrome and ciliopathies (Thomas et al., 2014, Fansa et al., 2016). Likewise, a recent study identified targeting the Rap1-PDE6D interaction in Alzheimer's disease models as a promising therapeutic strategy for protection against the neurodegenerative disease further highlighting the importance of PDE6D inhibition beyond the cancer context (Dumbacher et al., 2018).

Covalent inhibitors have experienced a renaissance in the past few years (Singh et al., 2011). Covalent inhibitors possess significant advantages including the fact that covalently reacting chemical warheads can target specific amino acid residues of a particular target protein, thus leading to the development of highly selective inhibitors (Singh et al., 2011, Aljoundi et al., 2020). Whilst the majority of rational covalent drug development efforts have focused on cysteine modifying small molecules, there is significant opportunity in the less explored area of lysine-modifying covalent inhibitor development (Singh et al., 2011). Our work with Calmirasone1 and OphA here exemplifies the potential applicability of a lysine modifying covalent inhibitor in oncology studies. Indeed, our novel covalent CaM inhibitor Calmirasone1 will add to the arsenal of covalent tool compounds to study CaM-associated cell biological processes specifically in unravelling the K-Ras/CaM associated stemness activity.

Developing effective anti-cancer agents not only requires new compounds but also the rational repurposing of already approved drugs for different diseases if they show significant anti-cancer benefits (Armando et al., 2020). Phenothiazines have been applied for the management of neurological conditions such as Schizophrenia for several decades and their safety for clinical applications is well documented. PTZs in addition to their neuroleptic effects have been reported to block cancers through the inhibition of CaM and PP2A activity (Hait et al., 1987, Gutierrez et al., 2014). Our findings in this thesis adds to the existing body of knowledge that these compounds possess relevant anti-cancer properties through multi-target engagement characteristics.

The following perspectives emerge from the results of this thesis:

- Building on our validation of the new design principle of PDE6D inhibitors, compounds with improved binding characteristics and resilience to Arl2-GTP unloading should be developed.

- To unravel the role of K-Ras in the emergence of cancer stem cells, the application of Calmirasone1 as a tool compound will be useful to aid the dissection of the role of K-Ras and CaM in cell fate determination.

- We have not fully studied the off-target activity of our CaM inhibitors, it is therefore plausible that CaM related proteins such as centrin-1, an EF-hand containing calcium binding protein with broad structural and functional similarity to CaM (Dantas et al., 2012), can also react with our compounds. Hence, the use of mass spectrometry to identify the full target-spectrum of our novel CaM inhibitor Calmirasone1 may be instructive in identifying any potential off-targets.

- In addition to being a cheaper option, another advantage of repurposing phenothiazines for oncology indications could be their already optimized chemistry for passage through the blood-brain barrier. Glioblastoma multiform (GBM) is a very aggressive form of brain cancer lacking sufficient beneficial therapeutic interventions (Shergalis et al., 2018). GBM is known to be reliant on Ras signaling in vivo (Holmen and Williams, 2005). Since the work of this thesis identifies a relationship between phenothiazine anti-cancer effects and Ras-MAPK dependence of cancers, it will be interesting to assess the activity of these compounds in GBM disease models.

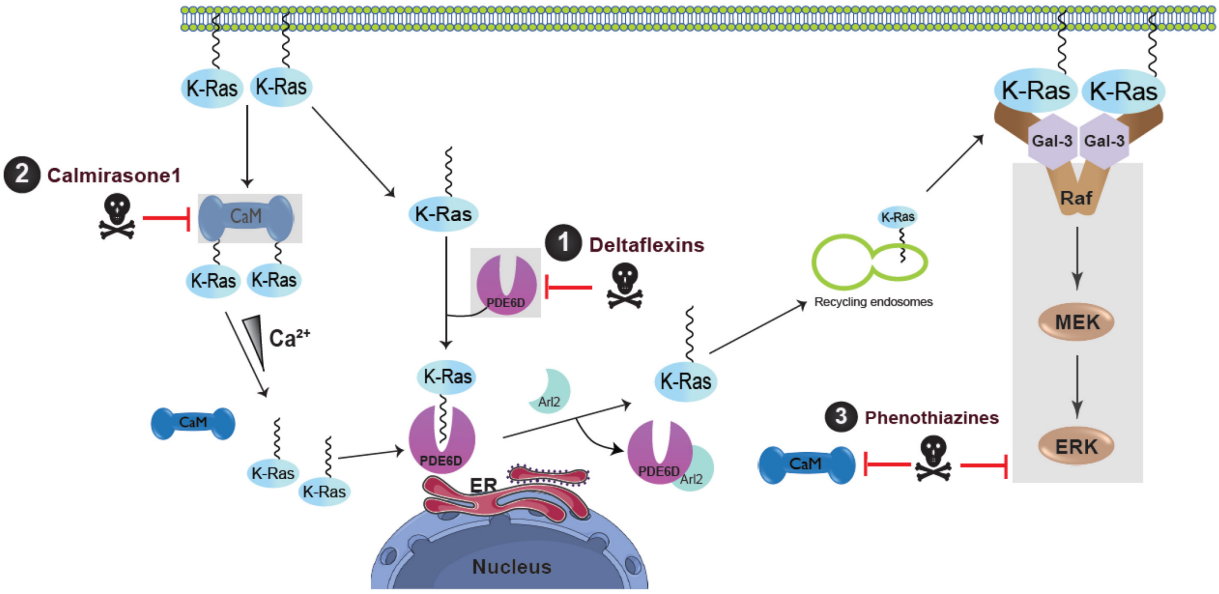

Figure 25. Schematic summary of thesis.

In this thesis, we developed and characterized novel covalent and non-covalent small molecules against K-Ras trafficking chaperones PDE6D (Deltaflexins) ***(1)*** *and CaM (Calmirasone1)* ***(2)****. Our results show that inhibiting these proteins more selectively interfered with K-Ras membrane localization and signaling. Similarly, we assessed the activity of phenothiazines which are reported CaM inhibitors and PP2A agonists* ***(3)*** *and show that these compounds decrease Ras-MAPK signaling output via a CaM and potentially PP2A dependent process.*

REFERENCES

7.0 References

ABANKWA, D. & GORFE, A. A. 2020. Mechanisms of Ras Membrane Organization and Signaling: Ras Rocks Again. *Biomolecules,* 10.

ABANKWA, D., GORFE, A. A. & HANCOCK, J. F. 2008a. Mechanisms of Ras membrane organization and signalling: Ras on a rocker. *Cell Cycle,* 7**,** 2667-73.

ABANKWA, D., GORFE, A. A., INDER, K. & HANCOCK, J. F. 2010. Ras membrane orientation and nanodomain localization generate isoform diversity. *Proc Natl Acad Sci U S A,* 107**,** 1130-5.

ABANKWA, D., HANZAL-BAYER, M., ARIOTTI, N., PLOWMAN, S. J., GORFE, A. A., PARTON, R. G., MCCAMMON, J. A. & HANCOCK, J. F. 2008b. A novel switch region regulates H-ras membrane orientation and signal output. *EMBO J,* 27**,** 727-35.

AGAMASU, C., GHIRLANDO, R., TAYLOR, T., MESSING, S., TRAN, T. H., BINDU, L., TONELLI, M., NISSLEY, D. V., MCCORMICK, F. & STEPHEN, A. G. 2019. KRAS Prenylation Is Required for Bivalent Binding with Calmodulin in a Nucleotide-Independent Manner. *Biophys J,* 116**,** 1049-1063.

AGARWAL, A., MACKENZIE, R. J., PIPPA, R., EIDE, C. A., ODDO, J., TYNER, J. W., SEARS, R., VITEK, M. P., ODERO, M. D., CHRISTENSEN, D. J. & DRUKER, B. J. 2014. Antagonism of SET using OP449 enhances the efficacy of tyrosine kinase inhibitors and overcomes drug resistance in myeloid leukemia. *Clin Cancer Res,* 20**,** 2092-103.

AHEARN, I., ZHOU, M. & PHILIPS, M. R. 2018. Posttranslational Modifications of RAS Proteins. *Cold Spring Harb Perspect Med,* 8.

AICH, A. & SHAHA, C. 2013. Novel role of calmodulin in regulating protein transport to mitochondria in a unicellular eukaryote. *Mol Cell Biol,* 33**,** 4579-93.

ALGAZI, A. P., ROTOW, J., POSCH, C., ORTIZ-URDA, S., PELAYO, A., MUNSTER, P. N. & DAUD, A. 2019. A dual pathway inhibition strategy using BKM120 combined with vemurafenib is poorly tolerated in BRAF V600(E/K) mutant advanced melanoma. *Pigment Cell Melanoma Res,* 32**,** 603-606.

ALJOUNDI, A., BJIJ, I., EL RASHEDY, A. & SOLIMAN, M. E. S. 2020. Covalent Versus Non-covalent Enzyme Inhibition: Which Route Should We Take? A Justification of the Good and Bad from Molecular Modelling Perspective. *Protein J,* 39**,** 97-105.

ALVAREZ-MOYA, B., LOPEZ-ALCALA, C., DROSTEN, M., BACHS, O. & AGELL, N. 2010. K-Ras4B phosphorylation at Ser181 is inhibited by calmodulin and modulates K-Ras activity and function. *Oncogene,* 29**,** 5911-22.

AMGEN 2021. FDA Approves LUMAKRAS™ (Sotorasib), The First And Only Targeted Treatment For Patients With KRAS G12C-Mutated Locally Advanced Or Metastatic Non-Small Cell Lung Cancer.

AOKI, Y., NIIHORI, T., INOUE, S. & MATSUBARA, Y. 2016. Recent advances in RASopathies. *J Hum Genet,* 61**,** 33-9.

APOLLONI, A., PRIOR, I. A., LINDSAY, M., PARTON, R. G. & HANCOCK, J. F. 2000. H-ras but not K-ras traffics to the plasma membrane through the exocytic pathway. *Mol Cell Biol,* 20**,** 2475-87.

ARMANDO, R. G., MENGUAL GOMEZ, D. L. & GOMEZ, D. E. 2020. New drugs are not enoughdrug repositioning in oncology: An update. *Int J Oncol,* 56**,** 651-684.

BACART, J., CORBEL, C., JOCKERS, R., BACH, S. & COUTURIER, C. 2008. The BRET technology and its application to screening assays. *Biotechnol J,* 3**,** 311-24.

BAKER, R., WILKERSON, E. M., SUMITA, K., ISOM, D. G., SASAKI, A. T., DOHLMAN, H. G. & CAMPBELL, S. L. 2013. Differences in the regulation of K-Ras and H-Ras isoforms by monoubiquitination. *J Biol Chem,* 288**,** 36856-62.

BARNETTE, M. S., DALY, R. & WEISS, B. 1983. Inhibition of calmodulin activity by insect venom peptides. *Biochem Pharmacol,* 32**,** 2929-33.

BATLLE, E. & CLEVERS, H. 2017. Cancer stem cells revisited. *Nat Med,* 23**,** 1124-1134.

BENAIM, G. & VILLALOBO, A. 2002. Phosphorylation of calmodulin. Functional implications. *Eur J Biochem,* 269**,** 3619-31.

BENDER, R. H., HAIGIS, K. M. & GUTMANN, D. H. 2015. Activated k-ras, but not h-ras or N-ras, regulates brain neural stem cell proliferation in a raf/rb-dependent manner. *Stem Cells,* 33**,** 1998-2010.

BERCHTOLD, M. W. & VILLALOBO, A. 2014. The many faces of calmodulin in cell proliferation, programmed cell death, autophagy, and cancer. *Biochim Biophys Acta,* 1843**,** 398-435.

BERY, N., CRUZ-MIGONI, A., BATAILLE, C. J., QUEVEDO, C. E., TULMIN, H., MILLER, A., RUSSELL, A., PHILLIPS, S. E., CARR, S. B. & RABBITTS, T. H. 2018. BRET-based RAS biosensors that show a novel small molecule is an inhibitor of RAS-effector protein-protein interactions. *Elife,* 7.

BERY, N. & RABBITTS, T. H. 2019. Bioluminescence Resonance Energy Transfer 2 (BRET2)-Based RAS Biosensors to Characterize RAS Inhibitors. *Curr Protoc Cell Biol,* 83**,** e83.

BIOSPACE. 2021. Amgen Moves One Step Closer to First Approved KRAS Inhibitor for Lung Cancer.

BIVONA, T. G., QUATELA, S. E., BODEMANN, B. O., AHEARN, I. M., SOSKIS, M. J., MOR, A., MIURA, J., WIENER, H. H., WRIGHT, L., SABA, S. G., YIM, D., FEIN, A., PEREZ DE CASTRO, I., LI, C., THOMPSON, C. B., COX, A. D. & PHILIPS, M. R. 2006. PKC regulates a farnesyl-electrostatic switch on K-Ras that promotes its association with Bcl-XL on mitochondria and induces apoptosis. *Mol Cell,* 21**,** 481-93.

BLACK, E. W., STRADA, S. J., GARRETT, R. L., JR., KVIETYS, P. R., THOMPSON, W. J. & NORMAN, J. A. 1989. Inhibition of gastric acid secretion in vivo and in vitro by a new calmodulin antagonist, CGS 9343B. *J Pharmacol Exp Ther,* 248**,** 208-14.

BLAIR, K., WRAY, J. & SMITH, A. 2011. The liberation of embryonic stem cells. *PLoS Genet,* 7**,** e1002019.

BLAZEVITS, O., MIDEKSA, Y. G., SOLMAN, M., LIGABUE, A., ARIOTTI, N., NAKHAEIZADEH, H., FANSA, E. K., PAPAGEORGIOU, A. C., WITTINGHOFER, A., AHMADIAN, M. R. & ABANKWA, D. 2016. Galectin-1 dimers can scaffold Raf-effectors to increase H-ras nanoclustering. *Sci Rep,* 6**,** 24165.

BLISS, C. I. 1939. The toxicity of poisons applied jointly. *Annals of Applied Biology*.

BLONS, H., EMILE, J. F., LE MALICOT, K., JULIE, C., ZAANAN, A., TABERNERO, J., MINI, E., FOLPRECHT, G., VAN LAETHEM, J. L., THALER, J., BRIDGEWATER, J., NORGARD-PETERSEN, L., VAN CUTSEM, E., LEPAGE, C., ZAWADI, M. A., SALAZAR, R., LAURENT-PUIG, P. & TAIEB, J. 2014. Prognostic value of KRAS mutations in stage III colon cancer: post hoc analysis of the PETACC8 phase III trial dataset. *Ann Oncol,* 25**,** 2378-2385.

BLUMENSCHEIN, G. R., JR., SMIT, E. F., PLANCHARD, D., KIM, D. W., CADRANEL, J., DE PAS, T., DUNPHY, F., UDUD, K., AHN, M. J., HANNA, N. H., KIM, J. H., MAZIERES, J., KIM, S. W., BAAS, P., RAPPOLD, E., REDHU, S., PUSKI, A., WU, F. S. & JANNE, P. A. 2015. A randomized phase II study of the MEK1/MEK2 inhibitor trametinib (GSK1120212) compared with docetaxel in KRAS-mutant advanced non-small-cell lung cancer (NSCLC)dagger. *Ann Oncol,* 26**,** 894-901.

BOSWELL-SMITH, V., SPINA, D. & PAGE, C. P. 2006. Phosphodiesterase inhibitors. *Br J Pharmacol,* 147 Suppl 1**,** S252-7.

BOURNE, H. R., SANDERS, D. A. & MCCORMICK, F. 1991. The GTPase superfamily: conserved structure and molecular mechanism. *Nature,* 349**,** 117-27.

BOURNET, B., MUSCARI, F., BUSCAIL, C., ASSENAT, E., BARTHET, M., HAMMEL, P., SELVES, J., GUIMBAUD, R., CORDELIER, P. & BUSCAIL, L. 2016. KRAS G12D

Mutation Subtype Is A Prognostic Factor for Advanced Pancreatic Adenocarcinoma. *Clin Transl Gastroenterol,* 7**,** e157.

BOUTE, N., JOCKERS, R. & ISSAD, T. 2002. The use of resonance energy transfer in high-throughput screening: BRET versus FRET. *Trends Pharmacol Sci,* 23**,** 351-4.

BOYARTCHUK, V. L., ASHBY, M. N. & RINE, J. 1997. Modulation of Ras and a-factor function by carboxyl-terminal proteolysis. *Science,* 275**,** 1796-800.

BREITHOLTZ, M., IVANOV, P., EK, K. & GOROKHOVA, E. 2020. Calmodulin inhibition as a mode of action of antifungal imidazole pharmaceuticals in non-target organisms. *Toxicol Res (Camb),* 9**,** 425-430.

BREMS, H., CHMARA, M., SAHBATOU, M., DENAYER, E., TANIGUCHI, K., KATO, R., SOMERS, R., MESSIAEN, L., DE SCHEPPER, S., FRYNS, J. P., COOLS, J., MARYNEN, P., THOMAS, G., YOSHIMURA, A. & LEGIUS, E. 2007. Germline loss-of-function mutations in SPRED1 cause a neurofibromatosis 1-like phenotype. *Nat Genet,* 39**,** 1120-6.

BUNDA, S., HEIR, P., SRIKUMAR, T., COOK, J. D., BURRELL, K., KANO, Y., LEE, J. E., ZADEH, G., RAUGHT, B. & OHH, M. 2014. Src promotes GTPase activity of Ras via tyrosine 32 phosphorylation. *Proc Natl Acad Sci U S A,* 111**,** E3785-94.

CAI, W. Q., ZENG, L. S., WANG, L. F., WANG, Y. Y., CHENG, J. T., ZHANG, Y., HAN, Z. W., ZHOU, Y., HUANG, S. L., WANG, X. W., PENG, X. C., XIANG, Y., MA, Z., CUI, S. Z. & XIN, H. W. 2020. The Latest Battles Between EGFR Monoclonal Antibodies and Resistant Tumor Cells. *Front Oncol,* 10**,** 1249.

CANCER GENOME ATLAS, N. 2015a. Comprehensive genomic characterization of head and neck squamous cell carcinomas. *Nature,* 517**,** 576-82.

CANCER GENOME ATLAS, N. 2015b. Genomic Classification of Cutaneous Melanoma. *Cell,* 161**,** 1681-96.

CANON, J., REX, K., SAIKI, A. Y., MOHR, C., COOKE, K., BAGAL, D., GAIDA, K., HOLT, T., KNUTSON, C. G., KOPPADA, N., LANMAN, B. A., WERNER, J., RAPAPORT, A. S., SAN MIGUEL, T., ORTIZ, R., OSGOOD, T., SUN, J. R., ZHU, X., MCCARTER, J. D., VOLAK, L. P., HOUK, B. E., FAKIH, M. G., O'NEIL, B. H., PRICE, T. J., FALCHOOK, G. S., DESAI, J., KUO, J., GOVINDAN, R., HONG, D. S., OUYANG, W., HENARY, H., ARVEDSON, T., CEE, V. J. & LIPFORD, J. R. 2019. The clinical KRAS(G12C) inhibitor AMG 510 drives anti-tumour immunity. *Nature,* 575**,** 217-223.

CAPIOD, T. 2013. The need for calcium channels in cell proliferation. *Recent Pat Anticancer Drug Discov,* 8**,** 4-17.

CASTELLANO, E. & DOWNWARD, J. 2011. RAS Interaction with PI3K: More Than Just Another Effector Pathway. *Genes Cancer,* 2**,** 261-74.

CHANDRA, A., GRECCO, H. E., PISUPATI, V., PERERA, D., CASSIDY, L., SKOULIDIS, F., ISMAIL, S. A., HEDBERG, C., HANZAL-BAYER, M., VENKITARAMAN, A. R., WITTINGHOFER, A. & BASTIAENS, P. I. 2011. The GDI-like solubilizing factor PDEdelta sustains the spatial organization and signalling of Ras family proteins. *Nat Cell Biol,* 14**,** 148-58.

CHEN, J., LI, Y., YU, T. S., MCKAY, R. M., BURNS, D. K., KERNIE, S. G. & PARADA, L. F. 2012. A restricted cell population propagates glioblastoma growth after chemotherapy. *Nature,* 488**,** 522-6.

CHIDLEY, C., TRAUGER, S. A., BIRSOY, K. & O'SHEA, E. K. 2016. The anticancer natural product ophiobolin A induces cytotoxicity by covalent modification of phosphatidylethanolamine. *Elife,* 5**,** e14601.

CHIEN, Y., KIM, S., BUMEISTER, R., LOO, Y. M., KWON, S. W., JOHNSON, C. L., BALAKIREVA, M. G., ROMEO, Y., KOPELOVICH, L., GALE, M., JR., YEAMAN, C., CAMONIS, J. H., ZHAO, Y. & WHITE, M. A. 2006. RalB GTPase-mediated activation of

the IkappaB family kinase TBK1 couples innate immune signaling to tumor cell survival. *Cell,* 127**,** 157-70.

CHIPPALKATTI, R. & ABANKWA, D. 2021. Promotion of cancer cell stemness by Ras. *Biochem Soc Trans,* 49**,** 467-476.

CHOI, J., CHIANG, A., TAULIER, N., GROS, R., PIRANI, A. & HUSAIN, M. 2006. A calmodulin-binding site on cyclin E mediates Ca2+-sensitive G1/s transitions in vascular smooth muscle cells. *Circ Res,* 98**,** 1273-81.

CHONG, H. & GUAN, K. L. 2003. Regulation of Raf through phosphorylation and N terminus-C terminus interaction. *J Biol Chem,* 278**,** 36269-76.

CHOU, J. J., LI, S., KLEE, C. B. & BAX, A. 2001. Solution structure of Ca(2+)-calmodulin reveals flexible hand-like properties of its domains. *Nat Struct Biol,* 8**,** 990-7.

CICALESE, A., BONIZZI, G., PASI, C. E., FARETTA, M., RONZONI, S., GIULINI, B., BRISKEN, C., MINUCCI, S., DI FIORE, P. P. & PELICCI, P. G. 2009. The tumor suppressor p53 regulates polarity of self-renewing divisions in mammary stem cells. *Cell,* 138**,** 1083-95.

CIMINO, P. J. & GUTMANN, D. H. 2018. Neurofibromatosis type 1. *Handb Clin Neurol,* 148**,** 799-811.

CLAING, A. 2013. beta-Arrestins: modulators of small GTPase activation and function. *Prog Mol Biol Transl Sci,* 118**,** 149-74.

CLARK, A. R. & OHLMEYER, M. 2019. Protein phosphatase 2A as a therapeutic target in inflammation and neurodegeneration. *Pharmacol Ther,* 201**,** 181-201.

CORDEDDU, V., DI SCHIAVI, E., PENNACCHIO, L. A., MA'AYAN, A., SARKOZY, A., FODALE, V., CECCHETTI, S., CARDINALE, A., MARTIN, J., SCHACKWITZ, W., LIPZEN, A., ZAMPINO, G., MAZZANTI, L., DIGILIO, M. C., MARTINELLI, S., FLEX, E., LEPRI, F., BARTHOLDI, D., KUTSCHE, K., FERRERO, G. B., ANICHINI, C., SELICORNI, A., ROSSI, C., TENCONI, R., ZENKER, M., MERLO, D., DALLAPICCOLA, B., IYENGAR, R., BAZZICALUPO, P., GELB, B. D. & TARTAGLIA, M. 2009. Mutation of SHOC2 promotes aberrant protein N-myristoylation and causes Noonan-like syndrome with loose anagen hair. *Nat Genet,* 41**,** 1022-6.

CORNU, M., ALBERT, V. & HALL, M. N. 2013. mTOR in aging, metabolism, and cancer. *Curr Opin Genet Dev,* 23**,** 53-62.

COX, J. A. 1988. Interactive properties of calmodulin. *Biochem J,* 249**,** 621-9.

CRISTOBAL, I., GARCIA-ORTI, L., CIRAUQUI, C., CORTES-LAVAUD, X., GARCIA-SANCHEZ, M. A., CALASANZ, M. J. & ODERO, M. D. 2012. Overexpression of SET is a recurrent event associated with poor outcome and contributes to protein phosphatase 2A inhibition in acute myeloid leukemia. *Haematologica,* 97**,** 543-50.

CRISTOBAL, I., GONZALEZ-ALONSO, P., DAOUD, L., SOLANO, E., TORREJON, B., MANSO, R., MADOZ-GURPIDE, J., ROJO, F. & GARCIA-FONCILLAS, J. 2015. Activation of the Tumor Suppressor PP2A Emerges as a Potential Therapeutic Strategy for Treating Prostate Cancer. *Mar Drugs,* 13**,** 3276-86.

CRIVICI, A. & IKURA, M. 1995. Molecular and structural basis of target recognition by calmodulin. *Annu Rev Biophys Biomol Struct,* 24**,** 85-116.

CUESTA, A. & TAUNTON, J. 2019. Lysine-Targeted Inhibitors and Chemoproteomic Probes. *Annu Rev Biochem,* 88**,** 365-381.

DALE, N. C., JOHNSTONE, E. K. M., WHITE, C. W. & PFLEGER, K. D. G. 2019. NanoBRET: The Bright Future of Proximity-Based Assays. *Front Bioeng Biotechnol,* 7**,** 56.

DANTAS, T. J., DALY, O. M. & MORRISON, C. G. 2012. Such small hands: the roles of centrins/caltractins in the centriole and in genome maintenance. *Cell Mol Life Sci,* 69**,** 2979-97.

DE, A., LOENING, A. M. & GAMBHIR, S. S. 2007. An improved bioluminescence resonance energy transfer strategy for imaging intracellular events in single cells and living subjects. *Cancer Res,* 67**,** 7175-83.

DE RUITER, N. D., WOLTHUIS, R. M., VAN DAM, H., BURGERING, B. M. & BOS, J. L. 2000. Ras-dependent regulation of c-Jun phosphorylation is mediated by the Ral guanine nucleotide exchange factor-Ral pathway. *Mol Cell Biol,* 20**,** 8480-8.

DEWHURST, L. O., GEE, J. W., RENNIE, I. G. & MACNEIL, S. 1997. Tamoxifen, 17beta-oestradiol and the calmodulin antagonist J8 inhibit human melanoma cell invasion through fibronectin. *Br J Cancer,* 75**,** 860-8.

DHARMAIAH, S., BINDU, L., TRAN, T. H., GILLETTE, W. K., FRANK, P. H., GHIRLANDO, R., NISSLEY, D. V., ESPOSITO, D., MCCORMICK, F., STEPHEN, A. G. & SIMANSHU, D. K. 2016. Structural basis of recognition of farnesylated and methylated KRAS4b by PDEdelta. *Proc Natl Acad Sci U S A,* 113**,** E6766-E6775.

DIETRICH, P., HELLERBRAND, C. & BOSSERHOFF, A. 2019. The Delta Subunit of Rod-Specific Photoreceptor cGMP Phosphodiesterase (PDE6D) Contributes to Hepatocellular Carcinoma Progression. *Cancers (Basel),* 11.

DONALDSON, J. G. & JACKSON, C. L. 2011. ARF family G proteins and their regulators: roles in membrane transport, development and disease. *Nat Rev Mol Cell Biol,* 12**,** 362-75.

DONG, H., CLAFFEY, K. P., BROCKE, S. & EPSTEIN, P. M. 2013. Expression of phosphodiesterase 6 (PDE6) in human breast cancer cells. *Springerplus,* 2**,** 680.

DOWNWARD, J. 2003. Targeting RAS signalling pathways in cancer therapy. *Nat Rev Cancer,* 3**,** 11-22.

DUAN, J., ZHAN, J. C., WANG, G. Z., ZHAO, X. C., HUANG, W. D. & ZHOU, G. B. 2019. The red wine component ellagic acid induces autophagy and exhibits anti-lung cancer activity in vitro and in vivo. *J Cell Mol Med,* 23**,** 143-154.

DUMBACHER, M., VAN DOOREN, T., PRINCEN, K., DE WITTE, K., FARINELLI, M., LIEVENS, S., TAVERNIER, J., DEHAEN, W., WERA, S., WINDERICKX, J., ALLASIA, S., KILONDA, A., SPIESER, S., MARCHAND, A., CHALTIN, P., HOOGENRAAD, C. C. & GRIFFIOEN, G. 2018. Modifying Rap1-signalling by targeting Pde6delta is neuroprotective in models of Alzheimer's disease. *Mol Neurodegener,* 13**,** 50.

DUNNETT-KANE, V., NICOLA, P., BLACKHALL, F. & LINDSAY, C. 2021. Mechanisms of Resistance to KRAS(G12C) Inhibitors. *Cancers (Basel),* 13.

DURONIO, V. 2008. The life of a cell: apoptosis regulation by the PI3K/PKB pathway. *Biochem J,* 415**,** 333-44.

EEROLA, I., BOON, L. M., MULLIKEN, J. B., BURROWS, P. E., DOMPMARTIN, A., WATANABE, S., VANWIJCK, R. & VIKKULA, M. 2003. Capillary malformation-arteriovenous malformation, a new clinical and genetic disorder caused by RASA1 mutations. *Am J Hum Genet,* 73**,** 1240-9.

EICHHORN, P. J., CREYGHTON, M. P. & BERNARDS, R. 2009. Protein phosphatase 2A regulatory subunits and cancer. *Biochim Biophys Acta,* 1795**,** 1-15.

EL BOUCHIKHI, I., BELHASSAN, K., MOUFID, F. Z., IRAQUI HOUSSAINI, M., BOUGUENOUCH, L., SAMRI, I., ATMANI, S. & OULDIM, K. 2016. Noonan syndrome-causing genes: Molecular update and an assessment of the mutation rate. *Int J Pediatr Adolesc Med,* 3**,** 133-142.

EL KHAMLICHI, C., REVERCHON-ASSADI, F., HERVOUET-COSTE, N., BLOT, L., REITER, E. & MORISSET-LOPEZ, S. 2019. Bioluminescence Resonance Energy Transfer as a Method to Study Protein-Protein Interactions: Application to G Protein Coupled Receptor Biology. *Molecules,* 24.

ENGELMAN, J. A., LUO, J. & CANTLEY, L. C. 2006. The evolution of phosphatidylinositol 3-kinases as regulators of growth and metabolism. *Nat Rev Genet,* 7**,** 606-19.

ETIENNE-MANNEVILLE, S. & HALL, A. 2002. Rho GTPases in cell biology. *Nature,* 420**,** 629-35.

FANSA, E. K., KOSLING, S. K., ZENT, E., WITTINGHOFER, A. & ISMAIL, S. 2016. PDE6delta-mediated sorting of INPP5E into the cilium is determined by cargo-carrier affinity. *Nat Commun,* 7**,** 11366.

FAUST, F. M., SLISZ, M. & JARRETT, H. W. 1987. Calmodulin is labeled at lysine 148 by a chemically reactive phenothiazine. *The Journal of biological chemistry,* 262**,** 1938-1941.

FIVAZ, M. & MEYER, T. 2005. Reversible intracellular translocation of KRas but not HRas in hippocampal neurons regulated by Ca2+/calmodulin. *J Cell Biol,* 170**,** 429-41.

FRANKFURT, O. S., SUGARBAKER, E. V., ROBB, J. A. & VILLA, L. 1995. Synergistic induction of apoptosis in breast cancer cells by tamoxifen and calmodulin inhibitors. *Cancer Lett,* 97**,** 149-54.

FRUMAN, D. A., CHIU, H., HOPKINS, B. D., BAGRODIA, S., CANTLEY, L. C. & ABRAHAM, R. T. 2017. The PI3K Pathway in Human Disease. *Cell,* 170**,** 605-635.

GELABERT-BALDRICH, M., SORIANO-CASTELL, D., CALVO, M., LU, A., VINA-VILASECA, A., RENTERO, C., POL, A., GRINSTEIN, S., ENRICH, C. & TEBAR, F. 2014. Dynamics of KRas on endosomes: involvement of acidic phospholipids in its association. *FASEB J,* 28**,** 3023-37.

GENTILE, D. R., RATHINASWAMY, M. K., JENKINS, M. L., MOSS, S. M., SIEMPELKAMP, B. D., RENSLO, A. R., BURKE, J. E. & SHOKAT, K. M. 2017. Ras Binder Induces a Modified Switch-II Pocket in GTP and GDP States. *Cell Chem Biol,* 24**,** 1455-1466 e14.

GILARDI, M., WANG, Z., PROIETTO, M., CHILLA, A., CALLEJA-VALERA, J. L., GOTO, Y., VANONI, M., JANES, M. R., MIKULSKI, Z., GUALBERTO, A., MOLINOLO, A. A., FERRARA, N., GUTKIND, J. S. & BURROWS, F. 2020. Tipifarnib as a Precision Therapy for HRAS-Mutant Head and Neck Squamous Cell Carcinomas. *Mol Cancer Ther,* 19**,** 1784-1796.

GOI, T., SHIPITSIN, M., LU, Z., FOSTER, D. A., KLINZ, S. G. & FEIG, L. A. 2000. An EGF receptor/Ral-GTPase signaling cascade regulates c-Src activity and substrate specificity. *EMBO J,* 19**,** 623-30.

GRABSKI, R., DEWIT, J., DE BRAEKELEER, J., MALICKA-BLASKIEWICZ, M., DE BAETSELIER, P. & VERSCHUEREN, H. 2001. Inhibition of T-cell invasion across cultured fibroblast monolayers by phenothiazine-related calmodulin inhibitors: impairment of lymphocyte motility by trifluoperazine and chlorpromazine, and alteration of the monolayer by pimozide. *Biochem Pharmacol,* 61**,** 1313-7.

GRANT, B. M. M., ENOMOTO, M., BACK, S. I., LEE, K. Y., GEBREGIWORGIS, T., ISHIYAMA, N., IKURA, M. & MARSHALL, C. B. 2020a. Calmodulin disrupts plasma membrane localization of farnesylated KRAS4b by sequestering its lipid moiety. *Sci Signal,* 13.

GRANT, B. M. M., ENOMOTO, M., BACK, S. I., LEE, K. Y., GEBREGIWORGIS, T., ISHIYAMA, N., IKURA, M. & MARSHALL, C. B. 2020b. Calmodulin disrupts plasma membrane localization of farnesylated KRAS4b by sequestering its lipid moiety. *Sci Signal,* 13**,** eaaz0344.

GRANT, B. M. M., ENOMOTO, M., IKURA, M. & MARSHALL, C. B. 2020c. A Non-Canonical Calmodulin Target Motif Comprising a Polybasic Region and Lipidated Terminal Residue Regulates Localization. *Int J Mol Sci,* 21.

GU, D., SCHLOTMAN, K. E. & XIE, J. 2016. Deciphering the role of hedgehog signaling in pancreatic cancer. *J Biomed Res,* 30**,** 353-360.

GUEN, V. J., CHAVARRIA, T. E., KROGER, C., YE, X., WEINBERG, R. A. & LEES, J. A. 2017. EMT programs promote basal mammary stem cell and tumor-initiating cell stemness by inducing primary ciliogenesis and Hedgehog signaling. *Proc Natl Acad Sci U S A,* 114**,** E10532-E10539.

GUO, Y. J., PAN, W. W., LIU, S. B., SHEN, Z. F., XU, Y. & HU, L. L. 2020. ERK/MAPK signalling pathway and tumorigenesis. *Exp Ther Med,* 19**,** 1997-2007.

GUTIERREZ, A., PAN, L., GROEN, R. W., BALEYDIER, F., KENTSIS, A., MARINEAU, J., GREBLIUNAITE, R., KOZAKEWICH, E., REED, C., PFLUMIO, F., POGLIO, S., UZAN, B., CLEMONS, P., VERPLANK, L., AN, F., BURBANK, J., NORTON, S., TOLLIDAY, N., STEEN, H., WENG, A. P., YUAN, H., BRADNER, J. E., MITSIADES, C., LOOK, A. T. & ASTER, J. C. 2014. Phenothiazines induce PP2A-mediated apoptosis in T cell acute lymphoblastic leukemia. *J Clin Invest,* 124**,** 644-55.

GUTIERREZ, L., MAGEE, A. I., MARSHALL, C. J. & HANCOCK, J. F. 1989. Post-translational processing of p21ras is two-step and involves carboxyl-methylation and carboxy-terminal proteolysis. *EMBO J,* 8**,** 1093-8.

HAIT, W. N., GLAZER, L., KAISER, C., CROSS, J. & KENNEDY, K. A. 1987. Pharmacological properties of fluphenazine-mustard, an irreversible calmodulin antagonist. *Mol Pharmacol,* 32**,** 404-9.

HALL, A. 1998. Rho GTPases and the actin cytoskeleton. *Science,* 279**,** 509-14.

HAMDAN, F. F., PERCHERANCIER, Y., BRETON, B. & BOUVIER, M. 2006. Monitoring protein-protein interactions in living cells by bioluminescence resonance energy transfer (BRET). *Curr Protoc Neurosci,* Chapter 5**,** Unit 5 23.

HANAHAN, D. & WEINBERG, R. A. 2011. Hallmarks of cancer: the next generation. *Cell,* 144**,** 646-74.

HANCOCK, J. F., PATERSON, H. & MARSHALL, C. J. 1990. A polybasic domain or palmitoylation is required in addition to the CAAX motif to localize p21ras to the plasma membrane. *Cell,* 63**,** 133-9.

HARRIS, J., OLIERE, S., SHARMA, S., SUN, Q., LIN, R., HISCOTT, J. & GRANDVAUX, N. 2006. Nuclear accumulation of cRel following C-terminal phosphorylation by TBK1/IKK epsilon. *J Immunol,* 177**,** 2527-35.

HARTLEY, D. & COOPER, G. M. 2002. Role of mTOR in the degradation of IRS-1: regulation of PP2A activity. *J Cell Biochem,* 85**,** 304-14.

HATZIVASSILIOU, G., HALING, J. R., CHEN, H., SONG, K., PRICE, S., HEALD, R., HEWITT, J. F., ZAK, M., PECK, A., ORR, C., MERCHANT, M., HOEFLICH, K. P., CHAN, J., LUOH, S. M., ANDERSON, D. J., LUDLAM, M. J., WIESMANN, C., ULTSCH, M., FRIEDMAN, L. S., MALEK, S. & BELVIN, M. 2013. Mechanism of MEK inhibition determines efficacy in mutant KRAS- versus BRAF-driven cancers. *Nature,* 501**,** 232-6.

HEALIO. 2021. FDA grants priority review to sotorasib for lung cancer subset.

HEGEMANN, L., TOSO, S. M., LAHIJANI, K. I., WEBSTER, G. F. & UITTO, J. 1993. Direct interaction of antifungal azole-derivatives with calmodulin: a possible mechanism for their therapeutic activity. *J Invest Dermatol,* 100**,** 343-6.

HELLMANN, M. D., KIM, T. W., LEE, C. B., GOH, B. C., MILLER, W. H., JR., OH, D. Y., JAMAL, R., CHEE, C. E., CHOW, L. Q. M., GAINOR, J. F., DESAI, J., SOLOMON, B. J., DAS THAKUR, M., PITCHER, B., FOSTER, P., HERNANDEZ, G., WONGCHENKO, M. J., CHA, E., BANG, Y. J., SIU, L. L. & BENDELL, J. 2019. Phase Ib study of atezolizumab combined with cobimetinib in patients with solid tumors. *Ann Oncol,* 30**,** 1134-1142.

HENNIG, A., MARKWART, R., ESPARZA-FRANCO, M. A., LADDS, G. & RUBIO, I. 2015. Ras activation revisited: role of GEF and GAP systems. *Biol Chem,* 396**,** 831-48.

HENRY, D. O., MOSKALENKO, S. A., KAUR, K. J., FU, M., PESTELL, R. G., CAMONIS, J. H. & WHITE, M. A. 2000. Ral GTPases contribute to regulation of cyclin D1 through activation of NF-kappaB. *Mol Cell Biol,* 20**,** 8084-92.

HERRMANN, C., AHMADIAN, M. R., HOFMANN, F. & JUST, I. 1998. Functional consequences of monoglucosylation of Ha-Ras at effector domain amino acid threonine 35. *J Biol Chem,* 273**,** 16134-9.

HIDAKA, H., SASAKI, Y., TANAKA, T., ENDO, T., OHNO, S., FUJII, Y. & NAGATA, T. 1981. N-(6-aminohexyl)-5-chloro-1-naphthalenesulfonamide, a calmodulin antagonist, inhibits cell proliferation. *Proc Natl Acad Sci U S A,* 78**,** 4354-7.

HILCHIE, A. L., SHARON, A. J., HANEY, E. F., HOSKIN, D. W., BALLY, M. B., FRANCO, O. L., CORCORAN, J. A. & HANCOCK, R. E. W. 2016. Mastoparan is a membranolytic anti-cancer peptide that works synergistically with gemcitabine in a mouse model of mammary carcinoma. *Biochim Biophys Acta,* 1858**,** 3195-3204.

HILLIG, R. C., SAUTIER, B., SCHROEDER, J., MOOSMAYER, D., HILPMANN, A., STEGMANN, C. M., WERBECK, N. D., BRIEM, H., BOEMER, U., WEISKE, J., BADOCK, V., MASTOURI, J., PETERSEN, K., SIEMEISTER, G., KAHMANN, J. D., WEGENER, D., BOHNKE, N., EIS, K., GRAHAM, K., WORTMANN, L., VON NUSSBAUM, F. & BADER, B. 2019. Discovery of potent SOS1 inhibitors that block RAS activation via disruption of the RAS-SOS1 interaction. *Proc Natl Acad Sci U S A,* 116**,** 2551-2560.

HOBBS, G. A., DER, C. J. & ROSSMAN, K. L. 2016. RAS isoforms and mutations in cancer at a glance. *J Cell Sci,* 129**,** 1287-92.

HOLDERFIELD, M., DEUKER, M. M., MCCORMICK, F. & MCMAHON, M. 2014. Targeting RAF kinases for cancer therapy: BRAF-mutated melanoma and beyond. *Nat Rev Cancer,* 14**,** 455-67.

HOLMEN, S. L. & WILLIAMS, B. O. 2005. Essential role for Ras signaling in glioblastoma maintenance. *Cancer Res,* 65**,** 8250-5.

HONG, D. S., FAKIH, M. G., STRICKLER, J. H., DESAI, J., DURM, G. A., SHAPIRO, G. I., FALCHOOK, G. S., PRICE, T. J., SACHER, A., DENLINGER, C. S., BANG, Y. J., DY, G. K., KRAUSS, J. C., KUBOKI, Y., KUO, J. C., COVELER, A. L., PARK, K., KIM, T. W., BARLESI, F., MUNSTER, P. N., RAMALINGAM, S. S., BURNS, T. F., MERIC-BERNSTAM, F., HENARY, H., NGANG, J., NGARMCHAMNANRITH, G., KIM, J., HOUK, B. E., CANON, J., LIPFORD, J. R., FRIBERG, G., LITO, P., GOVINDAN, R. & LI, B. T. 2020. KRAS(G12C) Inhibition with Sotorasib in Advanced Solid Tumors. *N Engl J Med,* 383**,** 1207-1217.

HU, Z. Y., GONG, Y. S. & HUANG, W. L. 1992. Interaction of berbamine compound E6 and calmodulin-dependent myosin light chain kinase. *Biochem Pharmacol,* 44**,** 1543-7.

HUANG, C., LAN, W., FRAUNHOFFER, N., MEILERMAN, A., IOVANNA, J. & SANTOFIMIA-CASTANO, P. 2019. Dissecting the Anticancer Mechanism of Trifluoperazine on Pancreatic Ductal Adenocarcinoma. *Cancers (Basel),* 11.

HUANG, J., MENG, L., YANG, B., SUN, S., LUO, Z. & CHEN, H. 2020. Safety Profile of Epidermal Growth Factor Receptor Tyrosine Kinase Inhibitors: A Disproportionality Analysis of FDA Adverse Event Reporting System. *Sci Rep,* 10**,** 4803.

HUMBERT, M. C., WEIHBRECHT, K., SEARBY, C. C., LI, Y., POPE, R. M., SHEFFIELD, V. C. & SEO, S. 2012. ARL13B, PDE6D, and CEP164 form a functional network for INPP5E ciliary targeting. *Proc Natl Acad Sci U S A,* 109**,** 19691-6.

HUNTER, J. C., MANANDHAR, A., CARRASCO, M. A., GURBANI, D., GONDI, S. & WESTOVER, K. D. 2015. Biochemical and Structural Analysis of Common Cancer-Associated KRAS Mutations. *Mol Cancer Res,* 13**,** 1325-35.

HWANG, J. H., YOON, J., CHO, Y. H., CHA, P. H., PARK, J. C. & CHOI, K. Y. 2020. A mutant KRAS-induced factor REG4 promotes cancer stem cell properties via Wnt/beta-catenin signaling. *Int J Cancer,* 146**,** 2877-2890.

HWANG, M. K., MIN, Y. K. & KIM, S. H. 2009. Calmodulin inhibition contributes to sensitize TRAIL-induced apoptosis in human lung cancer H1299 cells. *Biochem Cell Biol,* 87**,** 919-26.

IANEVSKI, A., GIRI, A. K. & AITTOKALLIO, T. 2020. SynergyFinder 2.0: visual analytics of multi-drug combination synergies. *Nucleic Acids Res,* 48**,** W488-W493.

ISMAIL, S. A., CHEN, Y. X., RUSINOVA, A., CHANDRA, A., BIERBAUM, M., GREMER, L., TRIOLA, G., WALDMANN, H., BASTIAENS, P. I. & WITTINGHOFER, A. 2011. Arl2-GTP and Arl3-GTP regulate a GDI-like transport system for farnesylated cargo. *Nat Chem Biol,* 7**,** 942-9.

ITO, H., WANG, J. Z. & SHIMURA, K. 1991. Inhibition of lung metastasis by a calmodulin antagonist, N-(6-aminohexyl)-5-chloro-1-naphthalenesulfonamide (W-7), in mice bearing Lewis lung carcinoma. *Anticancer Res,* 11**,** 249-52.

JAMES, J. R., OLIVEIRA, M. I., CARMO, A. M., IABONI, A. & DAVIS, S. J. 2006. A rigorous experimental framework for detecting protein oligomerization using bioluminescence resonance energy transfer. *Nat Methods,* 3**,** 1001-6.

JANES, M. R., ZHANG, J., LI, L. S., HANSEN, R., PETERS, U., GUO, X., CHEN, Y., BABBAR, A., FIRDAUS, S. J., DARJANIA, L., FENG, J., CHEN, J. H., LI, S., LI, S., LONG, Y. O., THACH, C., LIU, Y., ZARIEH, A., ELY, T., KUCHARSKI, J. M., KESSLER, L. V., WU, T., YU, K., WANG, Y., YAO, Y., DENG, X., ZARRINKAR, P. P., BREHMER, D., DHANAK, D., LORENZI, M. V., HU-LOWE, D., PATRICELLI, M. P., REN, P. & LIU, Y. 2018. Targeting KRAS Mutant Cancers with a Covalent G12C-Specific Inhibitor. *Cell,* 172**,** 578-589 e17.

JANG, H., BANERJEE, A., MARCUS, K., MAKOWSKI, L., MATTOS, C., GAPONENKO, V. & NUSSINOV, R. 2019. The Structural Basis of the Farnesylated and Methylated KRas4B Interaction with Calmodulin. *Structure,* 27**,** 1647-1659 e4.

JANSSENS, V. & GORIS, J. 2001. Protein phosphatase 2A: a highly regulated family of serine/threonine phosphatases implicated in cell growth and signalling. *Biochem J,* 353**,** 417-39.

JIANG, X., CHEN, Z., SHEN, G., JIANG, Y., WU, L., LI, X., WANG, G. & YIN, T. 2018. Psychotropic agent thioridazine elicits potent in vitro and in vivo anti-melanoma effects. *Biomed Pharmacother,* 97**,** 833-837.

JURA, N., SCOTTO-LAVINO, E., SOBCZYK, A. & BAR-SAGI, D. 2006. Differential modification of Ras proteins by ubiquitination. *Mol Cell,* 21**,** 679-87.

KAHL, C. R. & MEANS, A. R. 2003. Regulation of cell cycle progression by calcium/calmodulin-dependent pathways. *Endocr Rev,* 24**,** 719-36.

KARNOUB, A. E. & WEINBERG, R. A. 2008. Ras oncogenes: split personalities. *Nat Rev Mol Cell Biol,* 9**,** 517-31.

KAROULIA, Z., WU, Y., AHMED, T. A., XIN, Q., BOLLARD, J., KREPLER, C., WU, X., ZHANG, C., BOLLAG, G., HERLYN, M., FAGIN, J. A., LUJAMBIO, A., GAVATHIOTIS, E. & POULIKAKOS, P. I. 2016. An Integrated Model of RAF Inhibitor Action Predicts Inhibitor Activity against Oncogenic BRAF Signaling. *Cancer Cell,* 30**,** 501-503.

KASTRINSKY, D. B., SANGODKAR, J., ZAWARE, N., IZADMEHR, S., DHAWAN, N. S., NARLA, G. & OHLMEYER, M. 2015. Reengineered tricyclic anti-cancer agents. *Bioorg Med Chem,* 23**,** 6528-34.

KAUKO, O., O'CONNOR, C. M., KULESSKIY, E., SANGODKAR, J., AAKULA, A., IZADMEHR, S., YETUKURI, L., YADAV, B., PADZIK, A., LAAJALA, T. D., HAAPANIEMI, P., MOMENY, M., VARILA, T., OHLMEYER, M., AITTOKALLIO, T., WENNERBERG, K., NARLA, G. & WESTERMARCK, J. 2018. PP2A inhibition is a druggable MEK inhibitor resistance mechanism in KRAS-mutant lung cancer cells. *Sci Transl Med,* 10.

KAUKO, O. & WESTERMARCK, J. 2018. Non-genomic mechanisms of protein phosphatase 2A (PP2A) regulation in cancer. *Int J Biochem Cell Biol,* 96**,** 157-164.

KLEIN, C. H., TRUXIUS, D. C., VOGEL, H. A., HARIZANOVA, J., MURARKA, S., MARTIN-GAGO, P. & BASTIAENS, P. I. H. 2019. PDEdelta inhibition impedes the proliferation and survival of human colorectal cancer cell lines harboring oncogenic KRas. *Int J Cancer,* 144**,** 767-776.

KOHLER, M. & BRUMMER, T. 2016. B-Raf activation loop phosphorylation revisited. *Cell Cycle,* 15**,** 1171-3.

KOHNKE, M., SCHMITT, S., ARIOTTI, N., PIGGOTT, A. M., PARTON, R. G., LACEY, E., CAPON, R. J., ALEXANDROV, K. & ABANKWA, D. 2012. Design and application of in

vivo FRET biosensors to identify protein prenylation and nanoclustering inhibitors. *Chem Biol,* 19**,** 866-74.

KUBARA, K., YAMAZAKI, K., ISHIHARA, Y., NARUTO, T., LIN, H. T., NISHIMURA, K., OHTAKA, M., NAKANISHI, M., ITO, M., TSUKAHARA, K., MORIO, T., TAKAGI, M. & OTSU, M. 2018. Status of KRAS in iPSCs Impacts upon Self-Renewal and Differentiation Propensity. *Stem Cell Reports,* 11**,** 380-394.

KUO, Y. C., HUANG, K. Y., YANG, C. H., YANG, Y. S., LEE, W. Y. & CHIANG, C. W. 2008. Regulation of phosphorylation of Thr-308 of Akt, cell proliferation, and survival by the B55alpha regulatory subunit targeting of the protein phosphatase 2A holoenzyme to Akt. *J Biol Chem,* 283**,** 1882-92.

LABAER, J., GARRETT, M. D., STEVENSON, L. F., SLINGERLAND, J. M., SANDHU, C., CHOU, H. S., FATTAEY, A. & HARLOW, E. 1997. New functional activities for the p21 family of CDK inhibitors. *Genes Dev,* 11**,** 847-62.

LAKE, D., CORREA, S. A. & MULLER, J. 2016. Negative feedback regulation of the ERK1/2 MAPK pathway. *Cell Mol Life Sci,* 73**,** 4397-4413.

LAO, D. H., YUSOFF, P., CHANDRAMOULI, S., PHILP, R. J., FONG, C. W., JACKSON, R. A., SAW, T. Y., YU, C. Y. & GUY, G. R. 2007. Direct binding of PP2A to Sprouty2 and phosphorylation changes are a prerequisite for ERK inhibition downstream of fibroblast growth factor receptor stimulation. *J Biol Chem,* 282**,** 9117-26.

LAUDE, A. J. & PRIOR, I. A. 2008. Palmitoylation and localisation of RAS isoforms are modulated by the hypervariable linker domain. *J Cell Sci,* 121**,** 421-7.

LAVOIE, H., THEVAKUMARAN, N., GAVORY, G., LI, J. J., PADEGANEH, A., GUIRAL, S., DUCHAINE, J., MAO, D. Y., BOUVIER, M., SICHERI, F. & THERRIEN, M. 2013. Inhibitors that stabilize a closed RAF kinase domain conformation induce dimerization. *Nat Chem Biol,* 9**,** 428-36.

LE ROLLE, A. F., CHIU, T. K., ZENG, Z., SHIA, J., WEISER, M. R., PATY, P. B. & CHIU, V. K. 2016. Oncogenic KRAS activates an embryonic stem cell-like program in human colon cancer initiation. *Oncotarget,* 7**,** 2159-74.

LEE, H. W., SA, J. K., GUALBERTO, A., SCHOLZ, C., SUNG, H. H., JEONG, B. C., CHOI, H. Y., KWON, G. Y. & PARK, S. H. 2020. A Phase II Trial of Tipifarnib for Patients with Previously Treated, Metastatic Urothelial Carcinoma Harboring HRAS Mutations. *Clin Cancer Res,* 26**,** 5113-5119.

LEE, J., KIM, M. S., KIM, M. A. & JANG, Y. K. 2016. Calmidazolium chloride inhibits growth of murine embryonal carcinoma cells, a model of cancer stem-like cells. *Toxicol In Vitro,* 35**,** 86-92.

LEONARD, D., HUANG, W., IZADMEHR, S., O'CONNOR, C. M., WIREDJA, D. D., WANG, Z., ZAWARE, N., CHEN, Y., SCHLATZER, D. M., KISELAR, J., VASIREDDI, N., SCHUCHNER, S., PERL, A. L., GALSKY, M. D., XU, W., BRAUTIGAN, D. L., OGRIS, E., TAYLOR, D. J. & NARLA, G. 2020. Selective PP2A Enhancement through Biased Heterotrimer Stabilization. *Cell,* 181**,** 688-701 e16.

LESHCHINER, E. S., PARKHITKO, A., BIRD, G. H., LUCCARELLI, J., BELLAIRS, J. A., ESCUDERO, S., OPOKU-NSIAH, K., GODES, M., PERRIMON, N. & WALENSKY, L. D. 2015. Direct inhibition of oncogenic KRAS by hydrocarbon-stapled SOS1 helices. *Proc Natl Acad Sci U S A,* 112**,** 1761-6.

LETOURNEUX, C., ROCHER, G. & PORTEU, F. 2006. B56-containing PP2A dephosphorylate ERK and their activity is controlled by the early gene IEX-1 and ERK. *EMBO J,* 25**,** 727-38.

LEUNG, P. C., TAYLOR, W. A., WANG, J. H. & TIPTON, C. L. 1984. Ophiobolin A. A natural product inhibitor of calmodulin. *J Biol Chem,* 259**,** 2742-7.

LI, H. & VILLALOBO, A. 2002. Evidence for the direct interaction between calmodulin and the human epidermal growth factor receptor. *Biochem J,* 362**,** 499-505.

LI, M., MAKKINJE, A. & DAMUNI, Z. 1996. The myeloid leukemia-associated protein SET is a potent inhibitor of protein phosphatase 2A. *J Biol Chem,* 271**,** 11059-62.

LI, S., BALMAIN, A. & COUNTER, C. M. 2018. A model for RAS mutation patterns in cancers: finding the sweet spot. *Nat Rev Cancer,* 18**,** 767-777.

LI, W., HAN, M. & GUAN, K. L. 2000. The leucine-rich repeat protein SUR-8 enhances MAP kinase activation and forms a complex with Ras and Raf. *Genes Dev,* 14**,** 895-900.

LIAU, N. P. D., WENDORFF, T. J., QUINN, J. G., STEFFEK, M., PHUNG, W., LIU, P., TANG, J., IRUDAYANATHAN, F. J., IZADI, S., SHAW, A. S., MALEK, S., HYMOWITZ, S. G. & SUDHAMSU, J. 2020. Negative regulation of RAF kinase activity by ATP is overcome by 14-3-3-induced dimerization. *Nat Struct Mol Biol,* 27**,** 134-141.

LIU, G. X., SHENG, H. F. & WU, S. 1996. A study on the levels of calmodulin and DNA in human lung cancer cells. *Br J Cancer,* 73**,** 899-901.

LIU, W. N., YAN, M. & CHAN, A. M. 2017. A thirty-year quest for a role of R-Ras in cancer: from an oncogene to a multitasking GTPase. *Cancer Lett,* 403**,** 59-65.

LIU, Z., MA, L., WEN, Z. S., HU, Z., WU, F. Q., LI, W., LIU, J. & ZHOU, G. B. 2014. Cancerous inhibitor of PP2A is targeted by natural compound celastrol for degradation in non-small-cell lung cancer. *Carcinogenesis,* 35**,** 905-14.

MAGNANI, R., DIRK, L. M., TRIEVEL, R. C. & HOUTZ, R. L. 2010. Calmodulin methyltransferase is an evolutionarily conserved enzyme that trimethylates Lys-115 in calmodulin. *Nat Commun,* 1**,** 43.

MANOHARAN, G. B., KOPRA, K., ESKONEN, V., HÄRMÄ, H. & ABANKWA, D. 2019. High-throughput amenable fluorescence-assays to screen for calmodulin-inhibitors. *Anal Biochem,* 572**,** 25-32.

MARSHALL, C. B., NISHIKAWA, T., OSAWA, M., STATHOPULOS, P. B. & IKURA, M. 2015. Calmodulin and STIM proteins: Two major calcium sensors in the cytoplasm and endoplasmic reticulum. *Biochem Biophys Res Commun,* 460**,** 5-21.

MARTIN-GAGO, P., FANSA, E. K., KLEIN, C. H., MURARKA, S., JANNING, P., SCHURMANN, M., METZ, M., ISMAIL, S., SCHULTZ-FADEMRECHT, C., BAUMANN, M., BASTIAENS, P. I., WITTINGHOFER, A. & WALDMANN, H. 2017. A PDE6delta-KRas Inhibitor Chemotype with up to Seven H-Bonds and Picomolar Affinity that Prevents Efficient Inhibitor Release by Arl2. *Angew Chem Int Ed Engl,* 56**,** 2423-2428.

MARTIN-NIETO, J. & VILLALOBO, A. 1998. The human epidermal growth factor receptor contains a juxtamembrane calmodulin-binding site. *Biochemistry,* 37**,** 227-36.

MARTINELLI, S., DE LUCA, A., STELLACCI, E., ROSSI, C., CHECQUOLO, S., LEPRI, F., CAPUTO, V., SILVANO, M., BUSCHERINI, F., CONSOLI, F., FERRARA, G., DIGILIO, M. C., CAVALIERE, M. L., VAN HAGEN, J. M., ZAMPINO, G., VAN DER BURGT, I., FERRERO, G. B., MAZZANTI, L., SCREPANTI, I., YNTEMA, H. G., NILLESEN, W. M., SAVARIRAYAN, R., ZENKER, M., DALLAPICCOLA, B., GELB, B. D. & TARTAGLIA, M. 2010. Heterozygous germline mutations in the CBL tumor-suppressor gene cause a Noonan syndrome-like phenotype. *Am J Hum Genet,* 87**,** 250-7.

MARULLO, S. & BOUVIER, M. 2007. Resonance energy transfer approaches in molecular pharmacology and beyond. *Trends Pharmacol Sci,* 28**,** 362-5.

MASSOUD, T. F., PAULMURUGAN, R., DE, A., RAY, P. & GAMBHIR, S. S. 2007. Reporter gene imaging of protein-protein interactions in living subjects. *Curr Opin Biotechnol,* 18**,** 31-7.

MAZHAR, S., TAYLOR, S. E., SANGODKAR, J. & NARLA, G. 2019. Targeting PP2A in cancer: Combination therapies. *Biochim Biophys Acta Mol Cell Res,* 1866**,** 51-63.

MCDONALD, E. R., 3RD, DE WECK, A., SCHLABACH, M. R., BILLY, E., MAVRAKIS, K. J., HOFFMAN, G. R., BELUR, D., CASTELLETTI, D., FRIAS, E., GAMPA, K., GOLJI, J., KAO, I., LI, L., MEGEL, P., PERKINS, T. A., RAMADAN, N., RUDDY, D. A., SILVER, S. J., SOVATH, S., STUMP, M., WEBER, O., WIDMER, R., YU, J., YU, K., YUE, Y., ABRAMOWSKI, D., ACKLEY, E., BARRETT, R., BERGER, J., BERNARD, J. L., BILLIG,

R., BRACHMANN, S. M., BUXTON, F., CAOTHIEN, R., CAUSHI, J. X., CHUNG, F. S., CORTES-CROS, M., DEBEAUMONT, R. S., DELAUNAY, C., DESPLAT, A., DUONG, W., DWOSKE, D. A., ELDRIDGE, R. S., FARSIDJANI, A., FENG, F., FENG, J., FLEMMING, D., FORRESTER, W., GALLI, G. G., GAO, Z., GAUTER, F., GIBAJA, V., HAAS, K., HATTENBERGER, M., HOOD, T., HUROV, K. E., JAGANI, Z., JENAL, M., JOHNSON, J. A., JONES, M. D., KAPOOR, A., KORN, J., LIU, J., LIU, Q., LIU, S., LIU, Y., LOO, A. T., MACCHI, K. J., MARTIN, T., MCALLISTER, G., MEYER, A., MOLLE, S., PAGLIARINI, R. A., PHADKE, T., REPKO, B., SCHOUWEY, T., SHANAHAN, F., SHEN, Q., STAMM, C., STEPHAN, C., STUCKE, V. M., TIEDT, R., VARADARAJAN, M., VENKATESAN, K., VITARI, A. C., WALLROTH, M., WEILER, J., ZHANG, J., MICKANIN, C., MYER, V. E., PORTER, J. A., LAI, A., BITTER, H., LEES, E., KEEN, N., KAUFFMANN, A., STEGMEIER, F., HOFMANN, F., SCHMELZLE, T. & SELLERS, W. R. 2017. Project DRIVE: A Compendium of Cancer Dependencies and Synthetic Lethal Relationships Uncovered by Large-Scale, Deep RNAi Screening. *Cell,* 170**,** 577-592 e10.

MEJUCH, T., GARIVET, G., HOFER, W., KAISER, N., FANSA, E. K., EHRT, C., KOCH, O., BAUMANN, M., ZIEGLER, S., WITTINGHOFER, A. & WALDMANN, H. 2017. Small-Molecule Inhibition of the UNC119-Cargo Interaction. *Angew Chem Int Ed Engl,* 56**,** 6181-6186.

MINE, N., YAMAMOTO, S., SAITO, N., SATO, T., SAKAKIBARA, K., KUFE, D. W., VONHOFF, D. D. & KAWABE, T. 2017. CBP501 suppresses macrophage induced cancer stem cell like features and metastases. *Oncotarget,* 8**,** 64015-64031.

MISAKI, R., MORIMATSU, M., UEMURA, T., WAGURI, S., MIYOSHI, E., TANIGUCHI, N., MATSUDA, M. & TAGUCHI, T. 2010. Palmitoylated Ras proteins traffic through recycling endosomes to the plasma membrane during exocytosis. *J Cell Biol,* 191**,** 23-9.

MOHRI, T., KAMESHITA, I., SUZUKI, S., HIOKI, K., TOKUNAGA, R. & TAKATANI, S. 1998. Rapid adhesion and spread of non-adherent colon cancer Colo201 cells induced by the protein kinase inhibitors, K252a and KT5720 and suppression of the adhesion by the immunosuppressants FK506 and cyclosporin A. *Cell Struct Funct,* 23**,** 255-64.

MOON, B. S., JEONG, W. J., PARK, J., KIM, T. I., MIN DO, S. & CHOI, K. Y. 2014. Role of oncogenic K-Ras in cancer stem cell activation by aberrant Wnt/beta-catenin signaling. *J Natl Cancer Inst,* 106**,** djt373.

MOORE, A. R., ROSENBERG, S. C., MCCORMICK, F. & MALEK, S. 2020. RAS-targeted therapies: is the undruggable drugged? *Nat Rev Drug Discov,* 19**,** 533-552.

MOU, L., LIANG, B., LIU, G., JIANG, J., LIU, J., ZHOU, B., HUANG, J., ZANG, N., LIAO, Y., YE, L. & LIANG, H. 2019. Berbamine exerts anticancer effects on human colon cancer cells via induction of autophagy and apoptosis, inhibition of cell migration and MEK/ERK signalling pathway. *J BUON,* 24**,** 1870-1875.

MURTAUGH, T. J., SITARAMAYYA, A., WRIGHT, L. S. & SIEGEL, F. L. 1980. In vitro methylation of calmodulin. *Ann N Y Acad Sci,* 356**,** 412.

NAJUMUDEEN, A. K., JAISWAL, A., LECTEZ, B., OETKEN-LINDHOLM, C., GUZMAN, C., SILJAMAKI, E., POSADA, I. M., LACEY, E., AITTOKALLIO, T. & ABANKWA, D. 2016. Cancer stem cell drugs target K-ras signaling in a stemness context. *Oncogene,* 35**,** 5248-5262.

NASA, I. & KETTENBACH, A. N. 2018. Coordination of Protein Kinase and Phosphoprotein Phosphatase Activities in Mitosis. *Front Cell Dev Biol,* 6**,** 30.

NEEL, N. F., MARTIN, T. D., STRATFORD, J. K., ZAND, T. P., REINER, D. J. & DER, C. J. 2011. The RalGEF-Ral Effector Signaling Network: The Road Less Traveled for Anti-Ras Drug Discovery. *Genes Cancer,* 2**,** 275-87.

NEUHAUS, R. & REBER, B. F. 1992. Inhibition of membrane currents and rises of intracellular Ca2+ in PC12 cells by CGS 9343B, a calmodulin inhibitor. *Eur J Pharmacol,* 226**,** 183-5.

NEVIANI, P., SANTHANAM, R., OAKS, J. J., EIRING, A. M., NOTARI, M., BLASER, B. W., LIU, S., TROTTA, R., MUTHUSAMY, N., GAMBACORTI-PASSERINI, C., DRUKER, B. J., CORTES, J., MARCUCCI, G., CHEN, C. S., VERRILLS, N. M., ROY, D. C., CALIGIURI, M. A., BLOOMFIELD, C. D., BYRD, J. C. & PERROTTI, D. 2007. FTY720, a new alternative for treating blast crisis chronic myelogenous leukemia and Philadelphia chromosome-positive acute lymphocytic leukemia. *J Clin Invest,* 117**,** 2408-21.

NEWLACZYL, A. U., COULSON, J. M. & PRIOR, I. A. 2017. Quantification of spatiotemporal patterns of Ras isoform expression during development. *Sci Rep,* 7**,** 41297.

NOORI, S. & HASSAN, Z. M. 2014. Tehranolide inhibits cell proliferation via calmodulin inhibition, PDE, and PKA activation. *Tumour Biol,* 35**,** 257-64.

NORMAN, J. A., ANSELL, J., STONE, G. A., WENNOGLE, L. P. & WASLEY, J. W. 1987. CGS 9343B, a novel, potent, and selective inhibitor of calmodulin activity. *Mol Pharmacol,* 31**,** 535-40.

NUSSINOV, R., MURATCIOGLU, S., TSAI, C. J., JANG, H., GURSOY, A. & KESKIN, O. 2015. The Key Role of Calmodulin in KRAS-Driven Adenocarcinomas. *Mol Cancer Res,* 13**,** 1265-73.

NUSSINOV, R., TSAI, C. J. & JANG, H. 2020. Autoinhibition can identify rare driver mutations and advise pharmacology. *FASEB J,* 34**,** 16-29.

O'BRIEN, C. A., POLLETT, A., GALLINGER, S. & DICK, J. E. 2007. A human colon cancer cell capable of initiating tumour growth in immunodeficient mice. *Nature,* 445**,** 106-10.

OGRIS, E., DU, X., NELSON, K. C., MAK, E. K., YU, X. X., LANE, W. S. & PALLAS, D. C. 1999. A protein phosphatase methylesterase (PME-1) is one of several novel proteins stably associating with two inactive mutants of protein phosphatase 2A. *J Biol Chem,* 274**,** 14382-91.

OKAN, E., DREWETT, V., SHAW, P. E. & JONES, P. 2001. The small-GTPase RalA activates transcription of the urokinase plasminogen activator receptor (uPAR) gene via an AP1-dependent mechanism. *Oncogene,* 20**,** 1816-24.

OSTREM, J. M., PETERS, U., SOS, M. L., WELLS, J. A. & SHOKAT, K. M. 2013. K-Ras(G12C) inhibitors allosterically control GTP affinity and effector interactions. *Nature,* 503**,** 548-51.

OTTO, T. & SICINSKI, P. 2017. Cell cycle proteins as promising targets in cancer therapy. *Nat Rev Cancer,* 17**,** 93-115.

OWENS, D. M. & KEYSE, S. M. 2007. Differential regulation of MAP kinase signalling by dual-specificity protein phosphatases. *Oncogene,* 26**,** 3203-13.

OZDEMIR, E. S., JANG, H., GURSOY, A., KESKIN, O. & NUSSINOV, R. 2018. Arl2-Mediated Allosteric Release of Farnesylated KRas4B from Shuttling Factor PDEdelta. *J Phys Chem B,* 122**,** 7503-7513.

PANINA, S., STEPHAN, A., LA COUR, J. M., JACOBSEN, K., KALLERUP, L. K., BUMBULEVICIUTE, R., KNUDSEN, K. V., SANCHEZ-GONZALEZ, P., VILLALOBO, A., OLESEN, U. H. & BERCHTOLD, M. W. 2012. Significance of calcium binding, tyrosine phosphorylation, and lysine trimethylation for the essential function of calmodulin in vertebrate cells analyzed in a novel gene replacement system. *J Biol Chem,* 287**,** 18173-81.

PAPKE, B., MURARKA, S., VOGEL, H. A., MARTIN-GAGO, P., KOVACEVIC, M., TRUXIUS, D. C., FANSA, E. K., ISMAIL, S., ZIMMERMANN, G., HEINELT, K., SCHULTZ-FADEMRECHT, C., AL SAABI, A., BAUMANN, M., NUSSBAUMER, P., WITTINGHOFER, A., WALDMANN, H. & BASTIAENS, P. I. 2016. Identification of pyrazolopyridazinones as PDEdelta inhibitors. *Nat Commun,* 7**,** 11360.

PARK, E., RAWSON, S., LI, K., KIM, B. W., FICARRO, S. B., PINO, G. G., SHARIF, H., MARTO, J. A., JEON, H. & ECK, M. J. 2019. Architecture of autoinhibited and active BRAF-MEK1-14-3-3 complexes. *Nature,* 575**,** 545-550.

PARKER, C. & SHERBET, G. V. 1992. Modulators of intracellular Ca2+ and the calmodulin inhibitor W-7 alter the expression of metastasis-associated genes MTS1 and NM23 in metastatic variants of the B16 murine melanoma. *Melanoma Res,* 2**,** 337-43.

PARKER, J. A. & MATTOS, C. 2015. The Ras-Membrane Interface: Isoform-specific Differences in The Catalytic Domain. *Mol Cancer Res,* 13**,** 595-603.

PATGIRI, A., YADAV, K. K., ARORA, P. S. & BAR-SAGI, D. 2011. An orthosteric inhibitor of the Ras-Sos interaction. *Nat Chem Biol,* 7**,** 585-7.

PATRICELLI, M. P., JANES, M. R., LI, L. S., HANSEN, R., PETERS, U., KESSLER, L. V., CHEN, Y., KUCHARSKI, J. M., FENG, J., ELY, T., CHEN, J. H., FIRDAUS, S. J., BABBAR, A., REN, P. & LIU, Y. 2016. Selective Inhibition of Oncogenic KRAS Output with Small Molecules Targeting the Inactive State. *Cancer Discov,* 6**,** 316-29.

PENG, S. B., HENRY, J. R., KAUFMAN, M. D., LU, W. P., SMITH, B. D., VOGETI, S., RUTKOSKI, T. J., WISE, S., CHUN, L., ZHANG, Y., VAN HORN, R. D., YIN, T., ZHANG, X., YADAV, V., CHEN, S. H., GONG, X., MA, X., WEBSTER, Y., BUCHANAN, S., MOCHALKIN, I., HUBER, L., KAYS, L., DONOHO, G. P., WALGREN, J., MCCANN, D., PATEL, P., CONTI, I., PLOWMAN, G. D., STARLING, J. J. & FLYNN, D. L. 2015. Inhibition of RAF Isoforms and Active Dimers by LY3009120 Leads to Anti-tumor Activities in RAS or BRAF Mutant Cancers. *Cancer Cell,* 28**,** 384-98.

PEREIRA-LEAL, J. B. & SEABRA, M. C. 2001. Evolution of the Rab family of small GTP-binding proteins. *J Mol Biol,* 313**,** 889-901.

PERROTTI, D. & NEVIANI, P. 2013. Protein phosphatase 2A: a target for anticancer therapy. *Lancet Oncol,* 14**,** e229-38.

PETERSON, R. T., DESAI, B. N., HARDWICK, J. S. & SCHREIBER, S. L. 1999. Protein phosphatase 2A interacts with the 70-kDa S6 kinase and is activated by inhibition of FKBP12-rapamycinassociated protein. *Proc Natl Acad Sci U S A,* 96**,** 4438-42.

PFLEGER, K. D. & EIDNE, K. A. 2006. Illuminating insights into protein-protein interactions using bioluminescence resonance energy transfer (BRET). *Nat Methods,* 3**,** 165-74.

PLOWMAN, S. J., ARIOTTI, N., GOODALL, A., PARTON, R. G. & HANCOCK, J. F. 2008. Electrostatic interactions positively regulate K-Ras nanocluster formation and function. *Mol Cell Biol,* 28**,** 4377-85.

POTDAR, S., IANEVSKI, A., MPINDI, J. P., BYCHKOV, D., FIERE, C., IANEVSKI, P., YADAV, B., WENNERBERG, K., AITTOKALLIO, T., KALLIONIEMI, O., SAARELA, J. & OSTLING, P. 2020. Breeze: an integrated quality control and data analysis application for high-throughput drug screening. *Bioinformatics,* 36**,** 3602-3604.

POULIKAKOS, P. I., ZHANG, C., BOLLAG, G., SHOKAT, K. M. & ROSEN, N. 2010. RAF inhibitors transactivate RAF dimers and ERK signalling in cells with wild-type BRAF. *Nature,* 464**,** 427-30.

PRIOR, I. A. & HANCOCK, J. F. 2012. Ras trafficking, localization and compartmentalized signalling. *Semin Cell Dev Biol,* 23**,** 145-53.

PRIOR, I. A., HOOD, F. E. & HARTLEY, J. L. 2020. The Frequency of Ras Mutations in Cancer. *Cancer Res,* 80**,** 2969-2974.

PRIOR, I. A., MUNCKE, C., PARTON, R. G. & HANCOCK, J. F. 2003. Direct visualization of Ras proteins in spatially distinct cell surface microdomains. *J Cell Biol,* 160**,** 165-70.

QU, L., PAN, C., HE, S. M., LANG, B., GAO, G. D., WANG, X. L. & WANG, Y. 2019. The Ras Superfamily of Small GTPases in Non-neoplastic Cerebral Diseases. *Front Mol Neurosci,* 12**,** 121.

QUINLAN, M. P., QUATELA, S. E., PHILIPS, M. R. & SETTLEMAN, J. 2008. Activated Kras, but not Hras or Nras, may initiate tumors of endodermal origin via stem cell expansion. *Mol Cell Biol,* 28**,** 2659-74.

RAHMAN, M. M., PRUNTE, L., LEBENDER, L. F., PATEL, B. S., GELISSEN, I., HANSBRO, P. M., MORRIS, J. C., CLARK, A. R., VERRILLS, N. M. & AMMIT, A. J. 2016. The

phosphorylated form of FTY720 activates PP2A, represses inflammation and is devoid of S1P agonism in A549 lung epithelial cells. *Sci Rep,* 6**,** 37297.

RAJAKULENDRAN, T., SAHMI, M., LEFRANCOIS, M., SICHERI, F. & THERRIEN, M. 2009. A dimerization-dependent mechanism drives RAF catalytic activation. *Nature,* 461**,** 542-5.

RAUEN, K. A. 2013. The RASopathies. *Annu Rev Genomics Hum Genet,* 14**,** 355-69.

REYNHOUT, S. & JANSSENS, V. 2019. Physiologic functions of PP2A: Lessons from genetically modified mice. *Biochim Biophys Acta Mol Cell Res,* 1866**,** 31-50.

ROBERTSON, A. G., KIM, J., AL-AHMADIE, H., BELLMUNT, J., GUO, G., CHERNIACK, A. D., HINOUE, T., LAIRD, P. W., HOADLEY, K. A., AKBANI, R., CASTRO, M. A. A., GIBB, E. A., KANCHI, R. S., GORDENIN, D. A., SHUKLA, S. A., SANCHEZ-VEGA, F., HANSEL, D. E., CZERNIAK, B. A., REUTER, V. E., SU, X., DE SA CARVALHO, B., CHAGAS, V. S., MUNGALL, K. L., SADEGHI, S., PEDAMALLU, C. S., LU, Y., KLIMCZAK, L. J., ZHANG, J., CHOO, C., OJESINA, A. I., BULLMAN, S., LERAAS, K. M., LICHTENBERG, T. M., WU, C. J., SCHULTZ, N., GETZ, G., MEYERSON, M., MILLS, G. B., MCCONKEY, D. J., NETWORK, T. R., WEINSTEIN, J. N., KWIATKOWSKI, D. J. & LERNER, S. P. 2017. Comprehensive Molecular Characterization of Muscle-Invasive Bladder Cancer. *Cell,* 171**,** 540-556 e25.

RODRIGUEZ-VILARRUPLA, A., JAUMOT, M., ABELLA, N., CANELA, N., BRUN, S., DIAZ, C., ESTANYOL, J. M., BACHS, O. & AGELL, N. 2005. Binding of calmodulin to the carboxy-terminal region of p21 induces nuclear accumulation via inhibition of protein kinase C-mediated phosphorylation of Ser153. *Mol Cell Biol,* 25**,** 7364-74.

ROJAS, A. M., FUENTES, G., RAUSELL, A. & VALENCIA, A. 2012. The Ras protein superfamily: evolutionary tree and role of conserved amino acids. *J Cell Biol,* 196**,** 189-201.

SABLINA, A. A. & HAHN, W. C. 2008. SV40 small T antigen and PP2A phosphatase in cell transformation. *Cancer Metastasis Rev,* 27**,** 137-46.

SAITO, N., MINE, N., KUFE, D. W., VON HOFF, D. D. & KAWABE, T. 2017. CBP501 inhibits EGF-dependent cell migration, invasion and epithelial-to-mesenchymal transition of non-small cell lung cancer cells by blocking KRas to calmodulin binding. *Oncotarget,* 8**,** 74006-74018.

SAKAMOTO, K., MASUTANI, T. & HIROKAWA, T. 2020. Generation of KS-58 as the first K-Ras(G12D)-inhibitory peptide presenting anti-cancer activity in vivo. *Sci Rep,* 10**,** 21671.

SANGODKAR, J., FARRINGTON, C. C., MCCLINCH, K., GALSKY, M. D., KASTRINSKY, D. B. & NARLA, G. 2016. All roads lead to PP2A: exploiting the therapeutic potential of this phosphatase. *FEBS J,* 283**,** 1004-24.

SANGODKAR, J., PERL, A., TOHME, R., KISELAR, J., KASTRINSKY, D. B., ZAWARE, N., IZADMEHR, S., MAZHAR, S., WIREDJA, D. D., O'CONNOR, C. M., HOON, D., DHAWAN, N. S., SCHLATZER, D., YAO, S., LEONARD, D., BORCZUK, A. C., GOKULRANGAN, G., WANG, L., SVENSON, E., FARRINGTON, C. C., YUAN, E., AVELAR, R. A., STACHNIK, A., SMITH, B., GIDWANI, V., GIANNINI, H. M., MCQUAID, D., MCCLINCH, K., WANG, Z., LEVINE, A. C., SEARS, R. C., CHEN, E. Y., DUAN, Q., DATT, M., HAIDER, S., MA'AYAN, A., DIFEO, A., SHARMA, N., GALSKY, M. D., BRAUTIGAN, D. L., IOANNOU, Y. A., XU, W., CHANCE, M. R., OHLMEYER, M. & NARLA, G. 2017. Activation of tumor suppressor protein PP2A inhibits KRAS-driven tumor growth. *J Clin Invest,* 127**,** 2081-2090.

SASAKI, A. T., CARRACEDO, A., LOCASALE, J. W., ANASTASIOU, D., TAKEUCHI, K., KAHOUD, E. R., HAVIV, S., ASARA, J. M., PANDOLFI, P. P. & CANTLEY, L. C. 2011. Ubiquitination of K-Ras enhances activation and facilitates binding to select downstream effectors. *Sci Signal,* 4**,** ra13.

SCHMICK, M., VARTAK, N., PAPKE, B., KOVACEVIC, M., TRUXIUS, D. C., ROSSMANNEK, L. & BASTIAENS, P. I. H. 2014. KRas localizes to the plasma membrane by spatial cycles of solubilization, trapping and vesicular transport. *Cell,* 157**,** 459-471.

SEGEV, N. 2001. Ypt/rab gtpases: regulators of protein trafficking. *Sci STKE,* 2001**,** re11.

SENGUPTA, P., RUANO, M. J., TEBAR, F., GOLEBIEWSKA, U., ZAITSEVA, I., ENRICH, C., MCLAUGHLIN, S. & VILLALOBO, A. 2007. Membrane-permeable calmodulin inhibitors (e.g. W-7/W-13) bind to membranes, changing the electrostatic surface potential: dual effect of W-13 on epidermal growth factor receptor activation. *J Biol Chem,* 282**,** 8474-86.

SEZZI, M. L., ZUPI, G., DE LUCA, G., MATERAZZI, M. & BELLELLI, L. 1984. Effects of a calcium-antagonist (flunarizine) on the in vitro growth of B16 mouse melanoma cells. *Anticancer Res,* 4**,** 229-34.

SHALOM-FEUERSTEIN, R., PLOWMAN, S. J., ROTBLAT, B., ARIOTTI, N., TIAN, T., HANCOCK, J. F. & KLOOG, Y. 2008. K-ras nanoclustering is subverted by overexpression of the scaffold protein galectin-3. *Cancer Res,* 68**,** 6608-16.

SHEN, W. G., PENG, W. X., DAI, G., XU, J. F., ZHANG, Y. & LI, C. J. 2007. Calmodulin is essential for angiogenesis in response to hypoxic stress in endothelial cells. *Cell Biol Int,* 31**,** 126-34.

SHERGALIS, A., BANKHEAD, A., 3RD, LUESAKUL, U., MUANGSIN, N. & NEAMATI, N. 2018. Current Challenges and Opportunities in Treating Glioblastoma. *Pharmacol Rev,* 70**,** 412-445.

SHI, Y. 2009. Serine/threonine phosphatases: mechanism through structure. *Cell,* 139**,** 468-84.

SIDDIQUI, F. A., ALAM, C., ROSENQVIST, P., ORA, M., SABT, A., MANOHARAN, G. B., BINDU, L., OKUTACHI, S., CATILLON, M., TAYLOR, T., ABDELHAFEZ, O. M., LONNBERG, H., STEPHEN, A. G., PAPAGEORGIOU, A. C., VIRTA, P. & ABANKWA, D. 2020. PDE6D Inhibitors with a New Design Principle Selectively Block K-Ras Activity. *ACS Omega,* 5**,** 832-842.

SIDHU, R. S., CLOUGH, R. R. & BHULLAR, R. P. 2003. Ca2+/calmodulin binds and dissociates K-RasB from membrane. *Biochem Biophys Res Commun,* 304**,** 655-60.

SINGH, J., PETTER, R. C., BAILLIE, T. A. & WHITTY, A. 2011. The resurgence of covalent drugs. *Nat Rev Drug Discov,* 10**,** 307-17.

SPERLICH, B., KAPOOR, S., WALDMANN, H., WINTER, R. & WEISE, K. 2016. Regulation of K-Ras4B Membrane Binding by Calmodulin. *Biophys J,* 111**,** 113-22.

SPICZKA, K. S. & YEAMAN, C. 2008. Ral-regulated interaction between Sec5 and paxillin targets Exocyst to focal complexes during cell migration. *J Cell Sci,* 121**,** 2880-91.

SULLIVAN, R. J., INFANTE, J. R., JANKU, F., WONG, D. J. L., SOSMAN, J. A., KEEDY, V., PATEL, M. R., SHAPIRO, G. I., MIER, J. W., TOLCHER, A. W., WANG-GILLAM, A., SZNOL, M., FLAHERTY, K., BUCHBINDER, E., CARVAJAL, R. D., VARGHESE, A. M., LACOUTURE, M. E., RIBAS, A., PATEL, S. P., DECRESCENZO, G. A., EMERY, C. M., GROOVER, A. L., SAHA, S., VARTERASIAN, M., WELSCH, D. J., HYMAN, D. M. & LI, B. T. 2018. First-in-Class ERK1/2 Inhibitor Ulixertinib (BVD-523) in Patients with MAPK Mutant Advanced Solid Tumors: Results of a Phase I Dose-Escalation and Expansion Study. *Cancer Discov,* 8**,** 184-195.

SUN, Q., BURKE, J. P., PHAN, J., BURNS, M. C., OLEJNICZAK, E. T., WATERSON, A. G., LEE, T., ROSSANESE, O. W. & FESIK, S. W. 2012. Discovery of small molecules that bind to K-Ras and inhibit Sos-mediated activation. *Angew Chem Int Ed Engl,* 51**,** 6140-3.

SUN, X., GAO, H., YANG, Y., HE, M., WU, Y., SONG, Y., TONG, Y. & RAO, Y. 2019. PROTACs: great opportunities for academia and industry. *Signal Transduct Target Ther,* 4**,** 64.

SUNAGAWA, M., YOKOSHIKI, H., SEKI, T., NAKAMURA, M., LABER, P. & SPERELAKIS, N. 1999. Direct block of Ca2+ channels by calmidazolium in cultured vascular smooth muscle cells. *J Cardiovasc Pharmacol,* 34**,** 488-96.

SUNG, H., FERLAY, J., SIEGEL, R. L., LAVERSANNE, M., SOERJOMATARAM, I., JEMAL, A. & BRAY, F. 2021. Global cancer statistics 2020: GLOBOCAN estimates of incidence and mortality worldwide for 36 cancers in 185 countries. *CA Cancer J Clin*.

SZTUL, E., CHEN, P. W., CASANOVA, J. E., CHERFILS, J., DACKS, J. B., LAMBRIGHT, D. G., LEE, F. S., RANDAZZO, P. A., SANTY, L. C., SCHURMANN, A., WILHELMI, I., YOHE, M. E. & KAHN, R. A. 2019. ARF GTPases and their GEFs and GAPs: concepts and challenges. *Mol Biol Cell,* 30**,** 1249-1271.

TANAKA, N., LIN, J. J., LI, C., RYAN, M. B., ZHANG, J., KIEDROWSKI, L. A., MICHEL, A. G., SYED, M. U., FELLA, K. A., SAKHI, M., BAIEV, I., JURIC, D., GAINOR, J. F., KLEMPNER, S. J., LENNERZ, J. K., SIRAVEGNA, G., BAR-PELED, L., HATA, A. N., HEIST, R. S. & CORCORAN, R. B. 2021. Clinical acquired resistance to KRASG12C inhibition through a novel KRAS switch-II pocket mutation and polyclonal alterations converging on RAS-MAPK reactivation. *Cancer Discov*.

TEBAR, F., CHAVERO, A., AGELL, N., LU, A., RENTERO, C., ENRICH, C. & GREWAL, T. 2020. Pleiotropic Roles of Calmodulin in the Regulation of KRas and Rac1 GTPases: Functional Diversity in Health and Disease. *Int J Mol Sci,* 21.

TEBAR, F., LLADO, A. & ENRICH, C. 2002. Role of calmodulin in the modulation of the MAPK signalling pathway and the transactivation of epidermal growth factor receptor mediated by PKC. *FEBS Lett,* 517**,** 206-10.

TERRELL, E. M., DURRANT, D. E., RITT, D. A., SEALOVER, N. E., SHEFFELS, E., SPENCER-SMITH, R., ESPOSITO, D., ZHOU, Y., HANCOCK, J. F., KORTUM, R. L. & MORRISON, D. K. 2019. Distinct Binding Preferences between Ras and Raf Family Members and the Impact on Oncogenic Ras Signaling. *Mol Cell,* 76**,** 872-884 e5.

THOMAS, S., WRIGHT, K. J., LE CORRE, S., MICALIZZI, A., ROMANI, M., ABHYANKAR, A., SAADA, J., PERRAULT, I., AMIEL, J., LITZLER, J., FILHOL, E., ELKHARTOUFI, N., KWONG, M., CASANOVA, J. L., BODDAERT, N., BAEHR, W., LYONNET, S., MUNNICH, A., BURGLEN, L., CHASSAING, N., ENCHA-RAVAZI, F., VEKEMANS, M., GLEESON, J. G., VALENTE, E. M., JACKSON, P. K., DRUMMOND, I. A., SAUNIER, S. & ATTIE-BITACH, T. 2014. A homozygous PDE6D mutation in Joubert syndrome impairs targeting of farnesylated INPP5E protein to the primary cilium. *Hum Mutat,* 35**,** 137-46.

THORPE, L. M., YUZUGULLU, H. & ZHAO, J. J. 2015. PI3K in cancer: divergent roles of isoforms, modes of activation and therapeutic targeting. *Nat Rev Cancer,* 15**,** 7-24.

TIDOW, H. & NISSEN, P. 2013. Structural diversity of calmodulin binding to its target sites. *FEBS J,* 280**,** 5551-65.

TOUTENHOOFD, S. L. & STREHLER, E. E. 2000. The calmodulin multigene family as a unique case of genetic redundancy: multiple levels of regulation to provide spatial and temporal control of calmodulin pools? *Cell Calcium,* 28**,** 83-96.

UGI, S., IMAMURA, T., RICKETTS, W. & OLEFSKY, J. M. 2002. Protein phosphatase 2A forms a molecular complex with Shc and regulates Shc tyrosine phosphorylation and downstream mitogenic signaling. *Mol Cell Biol,* 22**,** 2375-87.

VAKANA, E., PRATT, S., BLOSSER, W., DOWLESS, M., SIMPSON, N., YUAN, X. J., JAKEN, S., MANRO, J., STEPHENS, J., ZHANG, Y., HUBER, L., PENG, S. B. & STANCATO, L. F. 2017. LY3009120, a panRAF inhibitor, has significant anti-tumor activity in BRAF and KRAS mutant preclinical models of colorectal cancer. *Oncotarget,* 8**,** 9251-9266.

VANDONSELAAR, M., HICKIE, R. A., QUAIL, J. W. & DELBAERE, L. T. 1994. Trifluoperazine-induced conformational change in Ca(2+)-calmodulin. *Nat Struct Biol,* 1**,** 795-801.

VARGA, A., SORIA, J. C., HOLLEBECQUE, A., LORUSSO, P., BENDELL, J., HUANG, S. A., WAGLE, M. C., OKRAH, K., LIU, L., MURRAY, E., SANABRIA-BOHORQUEZ, S. M., TAGEN, M., DOKAINISH, H., MUELLER, L. & BURRIS, H. 2020. A First-in-Human Phase I Study to Evaluate the ERK1/2 Inhibitor GDC-0994 in Patients with Advanced Solid Tumors. *Clin Cancer Res,* 26**,** 1229-1236.

VETTER, I. R. & WITTINGHOFER, A. 2001. The guanine nucleotide-binding switch in three dimensions. *Science,* 294**,** 1299-304.

VILLALOBO, A. & BERCHTOLD, M. W. 2020. The Role of Calmodulin in Tumor Cell Migration, Invasiveness, and Metastasis. *Int J Mol Sci,* 21.

VILLALONGA, P., LOPEZ-ALCALA, C., BOSCH, M., CHILOECHES, A., ROCAMORA, N., GIL, J., MARAIS, R., MARSHALL, C. J., BACHS, O. & AGELL, N. 2001. Calmodulin binds to K-Ras, but not to H- or N-Ras, and modulates its downstream signaling. *Mol Cell Biol,* 21**,** 7345-54.

WANG, J., LI, J., SANTANA-SANTOS, L., SHUDA, M., SOBOL, R. W., VAN HOUTEN, B. & QIAN, W. 2015a. A novel strategy for targeted killing of tumor cells: Induction of multipolar acentrosomal mitotic spindles with a quinazolinone derivative mdivi-1. *Mol Oncol,* 9**,** 488-502.

WANG, M. T., HOLDERFIELD, M., GALEAS, J., DELROSARIO, R., TO, M. D., BALMAIN, A. & MCCORMICK, F. 2015b. K-Ras Promotes Tumorigenicity through Suppression of Non-canonical Wnt Signaling. *Cell,* 163**,** 1237-1251.

WANG, Q., SHI, Y. L., ZHOU, K., WANG, L. L., YAN, Z. X., LIU, Y. L., XU, L. L., ZHAO, S. W., CHU, H. L., SHI, T. T., MA, Q. H. & BI, J. 2018. PIK3CA mutations confer resistance to first-line chemotherapy in colorectal cancer. *Cell Death Dis,* 9**,** 739.

WANG, T., YU, H., HUGHES, N. W., LIU, B., KENDIRLI, A., KLEIN, K., CHEN, W. W., LANDER, E. S. & SABATINI, D. M. 2017. Gene Essentiality Profiling Reveals Gene Networks and Synthetic Lethal Interactions with Oncogenic Ras. *Cell,* 168**,** 890-903 e15.

WEIS, K. 2003. Regulating access to the genome: nucleocytoplasmic transport throughout the cell cycle. *Cell,* 112**,** 441-51.

WEISS, B., PROZIALECK, W., CIMINO, M., BARNETTE, M. S. & WALLACE, T. L. 1980. Pharmacological regulation of calmodulin. *Ann N Y Acad Sci,* 356**,** 319-45.

WENNERBERG, K., ROSSMAN, K. L. & DER, C. J. 2005. The Ras superfamily at a glance. *J Cell Sci,* 118**,** 843-6.

WESTERMARCK, J. & NEEL, B. G. 2020. Piecing Together a Broken Tumor Suppressor Phosphatase for Cancer Therapy. *Cell,* 181**,** 514-517.

WHYTE, D. B., KIRSCHMEIER, P., HOCKENBERRY, T. N., NUNEZ-OLIVA, I., JAMES, L., CATINO, J. J., BISHOP, W. R. & PAI, J. K. 1997. K- and N-Ras are geranylgeranylated in cells treated with farnesyl protein transferase inhibitors. *J Biol Chem,* 272**,** 14459-64.

WILLIAMS, J. G., PAPPU, K. & CAMPBELL, S. L. 2003. Structural and biochemical studies of p21Ras S-nitrosylation and nitric oxide-mediated guanine nucleotide exchange. *Proc Natl Acad Sci U S A,* 100**,** 6376-81.

WINZKER, M., FRIESE, A., KOCH, U., JANNING, P., ZIEGLER, S. & WALDMANN, H. 2020. Development of a PDEdelta-Targeting PROTACs that Impair Lipid Metabolism. *Angew Chem Int Ed Engl,* 59**,** 5595-5601.

WLODARCHAK, N. & XING, Y. 2016. PP2A as a master regulator of the cell cycle. *Crit Rev Biochem Mol Biol,* 51**,** 162-84.

WU, C. H., BAI, L. Y., TSAI, M. H., CHU, P. C., CHIU, C. F., CHEN, M. Y., CHIU, S. J., CHIANG, J. H. & WENG, J. R. 2016. Pharmacological exploitation of the phenothiazine antipsychotics to develop novel antitumor agents-A drug repurposing strategy. *Sci Rep,* 6**,** 27540.

WU, H., ROSSI, G. & BRENNWALD, P. 2008. The ghost in the machine: small GTPases as spatial regulators of exocytosis. *Trends Cell Biol,* 18**,** 397-404.

WU, L. J., XU, L. R., LIAO, J. M., CHEN, J. & LIANG, Y. 2011. Both the C-terminal polylysine region and the farnesylation of K-RasB are important for its specific interaction with calmodulin. *PLoS One,* 6**,** e21929.

XU, F., XIA, Y., FENG, Z., LIN, W., XUE, Q., JIANG, J., YU, X., PENG, C., LUO, M., YANG, Y., WEI, Y. & YU, L. 2019. Repositioning antipsychotic fluphenazine hydrochloride for treating triple negative breast cancer with brain metastases and lung metastases. *Am J Cancer Res,* 9**,** 459-478.

XU, X., SOUTTO, M., XIE, Q., SERVICK, S., SUBRAMANIAN, C., VON ARNIM, A. G. & JOHNSON, C. H. 2007. Imaging protein interactions with bioluminescence resonance energy transfer (BRET) in plant and mammalian cells and tissues. *Proc Natl Acad Sci U S A,* 104**,** 10264-9.

XU, Y., PISTON, D. W. & JOHNSON, C. H. 1999. A bioluminescence resonance energy transfer (BRET) system: application to interacting circadian clock proteins. *Proc Natl Acad Sci U S A,* 96**,** 151-6.

XUE, J. Y., ZHAO, Y., ARONOWITZ, J., MAI, T. T., VIDES, A., QERIQI, B., KIM, D., LI, C., DE STANCHINA, E., MAZUTIS, L., RISSO, D. & LITO, P. 2020. Rapid non-uniform adaptation to conformation-specific KRAS(G12C) inhibition. *Nature,* 577**,** 421-425.

YADAV, B., PEMOVSKA, T., SZWAJDA, A., KULESSKIY, E., KONTRO, M., KARJALAINEN, R., MAJUMDER, M. M., MALANI, D., MURUMAGI, A., KNOWLES, J., PORKKA, K., HECKMAN, C., KALLIONIEMI, O., WENNERBERG, K. & AITTOKALLIO, T. 2014. Quantitative scoring of differential drug sensitivity for individually optimized anticancer therapies. *Sci Rep,* 4**,** 5193.

YAN, L., MIEULET, V., BURGESS, D., FINDLAY, G. M., SULLY, K., PROCTER, J., GORIS, J., JANSSENS, V., MORRICE, N. A. & LAMB, R. F. 2010. PP2A T61 epsilon is an inhibitor of MAP4K3 in nutrient signaling to mTOR. *Mol Cell,* 37**,** 633-42.

YANG, J. J., GAWTHROP, A. & YE, Y. 2003. Obtaining site-specific calcium-binding affinities of calmodulin. *Protein Pept Lett,* 10**,** 331-45.

YANG, L., SHI, P., ZHAO, G., XU, J., PENG, W., ZHANG, J., ZHANG, G., WANG, X., DONG, Z., CHEN, F. & CUI, H. 2020. Targeting cancer stem cell pathways for cancer therapy. *Signal Transduct Target Ther,* 5**,** 8.

YANG LI, Q. M., PING WANG, XIAOLEI LIU, QIUYU FU, YUTING XIE, YU ZHOU, XIANGBING QI, NIU HUANG 2020. Identification of PDE6D as a potential target of sorafenib via PROTAC technology.

BioRivX Preprint.

YANG, M. H., NICKERSON, S., KIM, E. T., LIOT, C., LAURENT, G., SPANG, R., PHILIPS, M. R., SHAN, Y., SHAW, D. E., BAR-SAGI, D., HAIGIS, M. C. & HAIGIS, K. M. 2012. Regulation of RAS oncogenicity by acetylation. *Proc Natl Acad Sci U S A,* 109**,** 10843-8.

YU, Y. Y., CHEN, Y., DAI, G., CHEN, J., SUN, X. M., WEN, C. J., ZHAO, D. H., CHANG, D. C. & LI, C. J. 2004. The association of calmodulin with central spindle regulates the initiation of cytokinesis in HeLa cells. *Int J Biochem Cell Biol,* 36**,** 1562-72.

YU, Z., PESTELL, T. G., LISANTI, M. P. & PESTELL, R. G. 2012. Cancer stem cells. *Int J Biochem Cell Biol,* 44**,** 2144-51.

ZHANG, M., JANG, H., LI, Z., SACKS, D. B. & NUSSINOV, R. 2021. B-Raf autoinhibition in the presence and absence of 14-3-3. *Structure*.

ZHANG, M., JANG, H. & NUSSINOV, R. 2019. The structural basis for Ras activation of PI3Kalpha lipid kinase. *Phys Chem Chem Phys,* 21**,** 12021-12028.

ZHANG, M., YOGESHA, S. D., MAYFIELD, J. E., GILL, G. N. & ZHANG, Y. 2013. Viewing serine/threonine protein phosphatases through the eyes of drug designers. *FEBS J,* 280**,** 4739-60.

ZHANG, Z., HE, F., CONSTANTINE, R., BAKER, M. L., BAEHR, W., SCHMID, M. F., WENSEL, T. G. & AGOSTO, M. A. 2015. Domain organization and conformational plasticity of the G protein effector, PDE6. *J Biol Chem,* 290**,** 12833-43.

ZHENG, H., LIU, A., LIU, B., LI, M., YU, H. & LUO, X. 2010. Ras homologue enriched in brain is a critical target of farnesyltransferase inhibitors in non-small cell lung cancer cells. *Cancer Lett,* 297**,** 117-25.

ZHOU, B., DER, C. J. & COX, A. D. 2016. The role of wild type RAS isoforms in cancer. *Semin Cell Dev Biol,* 58**,** 60-9.

ZHOU, Y. & HANCOCK, J. F. 2015. Ras nanoclusters: Versatile lipid-based signaling platforms. *Biochim Biophys Acta,* 1853**,** 841-9.

ZIMMERMANN, G., PAPKE, B., ISMAIL, S., VARTAK, N., CHANDRA, A., HOFFMANN, M., HAHN, S. A., TRIOLA, G., WITTINGHOFER, A., BASTIAENS, P. I. & WALDMANN, H. 2013. Small molecule inhibition of the KRAS-PDEdelta interaction impairs oncogenic KRAS signalling. *Nature,* 497**,** 638-42.

Appendices

SI Table 1. List of CaM inhibitors and their mechanisms of action in cancer

Table 7. List of CaM inhibitors and their mechanisms of action

#	Compound	Effects/Mechanism	Reference(s)
1	trifluoperazine	CaM antagonist, promotes apoptosis and necrosis in pancreatic adenocarcinoma	(Weiss et al., 1980, Huang et al., 2019)
2	E6 berbamine	CaM inhibitor, exerts anti-cancer effects on colon cancer cell line HT-29 by inducing autophagy and apoptosis	(Hu et al., 1992, Mou et al., 2019)
3	polistes mastoparan	Anti-cancer peptide that blocks mammary carcinoma in mouse through CaM inhibition	(Barnette et al., 1983, Hilchie et al., 2016)
4	CGS-9343B	CaM inhibitor that blocks gastric acid secretion in vitro and in vivo	(Norman et al., 1987, Black et al., 1989)
5	artemisinin (tehranolide)	CaM inhibitor which selectively blocks proliferation of K562 leukemia cell line	(Noori and Hassan, 2014)
6	CBP501	Blocks cancer proliferation, migration, EMT in NSCLC and suppresses macrophage induced CSC phenotypes through CaM inhibition	(Saito et al., 2017, Mine et al., 2017)
7	chlorpromazine	Blocks T-cell invasion across fibroblast monolayers through CaM inhibition	(Grabski et al., 2001)
8	flunarizine	Inhibits growth and survival of B16 mouse melanoma cell line through CaM/Ca^{2+} antagonism	(Sezzi et al., 1984)
9	J8	Antagonist of CaM, inhibits human melanoma cell invasion through fibronectin	(Dewhurst et al., 1997)
10	calmidazolium	Directly binds to CaM, inhibits cell adhesion and proliferation of colon cancer cells. Also reported to inhibit cancer stemness characteristics	(Lee et al., 2016, Najumudeen et al., 2016)

11	ophiobolin A	Covalently modifies Lysine residues on CaM, shown to block spheroid formation of Ras mutant breast cancer cell lines	(Najumudeen et al., 2016)
12	fluphenazine	CaM antagonist with anti-cancer effects on metastatic triple negative breast cancer	(Xu et al., 2019)
13	fluphenazine mustard	CaM covalent antagonist, sensitize lung cancer cell line H1299 to trail induced apoptosis	(Hwang et al., 2009)
14	W-7	Non covalent CaM antagonist shown to inhibit tumor cell growth, migration, invasiveness and metastasis in vivo	(Mohri et al., 1998, Parker and Sherbet, 1992, Ito et al., 1991)
15	miconazole	CaM inhibitor with activity against CaM mediated PDE activity	(Hegemann et al., 1993, Breitholtz et al., 2020)
16	econazole	CaM inhibitor with activity against CaM mediated PDE activity	(Hegemann et al., 1993)

Supplementary information for Manuscript 3: Phenothiazines synergistically block calmodulin and reactivate PP2A in Ras-MAPK driven cancers

SI Table 2. IC50 values of compounds assessed in 3D synergism spheroid assays N = 2

Table 8. IC50 values of compounds assessed in 3D synergism spheroid assays

Compound	***NCI H358 IC_{50} ± SEM/ µM***	***A375 IC_{50} ± SEM/ µM***	***MDA-MB-231 IC_{50} ± SEM/ µM***
DT-061	2.65 ± 0.25	2.1 ± 0.6	3 ± 0
CMZ	1.295 ± 0.005	1.3 ± 0.2	1.37 ± 0.76
CMZ + DT-061 (1 µM)	0.46 ± 0.03	0.7 ± 0.4	0.67 ± 0.06
CMZ + DT-061 (2 µM)	0.34 ± 0.05	0.6 ± 0.4	0.44 ± 0.21
trifluoperazine	0.7 ± 0.3	0.31 ± 0.06	0.59 ± 0.22
ARS-1620	0.5 ± 0.1	52 ± 4	58 ± 6

Supplementary Figures

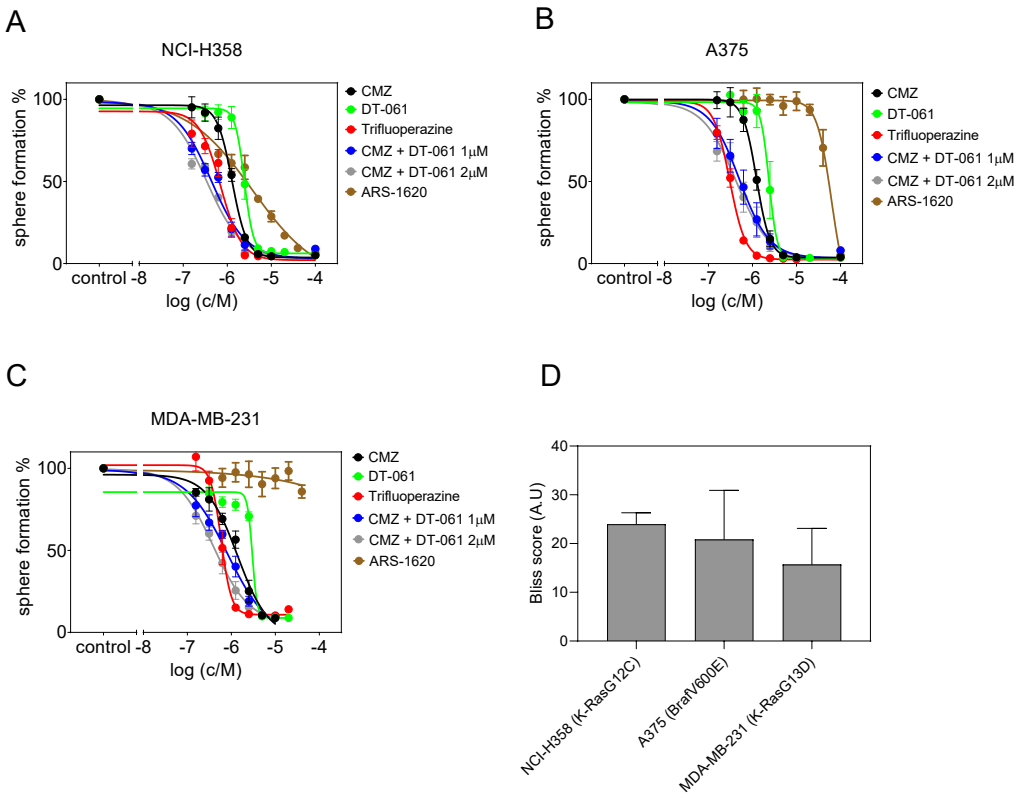

SI Figure 1. Synergistic assessment of CaM inhibitor and PP2A activator in Ras/MAPK mutated cancer cell lines. (A-C) *Dose response curves for various inhibitors in Ras pathway mutant cell lines NCIH-358* ***(A),*** *A 375* ***(B)*** *and MDA-MB-231* ***(C).*** *Compounds were tested as either single agents at concentration ranges of 0.2 µM – 10 µM (calmidazolium), 0.6 µM – 40 µM (DT-061), 0.2 µM – 40 µM (trifluoperazine) and 0.6 µM – 40 µM (ARS-1620) or in combination at a full dose response range of 0.2 µM – 10 µM for calmidazolium plus 1 or 2 µM of DT-061 added to all test conditions. Data represent mean values ± SEM, n = 2. The data were fit into log(inhibitor) vs. variable response (four parameters) function was used in the Prism (GraphPad) software to obtain the dose response curve.The actual curve fitting for Bliss calculation was done on the SynergyFinder website (https://synergyfinder.fimm.fi/).* ***(D)*** *Bliss synergism scores for combinatorial calmidazolium and DT-061 effects in Ras mutant cancer cell lines Data represent mean values ± SEM, n = 2*

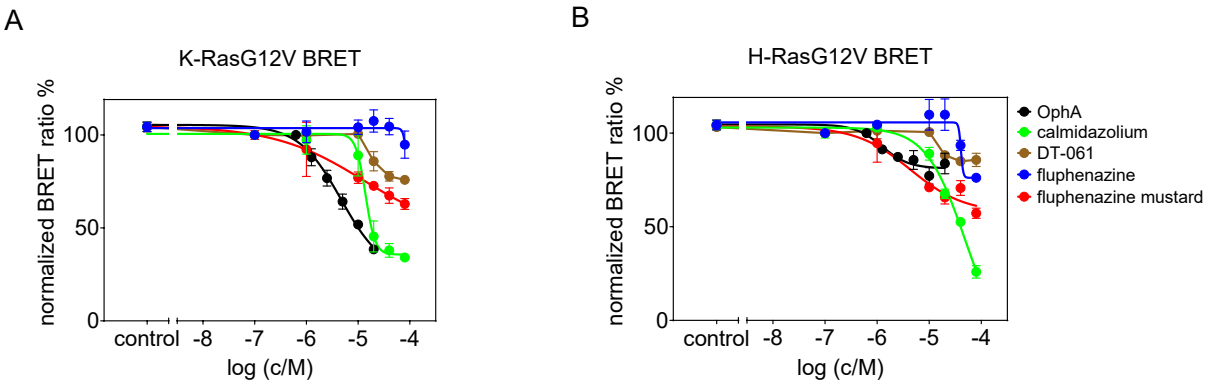

SI Figure 2. Cellular BRET assays indicates fluphenazine mustard inhibits both K-Ras and H-Ras nanoclustering. *(**A,B**) Dose response curves of phenothiazines (0.1 – 80 µM), calmidazolium (0.1 – 80 µM), DT-061 (0.1 – 80 µM) and OphA (0.3 – 20 µM) on K-RasG12V* ***(A)*** *and H-RasG12V* ***(B)*** *nanoclustering BRET. The A/D plasmid ratio was 4/1. Data represent mean values ± SEM, n ≥ 3. The data were fit into log(inhibitor) vs. variable response (four parameters) function was used in the Prism (GraphPad) software to obtain the dose response curve. The actual curve fitting for DSS_3 calculation was done on the breeze-site (https://breeze.fimm.fi/).*

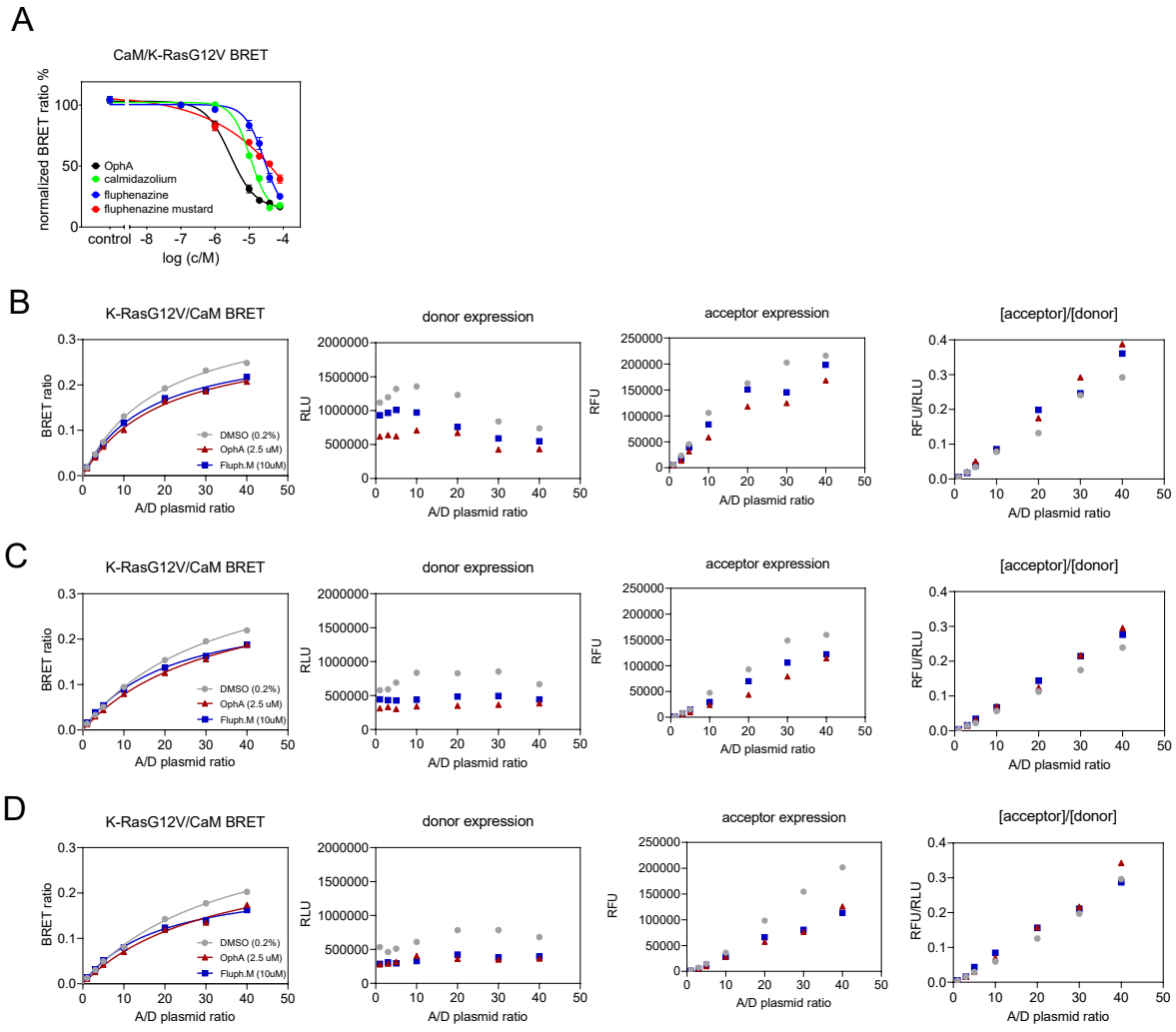

SI Figure 3. Assessment of the K-Ras/CaM on-target effects of CaM inhibitors and phenothiazines. (A) *Dose-response analysis of fluphenazine and its covalent mustard (0.1 – 80 μM) derivative as compared to OphA and calmidazolium (0.1 – 80 μM) using Rluc8-K-RasG12V/ GFP2-CaM BRET assay. The A/D plasmid ratio was 9/1. Data represent mean values ± SEM, n ≥ 2. The data were fit into log(inhibitor) vs. variable response (four parameters) function was used in the Prism (GraphPad) software to obtain the dose response curve. The actual curve fitting for DSS_3 calculation was done on the breeze-site (https://breeze.fimm.fi/).* ***(B-D)*** *Data from BRET pairs of Rluc8-K-RasG12V and GFP2-CaM after 24h treatment with DMSO (0.2% v/v in growth medium), OphA (2.5 μM) or fluphenazine mustard (10 μM). Each figure group represents individual biological repeats with (left to right) BRET ratio plotted against acceptor/donor plasmid ratio (A/D plasmid ratio), and then donor expression (RLU), acceptor expression (RFU) and relative expression of the two (RFU/RLU) plotted against acceptor/donor plasmid ratio (A/D plasmid ratio). Each biological repeat is the mean of four technical replicates (± SEM). The BRET ratio vs. relative expression data were fit with a hyperbolic function in Prism to obtain the $BRET_{max}$ and $BRET_{50}$ values.*

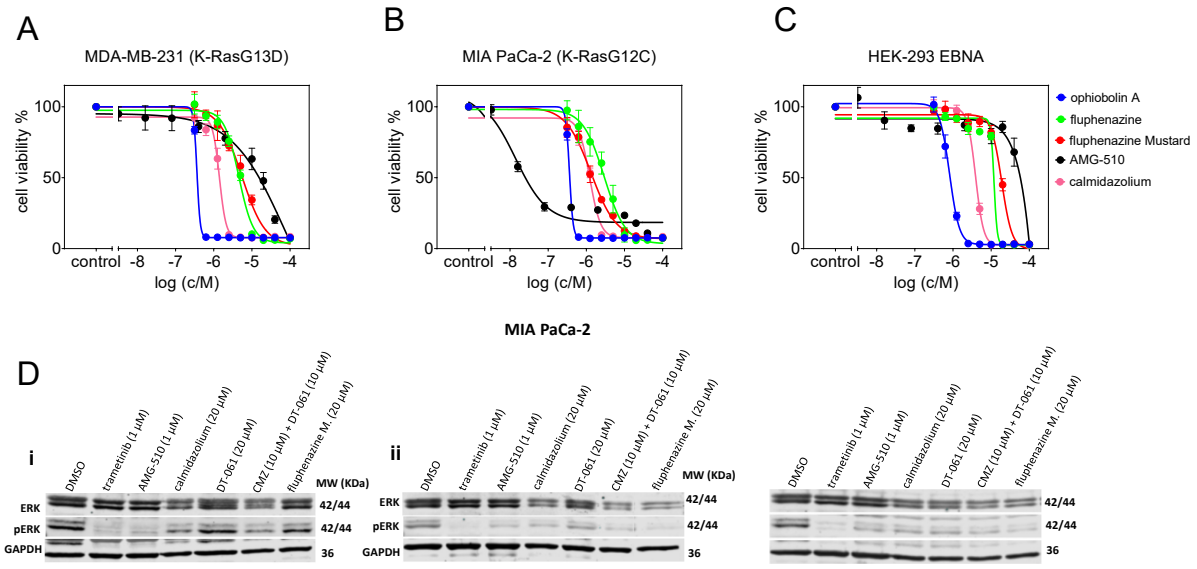

SI Figure 4. Phenotypic and signaling effects of inhibitors on Ras/MAPK mutated cancer cells. (A-C) *Comparison of effects of compounds on 2D monolayers derived from MDA-MB-231* ***(A)****, MIA PaCa-2* ***(B)*** *and HEK-293 EBNA* ***(C)****. Cells were treated with concentration range of 0.6 μM – 80 μM (fluphenazine and fluphenazine mustard), 0.3 μM – 40 μM (calmidazolium and OphA) and 0.003 μM – 40 μM (AMG-510). Data represent mean values ± SEM, n = 3. The data were fit to log (inhibitor) vs response – variable slope (four parameters) equation using the Prism (GraphPad) software.* ***(D)*** *MAPK signaling output measurement in MIA PaCa-2 upon treatment with control compounds trametinib (1 μM) and AMG-510 (1 μM), single agent treatment with camidazolium (20 μM) and DT-061 (20 μM) or in combination (DT-061 10 μM + CMZ 10 μM) as well as fluphenazine mustard (20 μM). pERK/ERK levels were assessed using a mouse monoclonal antibody against pERK and a rabbit polyclonal antibody against ERK. GAPDH was used as endogenous control for protein expression. Cells were seeded in 6-well plates for 24hrs, serum starved, treated with indicated concentrations of inhibitors for 2 h and then stimulated with EGF for 10 min. Blots shown represent images from 3 independent biological repeats.*